Geophysical characterisation of the Onewhero and Kellyville volcanic complexes, South Auckland Volcanic Field

A thesis submitted in partial fulfilment
of the requirements for the degree
of
Masters of Science
in Earth and Ocean Sciences
at
The University of Waikato
by

Kevin Joseph Chase Mullane

The University of Waikato
2015

THE UNIVERSITY OF
WAIKATO
Te Whare Wānanga o Waikato

Abstract

The Quaternary-aged (1.59 – 0.51 Ma) intraplate, monogenetic, basaltic South Auckland Volcanic Field consists of at least 82 volcanic centres that span an area of 300 km². This study focusses on the volcanic and sedimentary histories of the Onewhero and Kellyville maars, interpreted from additional geological observations, which build upon previous geological studies, and gravimetric and magnetic surveys.

New geological observations of the Onewhero maar reveal the presence of diatomaceous sediment, and at least one lava flow, that probably originated from the nearby Klondyke cone to the south, and which occupies a significant area of the crater floor. A geological investigation of the Kellyville maar reveals a crater that has been partially filled by a thick accumulation of basalt and scoria and overlain by Karapiro Formation sediments and diatomite. Available borehole stratigraphy suggests that the Glass Hill basalt cone present in the Kellyville maar was an early-stage volcanic product rather than a late-stage product as previously thought.

Gravimetric surveys in the Onewhero and Kellyville maars revealed contrasting crater fill deposits. Raw gravity data was acquired in the field, corrected for drift and then reduced to a Bouguer anomaly. The Onewhero maar is characterised by an anomaly of -5.8 mGal that has a concave profile. The post-eruption geological body present at Onewhero is two-dimensionally modelled with a density of 1.3 g/cm³, and has a maximum thickness of 100 m in the northwest of the crater. The Kellyville maar is characterised by an anomaly of +2.5 mGal that has a convex profile. The dominant geological body present in the crater is a lava-lake deposit that is two-dimensionally modelled with a density of 2.9 g/cm³, and has a maximum thickness of 60 m.

The total magnetic field strength of the Onewhero and Kellyville maars was recorded with a proton magnetometer and the values were mapped in ArcMap. In the Onewhero maar, two subdued anomalies were outliers. A positive magnetic anomaly (213 nT) with a broad crescent shape was identified in the middle of the crater and interpreted to be either an extrusive feeder dyke or an accumulation of highly magnetic volcanic sediment deposited in a topographic trough. A circular negative anomaly (-1057 nT) in the northwest of the crater is an accumulation of lake sediment with a low magnetic susceptibility. In the Kellyville maar, two contrasting anomalies were observed. The strongly positive anomaly (1275 nT) corresponds to the geographical position of Glass Hill, a basaltic cone. A strong negative anomaly (-3315 nT) in the middle of the crater corresponds to a known deposit of diatomite.

Overall, the structure of the Onewhero maar, as inferred by this investigation, is similar to many other maars globally and its sedimentary fill is remarkably similar to the Dottingen maar in Germany. The Kellyville maar has a more unique structure but can be compared to the Domain maar in the nearby Auckland Volcanic Field.

Acknowledgements

I would like to thank my supervisors Adrian Pittari, Beth Fox, and Andrew Gorman, for without them this study would not have been possible. Adrian, you anchored this project and provided the patience and personality that was needed to keep this ship afloat. Beth, you provided valuable information, and your extra knowledge was crucial. Without the support of the University of Otago, I would have been without equipment, so thank you Andrew.

Thank you to the rest of the staff in the Earth and Ocean Sciences department at the University of Waikato who all provided snippets of advice and inspired a love of the sciences throughout my years at university.

I am especially grateful to the landowners in Onewhero and Mercer who were all very approachable. Their generosity in allowing me to roam around their farms and borrow equipment should I need it ensured that I could gain full access to my field areas. Thank you to Nelson and the Black family from Mercer and the Green, Shakeshaft, Bovill, and Pellowe families from Onewhero.

I am very appreciative of funding received from the Broad Memorial Fund and internal University of Waikato research funds held by Adrian Pittari.

Cheers to the volcanology office crew (of which George is an honorary member) for the distractions and endless NBA procrastination (Billy).

To my family, thank you for instilling and nurturing in me a love for the natural world and for always being supportive of my endeavours.

Lastly to my field-helper Fiona, without your optimism, laughs and high-level off road skills we would never have made it through the fieldwork alive. Long live the Pokeno ice-cream trips.

Table of Contents

Abstract ..... **i**

Acknowledgements ..... **iii**

Table of Contents ..... **v**

List of Figures ..... **xi**

List of Tables ..... **xv**

Chapter One: Introduction **1**

1.1 Introduction 1

1.2 Objectives 2

1.3 Study area 2

1.4 Chapter outlines 3

Chapter Two: Formation and structure of maar volcanoes **5**

2.1 Introduction 5

2.2 Maar crater or tuff ring? 8

2.3 Geophysical case studies 9

2.4 North Island intraplate volcanism 11

2.5 South Auckland Volcanic Field 12

2.6 Country rock geology 14

2.7 Controls on volcanism 17

2.8 Eruption controls 17

2.9 Previous work: Kellyville Volcanic Complex 18

2.10 Previous work: Onewhero Volcanic Complex 19

Chapter Three: Geology of the Onewhero and Kellyville complexes **21**

3.1 Introduction 21

3.2 Geology of the Onewhero region 21

3.2.1 Introduction 21

3.2.2 Country rock geology 22
3.2.3 Volcanic geology 23
3.2.4 Borehole interpretation 24
3.2.5 Onewhero crater post-eruption fill 30
3.2.6 Onewhero crater lava flow 31
3.2.7 Updated geological map 33
3.3 Geology of the Mercer region 34
3.3.1 Introduction 34
3.3.2 Country rock geology 35
3.3.3 Volcanic geology 36
3.3.4 Borehole interpretation 36
3.3.5 Geological interpretations 42
3.3.6 Updated geological map 44
Chapter Four: Gravity investigation of the Onewhero and Kellyville volcanic complexes 45
4.1 Introduction 45
4.2 Gravity theory 46
4.3 Data collection 47
4.4 Base stations 48
4.5 Processing 48
4.5.1 Tide and machine drift 48
4.5.2 Latitude correction 49
4.5.3 Free-air correction 49
4.5.4 Bouguer correction 50
4.6 Potential sources of error in the raw data 51
4.7 Regional correction 51
4.8 Two-dimensional gravity modelling 52
4.9 Potential sources of error in the two-dimensional modelling 54

4.10 Onewhero gravity investigation....55
4.10.1 Gravity profiles.... 55
4.10.2 Onewhero two-dimensional gravity models 58
4.10.3 Discussion of the Onewhero gravity survey 60
4.11 Kellyville gravity investigation....61
4.11.1 Gravity profiles 61
4.11.2 Kellyville two-dimensional gravity models.... 64
4.11.3 Discussion of the Kellyville gravity survey.... 66
4.12 Chapter summary....67
Chapter Five: Magnetic investigation of the Onewhero and Kellyville volcanic complexes....69
5.1 Introduction....69
5.2 Magnetic Theory....69
5.3 Data collection....73
5.4 Processing....74
5.5 Onewhero magnetic investigation....76
5.5.1 Magnetic anomaly map.... 76
5.5.2 Points of interest 77
5.5.3 Interpretation of the points of interest.... 79
5.5.4 Discussion of the Onewhero magnetic investigation.... 81
5.6 Kellyville magnetic investigation....83
5.6.1 Magnetic anomaly map.... 83
5.6.2 Points of interest 84
5.6.3 Interpretation of points of interest 85
5.6.4 Discussion of the Kellyville magnetic investigation 86
5.7 Chapter summary....88
Chapter Six: Discussion....91
6.1 Introduction....91

6.2 Integration of the gravity and magnetic investigations 91
6.3 Structure of the Onewhero Volcanic Complex 98
6.4 Geological history of the Onewhero Volcanic Complex 99
6.4.1 Phase 1: Main vent initiation 99
6.4.2 Phase 2: Secondary vent initiation 99
6.4.3 Phase 3: Klondyke cone formation 99
6.4.4 Phase 4: Post-eruption sedimentary fill 100
6.5 Structure of the Kellyville Volcanic Complex 106
6.6 Geological history of the Kellyville Volcanic Complex 107
6.6.1 Phase 1: Basalt cone formation 107
6.6.2 Phase 2: Main vent initiation 107
6.6.3 Phase 3: Lava-lake/basalt plug formation 108
6.6.4 Phase 4: Post-eruption sedimentary fill 108
6.7 Maars or tuff rings? 113
6.7.1 Is the Onewhero crater a maar or a tuff ring? 114
6.7.2 Is the Kellyville crater a maar or a tuff ring? 116
6.8 Comparisons with the Auckland Volcanic Field 117
6.9 Comparisons with global monogenetic fields 118
6.10 Future directions for further investigations of the Onewhero and Kellyville volcanic complexes 122

Chapter Seven: Conclusions 125

7.1 Geological investigation 125
7.2 Gravity investigation 125
7.3 Magnetic investigation 126
7.4 Overall structure 127

References 129

Appendix A – Gravity investigation 137

A.1 Gravity correction equations 137

A.1.1 Latitude correction 137
A.1.2 Free-air correction 137
A.1.3 Bouguer correction 137
A.2 Gravity spreadsheets – raw data 138
A.2.1 Onewhero Y-Y' transect 138
A.2.2 Onewhero X-X' transect 140
A.2.3 Kellyville Y-Y' transect 142
A.2.4 Kellyville X-X' transect 144
A.3 Gravity corrections 146
A.3.1 Onewhero Y-Y' transect 146
A.3.2 Onewhero X-X' transect 148
A.3.3 Kellville Y-Y' transect 150
A.3.4 Kellyville X-X' transect 151
A.4 LINZ base-station tie 152
A.4.1 Onewhero base station tie 152
A.4.2 Kellyville base station tie 153
A.5 Raw two-dimensional gravity models 155
A.5.1 Onewhero Y – Y' transect 155
A.5.2 Onewhero X – X' transect 155
A.5.3 Kellyville Y – Y' transect 156
A.5.4 Kellyville X – X' transect 156
Appendix B – Magnetic investigation 157
B.1 Onewhero magnetic survey – raw data 157
B.2 Kellyville magnetic survey – raw data 179

List of Figures

Chapter Two: Formation and structure of maar volcanoes Page

Figure 2.1: General structure of a maar. 5

Figure 2.2: Magma fragmentation efficiency scale. 6

Figure 2.3: Maar diatreme and crater evolution. 7

Figure 2.4: Pukaki and Pukekiwiriki crater anomalies. 10

Figure 2.5: Volcanism in the North Island of New Zealand. 11

Figure 2.6: Distribution of volcanic centres in the SAVF. 13

Figure 2.7: SAVF fault-controlled eruption trends. 14

Figure 2.8: General country rock geology of the SAVF. 15

Chapter Three: Geology of the Onewhero and Kellyville volcanic complexes

Figure 3.1: Volcanoes of the Onewhero region. 22

Figure 3.2: Tuff ring outcrops in the Onewhero crater. 23

Figure 3.3: Chapter 3 borehole legend. 24

Figure 3.4: Location of boreholes in the Onewhero region. 25

Figure 3.5: OB1 visual log. 26

Figure 3.6: OB2 visual log. 27

Figure 3.7: OB3 visual log. 28

Figure 3.8: OB4 visual log. 29

Figure 3.9: OB5 visual log. 30

Figure 3.10: SEM images of diatoms in the Onewhero crater sediment. 31

Figure 3.11: Klondyke cone lava flow extent. 32

Figure 3.12: Onewhero intra-crater lava flow. 33

Figure 3.13: Geological map of the Onewhero maar. 34

Figure 3.14: Location of boreholes in the Mercer region. 37

Figure 3.15: MB1 visual log. 38

Figure 3.16: MB2 visual log. 39

Figure 3.17: MB3 visual log. 40

Figure 3.18: MB4 visual log. 41

Figure 3.19: Tuff deposit mantling Glass Hill. 43

Figure 3.20: Base surge disruption in the Kellyville maar. 43

Figure 3.21: Geological map of the Kellyville maar. 44

Chapter Four: Gravity investigation of the Onewhero and Kellyville volcanic complexes

Figure 4.1: Spring-based gravimeter theory. 47

Figure 4.2: Instrument drift at Onewhero maar. 49

Figure 4.3: Onewhero and Mercer regional gravity trends. 52

Figure 4.4: Gravity station measurements at Onewhero. 56

Figure 4.5: Onewhero Y – Y’ gravity transect. 57

Figure 4.6: Onewhero X – X’ gravity transect. 58

Figure 4.7: Onewhero Y – Y’ 2D model. 59

Figure 4.8: Onewhero X – X’ 2D model. 60

Figure 4.9: Gravity station measurements at Kellyville. 62

Figure 4.10: Kellyville Y – Y’ gravity transect. 63

Figure 4.11: Kellyville X – X’ gravity transect. 64

Figure 4.12: Kellyville Y – Y’ 2D model. 65

Figure 4.13: Kellyville X – X’ 2D model. 66

Chapter Five: Magnetic investigation of the Onewhero and Kellyville volcanic complexes

Figure 5.1: Magnetic dipole induction. 70

Figure 5.2: Secular variation at the South Magnetic Pole. 71

Figure 5.3: Total magnetic intensity vector diagram. 72

Figure 5.4: Magnetic susceptibility values. 73

Figure 5.5: Onewhero maar magnetic anomaly map. 76

Figure 5.6: Points of interest in the Onewhero maar. 77

Figure 5.7: Possible lava flow extent in the Onewhero maar. 80

Figure 5.8: Total field intensity in the Onewhero maar. 82

Figure 5.9: Kellyville maar magnetic anomaly map. 83

Figure 5.10: Points of interest in the Kellyville maar. 84

Figure 5.11: Total field intensity in the Kellyville maar. 87

Chapter Six: Discussion

Figure 6.1: X – X’ Bouguer anomaly for the Onewhero maar. 94

Figure 6.2: Y – Y’ Bouguer anomaly for the Onewhero maar. 94

Figure 6.3: X – X’ Bouguer anomaly for the Kellyville maar. 96

Figure 6.4: Y – Y’ Bouguer anomaly for the Kellyville maar. 96

Figure 6.5: Onewhero geological history, phase 1. 100

Figure 6.6: Onewhero geological history, phase 2. 100

Figure 6.7: Onewhero geological history, phase 3. 101

Figure 6.8: Onewhero geological history, phase 4. 102

Figure 6.9: Onewhero geological history, phase 5. 103

Figure 6.10: Kellyville geological history, phase 1. 107

Figure 6.11: Kellyville geological history, phase 2. 107

Figure 6.12: Kellyville geological history, phase 3. 108

Figure 6.13: Kellyville geological history, phase 4. 109

Figure 6.14: Kellyville geological history, phase 5. 110

Figure 6.15: Physical components of the Onewhero and Kellyville tuff. 113

Figure 6.16: Dottingen maar and Onewhero maar comparison. 117

Figure 6.17: Zuni Salt Lake maar. 118

Figure 6.18: Red Hill cone and lava flow. 119

List of Tables

Chapter Three: Geology of the Onewhero and Kellyville volcanic complexes

Table 3.1: Waikato Regional Council, OB1. 26

Table 3.2: Waikato Regional Council, OB2. 27

Table 3.3: Waikato Regional Council, OB3. 28

Table 3.4: Waikato Regional Council, OB4. 29

Table 3.5: Waikato Regional Council, OB5. 30

Table 3.6: Waikato Regional Council, MB1. 38

Table 3.7: Waikato Regional Council, MB2. 39

Table 3.8: Waikato Regional Council, MB3. 40

Table 3.9: Waikato Regional Council, MB4. 41

Chapter Four: Gravity investigation of the Onewhero and Kellyville volcanic complexes

Table 4.1: Onewhero modelled densities. 53

Table 4.2: Kellyville modelled densities. 54

Chapter Five: Magnetic investigation of the Onewhero and Kellyville volcanic complexes

Table 5.1: Onewhero and Kellyville magnetic parameters. 75

Chapter One: Introduction

1.1 Introduction

The geological archive represented by New Zealand's maar volcanoes can offer an insight into Quaternary paleoclimate through their ability to acquire and store climate-sensitive laminated sediments and other environmental proxies. They also pose a significant natural hazard threat to surrounding populations, particularly in Auckland and Northland.

Geophysical surveys have been extensively used to identify maars and their sedimentary fill, and this allows inferences to be made about their eruption history. The use of gravitational and magnetic signals to study these landforms is well documented (Pirrung et al., 2003; Cassidy et al., 2007; Loera, 2008; Mrlina et al., 2009; Blaikie et al., 2012). Maar craters are usually represented by a contrasting anomaly with the surrounding country rock. They typically occupy an area with a circular gravity low, caused by low density laminated lake sediments such as diatomite, with a corresponding circular magnetic high, representing a central iron mineral-rich diatreme (Jones, 2011).

The South Auckland Volcanic Field (SAVF) is a classic example of intraplate volcanism in New Zealand and is just one of multiple monogenetic volcanic fields in the North Island. The young age of the field (1.59 – 0.51 Ma) has allowed the Quaternary volcanic deposits, especially maar craters and tuff rings, with their post-eruption infill to remain intact (Briggs et al., 1994). Many of the 82 volcanic centres are easily accessed, situated in a semi-urban/rural setting.

The SAVF provides a complete geological record of a monogenetic field from activation to extinction. This is a particularly useful analogue in the context of the nearby Auckland Volcanic Field (AVF) which is currently still active and poses a significant natural hazard threat to all citizens living within the area (approximately 1.42 million (Statistics New Zealand, n.d., para. 1)).

The aim of this study is to constrain the subsurface geology of the Onewhero and Kellyville volcanic complexes by completing ground-based gravity and magnetic surveys. This will allow a better understanding of the volcanic and sedimentary processes that formed and filled these phreatomagmatic craters.

1.2 Objectives

Three objectives have been identified to help complete the aim of this study. The first of these is to reassess the geology of the Onewhero and Mercer regions. This will be completed by spending time in the field making geological observations and interpreting bore-hole data. The second objective is to determine any positive or negative gravity anomalies that may be present in the Onewhero and Mercer maars. This will be achieved by completing ground-based gravity surveys in the two craters. The third objective is to calculate any positive or negative magnetic anomalies that may be present in the Onewhero and Mercer complexes. This will be achieved by completing ground-based magnetic surveys in the two craters.

1.3 Study area

The South Auckland Volcanic Field covers an area of 300 km² (Schofield, 1958; Rafferty, 1977; Rafferty and Heming, 1979; Weaver and Smith, 1989) and encompasses the rural communities of Pukekohe, Bombay, Onewhero, Pukekawa, Tuakau, and Waiuku (Briggs et al., 1994). There are two study areas of interest in this thesis. The first is the Kellyville maar which is located in the southeast of the SAVF, south of Bombay and directly to the east of Mercer township. The second is the Onewhero maar which lies in the southern extent of the SAVF, about 15 km west of SH1, and 5 km south of the Waikato River.

1.4 Chapter outlines

The second chapter outlines New Zealand's tectonic and geological setting and how this affects intraplate volcanism in particular. Previous work in the South Auckland Volcanic Field will also be covered, with a brief outline of the dominant volcanic processes and field setting. The behaviour of this monogenetic field can be partially explained by acknowledging New Zealand's tectonic setting and development, and the characteristics of other intraplate monogenetic fields.

The third chapter investigates the background geology and stratigraphy by completing any further surface mapping that may be necessary to explain possible geophysical anomalies. The subsurface geology of the Kellyville and Onewhero volcanic centres will be interpreted from bore data obtained from the Waikato Regional Council. Features that may aid in the geophysical interpretations will also be discussed.

The fourth chapter focuses on the gravity data obtained from the Onewhero and Kellyville complexes. The gravity anomaly models will contribute to the discussion of eruption, evolution, and the infilling sequences of the Onewhero and Kellyville volcanic complexes, which will be discussed in Chapter 6.

The fifth chapter focuses on the magnetic data obtained from the Onewhero and Kellyville complexes. The magnetic anomaly models will contribute to the discussion of eruption, evolution and the infilling sequences of the Onewhero and Kellyville volcanic complexes, which will be discussed in Chapter 6.

The sixth chapter will combine the results of the gravity and magnetic surveys. I will discuss how well the two different geophysical methods complemented each other as well as interpreting the pre- and post-eruption history of the Onewhero and Kellyville volcanic complexes. Comparisons will be made between the results of this investigation and maar studies in a nearby monogenetic field and also in a global context.

The seventh and final chapter will conclude the geological, gravitational, and magnetic components of this study.

Chapter Two: Formation and structure of maar volcanoes

2.1 Introduction

Lorenz (1986, 2003) discussed maar formation and eruption processes. Below is a summary of his work.

Maar-forming eruptions are considered to be the second most common surface volcanic feature on Earth after scoria cones (Martin et al., 2007). Five structural features are generally present in maar volcanoes (Figure 2.1): an ejecta ring, post-eruption sedimentary infill, a diatreme, an explosion chamber and a feeder dyke (Lorenz, 1986).

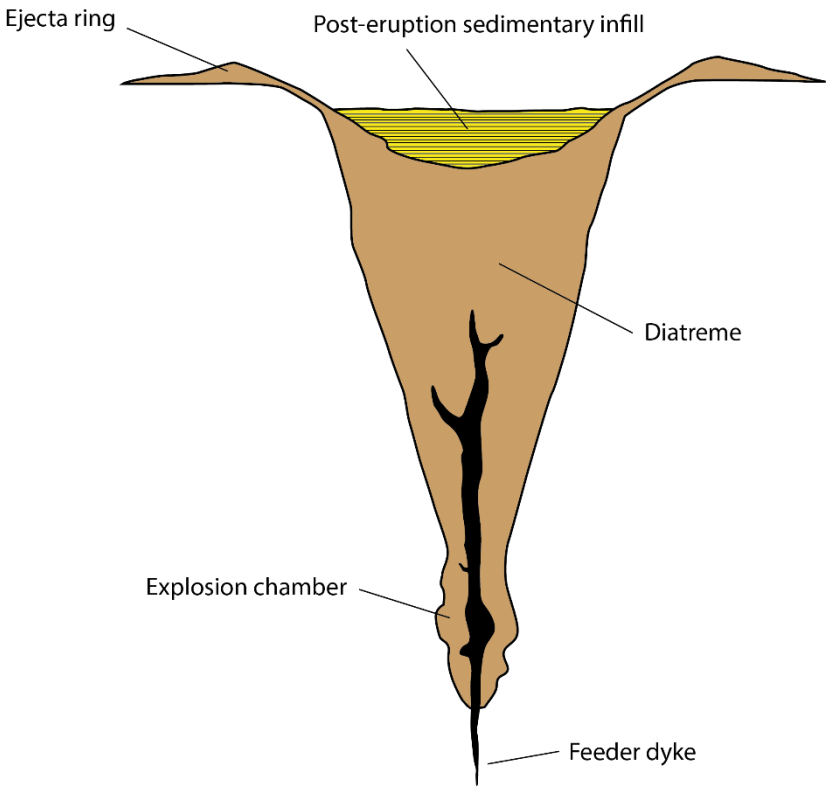

Figure 2.1: The general structure of a maar highlighting the five key structural features (adapted from Lorenz, 2003).

Phreatomagmatic volcanoes form when buoyant rising magma intersects groundwater. The mass ratio of water/magma determines the efficiency of energy transfer and the extent of magma fragmentation (Sheridan and Wohletz, 1981). A water/magma mass ratio of 0.3 – 0.8 can produce a highly energetic eruption accompanied by dry base surges (Figure 2.2). An efficient explosion shatters the surrounding country rock and excavates a funnel-shaped pit starting at the surface. The subsequent subsurface collapse pit is called a diatreme, and consists of fragmented country rock and volcanic breccia (Lorenz, 1986). Wall collapse is a characteristic maar-forming process. It is inferred that collapse can occur during an eruption as well as after an eruption as the steep conduit wall becomes increasingly unstable.

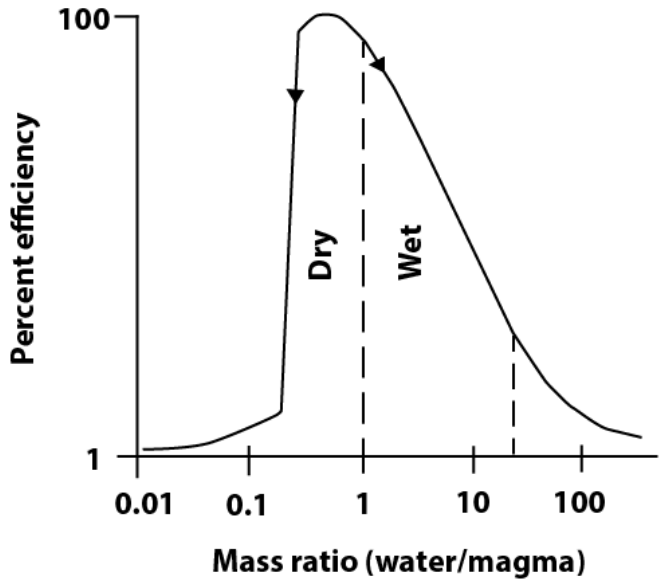

Figure 2.2: The magma fragmentation efficiency scale (adapted from Sheridan and Wohletz, 1981).

Any successive eruptions after the first initial blast will excavate the crater horizontally and vertically. Explosions can send shock-waves into the surrounding wall material, causing a decrease in rock density as the loose rock re-orientates (Lorenz, 1986). The explosion chamber evolves through every volcanic episode, deepening whilst being buried by the growing and increasingly unstable crater (Figure 2.3). The depth of succeeding eruptions has a direct effect upon the diameter of the maar crater at the surface. The shape of the diatreme is also dependent on the strength of the surrounding country rock. Studies have found that maar diatremes have much steeper diatreme wall angles when emplaced within hard basement rock

and very shallow diatreme wall angles when emplaced within sandstone or shale (Field and Scott-Smith, 1999; Jones, 2011)

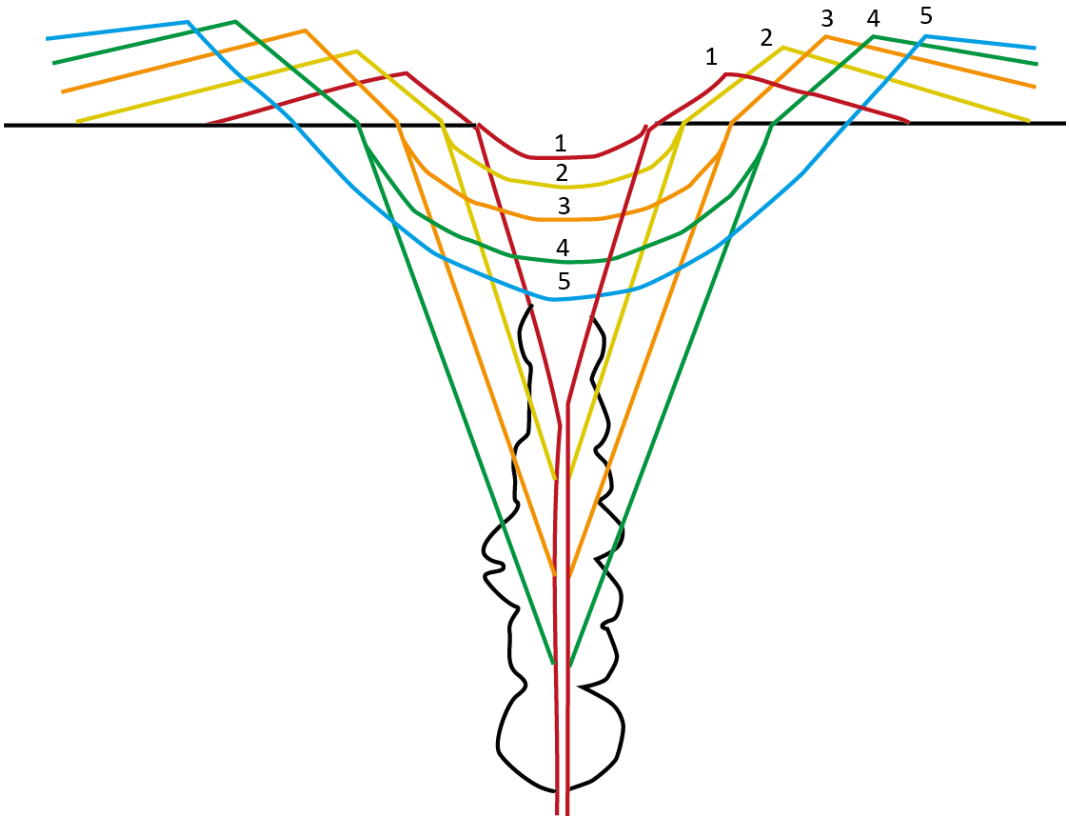

Figure 2.3: The vertical excavation of the diatreme and lateral build-up of the ejecta ring in stages from youngest (1) to oldest (5) (adapted from Lorenz, 2003).

The Waipiata Volcanic Field in the South Island of New Zealand consists of an ancient monogenetic field that was active in the Miocene (Coombs et al., 1986; Nemeth, 2001). Volcanic fields of this age are rarely still intact at the surface, but uplift and erosion can provide valuable outcrops where the subsurface geology can be investigated. Volcanic centres in the Waipiata Volcanic Field are characterised by having erupted with differing volcanic styles at different stages in the life of the volcano. At times, water-magma interactions were very efficient but could be interrupted by dry stages, producing basalt caps above diatremes (Karoly and White, 2003). The high strength of the Otago Schist often contains explosive maar behaviour, elongating the diatreme downwards and preventing it from growing outwards (Jones, 2011).

Lake Purrumbete maar in the Newer Volcanics Province, Australia, is a large maar crater with similar surface characteristics to the Onewhero crater. The maar was studied in detail by Jordan et al. (2013). The presence of such a large maar is due to a subsurface structure consisting of three coalesced vents. The three vents are responsible for a range of volcanic products. Six ash facies, six lapilli, two scoria, two ballistic ejecta, and an epiclastic volcanogenic sandy gravel facies have been identified. This huge range of facies from one 'monogenetic' event outlines the high geological diversity these volcanic events can evolve through.

2.2 Maar crater or tuff ring?

Comparisons between maar craters and tuff rings continually create intense debate. At present, there are specific criteria in place that are globally used to distinguish the two. However, a single monogenetic crater can evolve from a maar to a tuff ring or have multiple coalescing vents, and this often leads to some confusion when interpreting these volcanic landforms (Blaikie et al., 2012).

Lorenz (1973) identifies three main differences between the two landforms.

1. The density difference between the pyroclastic debris and country rocks
2. The difference in the distribution ratio between ejected material and debris remaining within the underlying diatreme
3. And most importantly, the total amount of juvenile material produced

The traditional distinction between maars and tuff rings can be defined by the difference in the depth of magma-water interaction and by the amount of juvenile material produced in the lifetime of the eruption.

Maar volcanoes react with groundwater at depth, usually intersecting an aquifer. This causes the vent to scour deep into the crust, up to 2.5 km. A large amount of country rock is excavated and therefore the ejecta ring is enriched in xenolith fragments compared to juvenile material.

Tuff rings differ by interacting with surface water or groundwater at a shallow depth. The vent is superficial since downward penetration of the diatreme does not

occur. Less country rock is incorporated into the surface deposits and this allows the ejecta ring to be enriched in juvenile material.

2.3 Geophysical case studies

Geophysical studies of maars are increasingly common as data collecting instruments become more affordable and compact. Gravity and magnetic signals are the most frequently used and are well suited to contrasting and defining low density lake sediment and higher density basalt diatreme features. Reduction of raw geophysical data and forward modelling has allowed the creation of striking subsurface imagery in many maar studies (Cassidy et al., 2007; Mrlina et al., 2009; Jones et al., 2011; Blaikie et al., 2014).

A geophysical study of maar-diatremes in the Auckland Volcanic Field by Cassidy et al. (2007) outlined the structure of four volcanic centres: Pukaki, Pukekiwiriki, Domain and Waitomokia. The volcanoes were emplaced in Plio-Pleistocene sediments and the alternating sandstones and siltstones of the Miocene aged Waitemata Group, within a probable extensional environment (Edbrooke et al. 1998).

The four maars studied were all similar sized with circular raised tuff rings. Gravity and magnetic signals outlined very different subsurface deposits in Pukaki and Pukekiwiriki. These two maars have a very similar surface geology, but the potential field modelling determined that the matching gravity and magnetic high (+8 g.u. and +160 nT) at Pukekiwiriki equated to a sizable basalt bowl underlying a thin layer of Pleistocene infill (Figure 2.4 b). No such gravity or magnetic high was recorded at Pukaki, so the two-dimensional gravity model consisted of a thick layer of Pleistocene infill to match a slight gravity low of -6 g.u. (Figure 2.4 a).

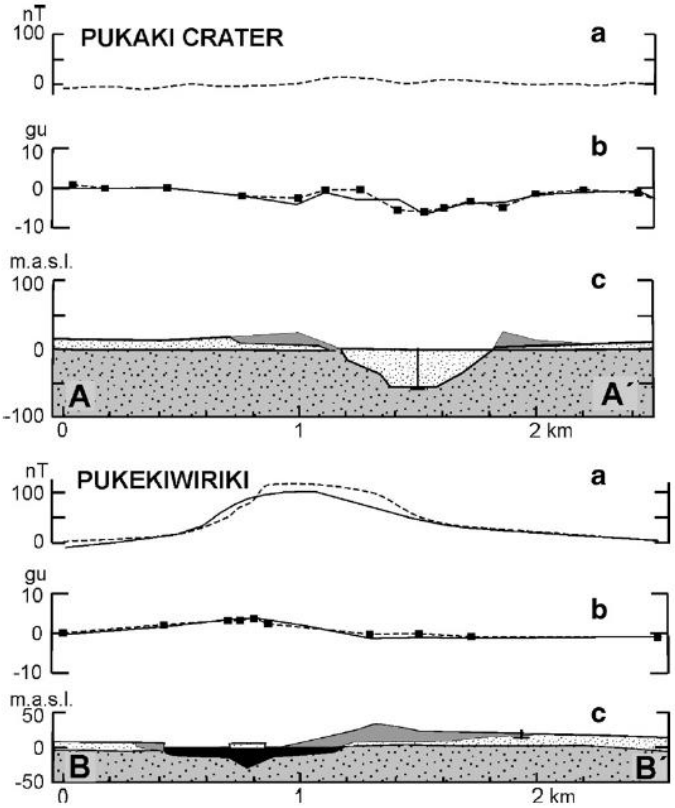

Figure 2.4: The Pukaki crater (a) and Pukekiwiriki crater (b) have contrasting magnetic and gravity anomalies as they have evolved through different stages of a maar eruption (from Cassidy et al., 2007).

A previously undiscovered maar in West Bohemia, Czech Republic, was confirmed with a gravity and magnetic survey. Mrlina et al. (2009) modelled a negative gravity anomaly with an amplitude of -2.30 mGal. The maar lay close to the Zelezna Hurka volcano and is the first phreatomagmatic landform found in the area.

The Ecklin maar in the Red Rock Volcanic Complex, Germany, was found to have a -1.9 mGal negative anomaly (Blaikie et al., 2014). The aim of the study was to image the subsurface of the maar to better understand eruption mechanisms. This investigation veered away from traditional forward modelling techniques by creating inverse models that built on the forward modelling results. This allows for less complex imaging, but the models are constrained by geological data at every stage and are much more robust as a result.

2.4 North Island intraplate volcanism

Intraplate volcanism in the North Island only occurs within the Indo-Australian plate (Johnson and Wellman, 1989). The Coromandel and Taupo volcanic zones are features of subduction-related volcanism (Cook et al., 2005). The Northland and Auckland intraplate volcanic provinces are believed to have no relationship with the active plate boundary that lies to the east and drives the andesitic-rhyolitic Coromandel and Taupo volcanic zones (Figure 2.5) (Weaver and Smith, 1989; Briggs et al., 1996; Cook et al., 2005).

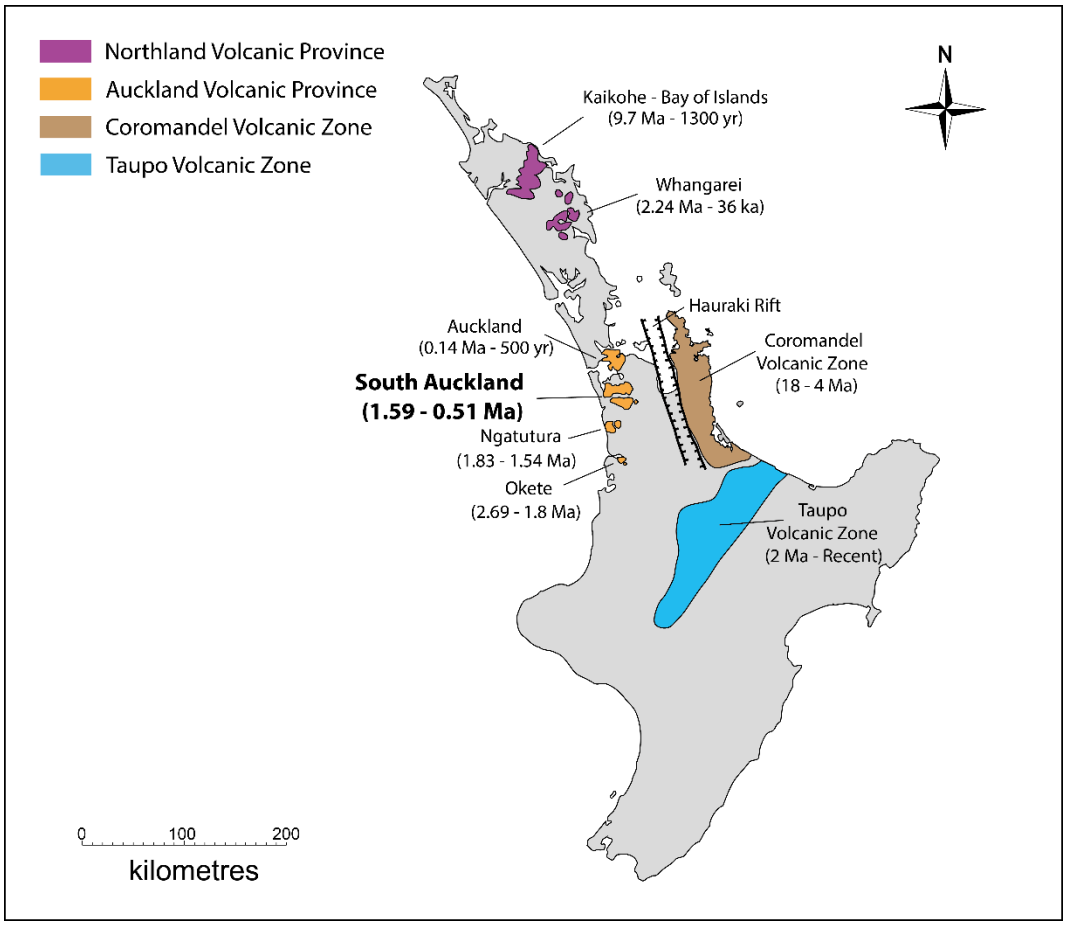

Figure 2.5: Volcanic fields of the North Island. Note the progressive younging to the north that is displayed by the Auckland Volcanic Province (Figure adapted from Weaver and Smith, 1989; Briggs et al., 1994; Cook et al., 2005).

The Northland province covers an area of approximately 2500 km² and can be separated into the Kaikohe-Bay of Islands Volcanic Field and the Whangarei Volcanic Field. The Auckland province covers an area of approximately 400 km² and can be broken down into the Auckland, South Auckland, Ngatutura, and

Okete volcanic fields. A progressive younging to the north characterises the Auckland Volcanic Province (Briggs et al., 1994) and should signify mantle source migration to the north. However actual plate movement dictates that the fields should progressively young towards the south (Briggs et al., 1994). Cook et al. (2005) suggests that the North Island intraplate volcanism could instead derive from adiabatic decompressional melting, promoted by regional tectonic extension events.

2.5 South Auckland Volcanic Field

The South Auckland Volcanic Field (SAVF) encompasses a ~300 km² area of lowland, mainly used for agriculture and horticulture (Figure 2.6). The field was active between 1.59 and 0.51 Ma (Briggs et al., 1994), and precedes the nearby Auckland Volcanic Field by 250 ka (Cook et al., 2005). Two eruption styles dominate volcanism in the SAVF. Magmatic eruptions produce positive relief landforms such as scoria cones, lava flows and small shield volcanoes. Phreatomagmatic eruptions commonly produce maar craters and tuff rings (Briggs et al., 1994). The volcanic activity observed in the SAVF was triggered by an extensional tectonic environment that thinned the crust and allowed rising magma easy access to the surface (Briggs et al., 1994; Cook et al., 2005). A large portion of the SAVF lies in an area of down-faulted Mesozoic greywackes, argillites and sandstones (Rafferty, 1977; Greig, 1989). Extensional environments account for most continental intraplate systems worldwide (Lesti et al., 2008; Valentine and Hirano, 2010).

Magmatic volcanism in the SAVF is a mixture of strombolian, hawaiian and surtseyan in style. The 82 volcanic centres in the SAVF comprise 38 tuff rings and maars formed from phreatomagmatic eruptions and 17 scoria cones and 40 lava shields/cones produced from hawaiian-strombolian eruptions (Briggs et al., 2012). Faulting in the SAVF is extensive and faults are thought to play a strong role in vent alignment and distribution (Rosenburg, 1991; Briggs et al., 2010). Approximately half of the volcanic centres in the SAVF occur on or in a close proximity to major faults (Briggs et al., 1994; Briggs et al., 2010). The Drury Fault and the Morley Road tuff rings in particular have a trend of volcanism to strongly support this theory (Figure 2.7). It is also very likely that many smaller faults are

completely buried beneath SAVF basalts and the actual fault controls are being underrepresented because of this (Briggs et al., 1994).

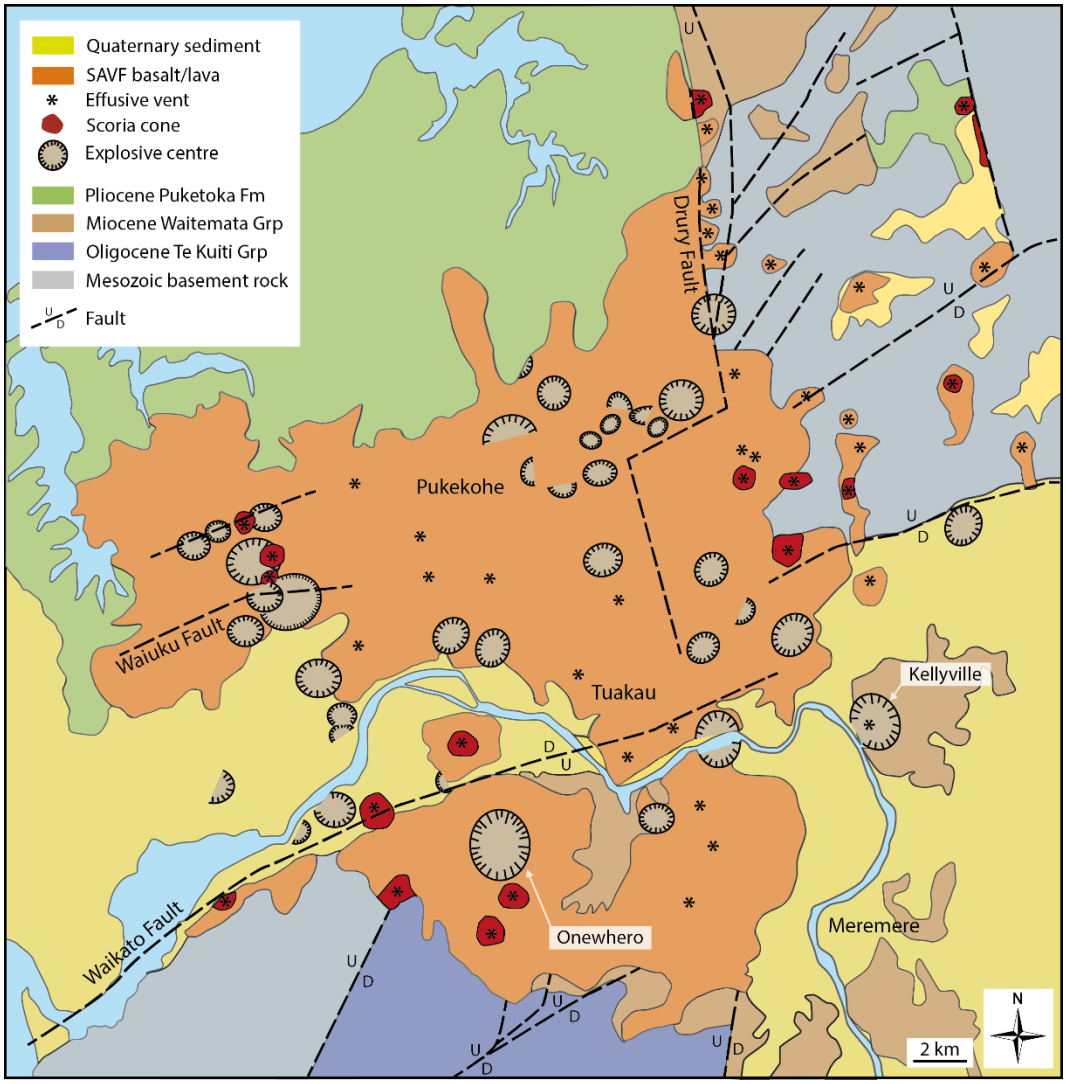

Figure 2.6: The geological structure and distribution of volcanic occurrences in the South Auckland Volcanic Field. Note the role that faulting plays in the alignment of vents in some areas (adapted from Briggs et al., 2010).

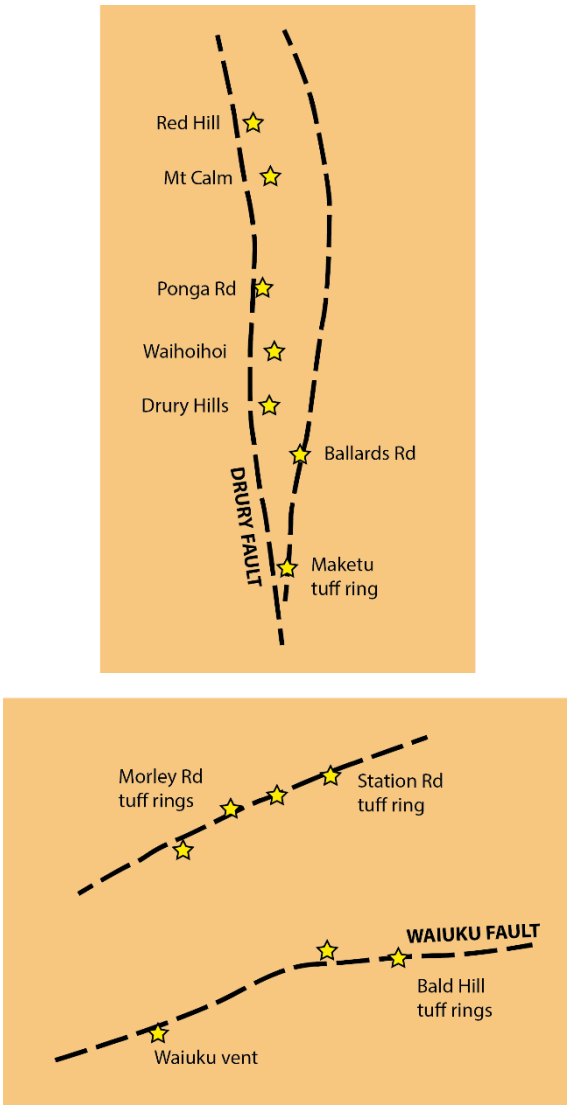

Figure 2.7: Many volcanic vents in the South Auckland Volcanic Field, especially the Drury and Waiuku faults, show evidence of fault controlled eruptions (adapted from Briggs et al., 2010).

2.6 Country rock geology

Figure 2.8 outlines the basic country rock geology for the South Auckland Volcanic Field. The basement of the SAVF is composed of late-Triassic to late-Jurassic Waipapa–Murihuku Group greywacke. This volcaniclastic accretionary wedge terrane outcrops in the field area only in the uplifted Hunua Ranges to the east of the Drury Fault (Vijevac et al., 2002).

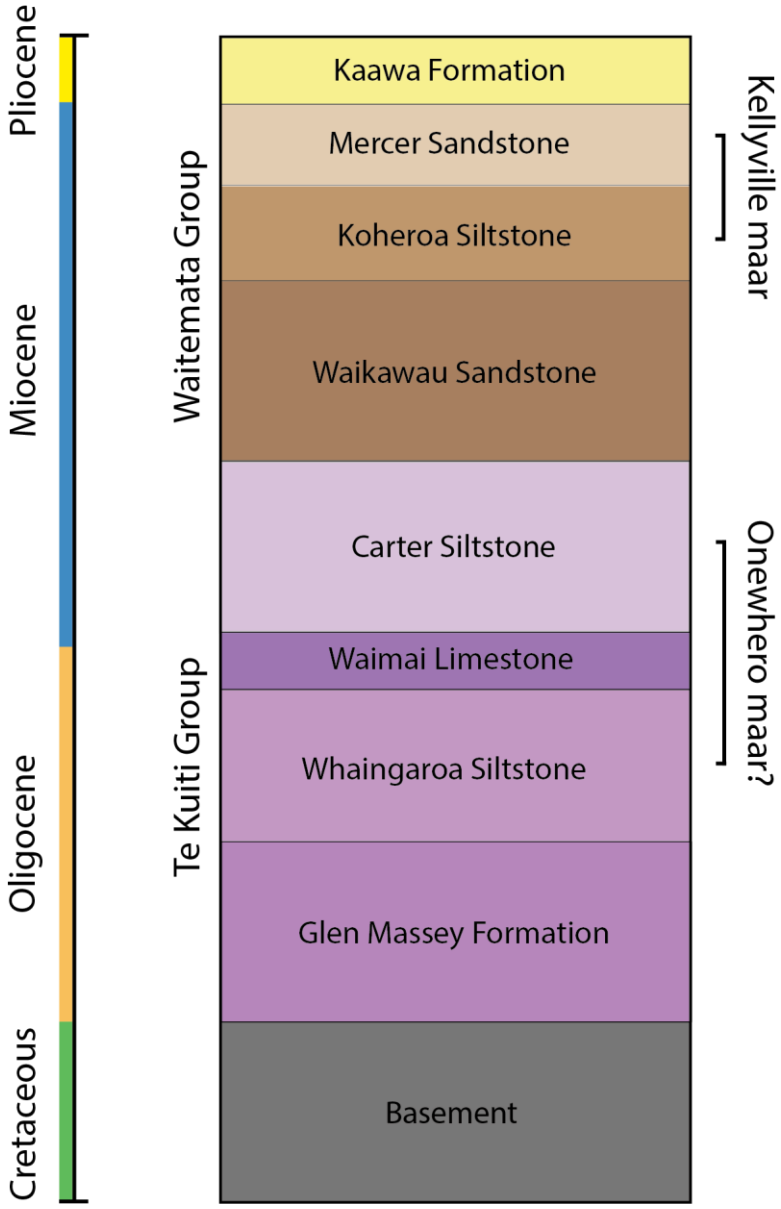

Figure 2.8: The general country rock geology of the South Auckland Volcanic Field. The Kellyville maar erupted through Waitemata Group sediment whereas the Onewhero maar probably erupted through Te Kuiti Group sediment.

The Waitemata Group rests unconformably atop the basement and underlies most of the SAVF (Vijevac et al., 2002). The group is laterally and vertically extensive, with Raglan and Whangarei being the southern and northern extents respectively. The sediments consist of mass-emplaced deposits transported via density currents in a subsiding basin (Ballance, 1974). Although the indurated sandstones and mudstones have relatively poor aquifer properties, the Waitemata Group is extensively deformed by faulting and also has sandy debrite formations that possess the ability to store significant water volumes (Hornibrook and Schofield, 1963;

Isaac et al., 1994). Aquifer transmissivity values in the fractured Waitemata Group sediments range from 20 – 60 m²/day (Greig, 1989)

The Te Kuiti Group is localised in its occurrence in the SAVF. It underlies the SAVF basalts that have been forced up in the Quaternary by the Waikato Fault (Figure 2.6). The Te Kuiti Group was first described by Kear and Schofield (1959) and further revised by White and Waterhouse (1993). The group consists of Eocene to Miocene calcareous sandstones, siltstones and limestones. The Carter Siltstone is the only member of the Te Kuiti Group that outcrops in the field area, and it does so to the north of the Onewhero maar. The Carter Siltstone is a light grey, highly calcareous, massive, sandy-siltstone (White and Waterhouse, 1993). The Carter Siltstone is not aquiferous and it is inferred that this was not the unit that supplied groundwater to the phreatomagmatic eruption that formed the Onewhero maar.

The Kaihu Group comprises Pliocene marine sediments that unconformably overlie the Waitemata Group (Vijevac et al., 2002). The basal member, the Kaawa Formation, is the most extensive and important of the SAVF aquifers. The Kaawa Formation consists of basal shell beds and alternating fine- to medium-grained sandstones that can reach thicknesses of up to 250 m in the south. It is found throughout the field area, only absent in the Karaka and Drury regions. The formation has a high transmissivity and is responsible for the majority of groundwater storage and release in the SAVF (Vijevac et al., 2002). Aquifer transmissivity values for the Kaawa Formation range from 30 – 500 m²/day, which is significantly higher than the Waitemata Group (Greig, 1989).

Eruption styles in the SAVF are largely regulated by the hydrology of the local country rock. Negative and low-relief landforms (maars and tuff rings) tend to occur in the lowlands to the north-east of the field. Here the underlying sediments represent a substantial aquifer and contain large amounts of groundwater year round. These aquiferous units allow rising magma to interact with groundwater at shallow depths, producing the highly efficient fragmentation that creates a phreatomagmatic eruption. Areas around fault lines provide a contrast to this trend, with effusive centres erupting in indurated greywackes that are generally of a low porosity and permeability (Briggs et al., 2010).

2.7 Controls on volcanism

The distribution and nature of volcanism in the South Auckland Volcanic Field is thought to be controlled by three factors. Many of the vents occur in close proximity to neighbouring faults. These **structural** plays have provided buoyant magma with a path of lower resistance. Volcanoes in the SAVF that lie directly over fault lines include the Bald Hill Road maar and the Ballards Road cone. Two intersecting faults can influence the precise vent location and this has occurred at the Maketu tuff ring and the Peach Hill cone (Rosenburg, 1991).

A majority of the SAVF occupies an area known as the Manukau lowlands. The underlying **lithology** of this area comprises downfaulted Mesozoic greywackes overlain by members of the Te Kuiti Group and the Kaawa Formation. To the east of the lowlands the same Mesozoic greywackes have been uplifted by up to 2.5 km. Eruptions in the shallow greywackes generally produce scoria cones and lava flows rather than maars and tuff rings. The Kaawa Formation in the west is very porous and highly permeable and the eruption products are dominated by 'dry' maars and tuff rings as a result.

Hydrology is the last of the three main volcanic controls. Phreatomagmatic volcanism occurs from the interaction of groundwater with ascending magma. Therefore strata can have different qualities that promote a more or less efficient eruption. Permeable sediments with high tranmissivity values meet the prerequisites required for efficient and energetic phreatomagmatic eruptions. In the Manukau Lowlands, precipitation is high, the water table is close to the surface, and the aquiferous Kaawa Formation is present throughout. This allows rising magma to explode phreatomagmatically in most cases.

2.8 Eruption controls

Lorenz (1986), considered the formation and growth of phreatomagmatic volcanoes to be influenced by three main variables: (1) the duration of the eruption, (2) the ejection of underlying country rock to the point of vent collapse, and (3) the depth and lowering of magma-water interaction. Rosenburg (1991) suggests that many of

the phreatomagmatic volcanoes in the South Auckland Volcanic Field have formed via similar processes to those outlined by Lorenz (1986).

2.9 Previous work: Kellyville Volcanic Complex

Kermode (1992) describes Kellyville maar as a tuff ring with a central basaltic plug. The eruption style is documented as being hawaiian/strombolian, with late activity forming the Glass Hill scoria cone. The tuff ring reaches a height of 110 m with internal terraces at 35 m and 55 m and a breach on the western side caused by an ancestral Waikato River flow path.

Kear and Schofield (1978) recognise Kellyville tuff ring as a breached tuff ring with a "small but prominent cone-shaped hill" composed of basaltic tuff and agglomerate. The tuff ring has been K-Ar dated to an age of 1.48 ± 0.10 Ma from a sample of *ne*-hawaiite basalt (Briggs et al., 1994).

A thesis study by Gibson (2011) comprehensively covered the volcanic geology and eruption history of the Kellyville Volcanic Complex, including stratigraphic logs, petrographic and geochemical analysis. Gibson measured the tuff ring height from the stratigraphic base to be 92 m, with the inner base of the tuff ring ranging from 10 to 12 m a.s.l. and the width of the tuff ring ranging from 200 to 600 m.

Gibson (2011) identified four tuff ring facies linked to different stages in the evolution of the eruption.

Facies A is a poorly to well-sorted, massive to weakly bedded tuff, with lithic-rich block and bombs. This facies represents an unsteady vent-clearing stage as the first water-magma interactions took place.

Facies B is a poorly sorted and massive lapilli, with fine lapilli to blocks and bombs. This facies represents a sustained, stable stage of the eruption where fall deposits comprise a mixture of lithics and juvenile material.

Facies C is a well-sorted, cross-laminated coarse to fine ash. This facies represents a stage where water-magma interaction was very stable and has allowed layers high in juvenile material to be deposited.

Facies D is a very well-sorted, planar laminated layer with coarse to fine ash. This facies represents a mixture of pyroclastic surge and fall deposits that form distinct layering and are high in juvenile material and lithics.

The Waikato Regional Council has groundwater data for seven localities in the Kellyville Volcanic Complex. The data outlines the subsurface stratigraphy with good to questionable data quality.

2.10 Previous work: Onewhero Volcanic Complex

Kermode (1992) describes Onewhero as a "tuff ring with an outlet to the north, infilled with sediments". He notes that the tuff ring is very well preserved and that this is the largest tuff ring in the SAVF, with a diameter of 2.5 km. The Onewhero maar has been K-Ar dated to 0.88 ± 0.06 Ma from a sample of alkali basalt (Briggs et al., 1994). The tuff ring is 87 m in height from the exposed base. Inferred Quaternary uplift due to vertical movement along the Waikato Fault has increased the elevation of the Onewhero volcanic complex to 182 m.a.s.l. at its maximum.

A gravity survey was produced and examined by Hochstein and Nunns (1976). The survey focussed mainly on the uplift of the Waikato Fault in the Onewhero region but the investigation passed close to the Onewhero tuff ring.

The Onewhero maar was also covered in the Gibson (2011) thesis. Stratigraphic logs and geochemical results were again the key datasets, linking physical geology to eruption processes.

Gibson (2011) identified two tuff ring facies:

Facies A is a well-sorted, cross-bedded, alternating fine and coarse ash layer. This facies represents an alternating surge and fall dominated stage of the eruption. Coarser beds are identifiable and consist of a large percentage of juvenile material with some lithics. This was interpreted as a drier stage of the eruption.

Facies B is a poorly to very well-sorted, fine ash to block-and-bomb layer. This facies represents a fall-dominated stage of the eruption. High moisture content in the eruption plume allowed finer particles to be deposited with higher density particles.

The Waikato Regional Council has groundwater data for five locations in the Onewhero Volcanic Complex, which is a poor coverage considering the size of the crater. The data outlines the subsurface stratigraphy with good to questionable data quality.

Chapter Three: Geology of the Onewhero and Kellyville complexes

3.1 Introduction

A geophysical model relies on having an extensive knowledge of the area being investigated. An area with tightly constrained geological data creates a robust model that needs fewer assumptions to become reliable. This chapter aims to better constrain the geology of the Onewhero and Mercer regions in order to create stronger gravity and magnetic models. This will be achieved by making observations in the field as well as interpreting bore-hole data provided by the Waikato Regional Council.

3.2 Geology of the Onewhero region

3.2.1 Introduction

A phreatomagmatic eruption 0.88 ± 0.06 Ma created the Onewhero Volcanic Complex in the South Auckland Volcanic Field (Briggs et al., 1994). Rising magma intersected Miocene-aged sediments, which could have been the Carter Siltstone or the Whaingaroa Siltstone of the Te Kuiti Group, or the Waikawau Sandstone and Koheroa Siltstone of the Waitemata Group (Kear, 1961; Tripathi et al., 2014). It has been suggested that uplift in the Quaternary Period along the Waikato Fault carried the maar from the level of the present day Waikato River to an elevation of 95 – 110 m.a.s.l (Briggs et al., 1994).

The Onewhero region has been highly modified by volcanic activity and is one of the more densely clustered volcanic regions in the SAVF (Figure 3.1). The uplifted block upon which the Onewhero tuff ring sits also has a noticeable

geomorphological contrast between the eastern and western regions (Figure 3.1). The smooth texture of the eastern section is caused by an extensive coverage of basalt lava flows from effusive vents such as the Klondyke and Kauri Road cones. This contrasts sharply with the rugged peaks of uplifted basement rock in the west.

Figure 3.1: The Onewhero maar is surrounded by other SAVF effusive and explosive vents. The

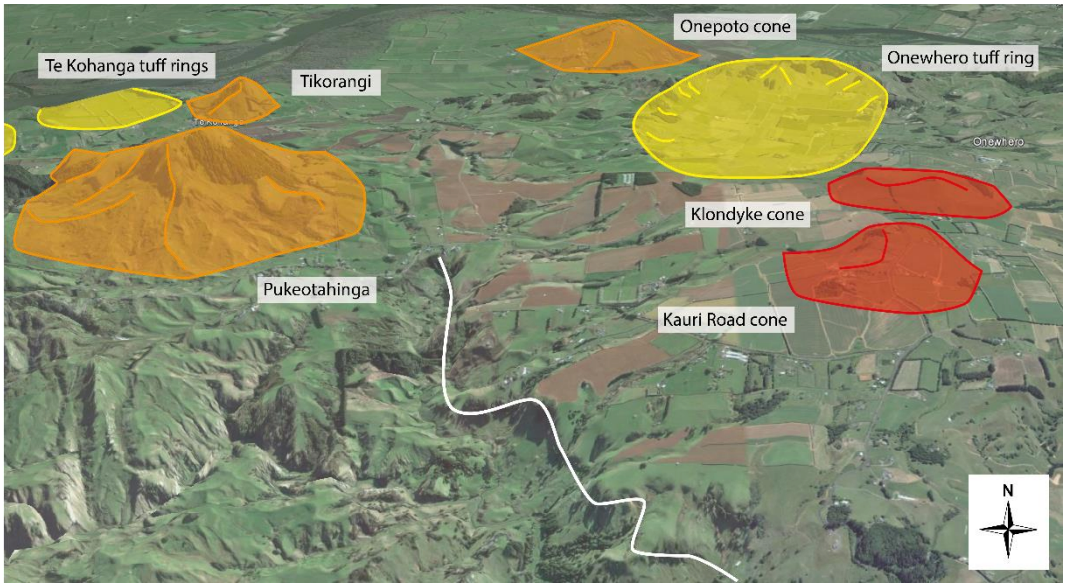

white line separates the smooth and the rugged geomorphology created by a thick surface layer of basalt in the east (base image: Google Earth).

3.2.2 Country rock geology

The Onewhero region is underlain by members of the Oligocene-Miocene aged Te Kuiti Group and the Miocene aged Waitemata Group. Both of these groups have been uplifted by the Waikato Fault and can be spatially localised; this makes the Onewhero region geologically complex. The formation underlying the Onewhero maar is inferred to be the Whaingaroa Siltstone. This unit was mapped by Waterhouse (1978) on the inside of the craters southwestern slope. Gibson (2011) suggested that the Carter Siltstone underlay the Onewhero maar due to the siltstone cropping out to the north of the crater at Maoa's Waterfall. This was confirmed as the Carter Siltstone with age dependent foraminifera being identified in the siltstone outcrop. Both the Whaingaroa and the Carter siltstones are generally massive, very calcareous, and glauconite rich in places. Due to their similar physical characteristics, depositional setting, and age, they are assumed in this study to be of

a similar density and which of the siltstones underlies the Onewhero maar is still disputable.

3.2.3 Volcanic geology

The Onewhero Volcanic Complex consists of an unusually large ejecta ring with no other obvious volcanic surface features aside from a basalt flow in the south of the crater. The tuff ring rises to 87 m from the crater floor (Gibson, 2011). Multiple outcrops of the tuff-ring deposits are easily accessed (Figure 3.2). Most of the suitable field localities outcrop in the north of the crater and occur towards the top of the ejecta deposit, therefore representing the later stages of the eruption. There are several important outcrops in the north-east of the crater where the Millers Stream has breached the crater providing a valuable cross-section of the ejecta ring in the early stages of the eruption. These outcrops were logged and documented from a physical volcanological perspective by Gibson (2011).

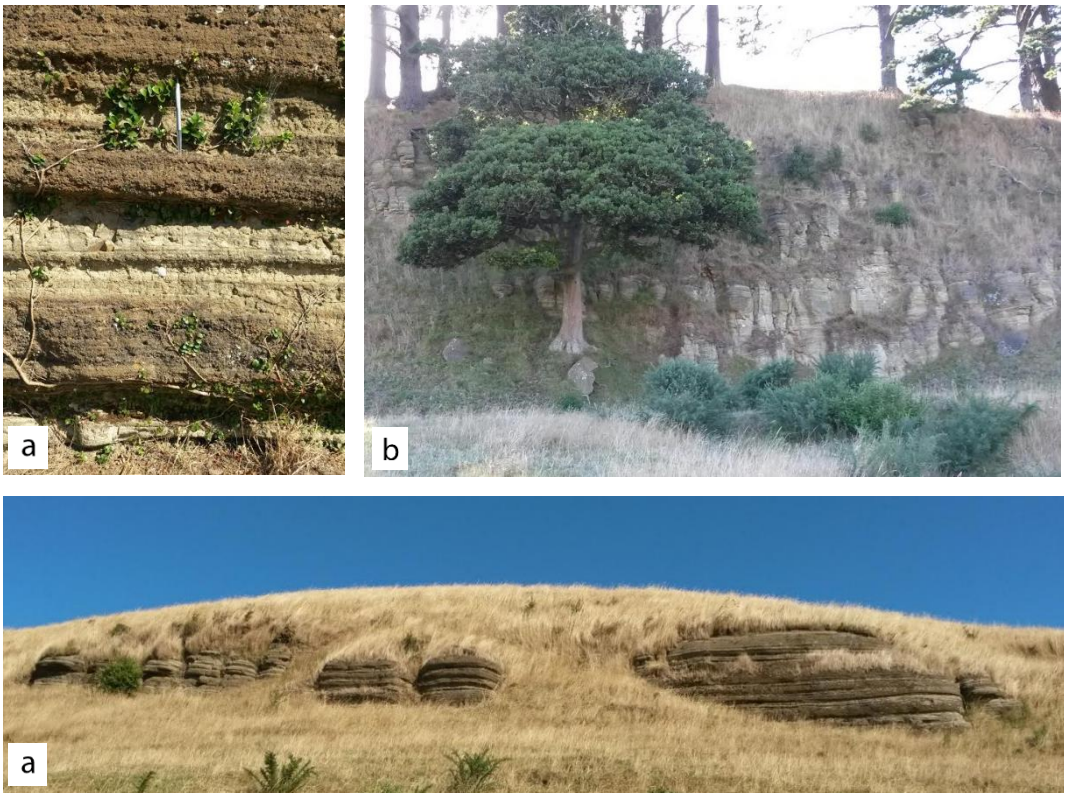

Figure 3.2: Outcrops of the ejecta ring in Onewhero are common and well preserved. The letters indicate the location of these outcrops on the updated geological map for the Onewhero maar (note the pen for scale in photo a).

3.2.4 Borehole interpretation

The borehole information was supplied by the Waikato Regional Council. It originally came in a text format but turning the text logs into a graphic representation made them more efficient to process (Figure 3.4). Having the borehole data allowed the geology of the Onewhero region to be further constrained and this was particularly useful for the two-dimensional gravity modelling.

Figure 3.3 is the legend for the borehole illustrations throughout this chapter are as follows:

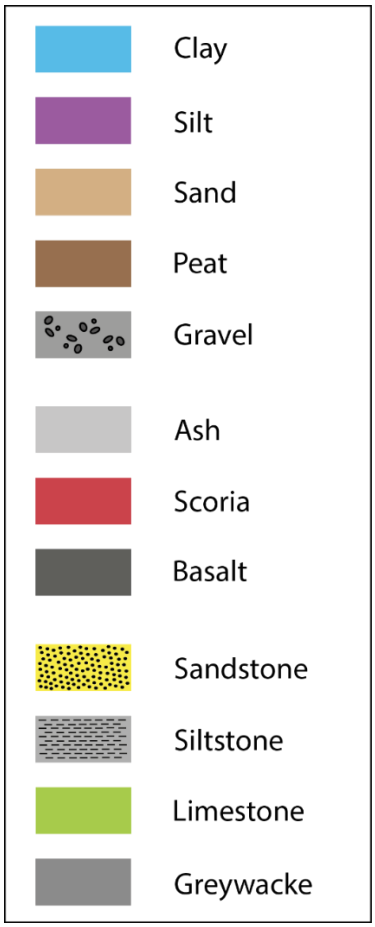

Figure 3.3: The borehole legend for Chapter 3.

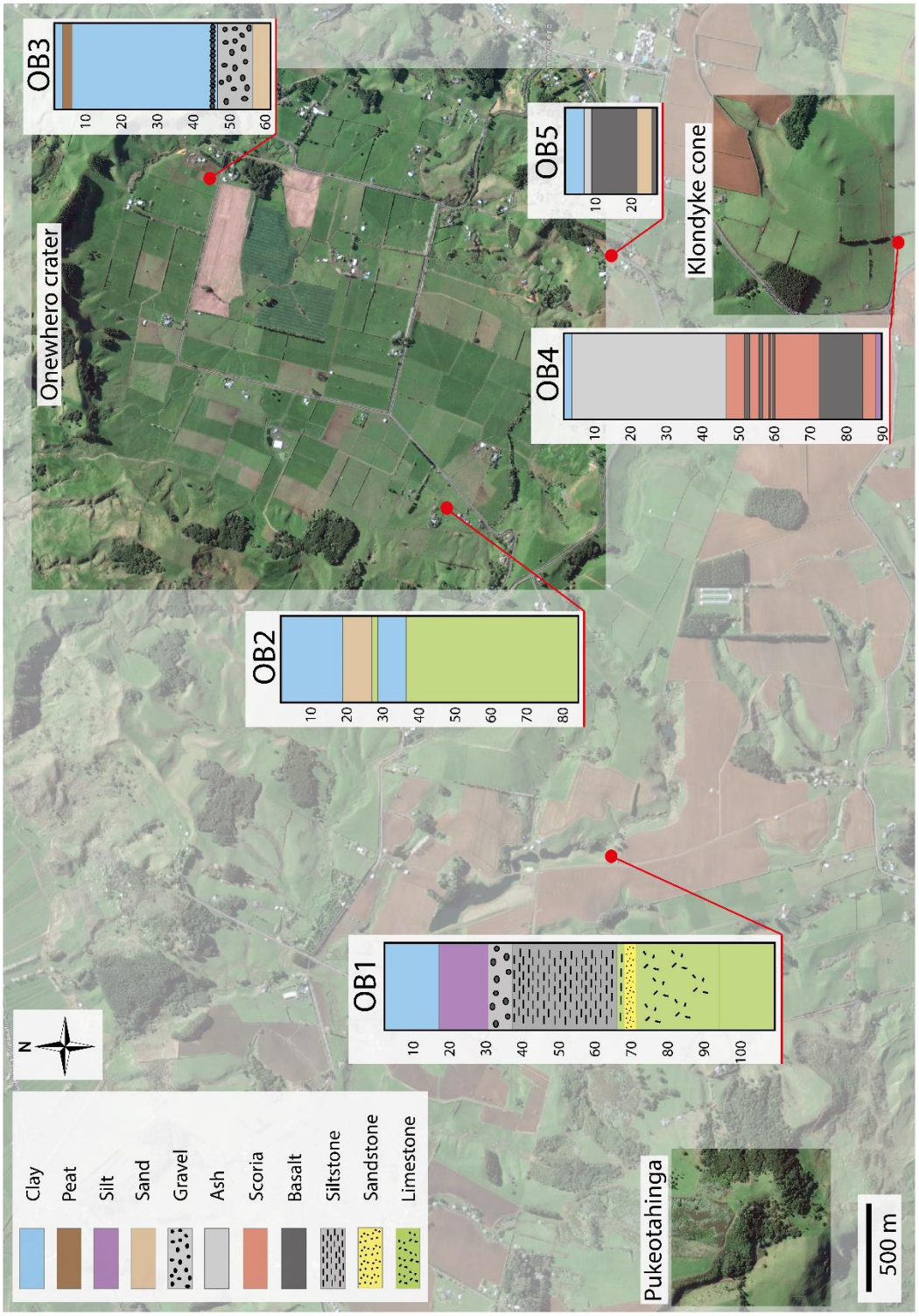

Figure 3.4: The locations of boreholes in the Onewhero region that are investigated and interpreted in this chapter.

Onewhero-bore 1 (OB1) (Table 3.1; Figure 3.5) is located to the southwest of the Onewhero crater (Figure 3.4). A fine, grading to coarse, limestone is present at the end of the bore. This unit is approximately 30 m thick and probably represents the Waimai Limestone of the Aotea Formation. This unit is known to grade from a flaggy limestone to a glauconitic grey sandstone and then to the grey siltstone of the Akatea Formation (Carter Siltstone), and this also occurs in this borehole (Edbrooke, 2001). The Carter Siltstone is inferred to have been deposited in an outer shelf environment with low sedimentation rates. This has allowed glauconite to form. This is also observed in the borehole description. Overlying the Carter Siltstone are layers of alluvial gravels and silts capped by a 15 m thick volcaniclastic clay.

Table 3.1: Waikato Regional Council, OB1.

Start depth (m)	End depth (m)	Lithology	Description
0	15	Clay	Volcanic clay
15	28	Silt	Brown-white silts
28	36	Gravels	Silty gravels
36	38.7	Silt	Blue-grey silts
38.7	76	Siltstone	Glauconitic siltstone
76	79	Sandstone	Sandstone
79	92	Limestone	Coarse limestone
92	108	Limestone	Fine limestone

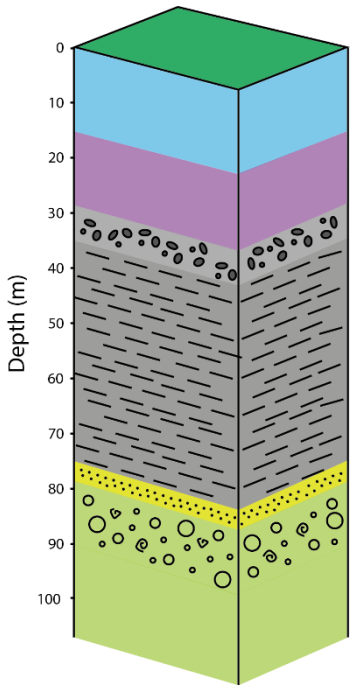

Figure 3.5: OB1 visual log.

Onewhero-bore 2 (OB2) (Table 3.2; Figure 3.6) is located in the south-west of the Onewhero crater (Figure 3.4). This bore is difficult to interpret due to a lack of detail. A >47 m layer of limestone is present starting from 35 m in depth. This unit has probably been misinterpreted as there are no known limestone units in either the Te Kuiti or Waitemata groups that reach thicknesses greater than 30 m. The Carter Siltstone of the Te Akatea Formation and the Whaingaroa Siltstone are both highly calcareous siltstone that can be observed with a sandy limestone at their base (Edbrooke, 2001). I believe the limestone actually represents one of these formations, probably the Waingaroa Siltstone as this was mapped on the inner slopes of the Onewhero maar by Waterhouse (1968). Resting on the limestone unit is an 8 m thick layer of clay that could be a weathered cap of limestone or represent the land surface before the eruption. Above this is a sandstone layer that is probably composed of reworked tuff that was eroded off the steep inner crater wall after the eruption. OB2 is capped by a 15 m layer of clay sediment that probably consists of post-eruption material and lake infill.

Table 3.2: Waikato Regional Council, OB2.

Start depth (m)	End depth (m)	Lithology	Description
0	17.37	Clay	Peaty, sandy, very soft
17.37	25.91	Sandstone	Soft to hard
25.91	35.05	Clay	-
35.05	82.3	Limestone	-

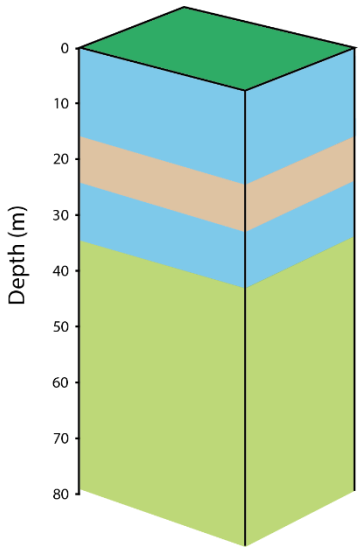

Figure 3.6: OB2 visual log.

Onewhero-bore 3 (OB3) (Table 3.3; Figure 3.7) lies in the north-east of the crater (Figure 3.4). A >3 m thick sandstone deposit lies at its base; this is likely a reworked tuff deposit. Overlying the sandstone are bands of fine gravels 3 – 4 m thick. These gravels probably represent crater-rim failure, in the form of slumps and debris flows. Pirrung et al. (2003) outlined a detailed stratigraphic description of a pre- to post-eruption maar infill. Gravel layers in the maar infill were suggested to be deposited days to decades after the eruption. The gravels were interpreted as being syn-/post-eruptive rockfalls, debris flows and slumps. Overlying the gravels are silty clay sediments that are interpreted here as post-eruption lake infill. A distinctive peat layer occurs 3 m below the surface. This would have formed during a period of anoxia in the area. The peat layer only occurs along the edge of the crater and this makes sense as vegetation would be concentrated in these areas. Swamp deposits are a common constituent of the sedimentary infill of a maar and they usually represent the end of a maar lakes life (Pirrung et al., 2003; Houben et al., 2013).

Table 3.3: Waikato Regional Council, OB3.

Start depth (m)	End depth (m)	Lithology	Description
0	3	Clay	-
3	4	Peat	-
4	44	Clay	Green-brown silts
44	56	Gravel	Fine, banded, cemented
56	59	Sandstone	-

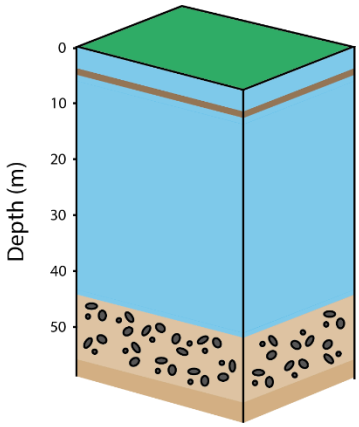

Figure 3.7: OB3 visual log.

Onewhero-bore 4 (OB4) (Table 3.4; Figure 3.8) is located on the southern slopes of the Klondyke cone (Figure 3.4) and comprises a repeating succession of interbedded scoria and basalt deposits that is approximately 40 m thick. The interbedded basalt and scoria represents a cycle of dry eruption styles from strombolian to hawaiian. Strombolian eruptions typically have higher gas contents and the resulting deposit is scoria. Hawaiian eruptions produce viscous basalt lavas with low gas contents (Mangan and Vergniolle, 2000). Overlying these deposits is a 45 m thick basaltic ash layer that is most likely associated with the Kauri Road cone that occurs nearby, to the south of the Klondyke cone.

Table 3.4: Waikato Regional Council, OB4.

Start depth (m)	End depth (m)	Lithology	Description
0	2	Clay	Basaltic
2	46	Ash	Basaltic
46	86	Basalt/scoria	Interbedded
86	88	Silt	White

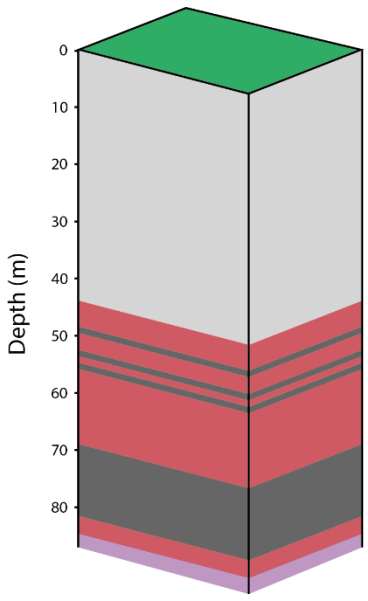

Figure 3.8: OB4 visual log.

Onewhero-bore 5 (OB5) (Table 3.5; Figure 3.9) is located on the southern outer slopes of the Onewhero maar's ejecta ring (Figure 3.4). The bore reveals a 10-12 m thick basalt lava flow that overlies basalt-rich, sandy volcaniclastic sediment. The flow lies halfway between the Klondyke cone and the basalt flow that mantles the southern inner tuff slope of the Onewhero crater. A thin layer of ash overlies the basalt flow and this is capped with a layer of weathered clay.

Table 3.5: Waikato Regional Council, OB5.

Start depth (m)	End depth (m)	Lithology	Description
0	5.8	Clay	Red brown
5.8	7.1	Ash	-
7.1	20	Basalt	Weathered
20	24	Sand	Cemented grey
24	26.6	Basalt	Hard

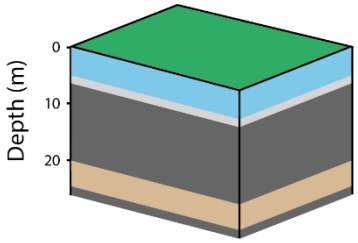

Figure 3.9: OB5 visual log.

3.2.5 Onewhero crater post-eruption fill

The eruption fill, as with most tuff-rings and maars, likely consists of a volcanic breccia above the vent that is overlain by a thin layer of fall and surge deposits. As soon as volcanic activity ceases, an influx of reworked sediment enters the crater. This is a normal erosion process and the majority of eroded material comes from the failure of the soft, unconsolidated ejecta ring. A freshly excavated drainage trench was found during the geophysical field work stage of this study. From this, a sample of clay was extracted. This was analysed using scanning electron microscopy (SEM) and was found to be full of diatoms, indicating that the late stages of crater sedimentation were influenced to some degree by a lacustrine environment (Figure 3.10) (pers. comm. B. Fox, 2015). The purity of the

diatomaceous sediment was not determined, but this find is still significant as diatomaceous earth has not been previously recorded at Onewhero. Similar clay was observed in the south of the crater near the lava flow, but this was not analysed by the SEM. The diatomaceous clay is probably widespread and may constitute a large portion of the post-eruption infill. The thick layers of fine clay in OB2 and OB3, up to 40 m in thickness, support this. Diatoms from Onewhero could also aid in approximating the age of the eruption as the original age could be in dispute. This is further discussed in section 3.2.6.

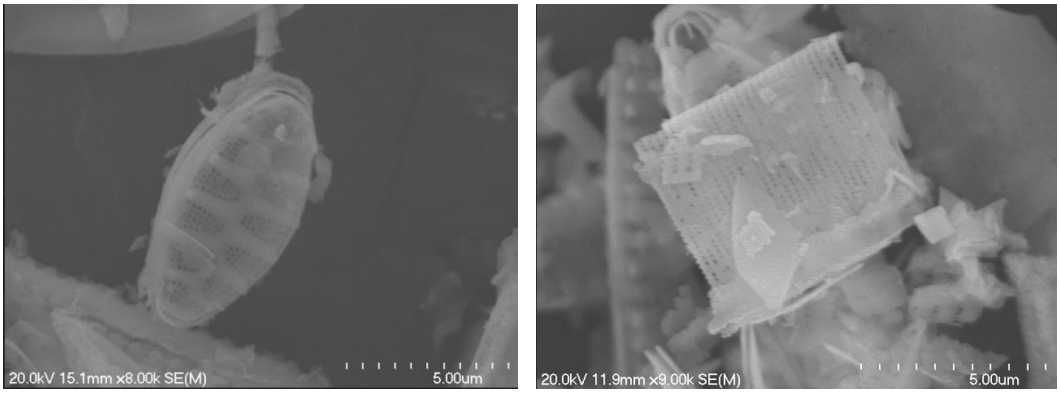

Figure 3.10: Scanning electron microscope images of assorted unidentified diatom frustules found within dry clay samples in the Onewhero crater (photos supplied by Bethany Fox).

3.2.6 Onewhero crater lava flow

The subsurface geology in the Onewhero crater is concealed from the surface by the post-eruption infill. The exception is a lava flow that outcrops in the south of the crater (Figure 3.12). The flow was mapped by GPS in the field by observing geomorphology and then comparing to the birds-eye-view geomorphology using Google Earth (Figure 3.13).

The basalt layer observed in OB5 is 13 m thick and appears, from above, to enter and flow into the crater from the south-east (Figure 3.13). Two effusive vents can be found in this direction; the nearby Klondyke cone and the Kauri Road cone. The flow itself covers at least a fifth of the inner crater slopes and floor. The basalt appears to be stratigraphically younger than the tuff deposits of the Onewhero tuff ring. In OB5, the lava flow is only overlain by a thin ash and weathered clay layer. The view from the top of the crater rim reveals that the Klondyke cone and its lava

flows have infilled any topography that would have been produced by the slopes of the outer ejecta ring deposits of the Onewhero tuff ring (Figure 3.11). The scoria and basalt deposits apparent in OB4 detail a volcanic history that was rich in magmatic products. It is my opinion that the basalt flow in the Onewhero crater originated from the Klondyke vent.

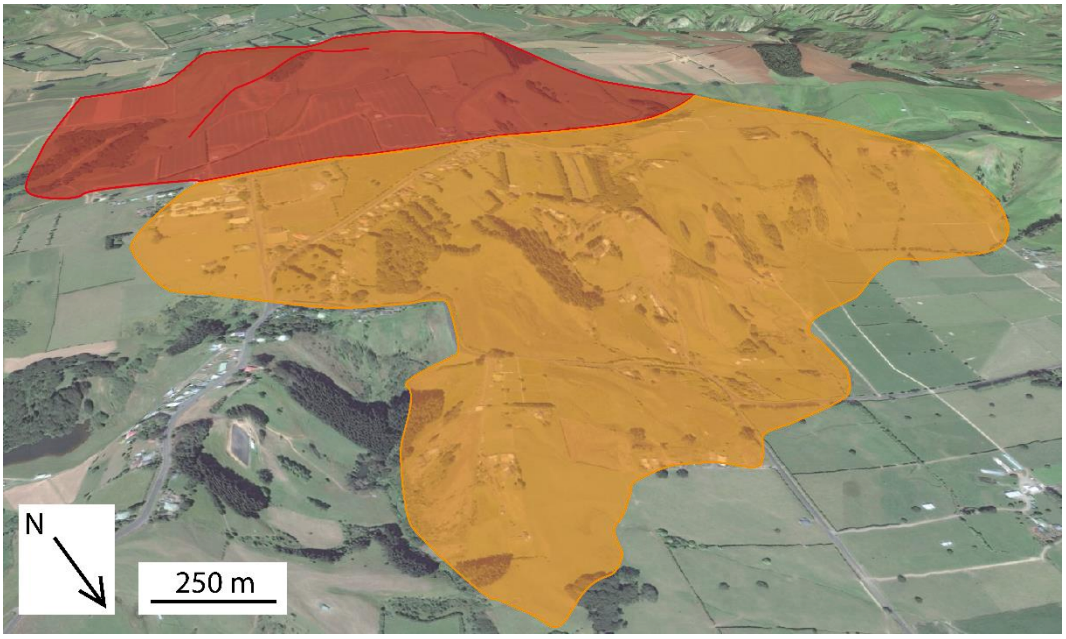

Figure 3.11: Klondyke cone (red) has erupted on the southern flanks of the Onewhero maar. Lava (orange) has filled in the existing topography and has entered and covered some of the maar's crater floor.

The basalt flow creates an interesting discrepancy in the age of the Onewhero maar. Briggs et al. (1994) dated the Onewhero crater using a sample of basalt in the southern portion of the field (pers. comm. R. Briggs, 2014) (Figure 3.11). When dating volcanic landforms it is advantageous to use basalt as a source, particularly when K-Ar dating as basalt is often the product least affected by long-term weathering (pers. comm. A. Pittari, 2015). I believe that the basalt used to K-Ar date the Onewhero maar came from the lava flow. This means the K-Ar age of 0.88 ± 0.06 Ma for the Onewhero maar could belong to the nearby Klondyke cone instead. An effusive vent has not been identified within the Onewhero crater so it is unlikely that the lava flow originated here.

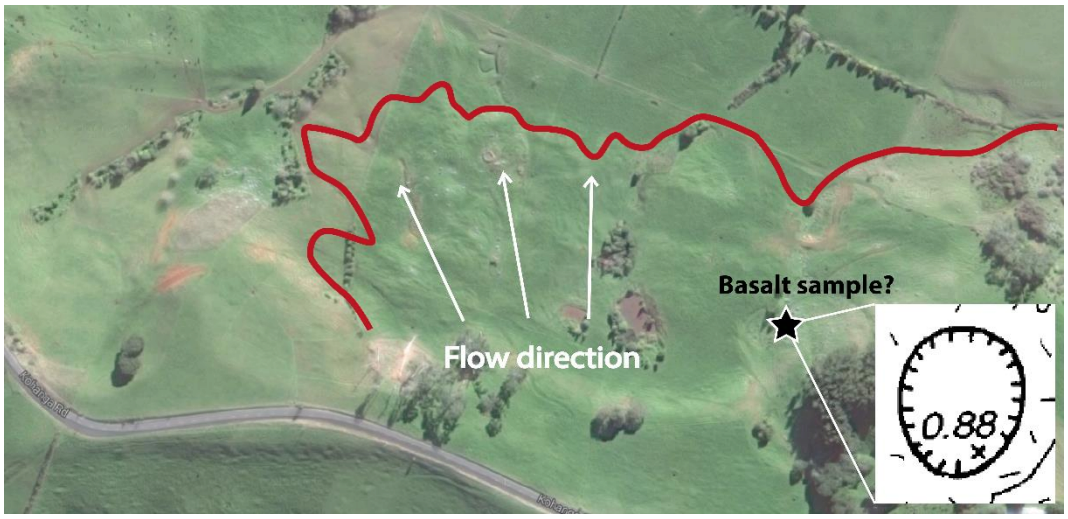

Figure 3.12: The Onewhero crater lava flow shows signs from above of a flow direction from the southeast. Inset is the location of basalt samples used to date the Onewhero tuff ring (Briggs et al, 1994).

3.2.7 Updated geological map

Figure 3.13 is an updated geologic map for the Onewhero region. It expands on a map previously illustrated by Gibson, (2011). The updated map incorporates the basalt flow in the south of the crater and draws attention to the lacustrine influence of the crater infill. The presence of diatoms in the upper layers of crater infill indicates that at least the latter stages of sediment deposition were in a lacustrine environment. The flat topography of the crater floor suggests that the lacustrine deposits are widespread. Previously, it was suggested that the sediment infill was deposited in an alluvial terrestrial environment (Gibson, 2011).

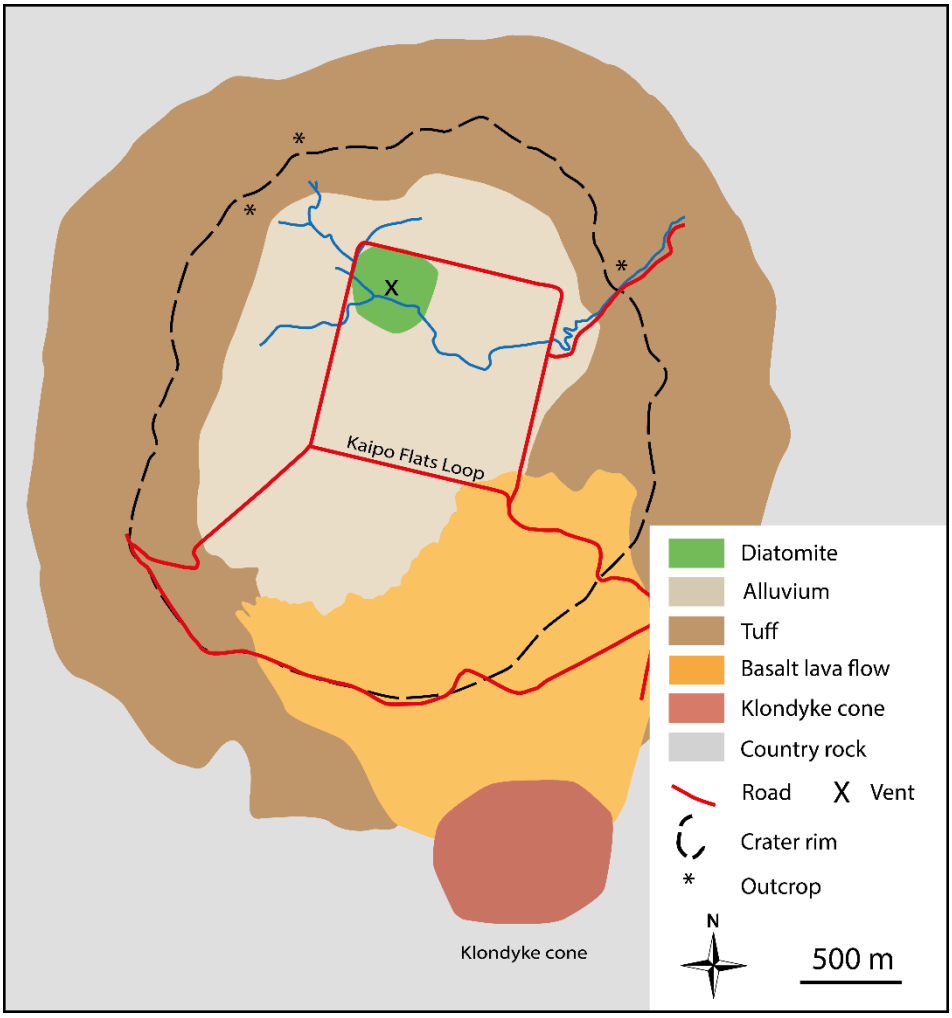

Figure 3.13: A geological map for the Onewhero tuff ring incorporating the lava flow and possible extent of post-eruption lake infill (adapted from Gibson, 2011, and using field observations and data from Google Earth).

3.3 Geology of the Mercer region

3.3.1 Introduction

An eruption at 1.48 ± 0.10 Ma produced the Kellyville Volcanic Complex (Briggs et al., 1994). The complex includes a highly eroded ejecta ring with two nested scoria cones in the middle of the crater. Rising magma intruded into the Koheroa Siltstone and the Mercer Sandstone, the main country rock formations. The post-eruption infill comprises diatomite and the sandy-pumiceous sediments of the Karapiro Formation. A conspicuous outcrop of diatomite on Koheroa Road confirms the presence of a Quaternary lake environment at some point after the

formation of the main ejecta ring (Waterhouse, 1980). The crater is breached and is exposed to the floodwaters of the nearby river system. When, or what caused the breach is unknown. Gibson (2011) suggests the Waikato River breached the rim. The Oruanui eruption 27 ka in the Taupo Volcanic Zone triggered the Waikato River to alter its course after volcanic debris blocked the river's previous path through the Hinuera Gap (McCraw, 2011). The breach in the ejecta ring could have been caused by catastrophic breakout floods after the Oruanui eruption. Alternatively Colchester (1968) suggests that the western section of the ejecta ring was continually washed away as it was deposited. A sandbar then developed, blocking the river system from entering the crater. This allowed a shallow lake to form in the topographic depression above the main eruption vent.

3.3.2 Country rock geology

The Mercer Sandstone is the youngest stratigraphic unit in the vicinity of the Kellyville Volcanic Complex. It crops out to the north of the crater and is generally massive, weakly indurated and poorly sorted (Kear and Schofield, 1978; Edbrooke, 2001). At a glance, the Mercer Sandstone has the physical characteristics of a high quality aquiferous rock. Poor sorting, weak induration and massive layering promote the movement and storage of groundwater. Therefore it is likely that rising magma interacted with groundwater in the Mercer Sandstone, initiating the first stage of the Kellyville eruption before moving into deeper strata. This was supported by Gibson's (2011) findings. The Mercer Sandstone made up a high proportion of the lithic content of the Kellyville tuff, upwards of 80% at most horizons.

Lying conformably below the Mercer Sandstone is the Koheroa Siltstone. Both of these units belong to the Waitemata Group, with the Koheroa Siltstone probably representing a continental shelf to slope deposit and the Mercer Sandstone probably representing a shelf to near-shore deposit. The Koheroa Siltstone makes up a small proportion of the xenoliths found in the Kellyville tuff facies, around 10 – 20% during most stages of the eruption (Gibson, 2011).

3.3.3 Volcanic geology

The Kellyville Volcanic Complex consists of a highly eroded ejecta ring and a nested basalt cone on the crater floor. Glass Hill is a medium sized basalt cone, reaching ~50 m in height it is the most recognisable crater feature. The tuff ring rises to 100 m above the crater floor in places and at first glance does not resemble a volcanic landform as the Onewhero tuff ring so obviously does. Multiple outcrops are available that display the middle and late stages of the eruption, the main being a road cutting outcrop in the east of the ejecta ring on Koheroa Road. Gibson (2011) made most of her interpretations based on this outcrop.

The eruption infill slightly differs to that of the Onewhero crater, with high quality diatomite being the most notable unit. However the breach of the ejecta ring in the west and the consequent drainage of the crater has allowed much of the infill to be washed away. What remains is likely to be a mixture of sediment from the well eroded tuff ring, lake fill, and deposits from the Taupo Volcanic Zone eruptions.

3.3.4 Borehole interpretation

Borehole data for the Mercer region is sporadic. However several drill profiles were provided by the Waikato Regional Council. The bore data was plotted from text file to a stratigraphic visualisation. The locations for the borehole data can be observed in Figure 3.14. This was useful for the later gravity and magnetic modelling.

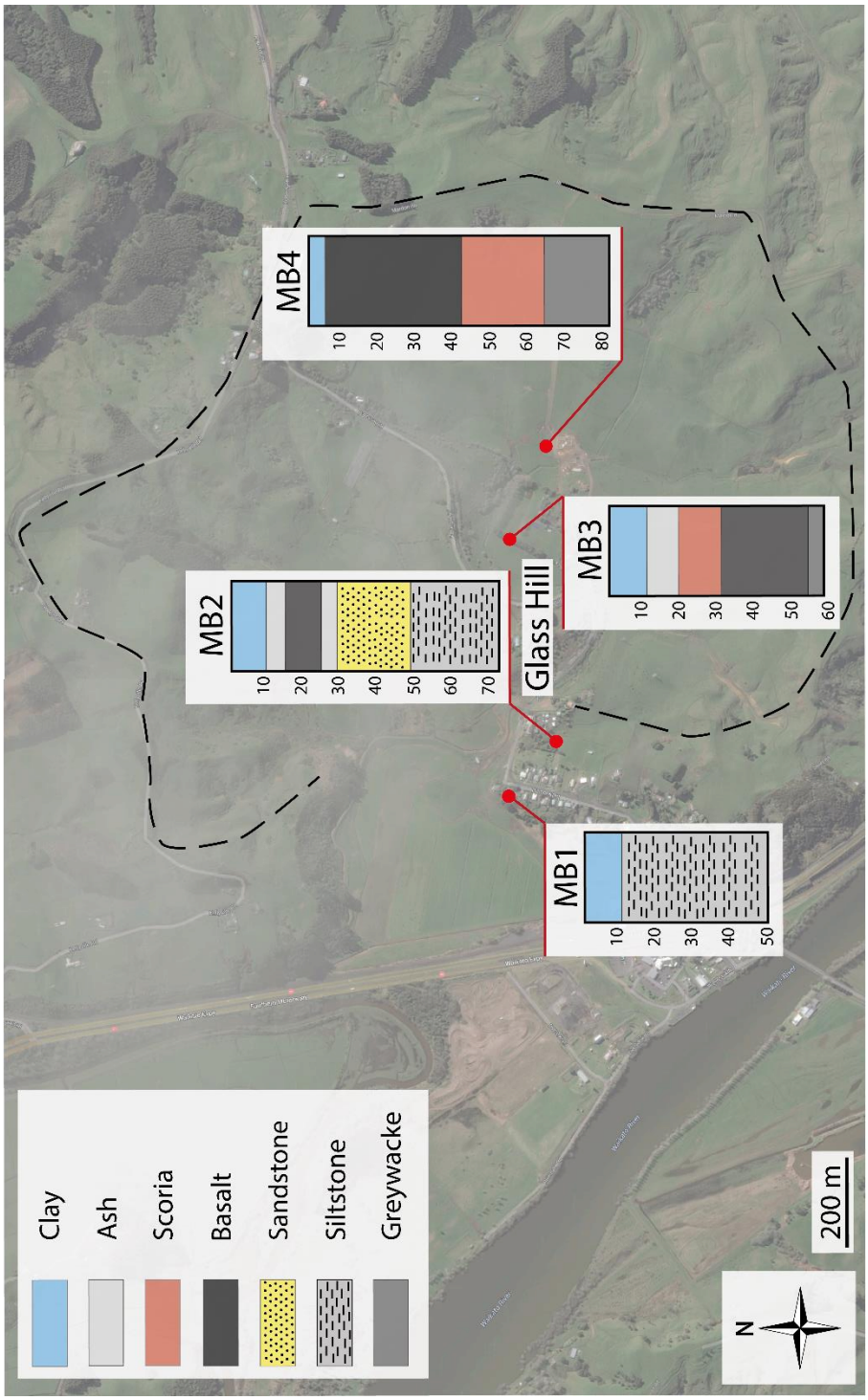

Figure 3.14: The locations of boreholes in the Mercer region that are investigated and interpreted in this chapter. The black dashed line is the present day ejecta ring rim.

Mercer-bore 1 (MB1) (Table 3.6; Figure 3.15) is located in the west of the Kellyville crater and reveals the erosion of the tuff ring by the Waikato River (Figure 3.14). In this position, a succession of tephra deposits should be visible, however clay directly overlies the main country rock in the area (Koheroa Siltstone).

Table 3.6: Waikato Regional Council, MB1.

Start depth (m)	End depth (m)	Lithology	Description
0	12	Clay	-
12	48	Siltstone	Grey, fractured

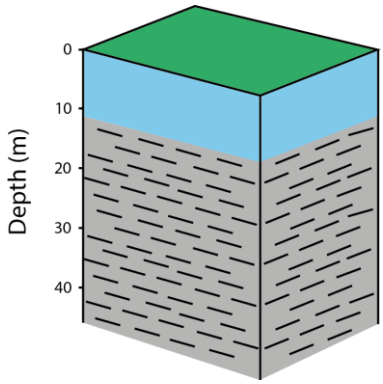

Figure 3.15: MB1 visual log.

Mercer-bore 2 (MB2) (Table 3.7; Figure 3.16) lies on the original boundary of the historic tuff ring (Figure 3.14). The log consists of weathered silty clay to 11 m underlain by a layer of ash. This ash probably originated from the main, central vent as that eruption succeeded the Glass Hill eruption. Underlying the ash is a 10 m thick basalt lava flow, also likely sourced from Glass Hill cone. This is underlain by another ash layer that was probably deposited during the initial stages of the Glass Hill cone eruption. Underlying the volcanic deposits is a 20 m thick sand layer. This deposit is firm and hard and probably represents the Mercer Sandstone of the Waitemata Group which is inferred to conformably overlie the Koheroa Siltstone (Edbrooke, 2001). The oldest unit in this log is the Koheroa Siltstone of the Waitemata Group, which is at least 23 m thick in the borehole data (Colchester, 1968; Kear and Schofield, 1978; Edbrooke, 2001).

Table 3.7: Waikato Regional Council, MB2.

Start depth (m)	End depth (m)	Lithology	Description
0	9	Clay	Brown-white
9	14	Ash	-
14	24	Basalt	Interbedded ash
24	27	Ash	-
27	48	Sandstone	Firm to hard
48	71	Siltstone	-

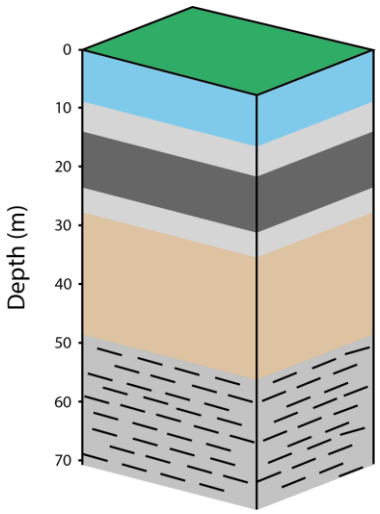

Figure 3.16: MB2 visual log.

Mercer-bore 3 (MB3) (Table 3.8; Figure 3.17) is located between the two scoria cones, and the stratigraphy reflects this (Figure 3.14). Lake infill/alluvium occupies the first 10 m of depth. The clay is volcaniclastic and probably consists of reworked tephra. The clay is underlain by an 8 m thick layer of ash, which is probably derived from central vent explosions. Underlying the ash is a thick scoria deposit with an interbedded, thin 2 m thick basalt flow. The complete thickness of the basalt/scoria deposit is 35 m. This bore could be intersecting deposits from Glass Hill cone or the main central vent, or the deposits could be a mixture of both of them. Towards the base of the bore the scoria overlies hard, fractured, greywacke basement.

Table 3.8: Waikato Regional Council, MB3.

Start depth (m)	End depth (m)	Lithology	Description
0	10	Clay	Volcanic clay and ash
10	18	Ash	Volcanic tuff and ash
18	31	Scoria	Scoriaceous basalt
31	53	Basalt	Interbedded hard and vesicular basalt
53	58	Greywacke	Hard, fractured, broken

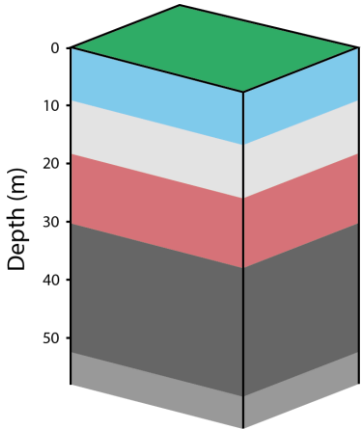

Figure 3.17: MB3 visual log.

Mercer-bore 4 (MB4) (Table 3.9; Figure 3.18) is located at the present day foot of Glass Hill cone (Figure 3.14). This bore is similar to MB3, with a thin layer of

reworked volcanic material and alluvium that is 5.5 m thick. This is underlain by thick alternating scoria and scoriaceous basalt layers. The interbedded basalt and scoria deposits equate to over 60 m. The base of the borehole again reveals greywacke basement.

Table 3.9: Waikato Regional Council, MB4.

Start depth (m)	End depth (m)	Lithology	Description
0	2.5	Clay	-
2.5	4.1	Silt	Pink and orange silts
4.1	5.5	Tuff	-
5.5	42	Basalt	Interbedded hard and vesicular basalt
42	66	Scoria	-
66	80	Greywacke	Hard, fractured

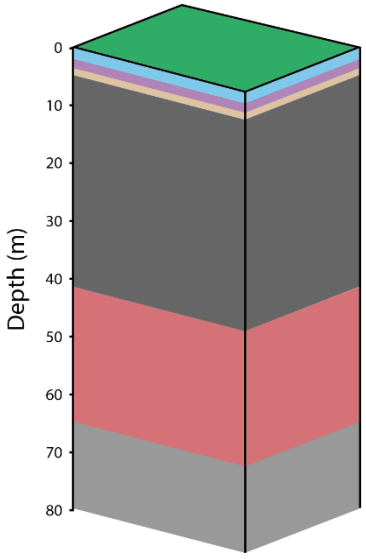

Figure 3.18: MB4 visual log.

3.3.5 Geological interpretations

The bore-hole information for the Kellyville Complex suggests that a large area of the crater floor is underlain by deposits of basalt and scoria of varying thickness. Lava lakes are not common features in maars and tuff rings, but they do occur and are well documented (Lorenz, 1986; Cassidy et al., 2007). The Kellyville crater appears to be underlain by lava lake deposits 300 – 500 m in diameter. The thickest accumulation of basalt and scoria lies in MB4, where 20 m of scoria and almost 40 m of basalt has been deposited by a feeder vent. This region was probably one of the topographic lows in the crater when the lava was being deposited. This region could also be close to the position of a vent, as the phreatomagmatic eruption that formed the tuff ring would have excavated a sizable crater. The gravity and/or magnetic survey should acknowledge the extent of subsurface lava lake deposits if they are present.

An interesting observation occurs in MB2. Basalt lies on a thin bed of ash. The ash is underlain by the Mercer Sandstone. The thin ash deposit probably originates from an early eruption-stage of the nearby Glass Hill and the overlying basalt, a late-stage eruption deposit from the same vent. This means Glass Hill most likely formed before the initiation of the main central vent of the Kellyville maar, contrary to previous suggestions (Gibson, 2011). This is further reinforced in the field. Deposits of generally massive, ungraded tuff with high lithic quantities, occur on the western flanks of Glass Hill (Figure 3.19). This tephra deposit is very similar to the tuff that comprises the surrounding ejecta ring. I suggest that Glass Hill formed before the initiation of the main vent and that the basalt cone blocked or diverted the tephra laden base surges that originated 200 m – 500 m to the east of the cone (Figure 3.20). This weakened the main tuff ring in the west of the Kellyville crater and hindered its development. This could be the cause for the breach in the ejecta ring.

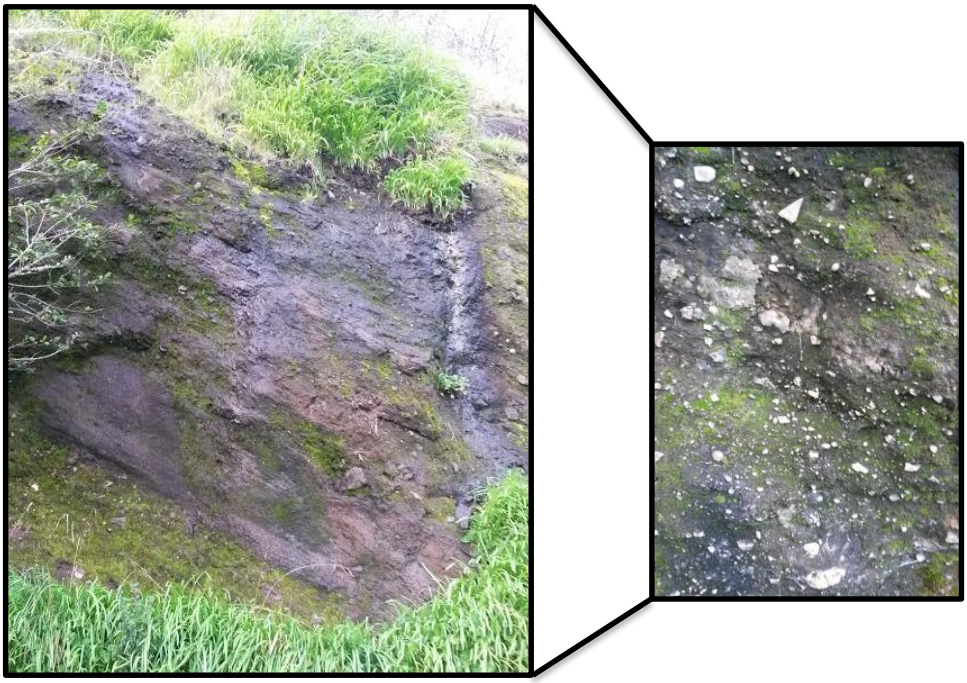

Figure 3.19: A massive, lithic-rich tuff deposit mantles the western slopes of Glass Hill basalt cone. This could be evidence for a revised sequence of events in the eruption history of the Kellyville maar.

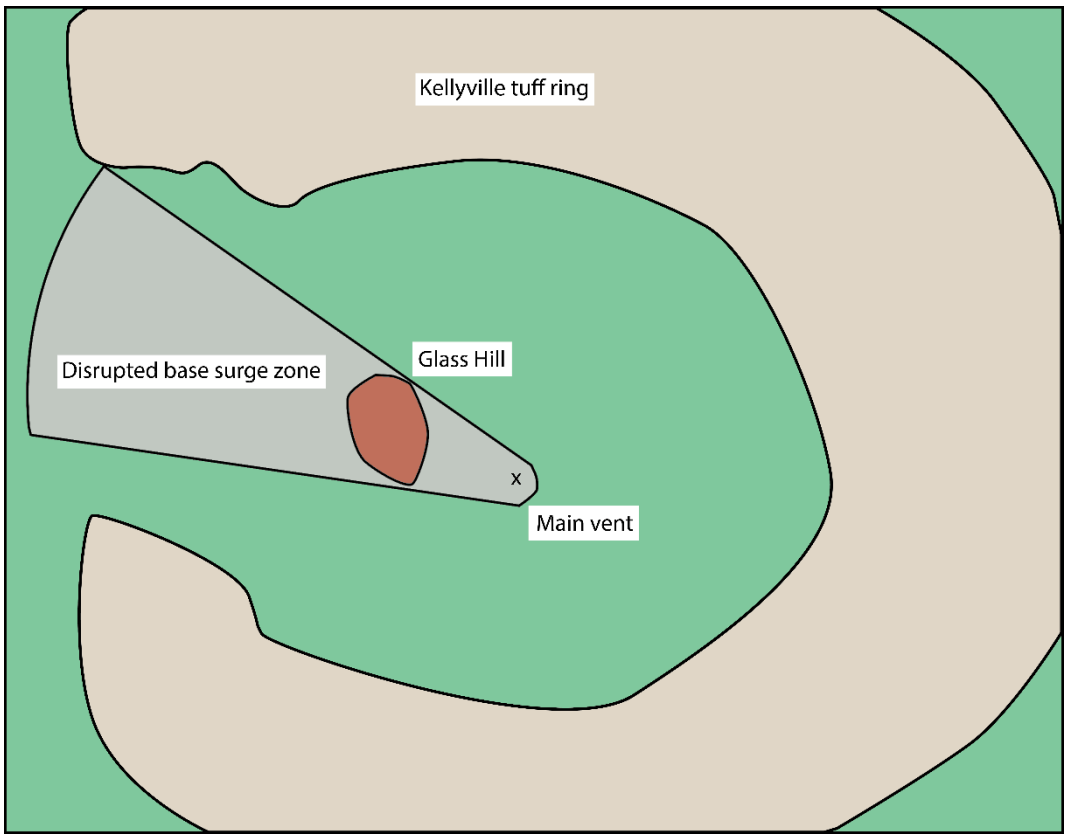

Figure 3.20: Glass Hill basalt cone could have disrupted the ability of base surges to efficiently carry and deposit tephra. This would result in a weakened section of the tuff ring.

3.3.6 Updated geological map

An updated geological map for the Kellyville maar is presented in Figure 3.19. This map combines observations from the borehole stratigraphy and includes regions with a low negative magnetic anomaly, which are interpreted in Chapter 5 as being deposits of diatomite. The map was adapted from Gibson (2011) and used Google Earth to provide spatial constraints.

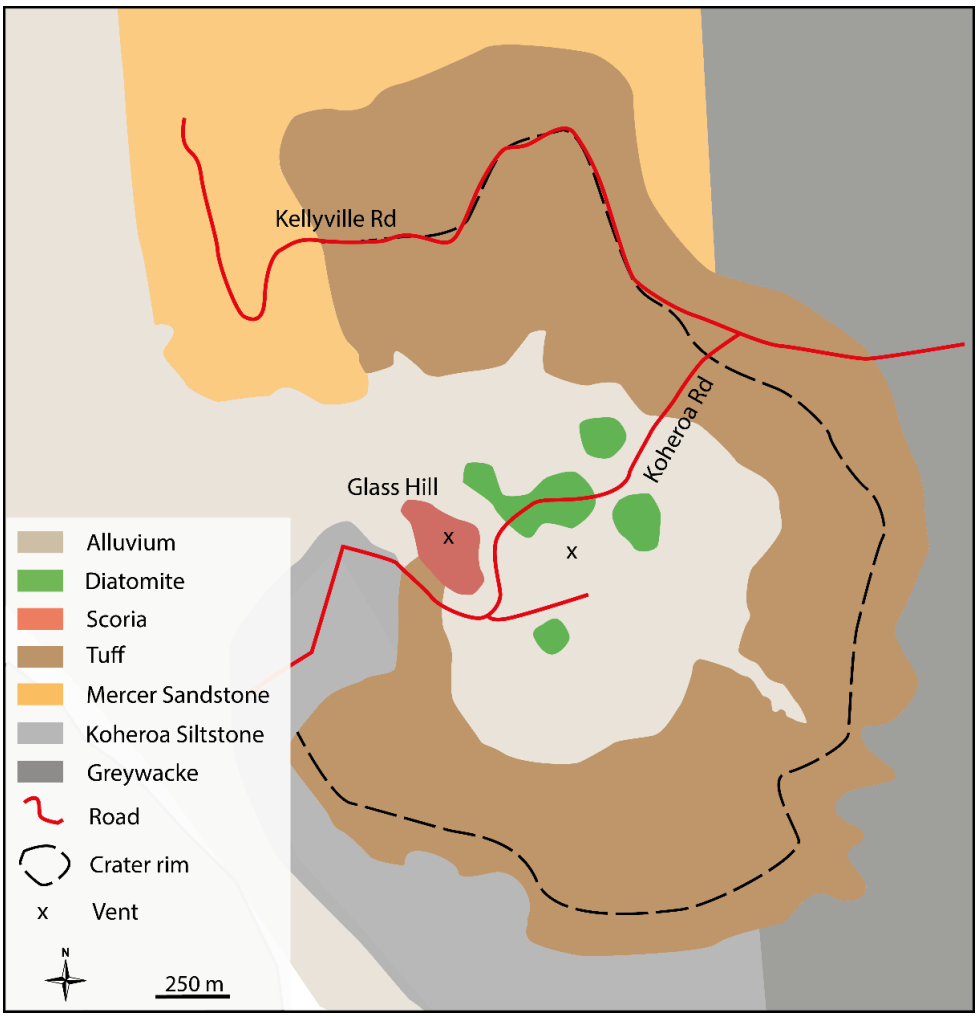

Figure 3.21: A geological map for the Kellyville maar (adapted from Colchester, 1968; Gibson, 2011, and using information from Google Earth).

Chapter Four: Gravity investigation of the Onewhero and Kellyville volcanic complexes

4.1 Introduction

Gravity surveys are well suited to the investigation of 'dry' phreatomagmatic volcanic landforms (Cassidy et al., 2007). The contrast in density between volcaniclastic products, post-eruption infill, and the surrounding country rock usually creates a characteristic negative concave profile. The flat crater floor also allows easy access to the areas required for data collection.

The gravity geophysical technique allows the user to make inferences about the subsurface geology of an area by modelling actual observations against calculated trends. To increase the accuracy and precision of gravity modelling the user can incorporate other physical or geophysical techniques. The most common techniques used to better constrain the geology are magnetic surveys, bore-hole drilling and seismic reflection profiling (Blaikie et al., 2014).

Gravity surveys have been carried out in many studies of volcanic edifaces, particularly of maar volcanoes (Cassidy et al., 2007; Mrlina et al., 2007; Blaikie et al., 2012; Blaikie et al., 2014).

This chapter begins with a brief outline of the basic theory behind Earth's gravitational field and how this allows gravity surveys to be particularly powerful modelling tools for subsurface interpretation. Secondly, an account of how the data was collected in the field at the Onewhero and Kellyville volcanic complexes and how the data was processed. This will be followed by the results of the gravity survey and some preliminary interpretations and implications for the subsurface geology based on the two-dimensional modelling. To conclude the chapter the results of the gravity data obtained at Onewhero and Kellyville will be discussed and summarised.

4.2 Gravity theory

Anything in the universe with mass has an attractive force called gravity. This force has an infinite range, but the attraction dwindles with increasing distance between two objects. Sir Isaac Newton famously noticed this force when he saw an apple fall out of a tree.

Newton's Law of Gravitation states that:

"the force of attraction F between two masses m_1 and m_2, whose dimensions are small with respect to the distance r between them, is given by

$$F = \frac{Gm_1m_2}{r^2}$$

where G is the gravitational constant (6.67×10^{-11} m^3 kg^{-1} s^{-2})" (Kearey et al., 2002).

The gravitational attraction of a mass is heavily influenced by the density of the mass. Density is mass per volume. So of two objects with identical radii, the object with the greater density will have an overpowering gravitational force.

Extremely sensitive instruments can detect the small variations in gravitational acceleration caused by the gravitational force of subsurface strata with contrasting densities. The science behind gravimeters revolves around the notion of a "causative body", where a rock unit with a density that is inconsistent with its surroundings causes a local warp in the gravity field, creating an anomaly.

The average value of gravitational acceleration at the surface of the earth is about 9.8 m s^{-2}. Other ways of expressing gravity data will be used in this study and it is important to know how to convert these to like units. The most common unit used in conjunction with most gravimeters is the gal (short for galileo):

$$1 \text{ mgal} = 10^{-3} \text{ gal} = 10^{-3} \text{ cm } s^{-2} = 10 \text{ gravity unit}$$

Gravimeters work by suspending a known constant mass on a spring balance (Figure 4.1). Variations in the gravitational acceleration exerted by subsurface strata cause the spring to extend or contract a small distance proportional to the gravitational attraction of the underlying mass. Gravimeters often measure the

relative gravity, so they are measuring the difference in gravity between local geological phenomena rather than the absolute value of gravity.

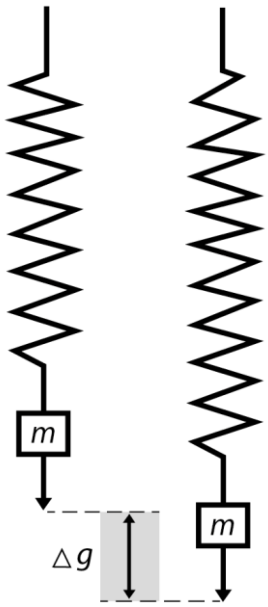

Figure 4.1: The theory behind a spring-based gravimeter. The instrument relies on variations in gravitational acceleration to extend or contract a precisely calibrated spring to make measurements (adapted from Keary et al., 2002).

4.3 Data collection

Gravity data collection commenced in October – November 2015 with the creation of a field base station at Onewhero and Mercer that was linked to the LINZ station in Mercer Township. This involved travelling between the field base station and the LINZ station as many times as possible over an 8 hour period to clarify and eliminate tidal effects. Linking the LINZ station to the Kellyville and Onewhero field base stations allows the gravity results to be linked and compared with the national grid.

69 gravity observations were then made along two profiles at Onewhero and 44 gravity observations were made along two profiles at Kellyville. The measurements were made with a Worden gravimeter (model 115) borrowed from the Department of Geology at the University of Otago. The gravity stations were spaced at 100 m

intervals along the ejecta ring and decreased to 50 m intervals when along the topographic surface of the crater basin. Four readings were taken at each gravity station to give a more accurate average reading for future processing. All stations had their locations saved on a hand-held Garmin GPS unit.

4.4 Base stations

The first stage of a gravity survey is to set up a field base station. This allows instrument drift and land tide disruptions to be corrected. Field base stations were set up at each of the field localities. The Onewhero field base station was located at the intersection of Kaipo Flats Road and Miller Road (S -37.317780, E 174.909566). The Mercer field base station was located at the end of Glass Road (S -37.276461, E 175.058804). The positions of both of the field base stations were chosen for their accessibility as they had to be revisited regularly throughout the gravity surveys. Field base stations were revisited every 1 – 2 hours; this allowed tide- and drift-based variations to be accurately accounted for and they could be easily removed during the data processing stage.

4.5 Processing

All data processing was completed in Microsoft Excel on spreadsheets. The raw gravimeter values must be transformed into a Bouguer anomaly and this occurs through a series of corrections. Raw and processed gravity data can be viewed in Appendix A.

4.5.1 Tide and machine drift

The first data correction is the removal of machine drift and land tide effects on the observed gravity. This was accomplished using a standard spreadsheet supplied by Andrew Gorman from the University of Otago. Instrument drift occurs when the spring holding the constant mass in the gravimeter undergoes creep. Creep is the permanent deformation of a solid material and is a slow process that is usually invisible. Instrument drift therefore usually has a linear value when plotted against time (Figure 4.2). Land tides are similar in theory to ocean tides but have much

smaller variations due to the solid nature of the underlying strata. These tides are unpredictable and are not linear due to local changes in geology, just as no two oceanic tides are ever the same.

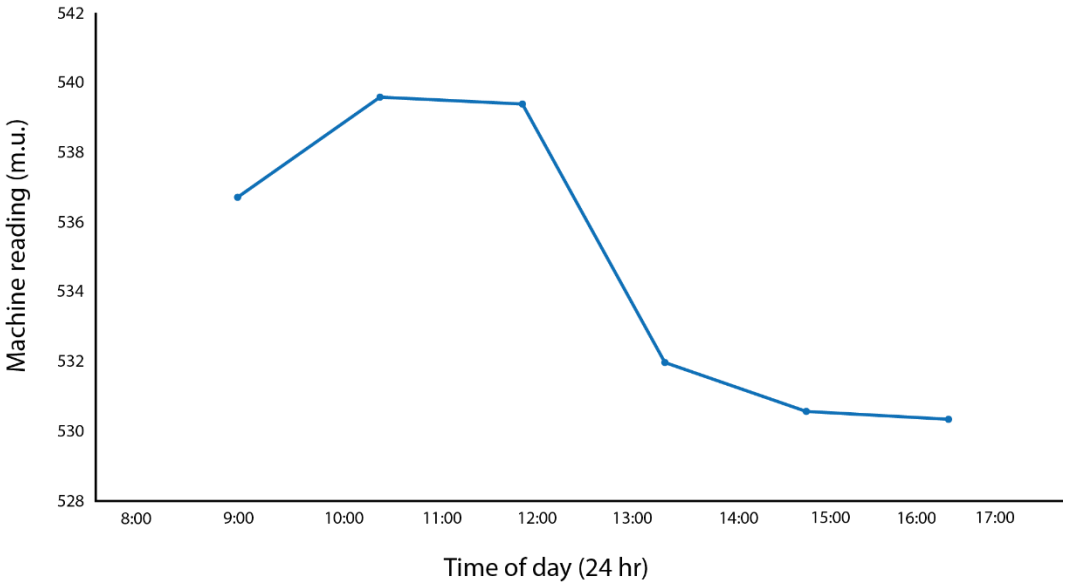

Figure 4.2: The fluctuation of land tides and machine drift through a day at Onewhero.

4.5.2 Latitude correction

Rotational momentum causes the earth's shape to flatten slightly at the poles, pulling the Earth into an oblate spheroid shape. Most of the earth's 'pulling' power comes from its very dense inner core; therefore gravity is stronger at the poles where the distance to earth's core is shorter. This deduction is called the latitude correction (Keary et al., 2002).

4.5.3 Free-air correction

The free-air correction works on similar principles to the latitude correction. As your elevation increases, so too does your distance from the centre of the earth. The free-air correction is added to the Bouguer anomaly if the survey was undertaken above sea-level and is subtracted if the survey was undertaken below sea-level.

4.5.4 Bouguer correction

The Bouguer correction corrects for the missing rock between the free-air elevation and sea level. The Bouguer correction assumes that the elevation difference is filled with an infinite slab with a density of 2.67 g/cm³.

With all these corrections we can reduce the data to a Bouguer anomaly. The equations used to reduce the gravity data in this study came from a geophysical exploration text book composed by Kearey et al., (2002):

$$BA = G_{obs} - LC + FAC - BC;$$

where *BA* is the Bouguer anomaly (mGal); and

G_{obs} is the observed gravity (machine units); and,

LC is the latitude correction (unitless); and,

FAC is the free-air correction (unitless); and,

and *BC* is the Bouguer correction (unitless).

A normal Bouguer anomaly generally incorporates a terrain correction which accounts for the gravitational pull of surrounding objects outside of the field area (Keary et al., 2002). This study uses a simple Bouguer anomaly which does not consider terrain correction in the calculations due to the complex country rock geology of the Onewhero region and the flat topography surrounding the Kellyville Volcanic Complex.

The spreadsheets with the raw and processed gravity data from Onewhero and Kellyville are located in Appendix A.

4.6 Potential sources of error in the raw data

Errors in the raw data could have arisen for the following reasons.

- Using the gravimeter in windy conditions can send small vibrations through the gravimeter causing small fluctuations in the spring reading [1].
- The instrumental error of the Garmin GPS had an average elevation error of up to 4 m, although with full satellite coverage it was much more accurate than this figure [2].

[1] If making a reading was affected by the wind I would stop and shelter the gravimeter so that the spring stopped moving enough to make a reading.

[2] Elevation measurements in a high-resolution survey are expected to have an error less than 10 cm.

4.7 Regional correction

The last correction to be applied to a gravity anomaly is the regional correction. Gravity surveys that need to cover large areas at a reasonable cost are often accomplished from a high elevation above the earth's surface using a gravimeter mounted to a plane. From this height, any local anomalies are masked by the overall regional gravity field. The regional field is influenced by larger scale geological occurrences such as the composition or thickness of basement rock, sedimentary basins, or plutonic intrusions (Keary et al., 2002). The regional gravity field for Onewhero increases gradually from about 38 mGal to 41 mGal in an east to west direction (Figure 4.3.a.). Ground-based gravity surveys measure localised gravity anomalies. Therefore the regional gravity is subtracted from the simple Bouguer anomaly to negate the effect of deeper geological structures. Subtracting the regional anomaly results in a Bouguer anomaly which can then be used for two-dimensional modelling. The regional gravity field for Mercer is negligible as the Kellyville Volcanic Complex occupies an area with a constant regional field so a correction did not need to be applied to the gravity values at Mercer (Figure 4.3.b.).

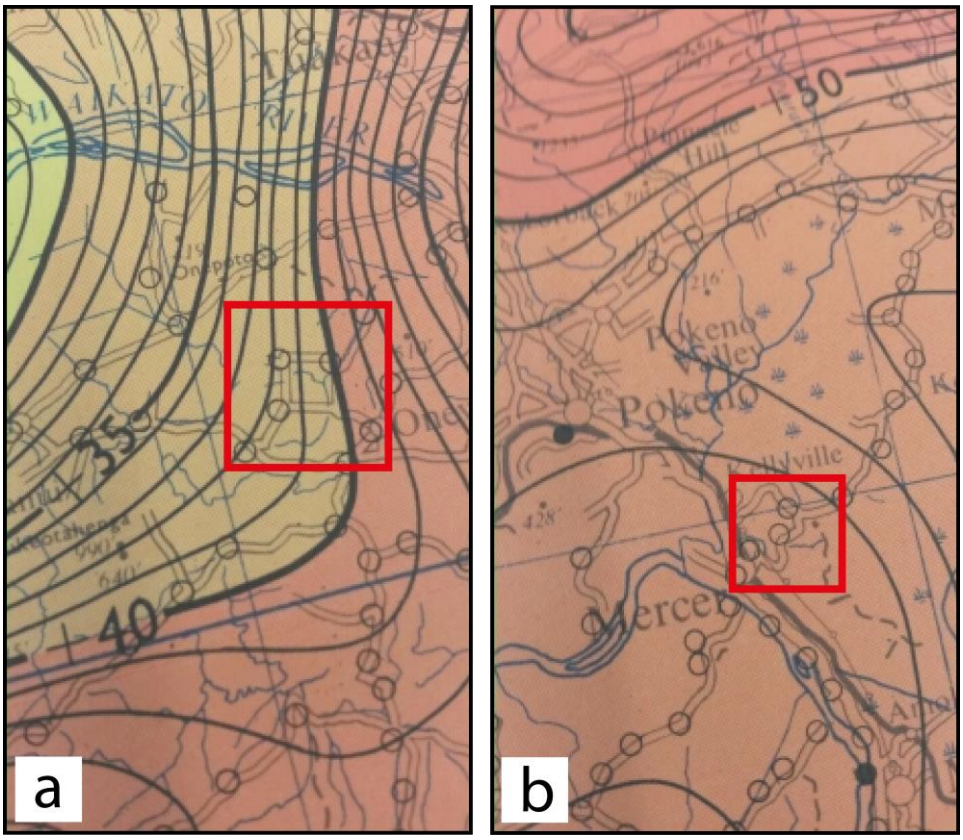

Figure 4.3: The regional gravity field for the Onewhero (a) and Mercer (b) regions (Woodward, 1971). The red box encapsulates the ejecta rings.

4.8 Two-dimensional gravity modelling

A free two-dimensional gravity modelling program called GravCadW was used to interpret the possible subsurface structure of the Onewhero and Kellyville craters (Sheriff, 1977). The program calculates the gravitational pull of modelled subsurface anomalies and matches these to the actual observed values. The program allows geological deposits to be manipulated into different shapes until the observed values closely match the calculated values.

Three geological bodies were modelled in the Onewhero crater: a lake infill deposit, a sandstone deposit, and a basalt deposit (Table 4.1). These geological bodies were chosen for their common occurrence in global phreatomagmatic craters or for their known occurrence in the crater either through outcrops at the surface or

identification in the bore-holes of Chapter 3 (Pirrung et al., 2003). The lake infill deposit includes all clay-sized sediment, silt, diatomaceous sediment, and peat occurrences in the crater. The sandstone deposit includes coarse volcaniclastics such as ash and reworked tuff that would have infilled the crater after the conclusion of the eruption. The basalt deposit consists solely of the lava flow/flows in the south of the crater.

The same geological bodies were modelled in the Kellyville crater: a lake infill deposit, a sandstone deposit and a basalt/scoria deposit (Table 4.2). The lake infill deposit includes all clay-sized sediment, silt, and diatomite in the crater. The lake infill is insignificant in much of the crater due to much of the sediment being lost to the Waikato River after the crater breach. The sandstone deposit includes coarse volcaniclastics such as ash and reworked tuff. The basalt deposit consists of Glass Hill basalt and underlying magmatic deposits that are mainly composed of fine-grained basalt (Colchester, 1968).

Table 4.1: The modelled densities (g/cm³) of applicable geological bodies in the Onewhero crater.

Onewhero geological densities		
Deposit	**Density[1]**	**Difference[2]**
Lake infill	1.3	-1.0
Reworked tuff	2.2	0.1
Country rock	2.3	0
Basalt	2.9	+0.5

[1] A density of 1.3 g/cm was modelled for the lake infill. This was measured by dividing the weight of a sample of Onewhero diatomaceous clay by its volume. This yielded a density of 1.1 g/cm³. This was then conservatively increased to 1.3 g/cm³ in an effort to model a density that represented the lake infill as a complete geological body.

The sandstone/tuff density was measured from a sample of tuff from the Onewhero ejecta ring. This will be used to represent reworked volcaniclastic sediment that likely underlies the lake infill body.

The likely country rock present under the Onewhero tuff ring is the Carter Siltstone. A publication was not found that mentioned the Carter Siltstone's density so a density of 2.3 g/cm³ was chosen.

A generic New Zealand basalt density of 2.9 g/cm³ was used for Onewhero (Cassidy et al., 2007).

[2] This column states that density difference of the geological bodies relative to the country rock upon which they are sitting.

Table 4.2: The modelled densities (g/cm³) of applicable geological bodies in the Kellyville crater.

Kellyville geological densities		
Deposit	**Density[1]**	**Difference**
Lake infill	1.3	- 1.0
Reworked tuff	2.2	-0.1
Country rock	2.4	0
Basalt	2.9	+0.6

[1] A density of 1.3 g/cm³ was modelled for the lake infill. This is due to the diatomite present at Mercer being less dense than water but the lake infill as a whole geological body includes clay, silt, Taupo Volcanic Zone pumiceous sediment, and groundwater.

The tuff density taken from the Onewhero tuff sample was used for the modelling of reworked volcaniclastic sediment for Kellyville.

A country rock density of 2.4 g/cm³ was used in Mercer. The Koheroa Siltstone is known to be denser than the Carter Siltstone and the density increase reflects that.

A generic basalt density of 2.9 g/cm³ was used for the basalt bodies modelled at Kellyville (Cassidy et al. 2007).

4.9 Potential sources of error in the two-dimensional modelling

Error in the two-dimensional modelling could have arisen for multiple reasons.

- Bore-hole information for the Mercer and Onewhero regions is sporadic and when available is poorly placed [1].

- The density measurements were calculated from field samples and do not represent the entire deposit [2].

- Due to the lack of accurate geological constraint, modelling of the gravity profiles is purely a best guess of the subsurface stratigraphy based on my own knowledge of the area [3].

[1] The bore-hole data that was available did help increase my geological knowledge of the area and I could therefore make better judgements when modelling.

[2] An effort was made to align densities so that they were closer to a 'bulk deposit' than they appeared at the surface.

[3] The geological models created and investigated below are the best estimates I can suggest from the limited constraints I have available. These are subject to change and be refined when additional data becomes available.

4.10 Onewhero gravity investigation

4.10.1 Gravity profiles

Two perpendicular gravity transects were made across the Onewhero tuff ring (Figure 4.4). Line Y – Y' consisted of 38 gravity readings and traversed the crater in a northeast to southwest direction. Line X – X' consisted of 31 gravity readings and traversed the crater in a southeast to northwest direction. The gravity values were corrected for latitude, elevation and regional effects and the resulting two-dimensional regionally-corrected Bouguer anomalies are shown in figures 4.4 and 4.5.

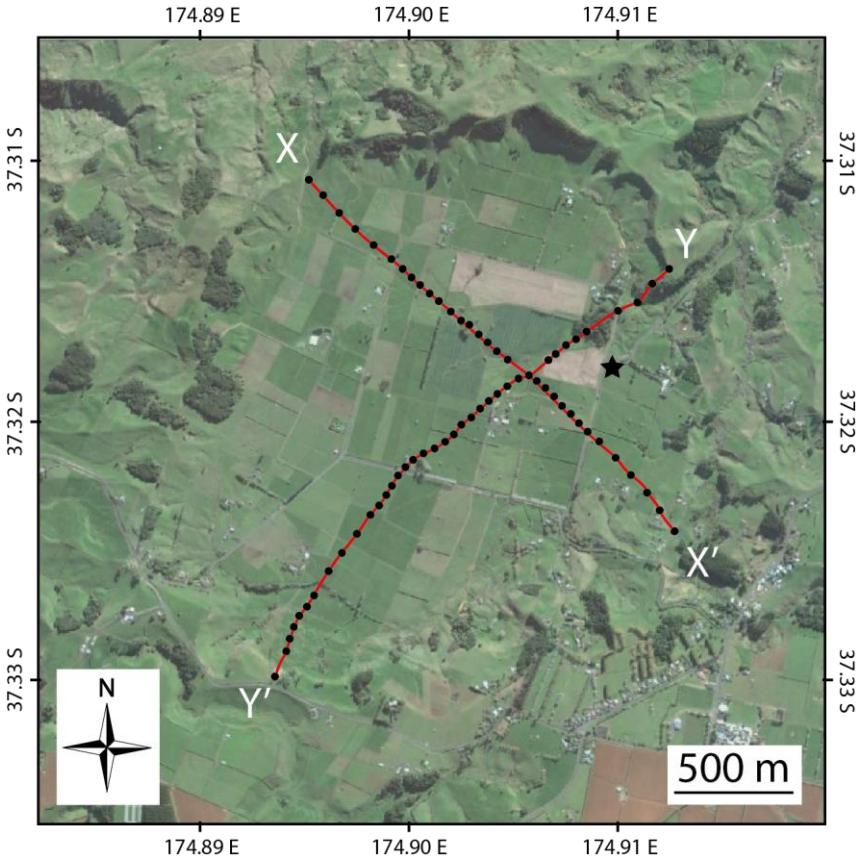

Figure 4.4: Aerial photograph from Google Earth showing the perpendicular transects that were measured for gravity in the Onewhero crater. Black circle = gravity station, black star = field base-station.

Figure 4.5 reveals the gravity anomalies for the Y – Y' transect. A shallow bowl of low gravity towards the centre of the crater reaches -3 mGal. A larger-than-expected gravity trend at the end of the profile in the south records a positive gravity value of +1 mGal at its peak.

Figure 4.6 reveals the gravity profile for the X – X' transect. It differs slightly from the Y – Y' transect. The gravity trend has a greater range and an anomaly reaches a maximum in the east, peaking at around +2 mGal. The gravity trend towards the west is the lowest in the crater, a minimum anomaly of -5.5 mGal is observed in this area.

In an ideal gravity survey involving a perfectly formed maar, one would expect to see a clear bowl-shaped negative anomaly. The gravity anomaly for the Onewhero crater differs somewhat from this ideal profile, but the general bowl shape is present here in both gravity profiles.

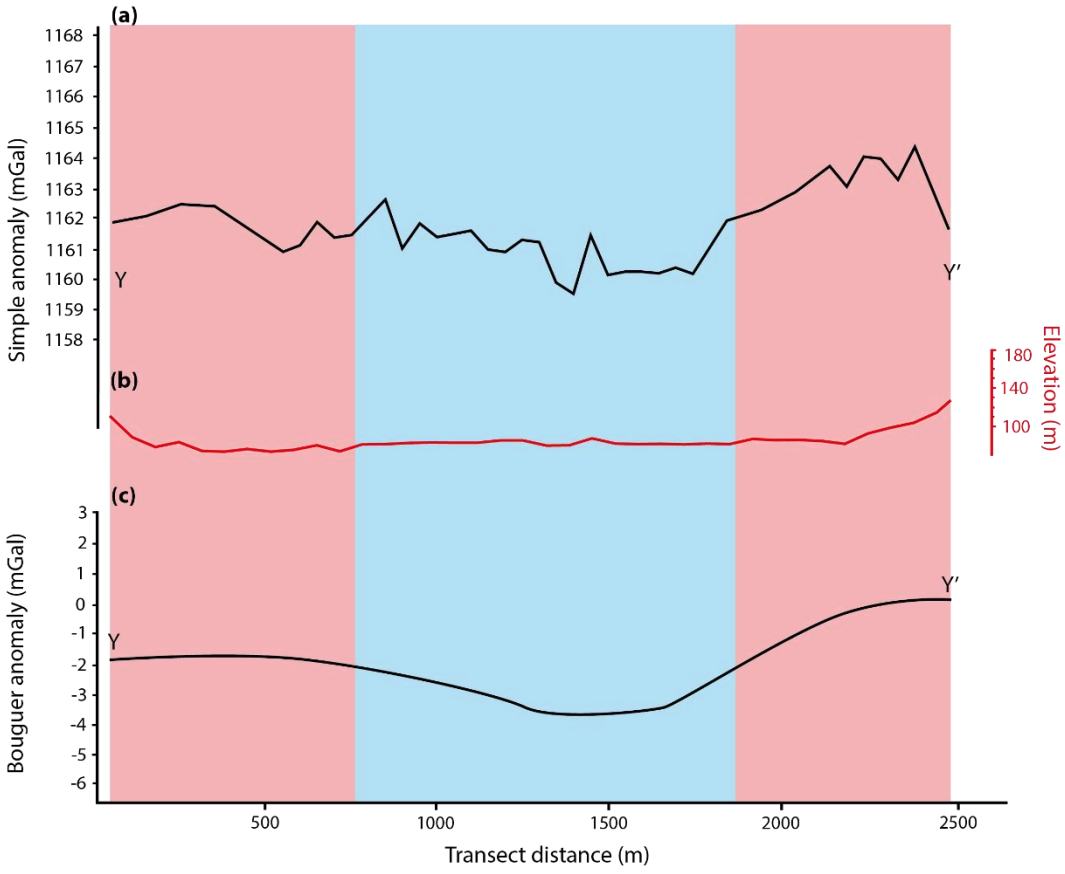

Figure 4.5: (a) The simple anomaly after corrections with (b) a topographic elevation guide (m.a.s.l.) for the profile Y – Y' (Figure 4.3). (c) The general gravity trend of the profile (a line of best fit) converted to the anomaly values that were used for two-dimensional modelling. The background shading represents high (red) and low (blue) regions of relative gravity.

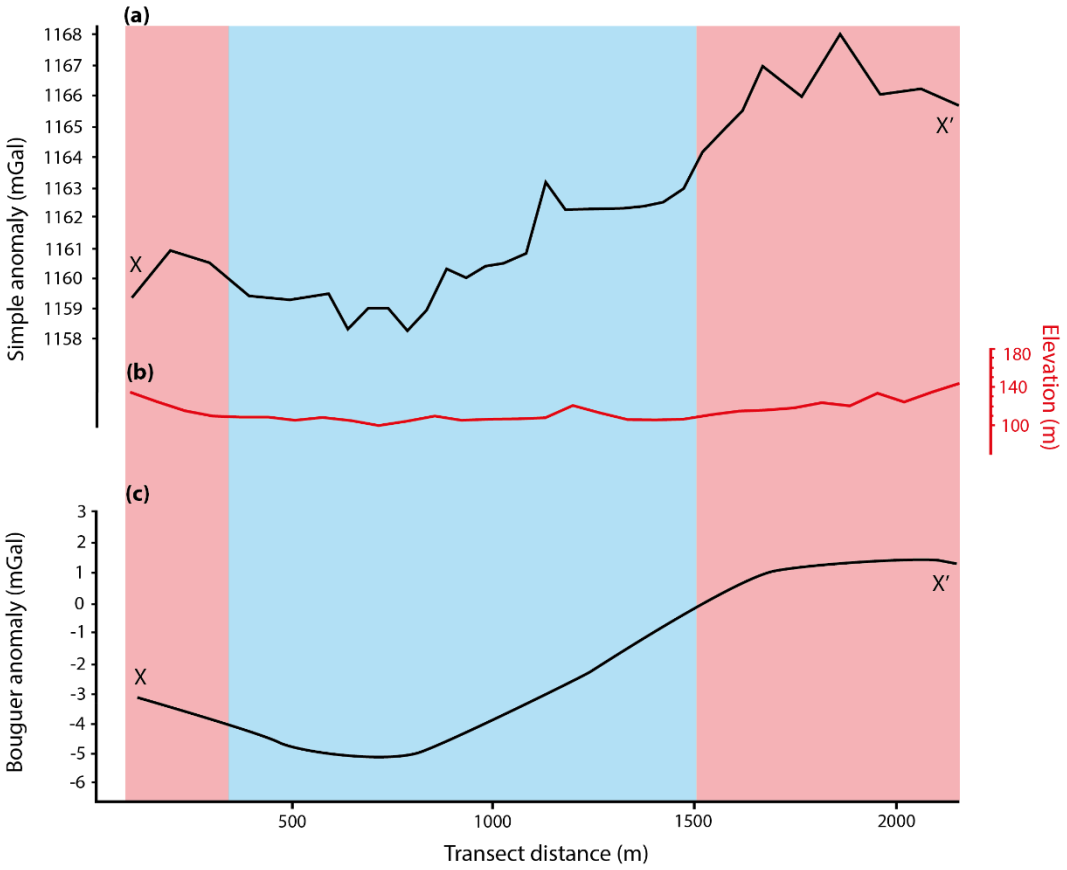

Figure 4.6: (a) The simple anomaly after corrections with (b) a topographic elevation guide (m.a.s.l.) for the profile X – X' (Figure 4.3). (c) The general gravity trend of the profile (a line of best fit) converted to the anomaly values that were used for two-dimensional modelling. The background shading represents high (red) and low (blue) regions of relative gravity.

4.10.2 Onewhero two-dimensional gravity models

Profile Y – Y'

Figure 4.7 is a two-dimensional model of the Y – Y' gravity transect at Onewhero. The general gravity of the inner crater is typically around -2.5 mGal. A gradual decrease in the gravity anomalies to the south was modelled as a lake deposit of low density clay infill that gradually thickened to the south with a maximum thickness of 75 m. An increase in gravity in the south of the crater can be attributed to the presence of a lava flow that spills over the Onewhero ejecta ring. The basalt flow in the south of the crater has a maximum modelled thickness of 20 m.

Profile X – X'

Figure 4.8 is a two-dimensional model of the X – X' gravity transect at Onewhero. The lake infill has a bowl shape that dips steeply in the west before thinning away to the east. It has a maximum depth of 100 m in this profile as the gravity anomaly dips to -5.8 mGal. There is a significant elevated gravity anomaly in the east, peaking at +4 mGal. A basalt flow has been modelled to account for this spike of gravity and it reaches a maximum modelled thickness of 25 m.

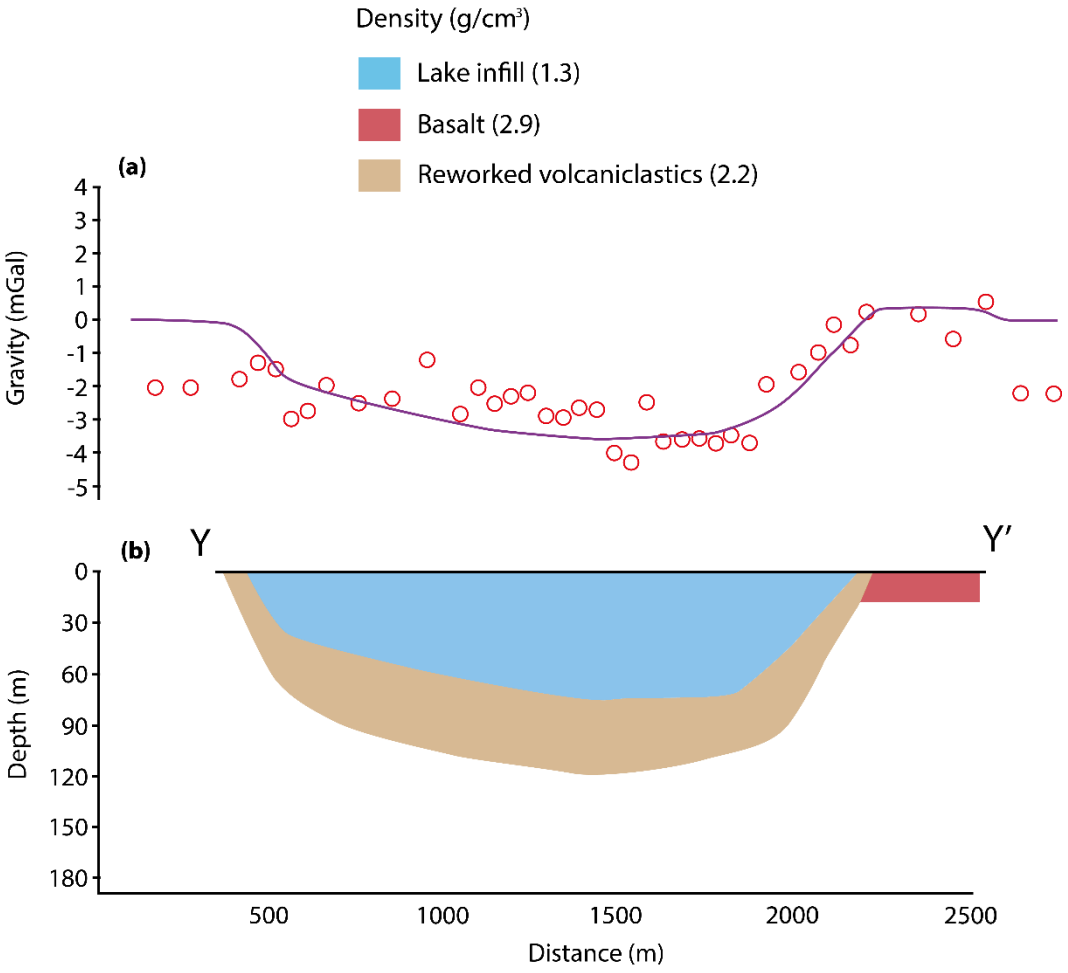

Figure 4.7: Two-dimensional gravity model of the Y – Y' transect. (a) The upper profile is the calculated versus observed gravity values with the red circles being the observed gravity values and the purple line representing the calculated values. (b) The bottom profile is the inferred geology that dictates a calculated gravity response (purple line).

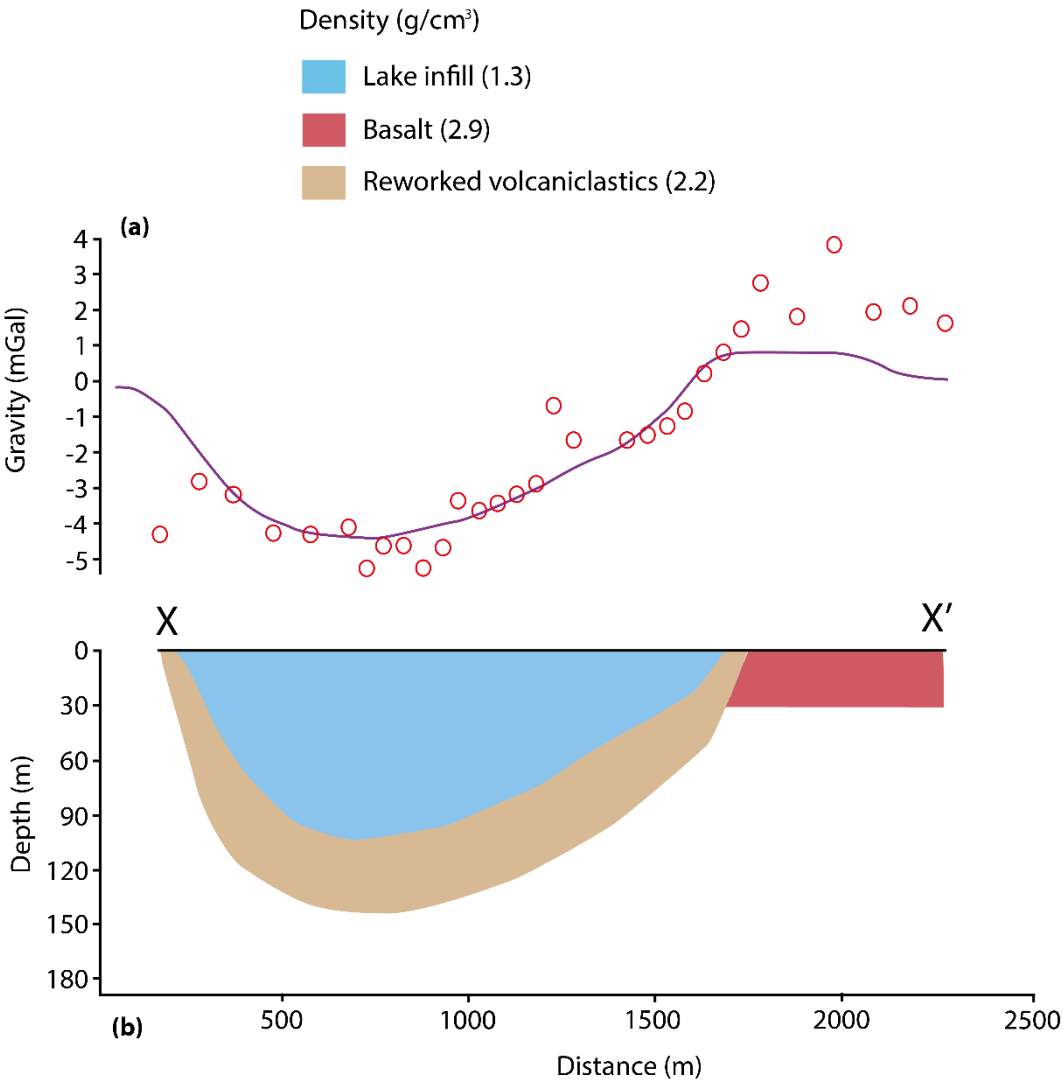

Figure 4.8: Two-dimensional gravity model of the X – X' transect. (a) The upper profile is the calculated versus observed gravity values with the red circles being the observed gravity values and the purple line representing the calculated values. (b) The bottom profile is the inferred geology that dictates a calculated gravity response (purple line).

4.10.3 Discussion of the Onewhero gravity survey

The Onewhero Volcanic Complex appears to be geologically simple at the surface. The few bore-holes that are available in the crater do not add further complexity. Although the constraints in this region are lacking I am confident that a large majority of the post-eruption infill in the Onewhero crater is composed of volcanic and lacustrine clay-sized sediment and this is a common occurrence in maars worldwide (Lorenz, 1986). The lava flow in the south of the crater has an obvious

effect on the gravity which is significantly elevated in the south and southeast. The gravity in the southeast on the X – X' transect is particularly high and the lava flow contributes to this. At the surface, the lava flow is much thicker in this region and it extends further into the crater from this direction. This could be the reason for the higher gravity relative to that recorded in the Y – Y' transect, and the lava flow was modelled as a thicker unit in the X – X' transect as a result. The post-eruption clay infill reaches a maximum thickness of 100 m in the northwest of the crater. This region was a low point in the crater when this infill was being deposited. The accumulation of low density sediment in this area is bowl-shaped and is much thicker than elsewhere in the crater and this is mirrored by the lowest Bouguer values measured at Onewhero. The rest of the crater has a post-eruption infill thickness that gradually decreases to about 60 m and then thins towards the walls of the ejecta ring.

4.11 Kellyville gravity investigation

4.11.1 Gravity profiles

Two perpendicular gravity transects were made across the Kellyville Volcanic Complex (Figure 4.9). Transects Y – Y' and X – X' consisted of 22 gravity readings each. Transect Y – Y' traversed the crater in a north to south direction and Line X – X' traversed the crater in a west to east direction. The gravity values were corrected for latitude and elevation effects allowing the simple and general gravity anomalies to be extracted.

Figure 4.10 reveals the Bouguer anomaly and general gravity trend for the Y – Y' transect in Kellyville maar. The general trend of the gravity anomalies is quite different from either of the Onewhero gravity trends. The general trend is an increase to the north from negative anomalies measuring -0.5 mGal to a peak in the anomaly measuring +1.2 mGal. The transect concludes with a decrease in gravity to -1.3 mGal.

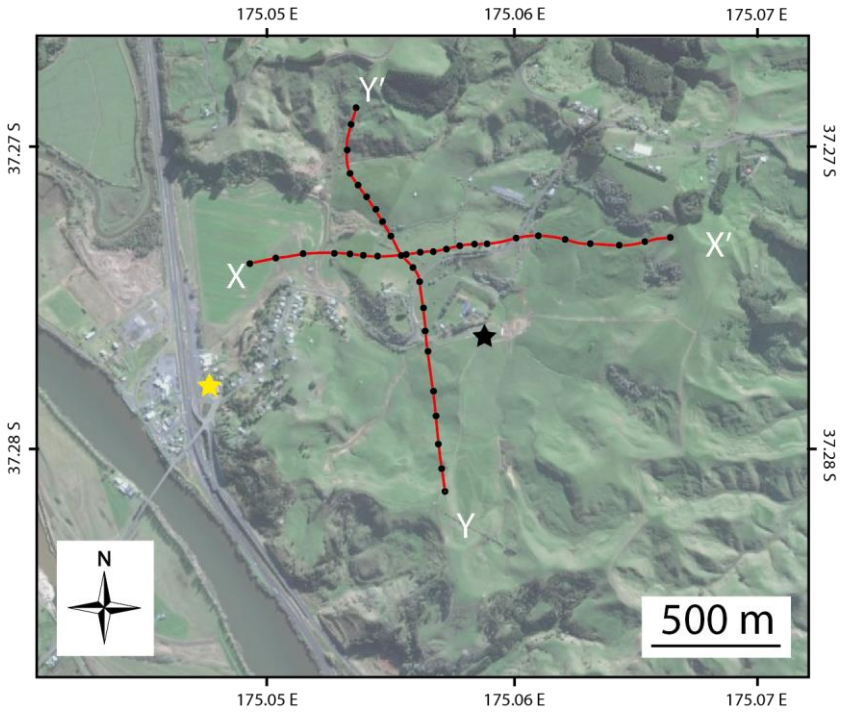

Figure 4.9: Aerial photograph from Google Earth showing the perpendicular transects that were measured for gravity in the Kellyville crater. Black circle = gravity station, black star = field base-station, yellow star = LINZ station.

Figure 4.11 reveals the Bouguer and general gravity trend for the X – X' transect in the Kellyville maar. The gravity profile differs, with a strong peak in the gravity anomaly near the start of the transect measuring +1.5 mGal. The maximum gravity value for the anomalies measured, occurs at 500 m into the transect and this peaks at +2.5 mGal. A shallow trough and crest occurs between 1000m and 1500 m that dips gradually to the east to a low gravity values of -2.5 mGal.

The gravity in the Kellyville crater is the opposite of the general gravity trend found in similar phreatomagmatic centres; instead of a negative bowl anomaly there is a convex-upwards gravity anomaly. This is an uncommon gravity feature in global maar-gravity surveys.

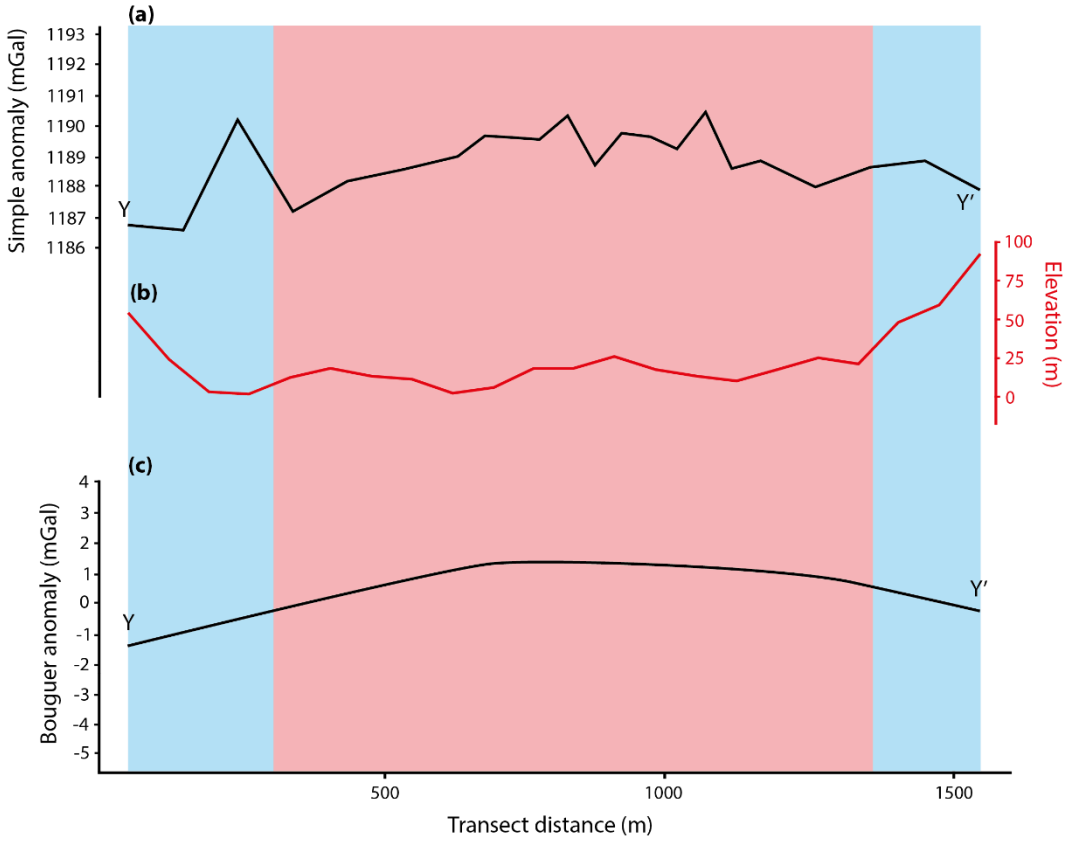

Figure 4.10: (a) The simple anomaly after corrections with (b) a topographic elevation guide (m.a.s.l.) for the profile Y – Y' (Figure 4.3). (c) The general gravity trend of the profile (a line of best fit) converted to the anomaly values that were used for two-dimensional modelling. The background shading represents high (red) and low (blue) regions of relative gravity.

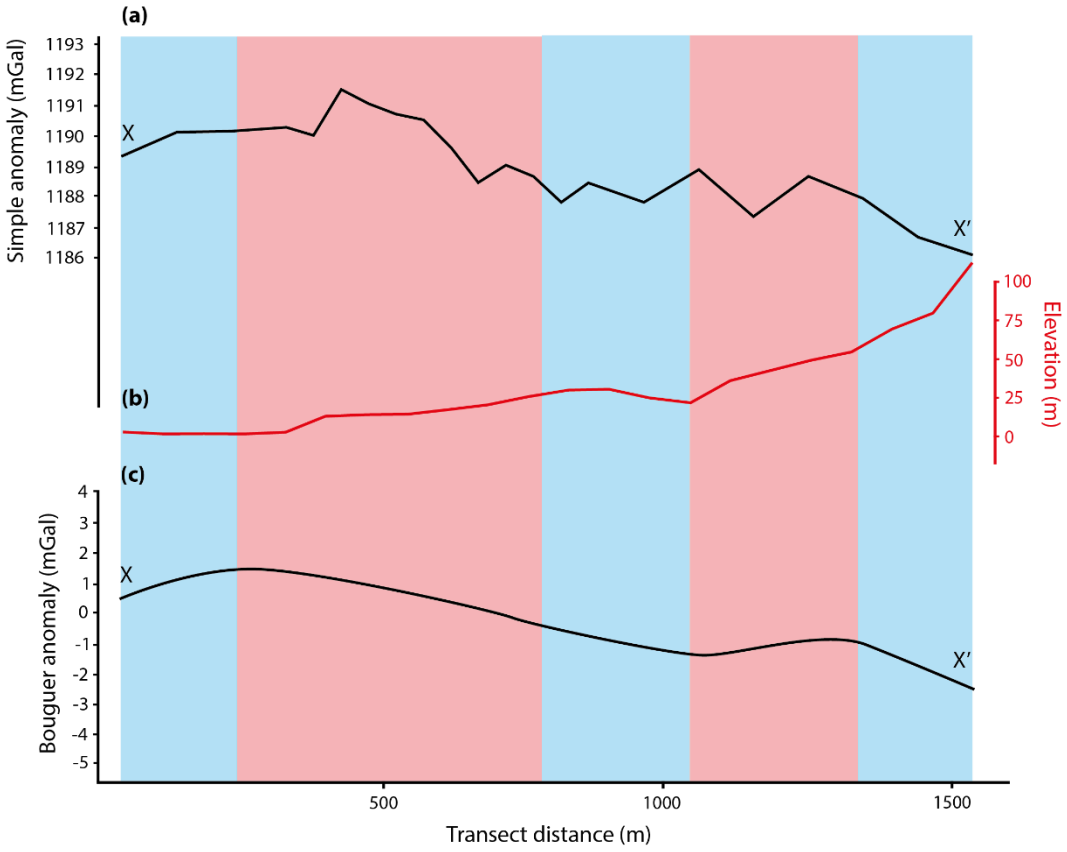

Figure 4.11: (a) The simple anomaly after corrections with (b) a topographic elevation guide (m.a.s.l.) for the profile X – X' (Figure 4.3). (c) The general gravity trend of the profile (a line of best fit) converted to the anomaly values that were used for two-dimensional modelling. The background shading represents high (red) and low (blue) regions of relative gravity.

4.11.2 Kellyville two-dimensional gravity models

Profile Y – Y'

Figure 4.12 is the two-dimensionally modelled illustration for the Y – Y' gravity transect. This profile traverses the crater in a north to south direction. The transect begins with a low gravity anomaly measuring -2.5 mGal. This is modelled as a thick accumulation of low density lake infill that reaches a maximum depth of 55 m. A steep rise in the gravity at around 500 m distance along the transect caused by thick

subsurface lava flows and eventually Glass Hill scoria cone deposits that reach a maximum thickness of 55 m. The gravity peaks at 1.25 mGal before falling due to the pinching out of basalt and a thickening of low density lake infill.

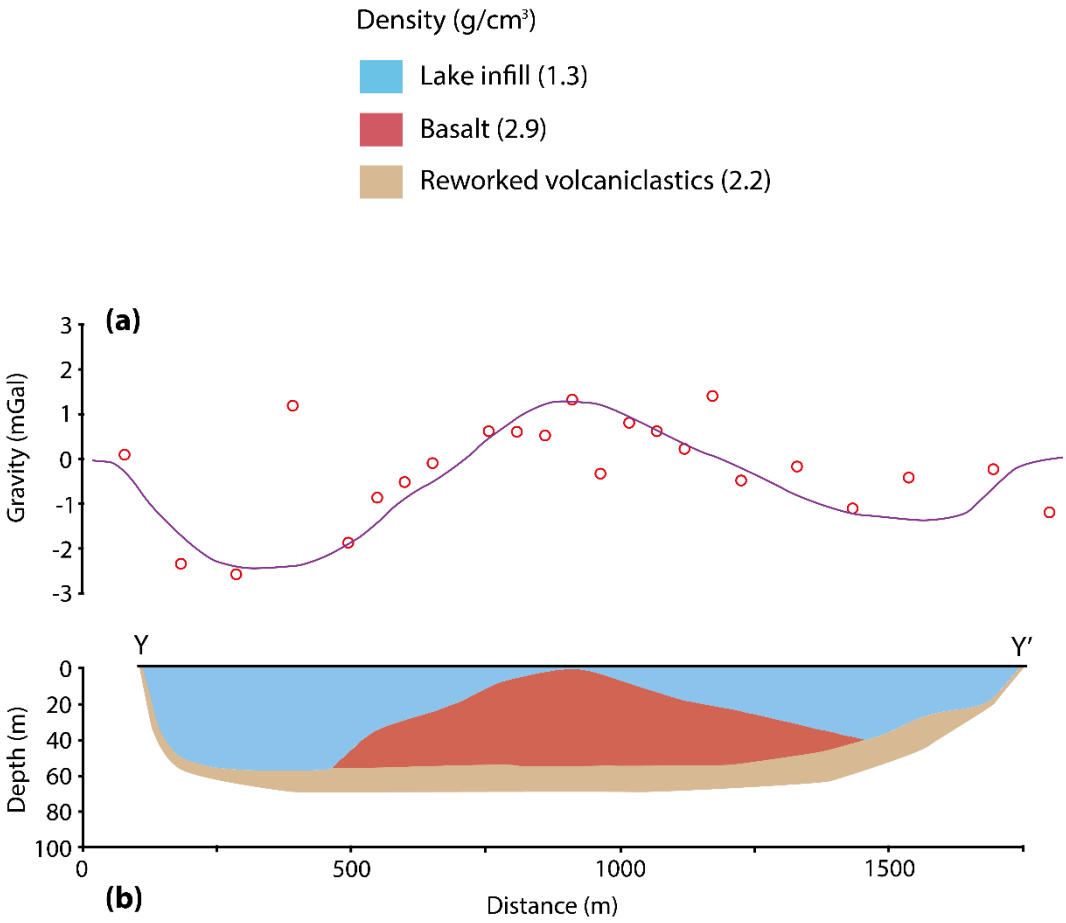

Figure 4.12: Two-dimensional gravity model of the Y – Y' transect. (a) The upper profile is the calculated versus observed gravity values with the red circles being the observed gravity values and the purple line representing the calculated values. (b) The bottom profile is the inferred geology that dictates a calculated gravity response (purple line).

Profile X – X'

Figure 4.13 is the two-dimensionally modelled illustration for the X –X' gravity transect. This profile traverses the crater in a west to east direction. The gravity anomaly increases from 0 mGal at the start of the transect to a peak of +2.3 mGal

towards the middle of the profile. This is modelled as an accumulation of basalt and scoria that increases in thickness as it approaches Glass Hill. The basalt deposit has a maximum thickness of 60 m and this causes the positive gravity anomaly. The gravity then dips and rises again towards the end of the transect. The profile ends with a negative gravity trend that is modelled as a pinching out of the basalt deposit and a thickening of low density lake infill that has a thickness of about 35 m.

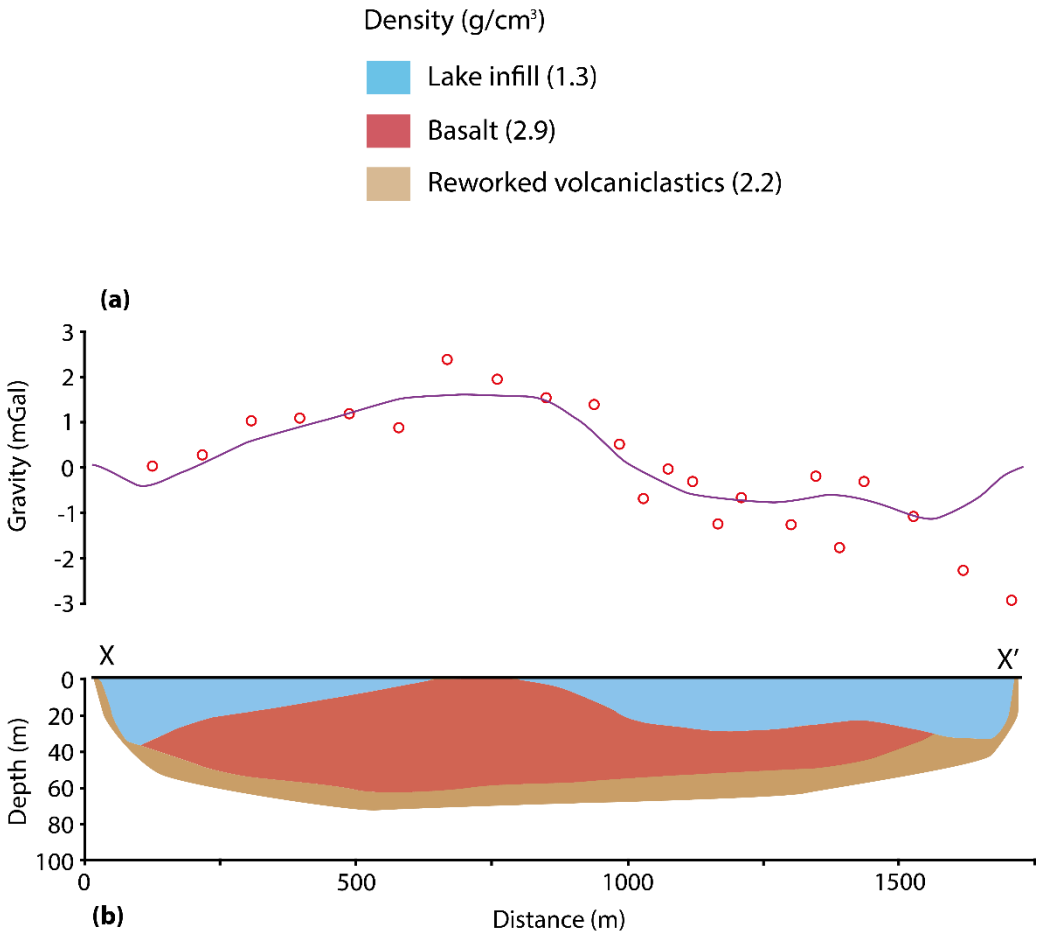

Figure 4.13: Two-dimensional gravity model of the Y – Y' transect. (a) The upper profile is the calculated versus observed gravity values with the red circles being the observed gravity values and the purple line representing the calculated values. (b) The bottom profile is the inferred geology that dictates a calculated gravity response (purple line).

4.11.3 Discussion of the Kellyville gravity survey

Unlike the Onewhero Volcanic Complex, which appears to be geologically simple from the surface, the Kellyville Volcanic Complex has volcanic features that are apparent at the surface. Glass Hill is the main surface feature and provided a basis

for modelling the thick accumulations of basalt that have been identified in the crater from the bore-hole data. The two-dimensional modelling of the Kellyville Volcanic Complex reveals a general gravity trend that opposes the trends seen at Onewhero. The positive trend in gravity suggests an extensive coverage of basalt up to 60 m thick around Glass Hill. The two-dimensional models indicate that multiple layers of lava could cover an area close to 1 km². In both of the profiles, the gravity reaches a maximum near the northern base of Glass Hill before dipping away from the extrusive vent. It appears as though the deposition of lacustrine infill was influenced by the post-eruption topography created by the extensive lava flows and possibly multiple effusive vents.

4.12 Chapter summary

Two South Auckland Volcanic Field craters were measured for their local gravity. 44 gravity measurements were made in the Kellyville Volcanic Complex and 69 gravity measurements were made in the Onewhero Volcanic Complex with a Worden gravimeter. The data was reduced to eliminate the effects of elevation and latitude. The regional gravity field was subtracted from the Onewhero gravity data but not the Kellyville gravity data due to the craters position in an area of constant regional gravity. This left a residual anomaly at Onewhero that had classic concave profile and at Kellyville that had an uncommon convex profile. The gravity anomalies were then modelled two-dimensionally using Steven Sheriff's GravCadW program. This software calculates the gravitational effects of geological bodies with contrasting densities that are superimposed upon each other. At Onewhero three distinct bodies were modelled. These were a post-eruption infill body with a density of 1.3 g/cm³, a reworked tuff/sandstone body with a density of 2.2 g/cm³, and a basalt body with a density of 2.9 g/cm³, these contrasted with the country rock which was modelled with a density of 2.3 g/cm³. At Kellyville three distinct bodies were also modelled. These were a post-eruption infill body with a density of 1.3 g/cm³, a reworked tuff/sandstone body with a density of 2.2 g/cm³, and a basalt body with a density of 2.9 g/cm³, these contrasted with the country rock which was modelled with a density of 2.4 g/cm³ The models were created based around the general maar structure described by Lorenz (1986). This includes a

breccia/reworked tephra deposit that forms on the crater floor immediately after the formation of the tuff ring for up to several decades as the ejecta ring stabilises. This sandy deposit of reworked tephra is deposited by mass wasting processes as the rim fails. Low density lacustrine sediment is then deposited on top of the sandstone creating a density contrast. In Chapter 6 these gravity models will be combined with the magnetic observations covered in Chapter 5 and this will eliminate some of the discrepancies and provide extra constraints for the geology of the Onewhero and Kellyville volcanic complexes.

Chapter Five: Magnetic investigation of the Onewhero and Kellyville volcanic complexes

5.1 Introduction

A typical maar volcano can be effectively identified in a magnetic survey due to the contrast in the high magnetic signature of basaltic diatreme fill and the low magnetic signature of the overlying post-eruption lake sediment and surrounding country rock. Mafic volcanic rock that has undergone limited fractional crystallisation is generally high in magnetite, a ferromagnetic mineral that preserves Earth's magnetic field.

The magnetic geophysical technique aims to define the intensity and spatial distribution of magnetized rocks (Everett, 2013). Magnetic measurements are made at the surface and are fast and non-destructive. Magnetic surveys are one of, if not the oldest of the geophysical analysis techniques (Nabighian et al., 2005). Magnetic surveys have been carried out in many volcanic studies due to the ease with which they pick up the subsurface characteristics of maar volcanoes (e.g. Cassidy et al., 2007; Mrlina et al., 2009; Blaikie et al., 2012; Blaikie et al., 2014).

This chapter begins with a brief outline of the basic theory behind Earth's magnetic field and how this allows magnetic surveys to be important tools for subsurface interpretation. This will be followed by an account of how the data was collected in the field at the Onewhero and Kellyville volcanic complexes and how the data was processed. Results will then be presented and interpretations for the Onewhero and Kellyville magnetic surveys will be outlined and discussed.

5.2 Magnetic Theory

All minerals possess an 'induced' magnetism when exposed to a magnetic field due to the sub-atomic effect of negatively charged electrons orbiting the nucleus. The

effects of induced magnetism are short-lived in most minerals; the precession of electrons within a mineral returns to normal as the magnetic field is removed. These processes are termed diamagnetism and paramagnetism and they generally produce magnetic "noise" rather than "signal" in a ground-based magnetic survey. Some iron-rich minerals, notably magnetite, retain their magnetism even when removed from a magnetic field. These minerals are ferromagnetic and have a strong positive magnetisation that can be measured in the field with a magnetometer.

The term "magnetic susceptibility" will be used later in this chapter when discussing magnetic anomalies. It is important to realise that magnetic susceptibility and induced magnetisation (which is the value being measured by the magnetometer) are not the same things but are closely related. In general, minerals with an induced magnetism have a high magnetic susceptibility and minerals that do not retain magnetism have a low magnetic susceptibility.

Volcanic rocks that are rich in magnetite can be thought of as assemblages of microscopic magnetic dipoles that are aligned in a direction imposed by an external magnetic field. A single magnetic dipole can be visualised as an extremely small loop of area relaying an electric current (Figure 5.1). The external magnetic field in this study is generated in Earth's outer core, the result of circulating masses of molten iron. The intensity of a magnetic field is measured by its magnetic flux. The SI unit for magnetic flux is the weber, but most studies use the term tesla (a derivative of the weber) when describing magnetic intensity. One tesla (T) is the flux density of one weber per metre squared (Wb/m^2). In this study the measure of magnetic field strength will be the nanotesla (nT) which is one billionth of a tesla.

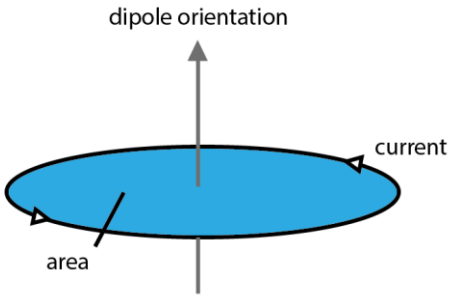

Figure 5.1: A magnetic dipole is induced by a loop of rotating current.

The magnetic poles, unlike the geographic poles, do not stay fixed in place over time. Both the north and south magnetic poles are continually wandering (Figure

5.2). This movement is known as secular variation (Everett, 2013). Secular variation is a process that is noticeable over several years, this is a different concept to magnetic reversals, which occur over a much longer timescale (hundreds of thousands of years).

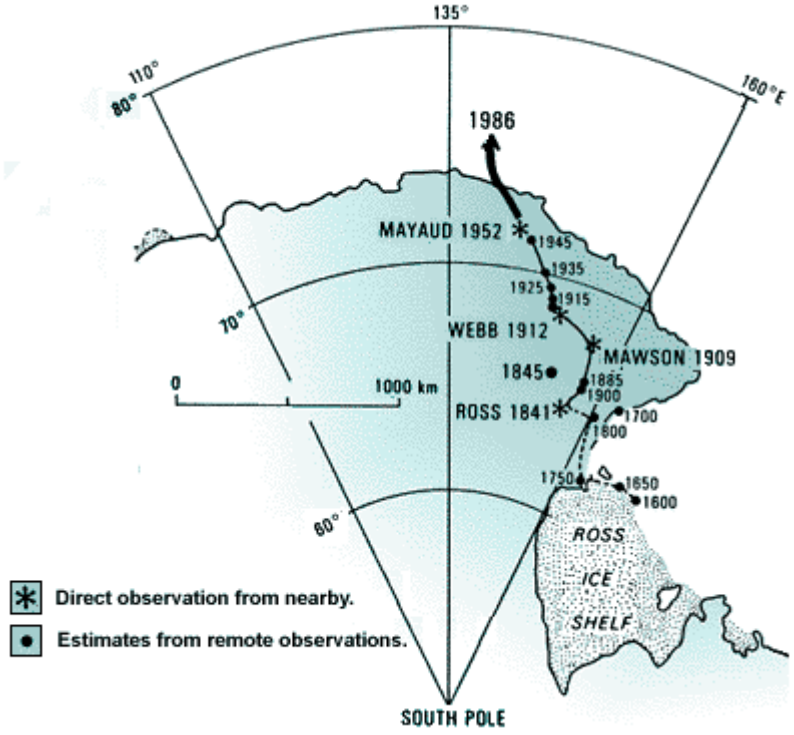

Figure 5.2: The South Magnetic Pole continually wanders in a movement known as secular variation. The historic direction of movement of the South Magnetic Pole is to the north (from Discover, 2011).

Slow changes in Earth's geomagnetic field create the need to update the model regularly, and this is achieved by adopting a new World Magnetic Model (WMM) or International Geomagnetic Reference Field (IGRF) model every five years. Earth's geomagnetic field direction and intensity can be visualised by conversion to a vector diagram (Figure 5.3). The total field intensity of a point is a product of horizontal (magnetic north) and vertical (downward projection) components.

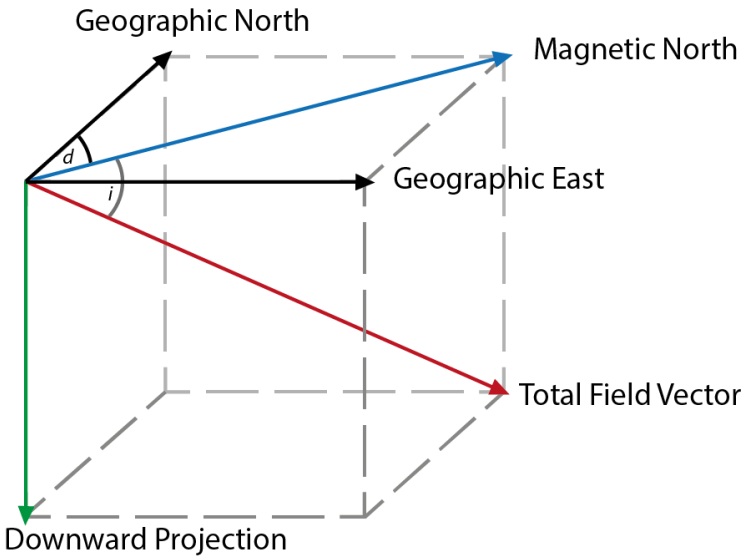

Figure 5.3: A vector diagram showing the intensity and orientation components that influence a local magnetic field. The inclination (*i*) is the angle between the surface of the earth and the local magnetic field lines in the area. The declination (*d*) is the angle between geographic north and magnetic north at a fixed position.

Magnetite is found in almost all volcanic rock but is found in particularly high concentrations in mafic or basaltic volcanic rock (Figure 5.4). In basalt, magnetite aligns to the current magnetic field as soon as it cools below its Curie temperature of 578^0 C which is well after most lava has solidified (Kearey et al., 2002). This effect is called remnant magnetisation and can be removed or increased in the negative direction if the external inducing magnetic field is reversed (Evans and Heller, 2007).

Magnetic anomalies are not only caused by subsurface geological structures. Diurnal variations occur often and are produced by solar processes such as sun-spots and flares. These abnormalities create electrical currents in the atmosphere causing variations in the geomagnetic field between 20 – 150 nT with larger events creating variation peaks that can exceed 1000 nT (Kearey et al., 2002).

Proton precession magnetometers are instruments that measure the total intensity of a magnetic field. A strong magnetic field is created in the instrument by passing a current through a solenoid that is surrounded by a hydrogen-rich liquid, such as kerosene. When subjected to a strong current, the protons (hydrogen) align themselves with the magnetic field and when the current is switched off the, protons

precess as they realign to Earth's magnetic field. The degree of precession is directly proportional to the strength of the surrounding magnetic field. This type of magnetometer is very precise and sensitivities of ~0.1 nT can be recorded if used correctly (Everett, 2013). The magnetometer used in this study was a G-856AX Memory-Mag Proton Precession Magnetometer created by Geometrics Inc. and borrowed from the Department of Geology at the University of Otago.

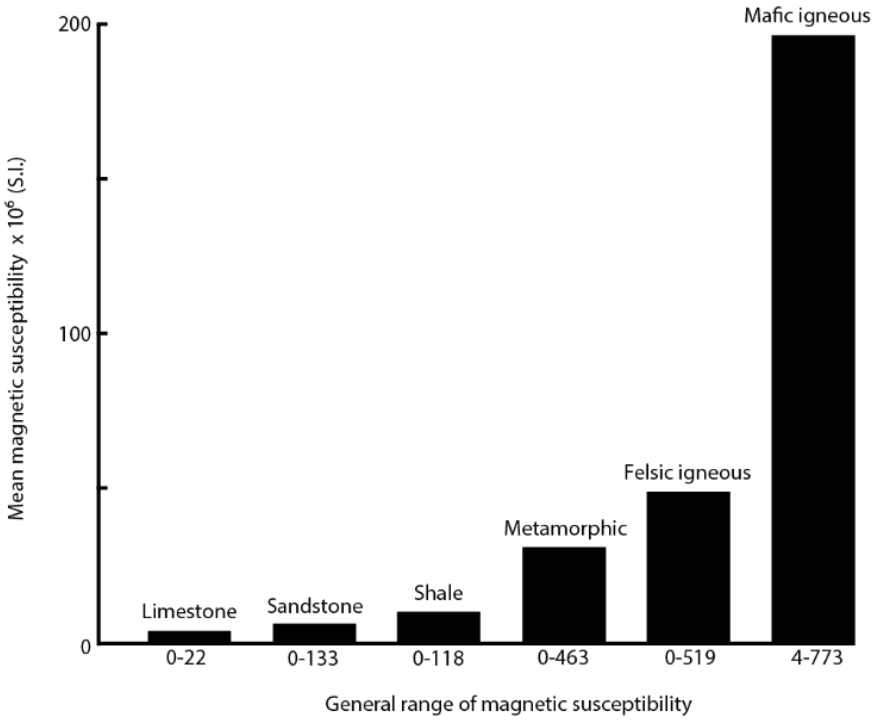

Figure 5.4: A figure showing the range of magnetic susceptibility of several rock types. Igneous rocks are generally much more susceptible than sedimentary rocks, which is important when surveying a volcanic structure.

5.3 Data collection

Magnetic data collection spanned the months from January through to April 2014. The G-856AX magnetometer does not use a mechanical process such as a spring to operate which means the instrument does not drift like the gravimeter, and magnetic signals are relatively unaffected by land tides so it was unnecessary to set up or return to a base station. 969 magnetic readings were made at Onewhero in a high resolution survey (Figure 5.5). Spacing between readings was approximately 30 m.

This spacing could not be set accurately and had to be paced out due to the small size of paddocks and length of grass in some paddocks hindered the use of a measurement wheel. 329 magnetic measurements were made at Kellyville. This was a slightly lower resolution survey as much of the volcanic geology at Kellyville is apparent at the surface. The spacing of measurements at Kellyville was irregular compared to Onewhero (Figure 5.9). This was acceptable as ArcMap, the program used to map the magnetic data, relied on a triangulated irregular network (TIN) layer where the spacing of measurements is maximised by an even coverage of the area rather than needing the straight, evenly-spaced lines that are crucial in other magnetic mapping programs. An effort was made to stay approximately 10 m away from any metallic objects such as fences, sheds, houses and transmission lines so as not to disrupt or distort the magnetic readings being made. However, even staying 10 m away from fences was not enough to fully eliminate the 'fence effect' (Figure 5.5). High-voltage transmission lines were not applicable in the Onewhero magnetic survey, but at Kellyville they were present within the survey area. The transmission lines in the Kellyville crater are probably 110 kV and this would create a substantial magnetic field around the conductors. No magnetic readings were taken within 50 m of transmission lines at Mercer and there is no apparent distortion in the magnetic anomaly map for the Kellyville maar as a result.

5.4 Processing

The raw magnetic data was processed in Microsoft Excel. An XYZ format was followed where the X value was the latitude, Y was the longitude, and Z was the height field, in this case, the magnetic intensity value. The magnetic anomaly for this study was created by subtracting the estimated magnetic field value from the observed magnetic reading obtained from the magnetometer. The estimated magnetic field values for the Mercer and Onewhero regions were obtained from a geomagnetic field calculator that used the newest World Magnetic Model. By inserting the geographical coordinates into the geomagnetic calculator the inclination, declination and total field values for Onewhero and Mercer townships were all made available (Table 5.1).

Table 5.1: The inclination, declination, and total field values for the Onewhero and Mercer regions. These values were obtained from the National Centers for Environmental Information (NOAA).

Onewhero	**Mercer**
Inclination: -63.13°	Inclination: -63.07°
Declination: 19.87°	Declination: 19.88°
Total Field: 54026 nT	Total Field: 53966 nT

The data containing the XYZ values was then exported into ArcMap and turned into a shapefile. A triangulated irregular network (TIN) function was used to extrapolate and display the magnetic anomaly values. The TIN layers were then fitted with contours and transformed using a raster function to create a smoother image.

5.5 Onewhero magnetic investigation

5.5.1 Magnetic anomaly map

Figure 5.5 is the magnetic anomaly map for the Onewhero crater created in ArcMap. Some of the magnetic features appear distorted, they are a product of the ArcGIS extrapolation. A set of stretched values in the middle of the map were probably distorted by the proximity to nearby fences as the paddocks in that area are thin and elongated. Five points of interest within the Onewhero crater were identified (Figure 5.6).

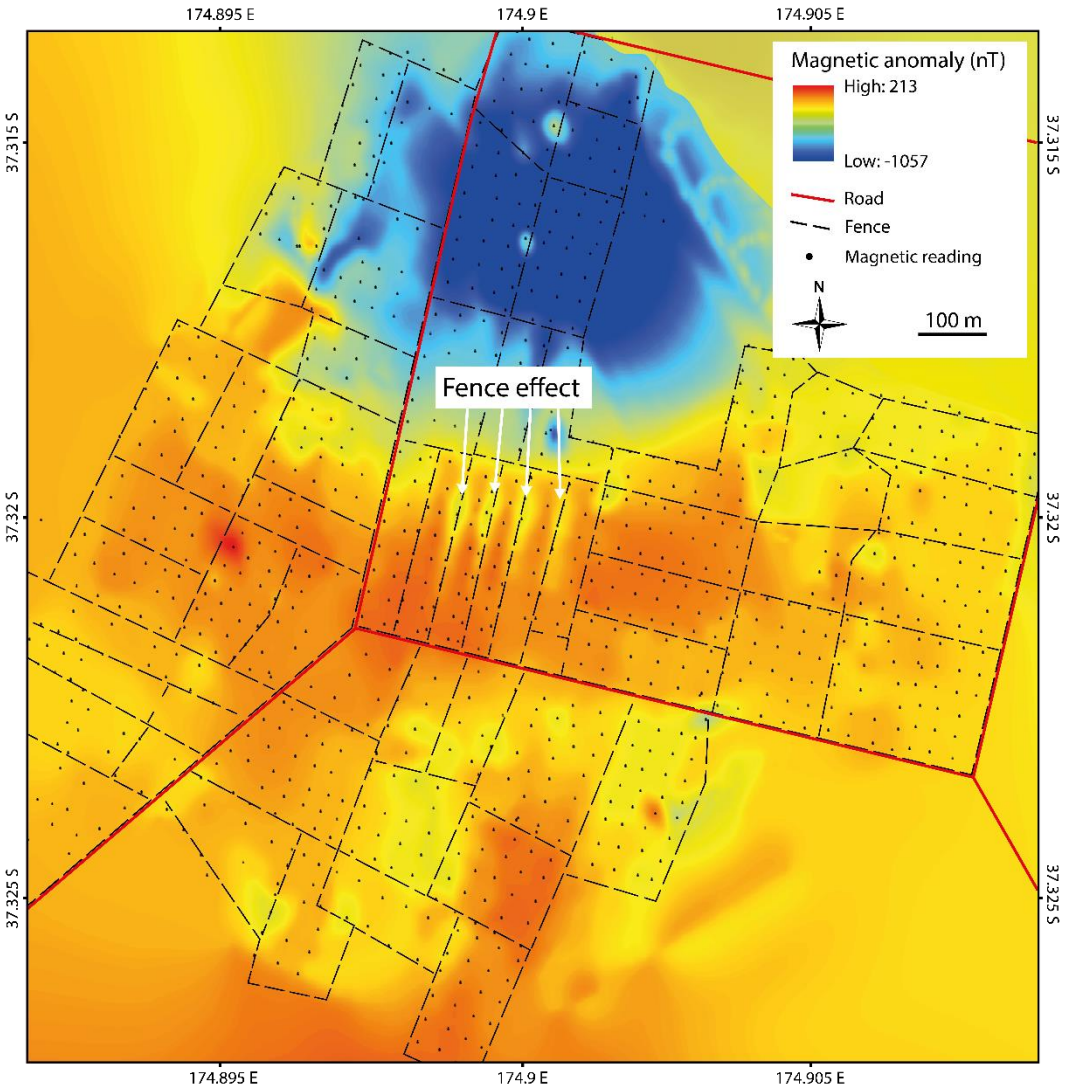

Figure 5.5: A magnetic anomaly map produced using ArcMap, for the Onewhero crater. Magnetic stations are present and you can see the way that they have had their values distorted by the closely spaced paddocks in the area.

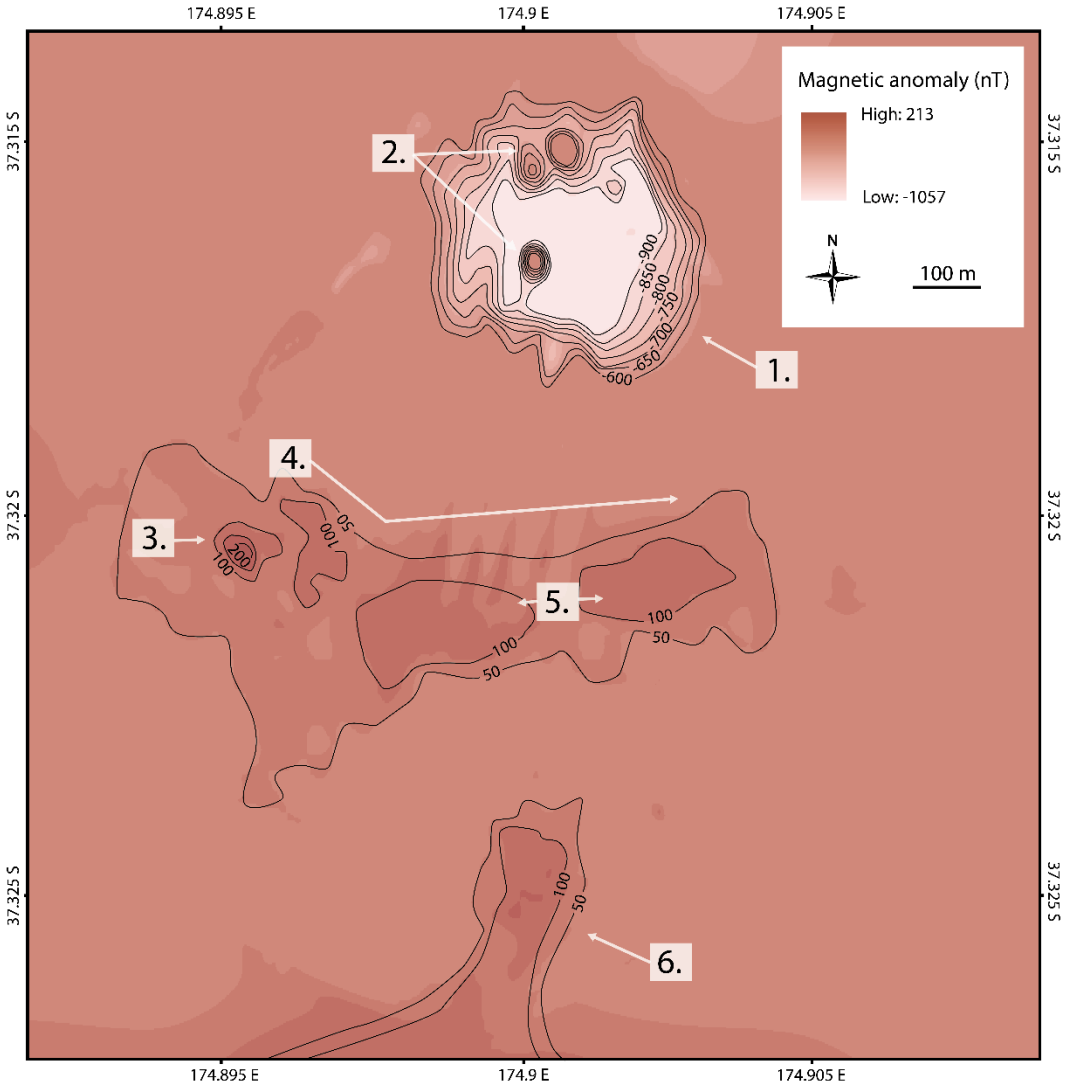

Figure 5.6: A magnetic anomaly map for the Onewhero crater outlining six magnetic observations that will be further described in this chapter. The main features are highlighted by 50 nT smoothed, best-fit contours that ignore the fence distortion and ArcMap's extrapolation where no data was recorded.

5.5.2 Points of interest

There are several sets of terminology used to describe magnetic anomaly relationships further on in this chapter.

Subsurface geological bodies that are high in magnetic minerals can produce short and/or long wavelength magnetic features. A body of basalt that is close to the surface will produce a sharp, magnetically intense feature with closely spaced contours; this is known as a short wavelength magnetic feature. The same body of basalt buried under 50 m of alluvium will produce a vague, faded, magnetic feature

with a much lower magnetic value outlined by broad contours; this is known as a long wavelength magnetic feature.

The amplitude refers to the magnetic value of a feature. A high amplitude body is likely a subsurface deposit of primary volcanic material, such as a dyke, or a basalt flow. A low amplitude body likely has a negative magnetic value and corresponds to a geological body made up of sediment with a very low magnetic susceptibility.

Six interesting magnetic and non-magnetic anomalies have been identified in the Onewhero crater and these will be outlined and interpreted below.

1. The lowest magnetic readings in the survey occur in the north of the crater. The lowest negative anomaly is -1057 nT and the anomaly reduces with distance in a circular basin shape.

2. Two high amplitude readings occur within the low magnetic intensity region. The northern high has an anomaly of -222 nT and the southern high has an anomaly of -260 nT. These points provide a stark contrast with the surrounding low intensity region.

3. The highest magnetic reading in the survey occurs in the west of the central high amplitude ridge. The region has a medium wavelength magnetic intensity anomaly of 213 nT that forms a steep intensity gradient with the surrounding positive anomaly ridge.

4. An elongated magnetic ridge with a long wavelength and a high amplitude stretches across the middle of the crater in a west to east trend.

5. Two long wavelength regions occur in the centre of the magnetic ridge with magnetic anomalies greater than 100 nT.

6. A positive long wavelength magnetic anomaly occurs in the south of the crater with a maximum anomaly of 110 nT.

5.5.3 Interpretation of the points of interest

1. The negative magnetic anomaly in the north of the crater is most likely a thick accumulation of sediment with negative magnetic susceptibility. Due to the presence of diatomaceous sediment in the crater-infill (Figure 3.10), we can assume that this region of negative magnetic amplitude originated as a bowl like depression in the post-eruption topography. This allowed a thicker lake sediment body to infill this area of the lake bed compared to the rest of the crater. The geometry of the basin is consistent with an explosion crater and I suggest that underlying the circular basin is a diatreme.

2. Two locally high anomalies occur within the low amplitude basin. I suggest that they are volcanic in origin and are related to the explosion crater outlined in the previous paragraph as they have a difference in value from the surrounding lake material exceeding 800 nT. They could be late-stage intrusions that intruded the diatreme near the end of the eruption, forming small basalt plugs. It is also possible that these elevated values were caused by human-buried material or they could simply be machine errors.

3. The region with the highest positive anomalies lies to the southwest of the low intensity basin. The anomaly peaks at 213 nT and the steep gradient from the surrounding magnetic material indicates vertical extent. This is probably related to a small extrusive vent that has formed a basalt spatter or scoria cone.

4. This magnetic ridge is probably basalt lava originating from the effusive vent inferred in (3.) above. The elongated west to east direction suggests the flows have been influenced by the topography that existed at the time. This could have been a terrace that prevented northward lateral migration or a valley that funnelled lava to the west. Another possibility is that the ridge of positive magnetic intensity is the result of an accumulation of weathered iron-rich sediment that has been eroded from the extrusive vent inferred above (3.), or the lava flow to the south. Again there would need to be some

kind of topographic feature that funnelled the magnetic sediment into the crescent shape observed on the magnetic anomaly map.

5. These circular regions could be vents due to their proximity to the centre of the crater and their relatively short wavelength compared to some of the other magnetic features. The short wavelength suggests that they are unsubstantial magnetic features at a shallow depth or substantial magnetic features at a greater depth. They could also be pools of lava thicker than the surrounding flows that were emplaced in shallow topographic depressions. Again the topography of these depressions could have been influenced by the presence of a vent.

6. This magnetic feature is also located in close proximity to the observed lava flow in the south of the crater. The lava flow is outlined in Figure 3.11 but this is only a surface contact. It is likely that the lava flow continues further on its path but has been partially buried by infill since it was emplaced (Figure 5.7). Alternatively the positive anomaly could be iron-rich sediment derived from the basalt flow nearby.

Figure 5.7: The geographic positions of the Onewhero crater lava flow (black) and the possible lava flow extent (red) inferred from the magnetic anomaly map.

5.5.4 Discussion of the Onewhero magnetic investigation

A high-resolution magnetic survey of the Onewhero Volcanic Complex has revealed a crater that is more complex than the geology appears at the surface. Three major features have been confidently identified: a large negative magnetic anomaly in the north of the crater, a positive magnetic ridge in the middle of the crater, and a positive magnetic region in the south of the crater. The percentage of the crater that is higher than the average magnetic intensity for the South Auckland region is low, suggesting a small volume of primary volcanic material (Figure 5.8).

The geological investigation of the crater in Chapter 3 improves confidence of two of the above interpretations.

The low amplitude basin in the north of the crater is a basin filled with lacustrine sediment. The low magnetic signal of this feature could be due to the thickness of the deposit, the purity of the diatomaceous sediment present, or a combination of the two. The diatomaceous clay found in the Onewhero crater was not as pure as the diatomite that occurs in outcrop in the Kellyville crater. Therefore, the magnetic low likely results from an accumulation of low-medium purity diatomaceous sediment that has been deposited in a topographic low, allowing a thick accumulation of the deposit to occur. This will be further discussed in Chaper Six by integrating the gravity results.

The positive magnetic region in the south of the crater can also be explained with high confidence by reference to the known geology. The magnetic survey did not cover the area partially covered by a lava flow in the south of the crater. However, the survey did start approximately 100 m to the north of the lava flow. The high, positive magnetic anomaly that was recorded in the south of the crater is probably a continuation of the exposed lava flow. In Chapter 3 the lava flow is confidently identified as originating from the Klondyke cone, if this is correct, the lava flow is younger than the ejecta ring. The strong magnetic feature in the south of the crater is the extent of the Klondyke cone's lava flow into the crater, where it has been partially buried by Holocene sediment. The one significant magnetic observation in the Onewhero crater that cannot be easily explained is the high magnetic intensity region in the middle of the crater. The positive anomaly has been completely buried by post-eruption infill and therefore the origin and structure of the feature has to be

assumed. The point of maximum intensity rises steeply from the surrounding positive magnetic ridge. This suggests that the feature has a vertical component that contrasts from its surroundings. This feature could be an extrusive vent, originating from a secondary dyke. The shape of the flow originating from this vent would have been heavily influenced by the pre-existing topography.

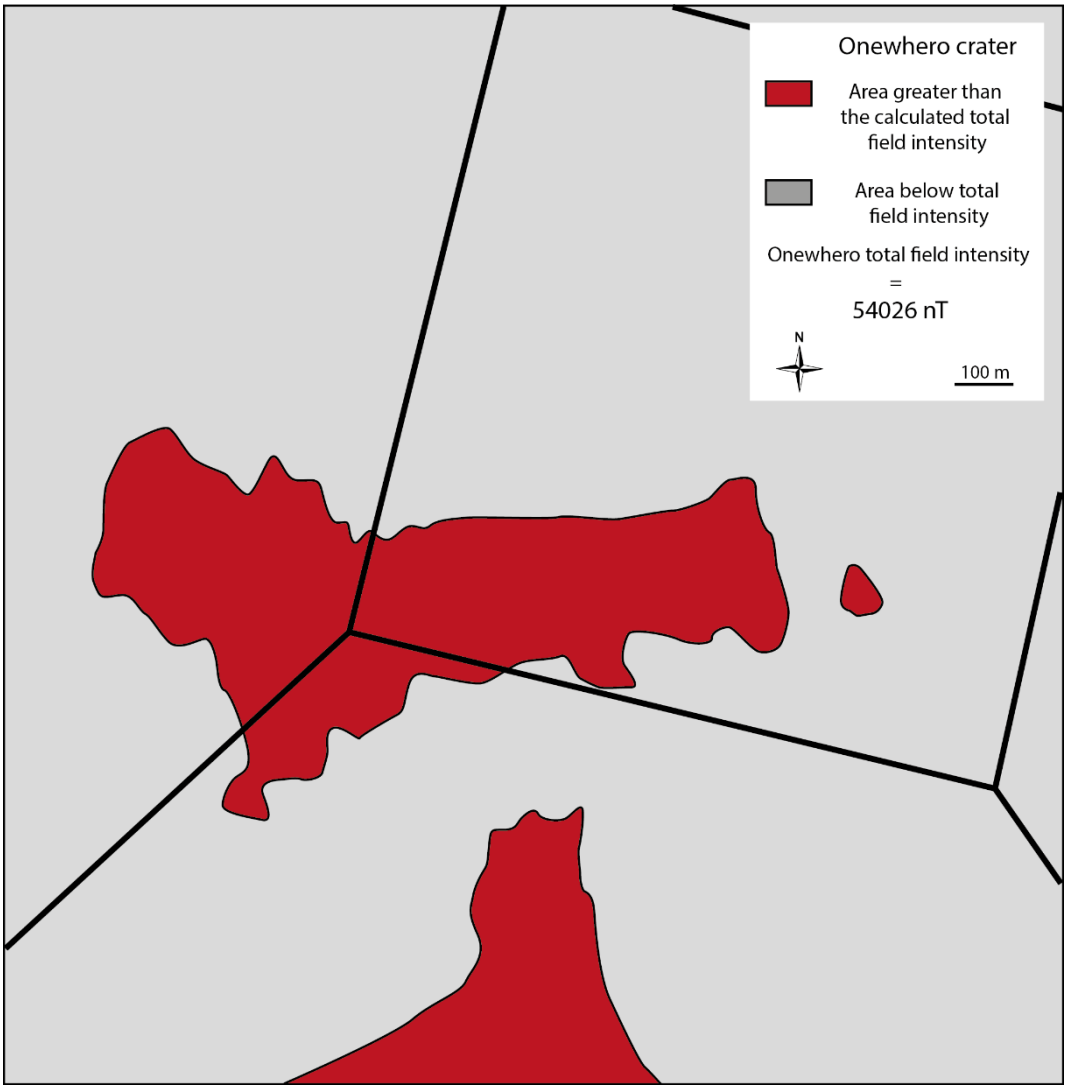

Figure 5.8: A map outlining the area in the Onewhero crater that is above what was calculated as the normal magnetic intensity for the Onewhero region.

5.6 Kellyville magnetic investigation

5.6.1 Magnetic anomaly map

Figure 5.9 is the magnetic anomaly map for the Kellyville Volcanic Complex. There is an elongated high intensity magnetic feature in the west that curves in a crescent shape to the north and south. East of the crescent are scattered regions of very low magnetic intensity. Most of the magnetic features in the Kellyville region have a high wavelength, this suggests that the material producing the magnetic anomaly is located at a shallow depth. Points of interest are outlined in Figure 5.10.

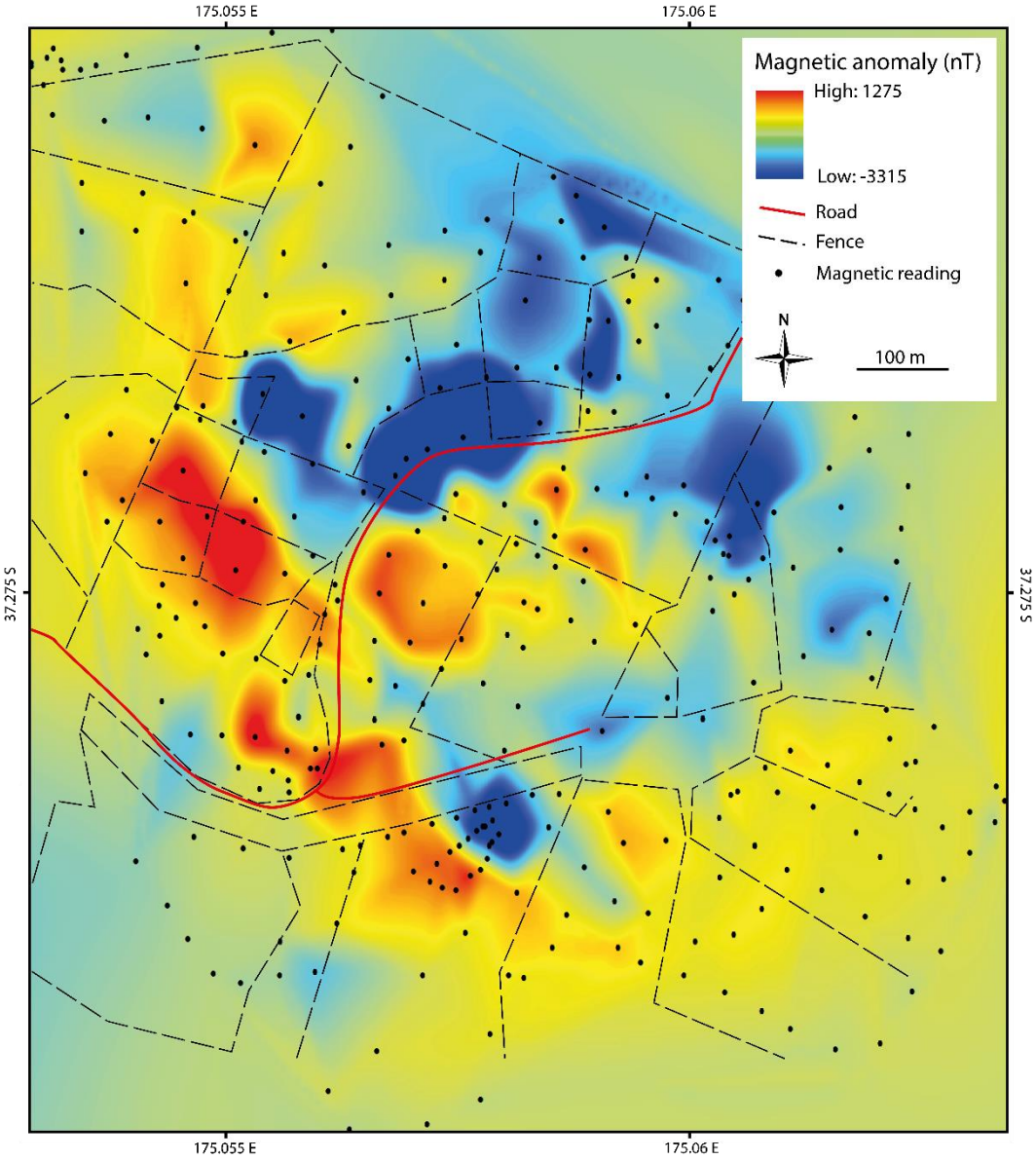

Figure 5.9: A magnetic anomaly map produced using ArcMap, for the Kellyville crater. Magnetic stations are present and there appears to be no significant fence distortion.

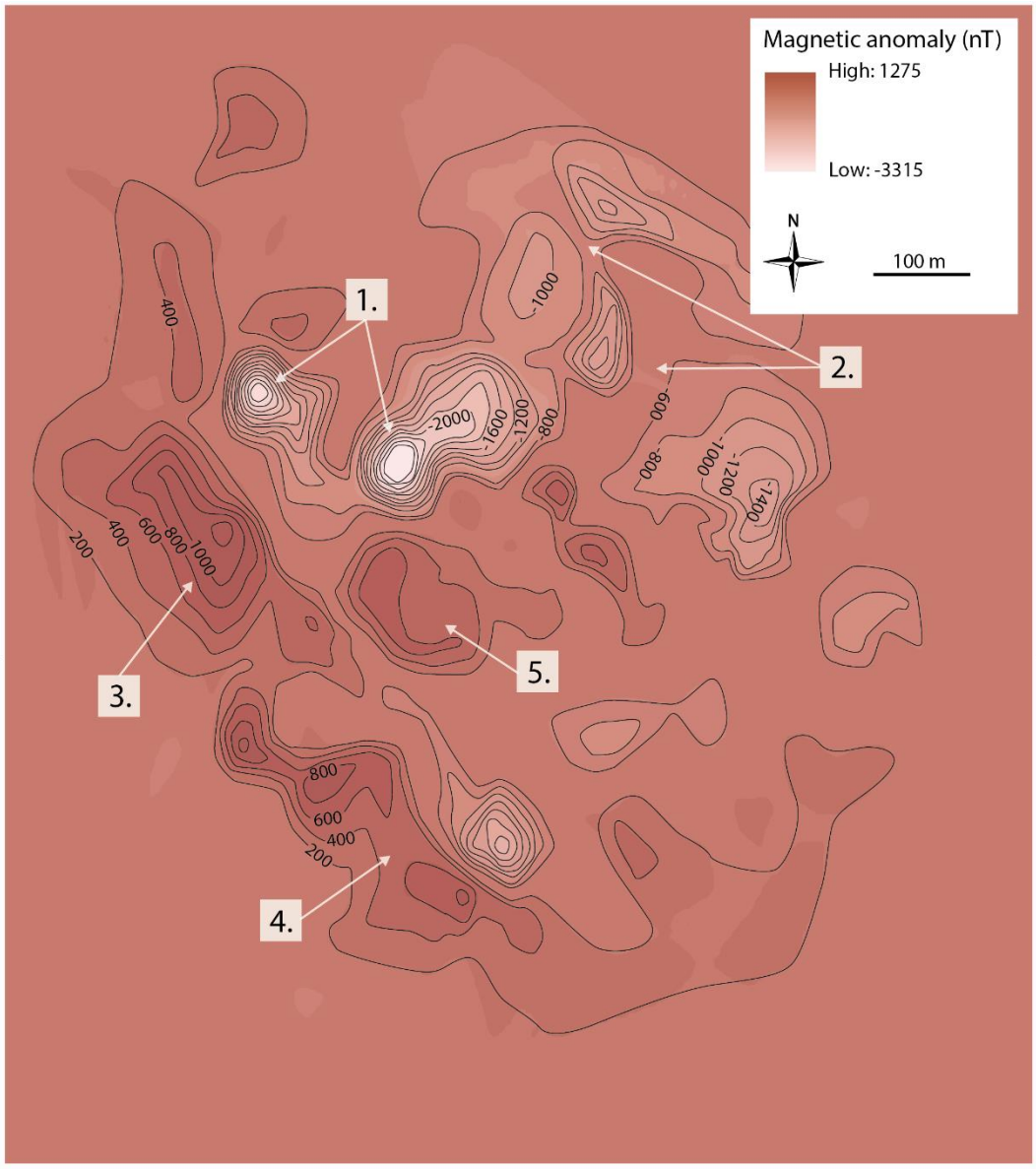

Figure 5.10: A magnetic anomaly map for the Kellyville crater outlining six magnetic observations that will be further described. The main features are highlighted by 200 nT smoothed, best-fit contours that ignore the fence distortion and ArcMap's extrapolation where no data was recorded.

5.6.2 Points of interest

The magnetic survey of the Kellyville crater instantly reveals a map that is much more complex than the Onewhero crater. Five interesting regions have been identified and they will be outlined and interpreted below.

1. The lowest anomaly values in the Kellyville survey are found just north of the centre of the crater. The lowest intensity in this negative magnetic anomaly is -3315 nT.

2. Two ridges that separate areas of low magnetic intensity. These are located in the north-east of the crater.

3. An area with a strong, positive magnetic signal exists slightly to the west of the centre of the crater. The maximum magnetic intensity in this anomaly is 1275 nT.

4. A crescent-shaped magnetic high occurs in the northwest of the crater and swings to the southeast.

5. A positive circular anomaly is found in the centre of the crater, directly to the east of Glass Hill. This anomaly ranges from 200 – 600 nT.

5.6.3 Interpretation of points of interest

1. Several zones of very low magnetic intensity are found around Koheroa Road. This material has a very short wavelength and also has the lowest collective magnetic amplitude of any region in the Kellyville crater. Due to Koheroa Road running through this area of low magnetic intensity and having observed the diatomite outcrop in this region, this negative magnetic anomaly can be confidently attributed to a subsurface layer of diatomite. The diatomite in this region has been studied in detail and this deposit is no more than 8 – 10 m thick (Waterhouse, 1967; Waterhouse, 1980).

2. The ridges of higher magnetic intensity than the surrounding non-magnetic mounds are likely due to the geomorphology of the area. I suggest that these features are caused by erosional gullies that have been cut into the surrounding post-eruption crater infill. This creates a magnetic contrast as the gullies have less lake infill to mask the local magnetic signature of the underlying crater.

3. This magnetically intense feature has a short wavelength that peaks at 1275 nT. This positive magnetic anomaly can be confidently attributed to the Glass Hill scoria cone due to the surface expression of this feature.

4. The crescent-shaped positive magnetic anomaly that stretches north and south of Glass Hill is probably produced by lava flows. Basalt covers much of the Kellyville crater floor, and these are likely to be flows that were deposited in a topographic low and are therefore much thicker than any other lateral flows. Another interpretation is that the elongated magnetic anomaly that travels southwards could be a part of the tuff ring which Colchester (1968) interpreted as curling up from the south almost to Glass Hill scoria cone. However it is unlikely that the amount of fragmented volcanic material in the ejecta ring warrants the magnetic anomaly values (200 – 800 nT) observed in this area.

5. The circular region of high magnetic intensity could be the primary vent. The wavelength of this feature is relatively long and this means it probably occurs deeper than any of the previous anomalies. Geographically, it is located in the centre of the surrounding ejecta ring. Its circular anomaly shape and the long wavelength hint at a vent origin. The bore-hole data outlined in Chapter 3 show thick layers of basalt and scoria in the centre of the crater. The vent is probably plugged with basalt instead of filling with post-eruption sediment which is the opposite of the interpretation made for the possible vent in the Onewhero crater. Another interpretation is that the positive anomaly is being produced by volcaniclastic sediments derived from the erosion of Glass Hill and any other basalt rock in the crater.

5.6.4 Discussion of the Kellyville magnetic investigation

The Kellyville crater is much more magnetically complex than the Onewhero crater. This is clear from the percentage of the crater that is characterised by a positive anomaly (Figure 5.11). The measured magnetic anomalies are much greater than that of the Onewhero crater, and this can be attributed to the volcanic

complexity of the Kellyville Volcanic Complex. It is likely that an even greater percentage of the crater would have a positive anomaly if it were not being masked by the magnetically negative diatomite deposits.

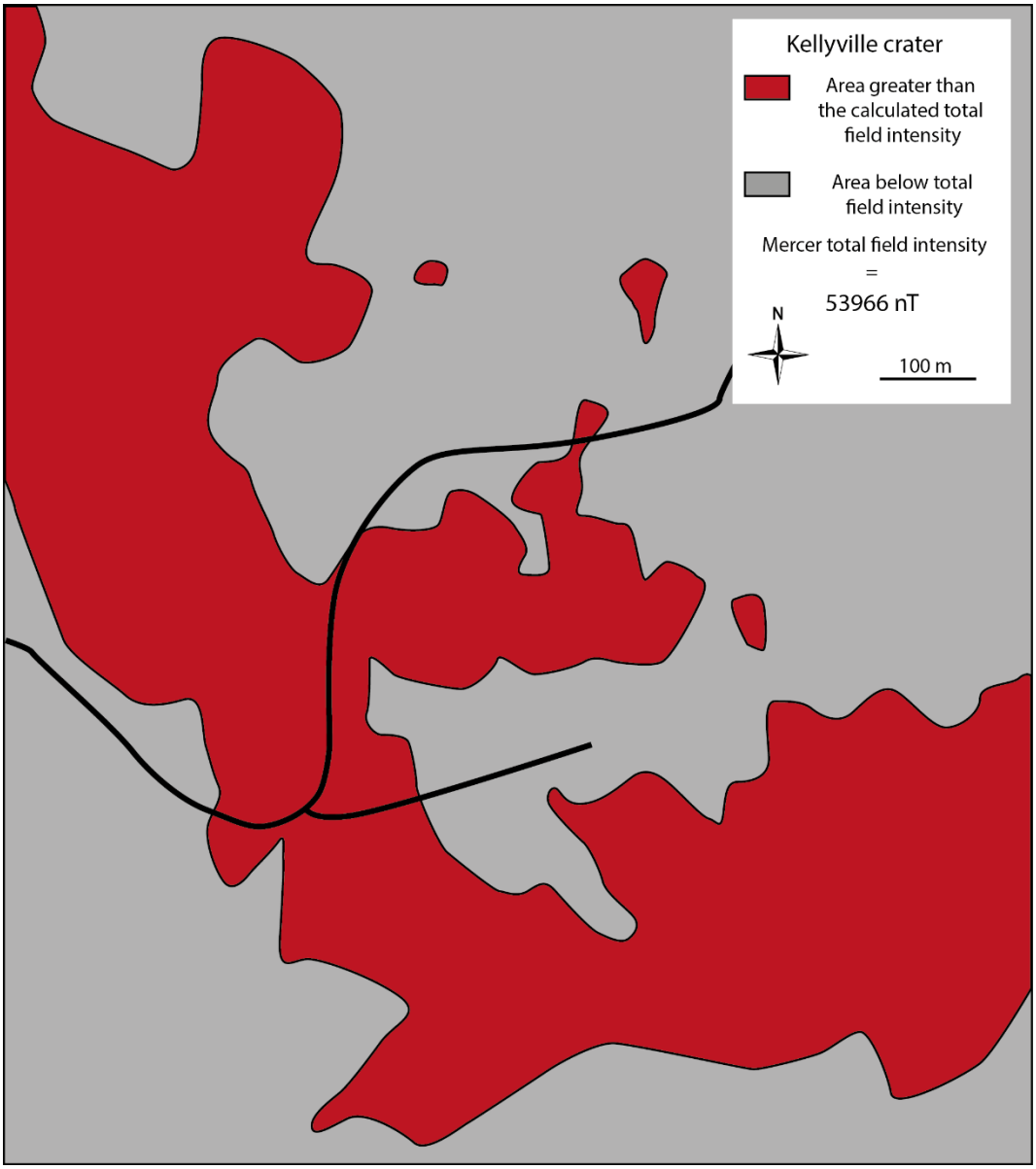

Figure 5.11: A map outlining the area in the Kellyville crater that is above what was calculated as the normal magnetic intensity for the Mercer region.

The magnetic anomaly map (Figure 5.9) reveals a mixture of low and high intensity magnetic features. Due to the erosion of much of the crater infill after the crater breach, some of the magnetic anomalies observed in the Kellyville Volcanic Complex can be confidently attributed to known geological features. These observations then make the interpretation of subsurface anomalies less prone to

error. An example of this is Glass Hill cone. I am reasonably confident that the elongate, highly magnetic positive anomalies in the west of the crater (4.) are produced by deposits of the scoria cone nearby. I am less confident about the position of the vent in the Kellyville crater. The position of the circular magnetic anomaly (5.) in the middle of the crater and the long wavelength characteristics of this features make this interpretation the best fit for the data available.

The extent of high purity, or relative thickness, of diatomite in the Kellyville crater is also made apparent from the magnetic survey. Two regions with a negative magnetic anomaly less than -2000 nT were identified. These areas are likely to be deposits of diatomite that are thicker or of a higher purity than the surrounding post-eruption lake infill.

5.7 Chapter summary

Magnetic surveys of the Onewhero and Kellyville craters were undertaken in the 2014 – 2015 summer. 969 magnetic readings were recorded at Onewhero and 329 magnetic readings were recorded at Kellyville. The measurements were made with a G-856AX Memory-Mag Proton Precession Magnetometer. An effort was made to take readings away from metallic-based objects that could distort magnetic values. Aside from this, no further corrections were required to process the data.

An investigation of the Onewhero magnetic anomaly map yields six interesting features. The most intense positive anomaly belongs to a feature that is interpreted as an extrusive vent or scoria cone. Linked to this vent is a ridge of lower, but still positive, magnetic anomalies that stretch away across the crater to the east. This is interpreted as a lava flow extending out from the dyke-fed vent.

A separate region of high magnetic intensity occurs in the south of the crater and it is suggested that this belongs to the known lava flow that probably originates from the Klondyke cone. The lava flow does not crop out at the surface in the area covered by the magnetic survey, but it is likely that it dips below the younger post-eruption infill and into the magnetic survey area.

The last major magnetic anomaly feature is a very low intensity region towards the north of the crater. The low magnetic anomaly in this area is interrupted by two locally high intensity magnetic readings. The feature as a whole is interpreted as dykes that erupted at the surface, creating a localised depression into which lake sediments were deposited that have a very low magnetic susceptibility.

An investigation of the Kellyville magnetic anomaly map yields five interesting features. Two negative magnetic anomalies occur near the middle of the crater. These are interpreted as being deposits of diatomite with a very low magnetic susceptibility. The evidence of one of the negative magnetic features can be confirmed due to a diatomite outcrop that is cut by Koheroa Road.

Valleys separate many of the low magnetic anomalies. These are interpreted as erosional valleys that formed when the crater was breached and allowed unconsolidated sediment with a negative magnetic susceptibility to be washed out into the river system.

A positive anomaly with a short wavelength feature occurs in the west of the crater. This feature can be identified from the surface; it is the scoria cone known as Glass Hill. Ridges that have a positive magnetic intensity radiate away from Glass Hill and these are interpreted as basalt flows.

The last magnetic feature is noticeably different to anything else observed in the crater. It is a circular region with a relatively long wavelength, this means it probably occurs deeper than any of the other high-intensity magnetic structures. It occurs in the centre of the Kellyville crater and could be the initial eruption vent or a basin of eroded iron-rich sediment.

Chapter Six: Discussion

6.1 Introduction

Chapter 6 consists of five sections. The first section integrates the gravimetric and magnetic geophysical data for the Onewhero and Kellyville volcanic complexes. A final interpretation of the subsurface geology for these two craters will be provided based on the best fit available from the bore-hole data, the gravity data, and the magnetic data. I will also comment on how well the gravimetric and magnetic data supports or obscures each other. The second section will describe and discuss the syn- and post-eruption history for the Onewhero and Kellyville volcanic complexes. Comments will be made on whether these phreatomagmatic centres satisfy the geological conditions needed to classify them as tuff rings or maar volcanoes. The third section will discuss the similarities and differences between the Onewhero and Kellyville volcanic complexes and other phreatomagmatic localities in the nearby Auckland Volcanic Field. In the fourth section I will investigate and discuss similarities and differences between the Onewhero and Kellyville volcanic complexes and selected phreatomagmatic localities in a global context. In the fifth and final section of Chapter 6 I will propose a direction for further studies of the Onewhero and Kellyville craters as well as other volcanoes in the South Auckland Volcanic Field.

6.2 Integration of the gravity and magnetic investigations

The reliability of a subsurface geophysical model can be increased by adding constraints. Many geophysical investigations combine magnetic and gravimetric data to interpret subsurface geology due to the speed and low cost of these surveys (Pirrung et al. 2003; Schulz et al., 2005; Cassidy et al., 2007; Loera et al., 2008; Mrlina et al., 2009; Blaikie et al., 2012; Jordan et al., 2013).

The gravimetric and magnetic data obtained and interpreted in this investigation can be integrated to form best-fit geological models for the Onewhero and Kellyville craters.

At Onewhero the magnetic and gravimetric data supported each other to a mixed degree. Figure 6.1 is an overlay of the Bouguer anomaly with the magnetic values across the X – X' transect in the Onewhero crater. Low density maar sediments are often composed of silica-rich diatomite or oil-shales that do not retain magnetisation (Pirrung et al., 2003). Therefore a two-dimensional profile comparing gravity and magnetic anomalies should show the same general trends. Figure 6.1 outlines this clearly: the low gravity anomaly in the northwest of the crater is mirrored by the low magnetic anomaly in the same area. This area of the crater is a depocentre for low density sediment, and due to the negative magnetic anomaly the sediments must have a low susceptibility to an external magnetic field. Due to the known presence of diatomaceous clay at the surface I can confidently interpret this negative magnetic and gravimetric region as a thick (modelled as 90 – 100 m thick) accumulation of low-density, diatom-rich sediment.

Figure 6.2 is a two-dimensional magnetic and gravimetric profile overlay for the Y – Y' transect. The magnetic and gravimetric results here do not support each other. The gravity anomaly in this profile indicates the presence of low density sediments. The gravity minimum in this profile is -4.5 mGal, compared to almost -6 mGal for the X – X' transect. The change in these minimum values comes from either a difference in the density of the underlying sediment in the area or a difference in the thickness of the sediment body. In Chapter 4, the post-eruption infill body is modelled as the same density throughout, and therefore it is assumed that the sediment is thinner in the Y – Y' transect and this is the reason for the higher Bouguer anomaly. The magnetic profile for this region suggests that the sediment should be composed of material with a higher magnetic susceptibility. The post-eruption infill in the X – X' transect produces a magnetic anomaly ranging from 0 to -1000 nT but in the Y – Y' transect the values range from about 50 to -200 nT. This could be due to ferrimagnetic material below the post-eruption infill or alternatively the post-eruption infill in this region of the crater could contain a higher percentage of sediment derived from the ejecta ring or the nearby basalt.

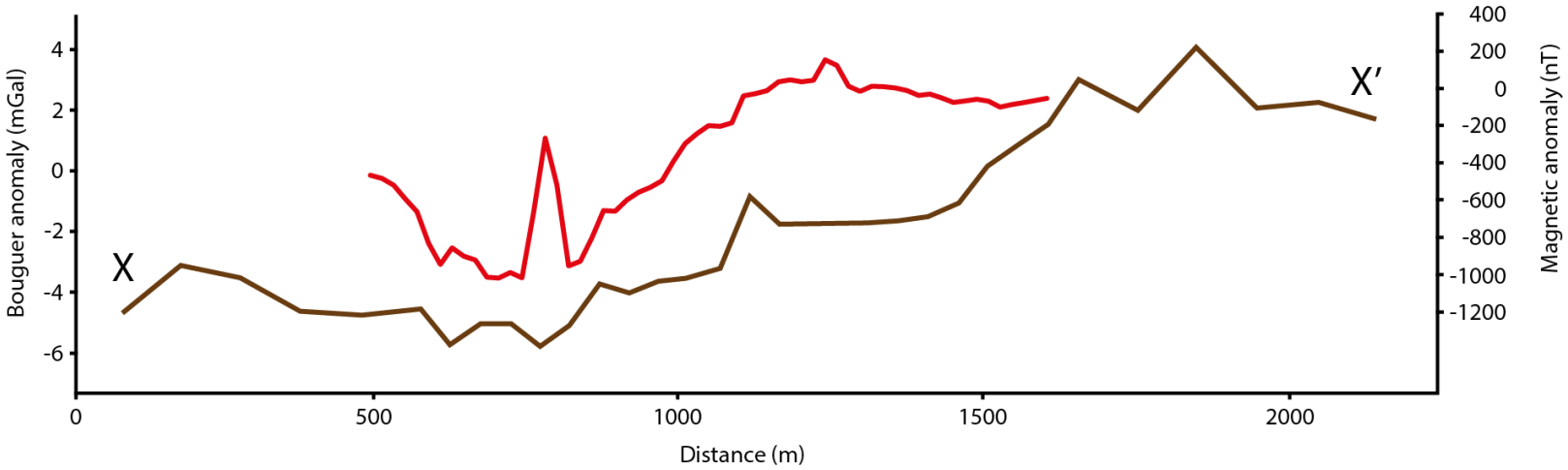

Figure 6.1: The X – X' Bouguer anomaly (Onewhero) overlain with the magnetic anomaly (red line) for the same transect.

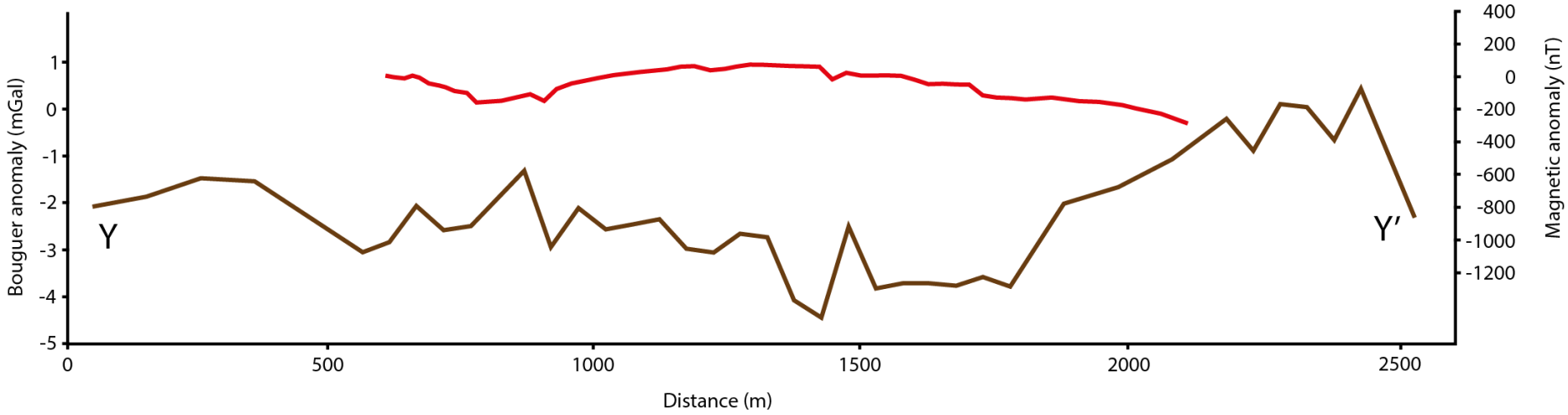

Figure 6.2: The Y – Y' Bouguer anomaly (Onewhero) overlain with the magnetic anomaly (red line) for the same transect.

At Kellyville the magnetic and gravimetric data support each other to a mixed degree. Figure 6.3 is an overlay of the Bouguer anomaly with the magnetic values across the X – X' transect that crosses the Kellyville crater in a west to east direction. In this profile the geophysical data is complementary: in general the highs and lows of the magnetic and Bouguer anomalies follow the same trends. The magnetic anomalies in the X – X' transect appear to support the presence of a thick basalt body that is overlain by low density sediments that are diamagnetic. Between 400 m and 600 m, Glass Hill scoria cone is present as a peak in the maximum Bouguer and magnetic anomalies. Both of the anomalies decrease after leaving the slopes of Glass Hill as they cross over the known diatomite deposit that is dissected by Koheroa Road. Figure 6.4 is a Bouguer-magnetic anomaly overlay for the Y – Y' transect that traverses the Kellyville crater in a north to south direction. The gravimetric and magnetic anomalies do not correlate as well as in Figure 6.3, although the general trends can still be made out. Between 300 m and 700 m, the Bouguer and magnetic anomalies both gradually increase. The increase in this region is interpreted in the two-dimensional gravity modelling as the start of subsurface basalt or basalt-derived sediment, probably originating from Glass Hill. The Bouguer-magnetic anomalies begin to decline again at 1200 m as the transect leaves the other side of Glass Hill and any of its volcanic products. The steep trench in the magnetic anomaly at 750 m is due to a deposit of negatively magnetised material that lies north-northeast of Glass Hill. This deposit is located in close proximity to the main diatomite outcrop and has a very similar negative magnetic anomaly. The two diamagnetic sediment bodies are probably very pure deposits of diatomite.

In this investigation, the creation and interpretation of a geological model for both the Onewhero and Kellyville volcanic complexes has been aided by integrating existing bore-hole data with gravimetric and magnetic surveys. Each layer of geological/geophysical data has strengthened the geological models for the two craters.

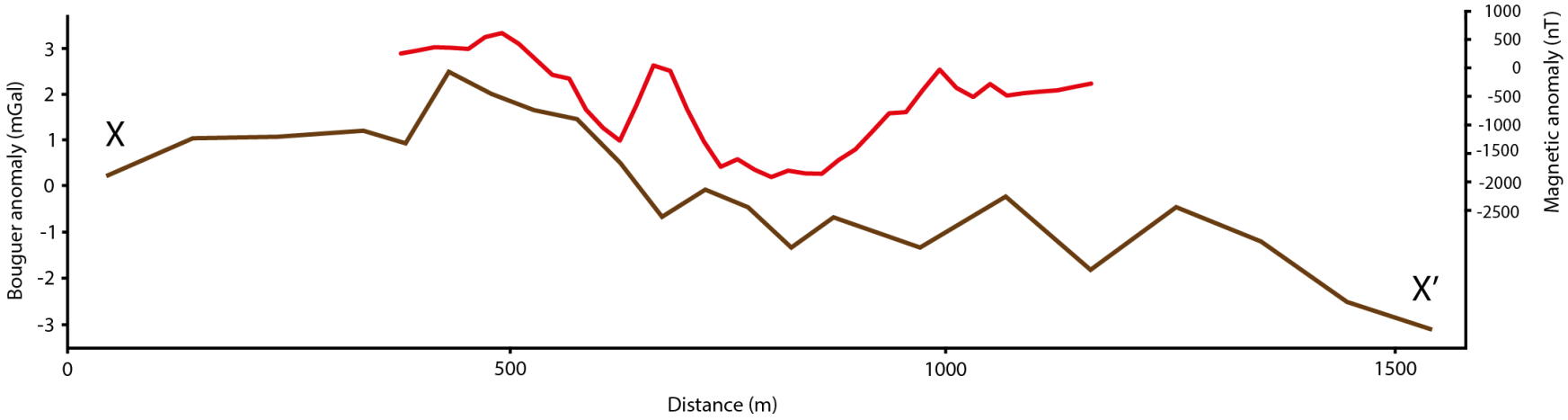

Figure 6.3: The X – X' Bouguer anomaly (Kellyville) overlain with the magnetic anomaly (red line) for the same transect.

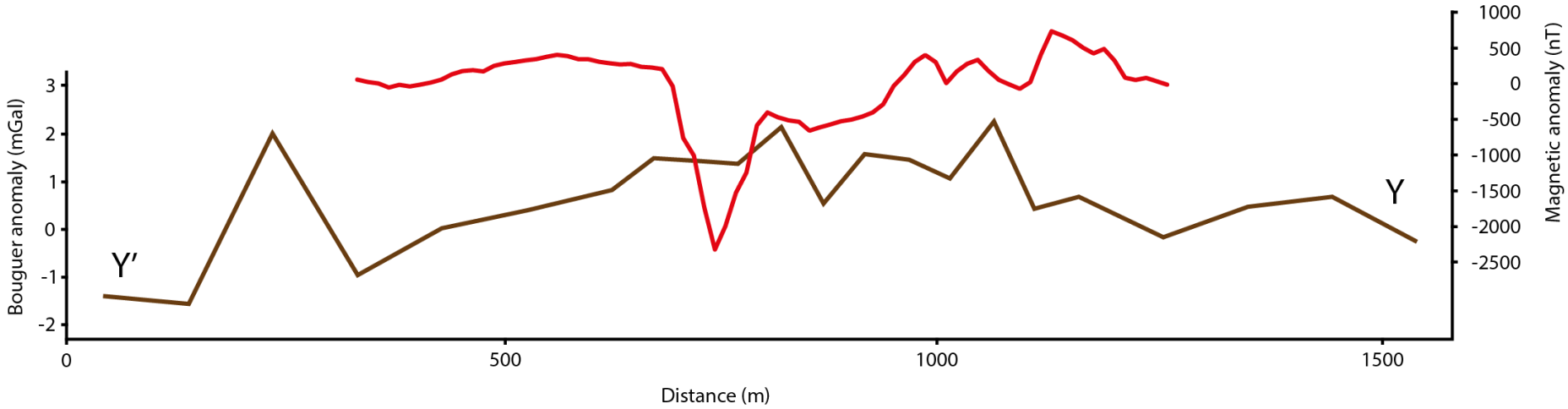

Figure 6.4: The Y – Y’ Bouguer anomaly (Kellyville) overlain with the magnetic anomaly (red line) for the same transect.

6.3 Structure of the Onewhero Volcanic Complex

The Onewhero Volcanic Complex appears to be structurally simple compared to other maar volcanoes (e.g., Blaikie et al., 2012; Jordan et al., 2013). Although it is not as complex as the Kellyville Volcanic Complex, the model relied on three constraints, and even then the geological model still has plenty of room to improve. The overall structure of the Onewhero Volcanic Complex has been defined by interpreting existing bore-hole data, and by studying Bouguer and magnetic anomalies.

Bore-hole, gravimetric, and magnetic data all unambiguously indicate the occurrence of a significant body representing post-eruption infill, that in localised areas, if not all areas, of the crater contains diatom-rich sediment. The post-eruption infill is characterised by a 0 – -6 mGal Bouguer anomaly and has a modelled thickness of 30 – 80 m in the majority of the crater and a maximum modelled thickness of 110 m in the northwest of the crater.

A less well constrained geological body occurs in the middle of the crater. It was suggested in Chapter 5 that this structure is volcanic in origin, as it has a detectable magnetic anomaly that peaks at a maximum of 213 nT. The body does not clearly appear in the Bouguer anomalies and bore-hole data in the area is not available. All evidence is consistent with this body being a secondary feeder-dyke that has produced topography-controlled lava flows.

A third geological body in the Onewhero crater was identified in the bore-hole data and the gravity and magnetic surveys. Lava flows from the Klondyke cone have infilled the topography between the two volcanic centres and have spilled over the Onewhero ejecta ring and onto the crater floor. It is inferred from positive magnetic anomalies that the flows have either been partially submerged by post-eruption deposition or the anomalies represent concentrations of lava-flow-derived sediment.

6.4 Geological history of the Onewhero Volcanic Complex

6.4.1 Phase 1: Main vent initiation

Rising basaltic magma intersected ground or surface water sometime before 0.88 ± 0.06 Ma in the Onewhero region, creating plumes of fragmented ash and country rock lithics (Figure 6.5). Hypersthene, quartz, and plagioclase lithic clasts in the resulting ejecta ring suggest that the initial phreatomagmatic eruption occurred close to sea level in an alluvial river system, although these minerals are also common in mafic magma (Briggs et al., 2010; Gibson, 2011). As the volcanic eruption progressed, the feeder dyke grew deeper and incorporated underlying country-rock lithic clasts. Base-surges derived from efficient magma fragmentation continued to accumulate around the vent producing a tuff ring (Gibson, 2011).

6.4.2 Phase 2: Secondary vent initiation

The elliptical shape of the ejecta ring raises doubt that the complex followed the conventional single-vent maar eruption. The elongated geometry of the tuff ring was probably influenced by a second nearby vent, and evidence for this was found in the magnetic survey of the crater (Figures 6.1; 6.2; 6.6). The magnetic survey also outlined a large circular negative anomaly in the north of the crater. This main vent would have produced the majority of the erupted tephra. It is possible that the second feeder dyke produced a dry eruption because the already existing ejecta ring had inhibited the flow of surface water in the crater which was previously located in a deltaic/lowland river environment. It is also possible that either of the vents migrated through the country rock at an angle (instead of vertically), forcing tephra to concentrate south of the vent (Loera et al., 2008). After exhausting the groundwater supply, it appears as though a secondary feeder-dyke has produced a small scoria or spatter cone with thin, topography-controlled lava flows (Figure 6.7).

6.4.3 Phase 3: Klondyke cone formation

A rising magma source on the outer southern slopes of the Onewhero maar's ejecta ring produced a dominantly dry eruption that consisted mainly of basaltic lava flows (Figures 6.7; 6.8) (Briggs et al., 1994). This vent is now known as Klondyke cone and K-Ar dating reveals an age of 0.88 ± 0.06 Ma (Brigg et al., 1994). The magma

volume erupted at this vent was reasonably large and after some time the lava flows filled in the surrounding topography, and an unknown number of flows entered the Onewhero tuff ring and cooled on the crater floor (Figure 3.11). As basalt samples from this lava flow were K-Ar dated (dating was meant for the Onewhero tuff ring) and this means the Onewhero tuff ring is probably undated (Briggs et al., 1994). Simultaneous to the formation of the Klondyke cone, the Onewhero maar would have been quickly filling with surface water, as no outflow through the tuff ring existed. Diatoms flourished in the calm waters of the lake and the lake was deepest in the north of the crater about the primary vent. In the deepest reaches of the lake, the water may have been anoxic and the diatom frustules preserved in a reducing environment (Pirrung et al., 2003).

6.4.4 Phase 4: Post-eruption sedimentary fill

Immediately after the Onewhero tuff ring formed and for some decades after the eruption, weathering processes worked to destabilise the fresh ejecta ring and mass-wasting would have deposited layers of reworked tephra and gravel on the crater floor (Figure 6.9) (Pirrung et al., 2003). The reworked tuff and gravel has been characterised in the gravity modelling as having a density of 2.2 g/cm^3. Simultaneously, a lake environment would have been forming as the fresh ejecta ring prevented water outflow. The crater-lake was probably anoxic at depth and this would have allowed mats of diatoms to be deposited in a reducing environment. The thickest deposits of diatom-rich clay occur in a circular basin in the north of the crater. The modelled maximum thickness of this deposit was 110 m. The build-up of diatom-rich lacustrine sediment would have occurred over thousands of years, all the while being mixed with silts, sands, and gravels of the continually degrading ejecta ring (Pirrung et al., 2003). Bore-holes that dissect the crater's marginal facies all encounter plant-rich sediment in the form of peat. Terrestrial, biogenic inputs are known to signal the end of a maar lake's cycle, and this was the last major phase in the evolution of the Onewhero crater (Pirrung et al., 2003).

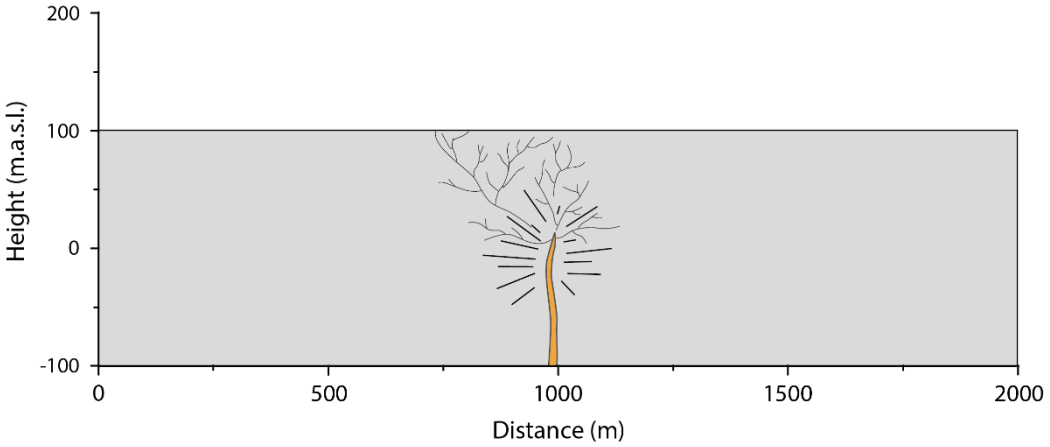

Figure 6.5: Onewhero geological history, phase 1. Rising basaltic magma explodes when it encounters ground or surface water, shattering the surrounding country rock.

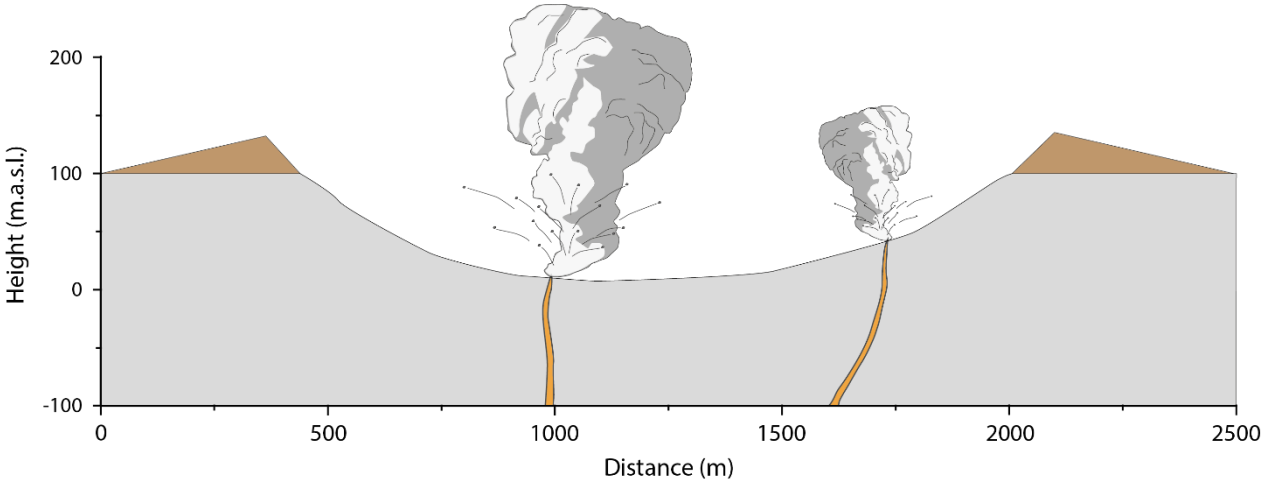

Figure 6.6: Onewhero geological history, phase 2. The primary vent deepens and widens creating a large tuff ring around the diatreme. Initiation of a secondary feeder dike.

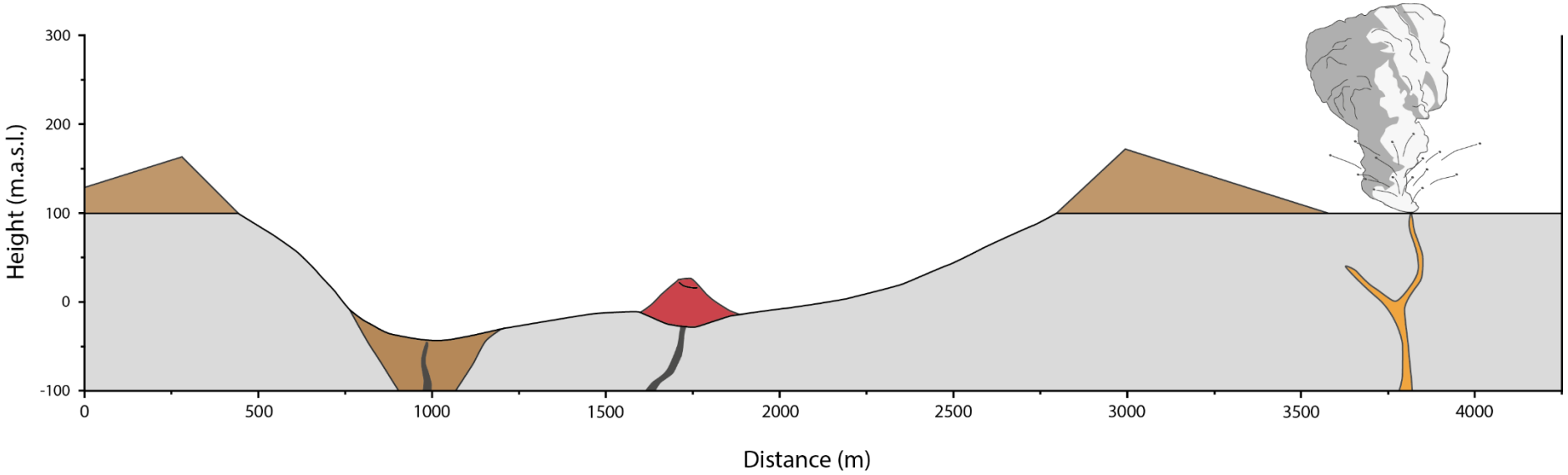

Figure 6.7: Onewhero geological history, phase 3. A small scoria cone forms in the crater as ground/surface water retreats and magma keep rising. The surrounding ejecta ring fails and breccia-gravels are deposited on the crater floor via debris flows and slumps. To the south the Klondyke vent initiates.

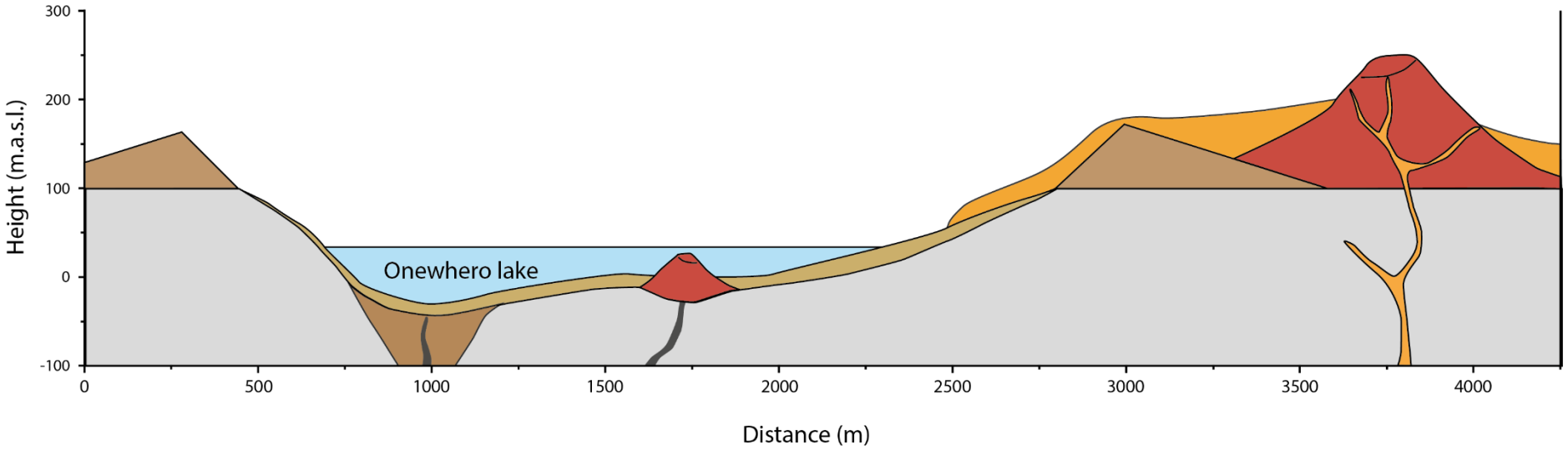

Figure 6.8: Onewhero geological history, phase 4: Klondyke cone grows into a large scoria cone, the lava has a low viscosity and infills the surrounding topography, eventually it flows over the top of the Onewhero maar's ejecta ring and hardens on the crater floor. A maar lake forms and biogenic clays and silts are deposited on the lake floor. Light brown crater infill represents gravel and sands eroded from the fresh tuff ring.

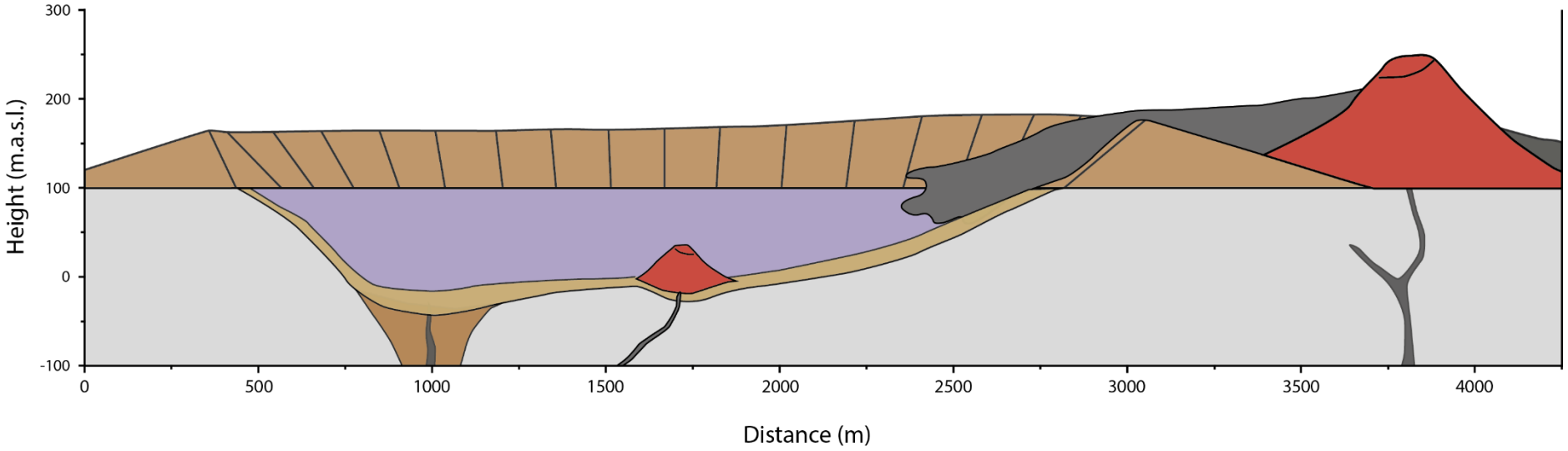

Figure 6.9: Onewhero geological history, phase 5. After hundreds of thousands of years >100 m of diatomaceous sediment and reworked tephra fill the crater (purple). The maar lake is shallow, reeds and riparian plant species flourish. Thin layers of peat form around the edges of the crater, signalling the end of the maar lakes life.

6.5 Structure of the Kellyville Volcanic Complex

The geological complexity of the Kellyville Volcanic Complex is apparent at the surface. A breached crater, a nested scoria cone and a diatomite road-cutting are all noticeable surface features. In this investigation, a geological model has been created to interpret and define the structure of the Kellyville Volcanic Complex by integrating bore-hole data and Bouguer and magnetic anomalies.

The bore-hole data, Bouguer and magnetic anomalies in the Kellyville crater reveal a subsurface that is characterised by thick accumulations of hard, fine-grained to scoriaceous basalt. The basalt deposits dominate the Bouguer anomaly, producing a convex gravity profile, with a maximum of 2.2 mGal, which differs from the normal concave anomaly that characterises a maar. The maximum modelled thickness of the basalt is 65 m. In the bore-hole data it reaches a maximum thickness of 60 m. Gibson (2011) described a 2.6 m high exposed scoria section as a second nested scoria cone (School Hill). In this study the absence of a strong, positive magnetic anomaly in this area is not consistent with a cone. The scoria outcrop is a lava flow deriving from Glass Hill scoria cone, or from the now hidden initial vent. The "lake" of lava that is revealed in MB5 could be located in any part of the primary diatreme or it could belong to lava flows from Glass Hill scoria cone that have accumulated in a massive depression, also possibly relating to a diatreme structure. Colchester (1968) noted that soils south of Koheroa Road were a distinctive red-brown colour. The soils underlie the pumiceous silts that cover most of the crater floor and it has been suggested that these red-brown clays have formed on top of weathered basalt, which is consistent with the Bouguer and magnetic anomalies in this investigation.

The post-eruption infill in the Kellyville crater is composed of medium- to high-purity diatomite with interbedded Taupo Volcanic Zone pumiceous sands and reworked ejecta ring tuff. The distribution of this material is patchy due to the crater breach in the west that allowed the crater to be drained. Consequently the crater floor was open to flooding from the surrounding low-lying riverine environment. The magnetic survey proved a useful tool in the Kellyville crater and the purest diatomite deposits could be outlined due to their incredibly low susceptibility to a magnetic field. According to the magnetic survey, two zones of high-quality

diatomite occur in the road-cutting section and just to the northeast of Glass Hill scoria cone.

6.6 Geological history of the Kellyville Volcanic Complex

6.6.1 Phase 1: Basalt cone formation

Glass Hill cone appears to have been created at some point near the start of the eruption. This is inferred from two observations (Figures 6.10; 6.11). Firstly, in the bore MB2, basalt lava flows lie almost directly on Koheroa Siltstone. If Glass Hill cone was a late-stage volcanic product the lava flows would have been emplaced upon or blocked by tuff deposits. Secondly, mantling Glass Hill on its western slope is a massive to weakly bedded tuff deposit that has the same characteristics as the Kellyville ejecta ring. The mantling suggests that the cone was in place before the majority of the tephra was erupted. The feeder dyke beneath Glass Hill must have supplied lava at a rapid rate to have been able to produce a basalt cone in what was probably a seasonally flooded lowland environment. A mixture of hawaiian and strombolian eruption styles quickly created the Glass Hill edifice. Colchester (1968) noted that the majority of Glass Hill is fine-grained basalt with vesicular scoria only occurring on the outer slopes of the cone. The fine-grained basalt has a low gas content and its low viscosity allowed the flows to move some distance from the vent. This was mapped in the Kellyville magnetic survey.

6.6.2 Phase 2: Main vent initiation

Shortly after the formation of the cone, or simultaneously, the main vent began to form (Figures 6.11; 6.12). The main vent erupted 300 m to the east of Glass Hill and initial explosions were shallow and efficient, with a high degree of fragmentation (Wohletz and Sheridan, 1983; Gibson, 2011). An ejecta ring started forming around the main vent that consisted mostly of juvenile material with a low quantity of lithics. I suggest that the height and width of Glass Hill influenced the thickness of the tuff ring behind the scoria cone. The >50 m hill would have diverted base surges, weakening and thinning the ejecta ring and allowing it to be easily breached later on. Towards the end of the phreatomagmatic activity, the vent

deepened and the explosions started incorporating more country rock. Lithic percentages in the expelled tuff reached over 30% in these stages (Gibson, 2011).

6.6.3 Phase 3: Lava-lake/basalt plug formation

The volume of magma exceeded the quantity of water needed for efficient fragmentation somewhere near the end of the eruption. This allowed lava to spill out into the crater floor where is pooled into thick scoriaceous to fine-grained basaltic deposits that were created by strombolian and hawaiian eruption styles (Figure 6.13). This is particularly evident in MB4: this bore reveals a deposit of alternating scoriaceous-fine grained basalt that is 60 m thick.

6.6.4 Phase 4: Post-eruption sedimentary fill

The sedimentary fill history of the Kellyville crater begins with the deposition of fine rhyolitic sands of the Karapiro Formation (Colchester, 1968). Colchester (1968) describes the sands as pumiceous and massive and they are noted as occurring up to 50 feet thick. The Karapiro Formation was deposited in the crater by the river system of the time, which means the weakened tuff ring was breached shortly after volcanic activity ceased. A shallow lake formed and this allowed diatoms to flourish in its calm, shallow waters (Figure 6.14). The deposition of diatomite at the bottom of the lake was frequently disrupted by flooding events from the nearby river which brought thin layers of pumice-rich sediment to lie on the lake bed. The diatomite at Mercer is also high in organic matter, which suggests that the lake was shallow and the crater was filled with vegetation (Pirrung et al., 2003).

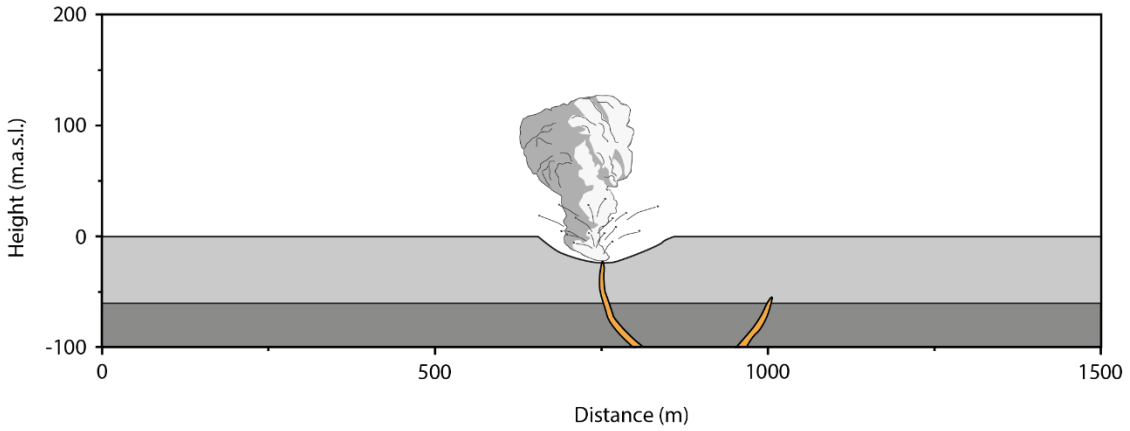

Figure 6.10: Kellyville geological history, phase 1. Glass Hill vent initiates as fast rising magma produces a magmatic eruption.

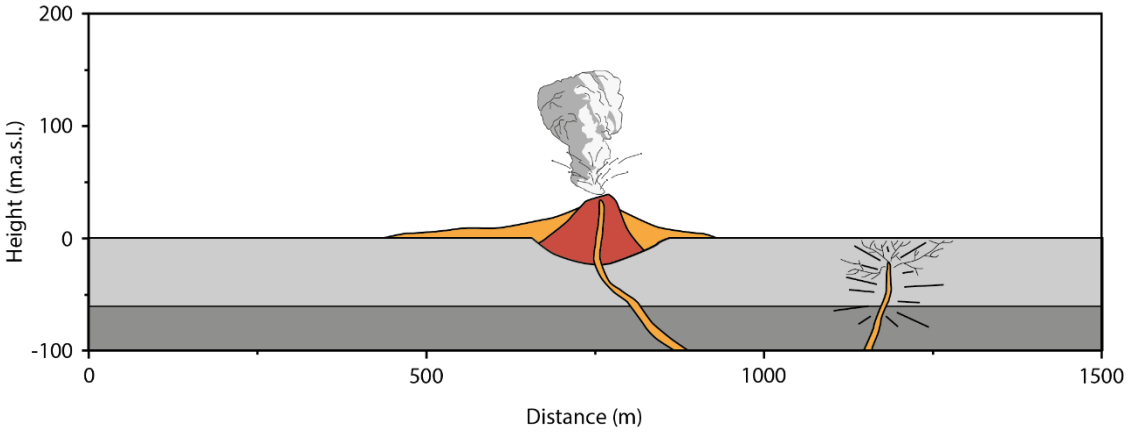

Figure 6.11: Kellyville geological history, phase 2. Glass Hill cone grows in size as low viscosity basalt flows away from the vent. The main, central vent initiates, fracturing the surrounding country rock.

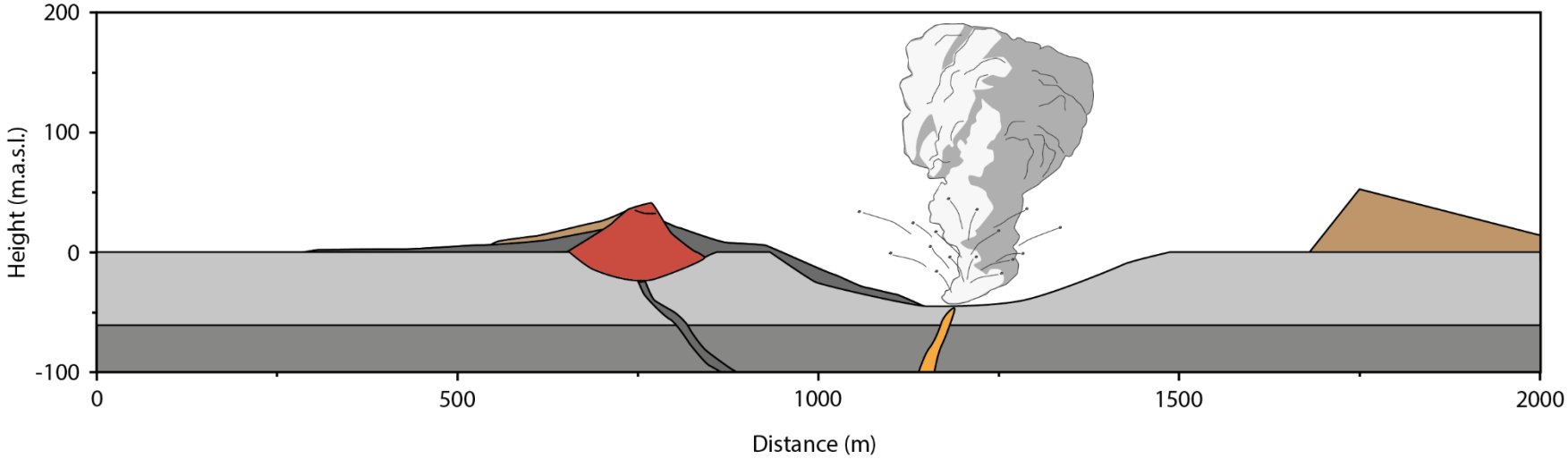

Figure 6.12: Kellyville geological history, phase 3. The main, central crater excavates country rock and the fragmented tephra builds up around the vent.

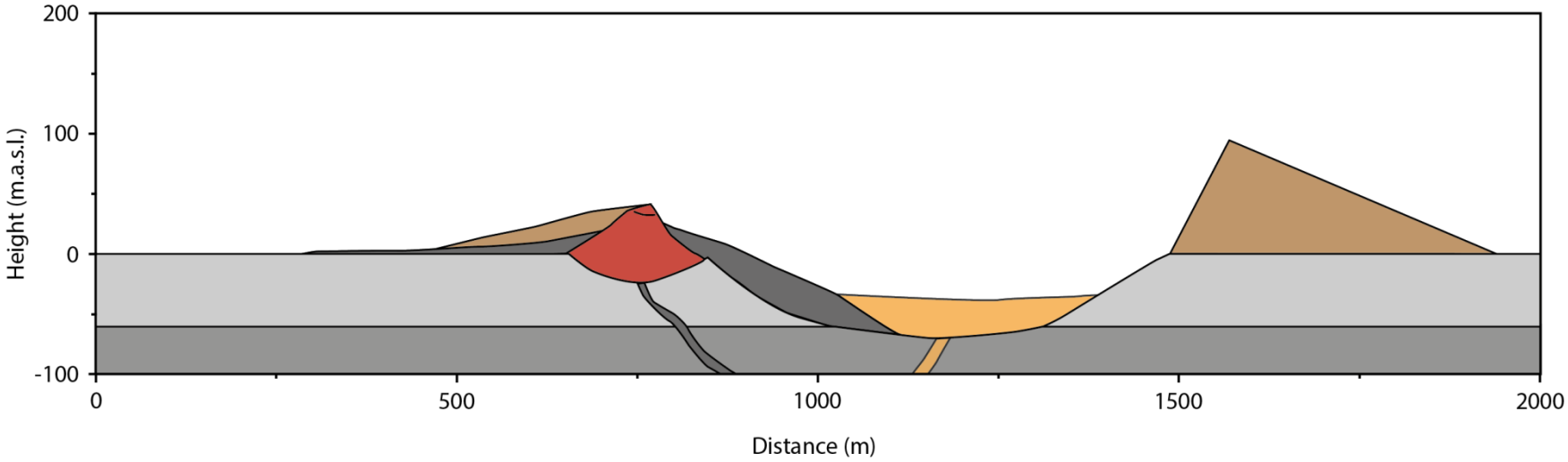

Figure 6.13: Kellyville geological history, phase 3. Inefficient eruptions begin as rising magma outweighs surface/groundwater. Lava ponding occurs above the diatreme.

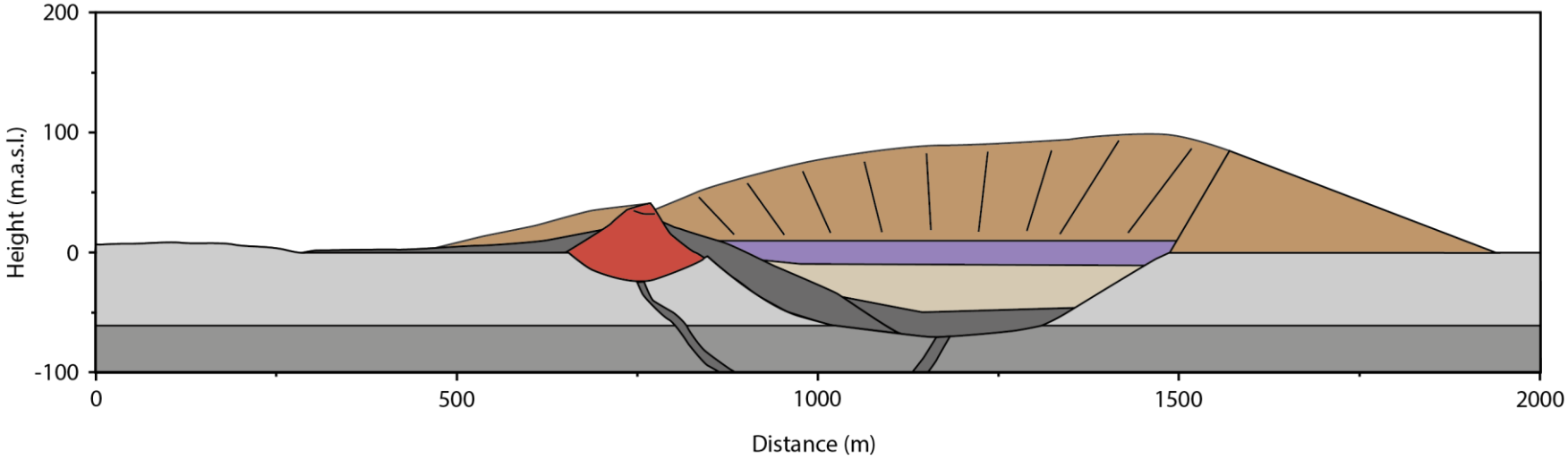

Figure 6.14: Kellyville geological history, phase 4. Pumiceous sediment (tan) of the Karapiro Formation from the Taupo Volcanic Zone is deposited onto the crater floor every time the nearby river floods. Eventually a shallow lake forms in the crater and diatoms flourish, creating a thin deposit of diatomite (purple) over time.

6.7 Maars or tuff rings?

Maar volcanoes and tuff rings are notoriously difficult to distinguish in some cases, due to the potential for a crater to evolve through both styles. However, in general, the following characteristics are more frequently possessed by maar volcanoes:

- A high percentage of country rock fragments in the ejected tuff. This is due to the diatreme initiating at depth, expelling large quantities of country rock to be included in the ejecta ring as xenoliths (Lorenz, 1973; Francis and Oppenheimer, 2004; Carey and Houghton, 2010).

- Maar volcanoes are usually negative relief landforms. The development of the diatreme at depth expels country rock and creates unstable vent walls which periodically collapse in on themselves, creating a deep pit. When the magma source recedes, the crater can collapse even further into the empty chamber. It is common to see the country rock in the crater wall of a maar volcano due to these eruption processes (Lorenz, 1973; 1986; 2003).

- Crater lakes are common occurrences in maar volcanoes due to the low or negative elevation. If the conditions are right in the lake, diatoms will flourish and their frustules will settle out of suspension to form diatomite. The lake infill deposits can be protected for long periods of time as the surrounding ejecta ring provides shelter against weathering and erosion processes.

Tuff rings generally possess subtly different characteristics:

- A high percentage of fragmented juvenile material compared to country rock lithics. Eruptions that form tuff rings tend to initiate at the surface or at shallow depths. The diatreme does not migrate downwards and therefore country rock lithics are poorly represented in the ejecta.

- Tuff ring explosions generally create a shallow crater with a thick ejecta ring that has roughly equal inner and outer slope angles (Cas and Wright,

1987). The crater is often at the same elevation or higher than the surrounding environment.

- Tuff rings often form nested scoria cones and effusive flows when surface water runs out (Cas, 1989).

6.7.1 Is the Onewhero crater a maar or a tuff ring?

The Onewhero Volcanic Complex is commonly referred to as the Onewhero tuff ring although the crater is characterised by features commonly observed at both maar volcanoes and tuff rings (Briggs et al., 1994; Gibson, 2011). The crater has a diameter that ranges from 2 – 2.5 km wide with an elliptic shape. This is quite large for a maar, but larger maar craters do exist (Jordan et al., 2013; Otterloo et al., 2013; Blackfield et al., 2014).

The ejecta ring that encompasses the Onewhero crater is composed of a mixture of ash, fragmented scoria, olivine crystals, and country rock lithics. In a lithological investigation by Gibson (2011), it was found that only 5 – 20% of the ejecta ring was composed of country rock material, which is low for a maar-forming eruption (Figure 6.15).

Gibson (2011) also noted inner slope angles of 14 – 25° and outer slope angles of 6 – 7°. These slope angles are consistent with a maar-formed ejecta ring, but this is not a fair representation, as the tuff ring at Onewhero has had more than 0.88 ± 0.06 Myr of ejecta ring deterioration. The elevation of the crater floor ranges from about 99 – 111 m, due to inferred Quaternary displacement across the nearby Waikato fault. The elevation of the topography surrounding the crater ranges from 100 – 200 m. Even if the initial eruption occurred at close to sea-level, the two-dimensional gravity modelling revealed an eruption crater that was up to 120 m deep before sedimentary infill. It was shown earlier in this investigation (section *3.2.5*) by the presence of diatomaceous sediment found in the crater that a lake formed some time during the post-eruption period. The ejecta ring slope angles, negative elevation of the original crater floor, and presence of a crater lake are consistent with a maar-forming eruption.

On a geological map for the Onewhero region (Waterhouse, 1978) an outcrop of Whaingaroa Siltstone appears on the inside of the tuff ring in the southwest of the crater. If this is reliable, it means that much of the crater floor is below the original surface. This is probably the best physical evidence for confirming whether or not a phreatomagmatic landform is a maar volcano or a tuff ring. If Waterhouse (1978) is correct in his observations I am confident in proposing that the Onewhero crater is a maar until further evidence to the contrary.

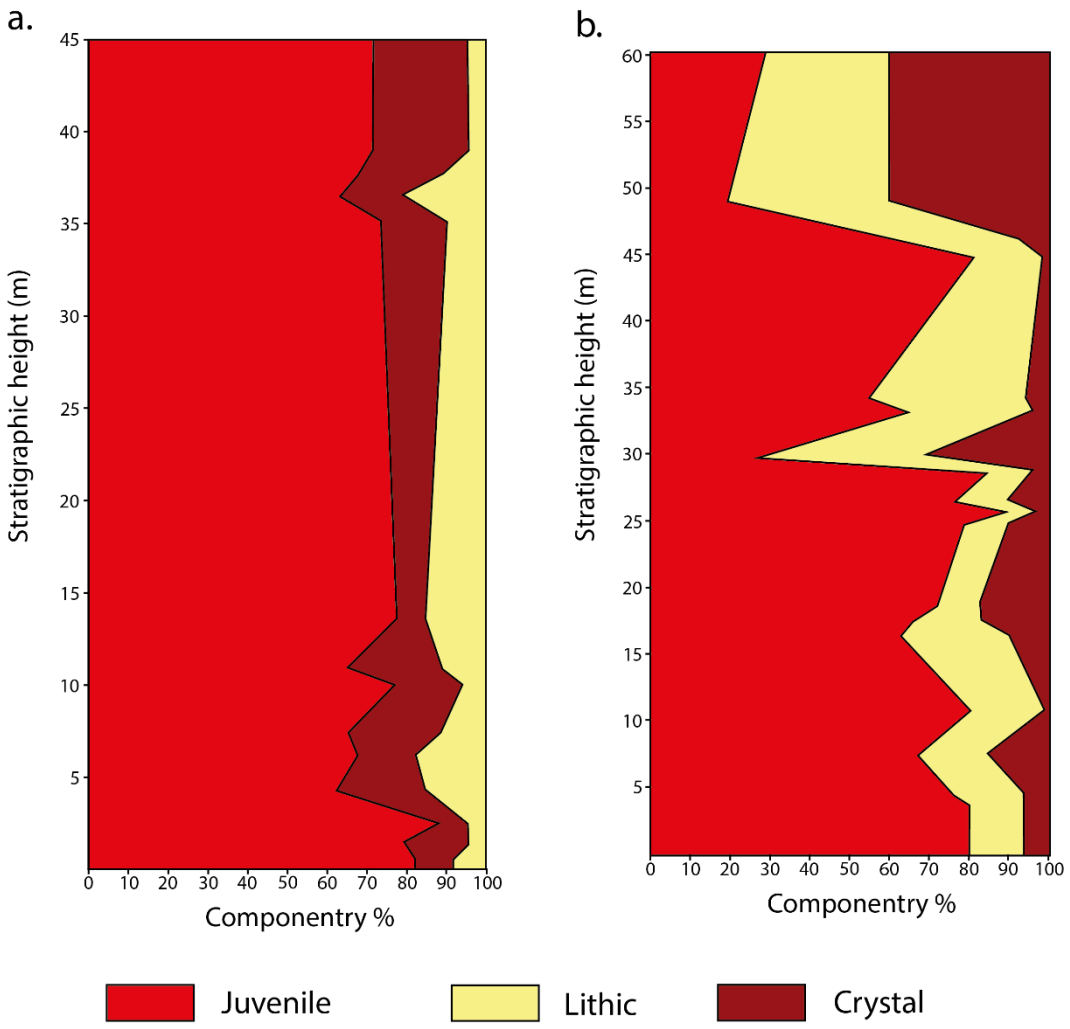

Figure 6.15: Physical components of the Onewhero (a.) and Kellyville (b.) tuff rings (Gibson, 2011).

6.7.2 Is the Kellyville crater a maar or a tuff ring?

The Kellyville Volcanic Complex is commonly referred to as the Kellyville tuff ring, although the crater has features consistent with both a maar and a tuff ring (Briggs et al., 1994; Gibson, 2011). The crater has a diameter that ranges from about 1 – 1.5 km wide.

The base of the ejecta ring at Kellyville is dominated (80%) by juvenile material (Figure 6.15). There is a trend of increasing crystal and lithic content up through the tuff deposits with the crystal and lithic content increasing markedly to the point where lithics make up almost 50% of the tuff ring (Gibson, 2011). This could be due to the diatreme deepening and incorporating more country rock. The percentage of lithics in the Kellyville tuff is far more consistent with a maar-forming eruption than that of the Onewhero tuff.

Gibson (2011) noted an inner slope angle of 10° and outer slope angles of 7 – 9°. These angles are very similar, and this, combined with a minimum tuff ring height of 92 m, is compelling evidence for the presence of a tuff ring.

The argument for the presence of a maar is just as strong. A crater lake was present sometime after the eruption, as confirmed by an outcrop of pure diatomite. Colchester (1968) also identified the Mercer Sandstone in outcrop, lying unconformably beneath the pyroclastic deposits. The two-dimensional gravity modelling revealed a crater-fill of basalt that reaches a thickness greater than 60 m. This suggests that the eruption cut considerably into the pre-eruptive surface. These three pieces of evidence are all consistent with maar-forming eruptions.

The evidence for the presence of a maar or a tuff ring is inconclusive. I believe that the Kellyville crater has maar-like subsurface features but it also has tuff ring-like surface features. In this investigation I have referred to the crater in Mercer as the Kellyville maar.

6.8 Comparisons with the Auckland Volcanic Field

The Auckland Volcanic Field is a small Quaternary monogenetic field in the Auckland region with 50 eruptive centres (Hayward et al., 2011; Bebbington, 2015). The Auckland Volcanic Field shares many characteristics with the South Auckland Volcanic Field. Both are Quaternary monogenetic basaltic fields, with the AVF having erupted erratically for the last 250 ka (Agustin-Flores et al., 2014). Both fields are well represented by phreatomagmatic activity (75% in the AVF, ~50% in the SAVF). Rosenburg (1991) determined that phreatomagmatic and magmatic behaviour in the South Auckland Volcanic Field was controlled by country rock lithology and hydrology. The comparable volcanic behaviour in these two neighbouring fields can be attributed to the volcanic centres erupting through the same Miocene sedimentary successions in an extensional tectonic setting, and hydrological environments that are similar (Smith, 1989; Sporli and Eastwood, 1997; Cassidy et al., 2007; Agustin-Flores, 2014).

A geophysical study of Auckland Volcanic Field maar volcanoes by Cassidy et al. (2007) revealed the volcanic geology of a sediment-filled crater (Pukaki maar), with similar characteristics to the Onewhero maar, and a basalt plugged crater (Domain maar), with similar characteristics to the Kellyville maar.

Pukaki maar is a small feature with a negative gravity anomaly of -0.6 mGal and subdued magnetic anomaly of <20nT. The combined two-dimensional geophysical model revealed a crater with a 50 m thick Plio-Pleistocene crater fill, surrounded by a thin ejecta ring. The model is a smaller scale version of the Onewhero maar, which has roughly ten-fold larger gravity and magnetic anomalies (-3 to -6 mGal, and ~200 nT). The main difference between the Pukaki and Onewhero maars was the size of the eruptions. The Onewhero maar has a large tuff ring that was probably close to 100 m high with a diameter over 2000 m. The Pukaki maar has a thin tuff ring that only has a ~700 m diameter. The Pukaki maar is filled with marine muds that do not produce a large density contrast with the surrounding Miocene flysch. This is the reason for the weak negative gravity anomaly that was recorded in the crater. The sedimentary fill in the Onewhero maar differs in that it is composed of diatom-rich clay with a high density contrast with the surrounding Oligocene

siltstones and sandstones, thus giving rise to a much stronger negative gravity anomaly.

Domain maar is a similar size to Pukaki maar but has a very different gravity and magnetic signature. The gravity anomaly is +2.1 mGal and this is accompanied by a strong +310 nT magnetic anomaly in the centre of the crater. This is comparable to Kellyville maar, which has up to a +3 mGal gravity peak and an associated ~800 nT magnetic anomaly. Both craters were modelled as having thick accumulations of basalt. In Domain maar, a twin-vent crater, the sedimentary infill is minimal and does not mask the strong magnetic signals produced by the mafic basalt plugs. In the Kellyville maar, conditions were right for lake formation, and the resulting diatomite deposits have masked the underlying positive magnetic signature of volcanic material in the crater. If the entire Kellyville crater was covered in diatomite it might have completely masked the basalt plugs present. This is where dual-geophysical datasets have an advantage: even if the magnetic signals are being masked, positive gravity anomalies would show a subsurface accumulation of dense volcanic material.

The inability of dual gravity-magnetic surveys to outline a clear diatreme structure in the two Auckland Volcanic Field maars was surprising and this occurs in this investigation as well. In this study, the diatreme structure in the Onewhero crater was probably masked by post-eruption lake infill and in the Kellyville crater by a basalt pond. Alternatively, the diatremes beneath the Onewhero and Kellyville craters may not be highly evolved or may not exist at all, and this may be the reason for their absence in the geophysical data. If the diatreme structures are missing in the Onewhero and Kellyville volcanic complexes, the landforms would not satisfy the structural requirements for a maar and they would instead be defined as tuff rings.

6.9 Comparisons with global monogenetic fields

The Onewhero maar has a similar post-eruption deposition history to the Dottingen maar of the Hocheifel Volcanic Field (Figure 6.16) (Pirrung et al., 2003). Cores through the infill sequence at Dottingen maar reveal a post-eruption succession of

lithozones. The basic succession starts immediately after the eruption. Lithozone A is a country rock breccia that is interpreted as being deposited by syneruptive rock falls. Lithozones B and C are post-eruption rock falls and subaquatic debris flows deposited weeks to years after the eruption. Lithozone D is biogenic/minerogenic lake sediments with interbedded gravelly layers from occasional debris flows; these layers occur for some ten thousands of years. Lithozone E represents layers of peat from swamp deposits, this generally signals the end of a maar's sedimentary fill. OB3 in the Onewhero crater has a sedimentary fill that is very similar to the Dottingen maar and this suggests that the Onewhero maar sedimentary fill could have evolved through similar post-eruption processes.

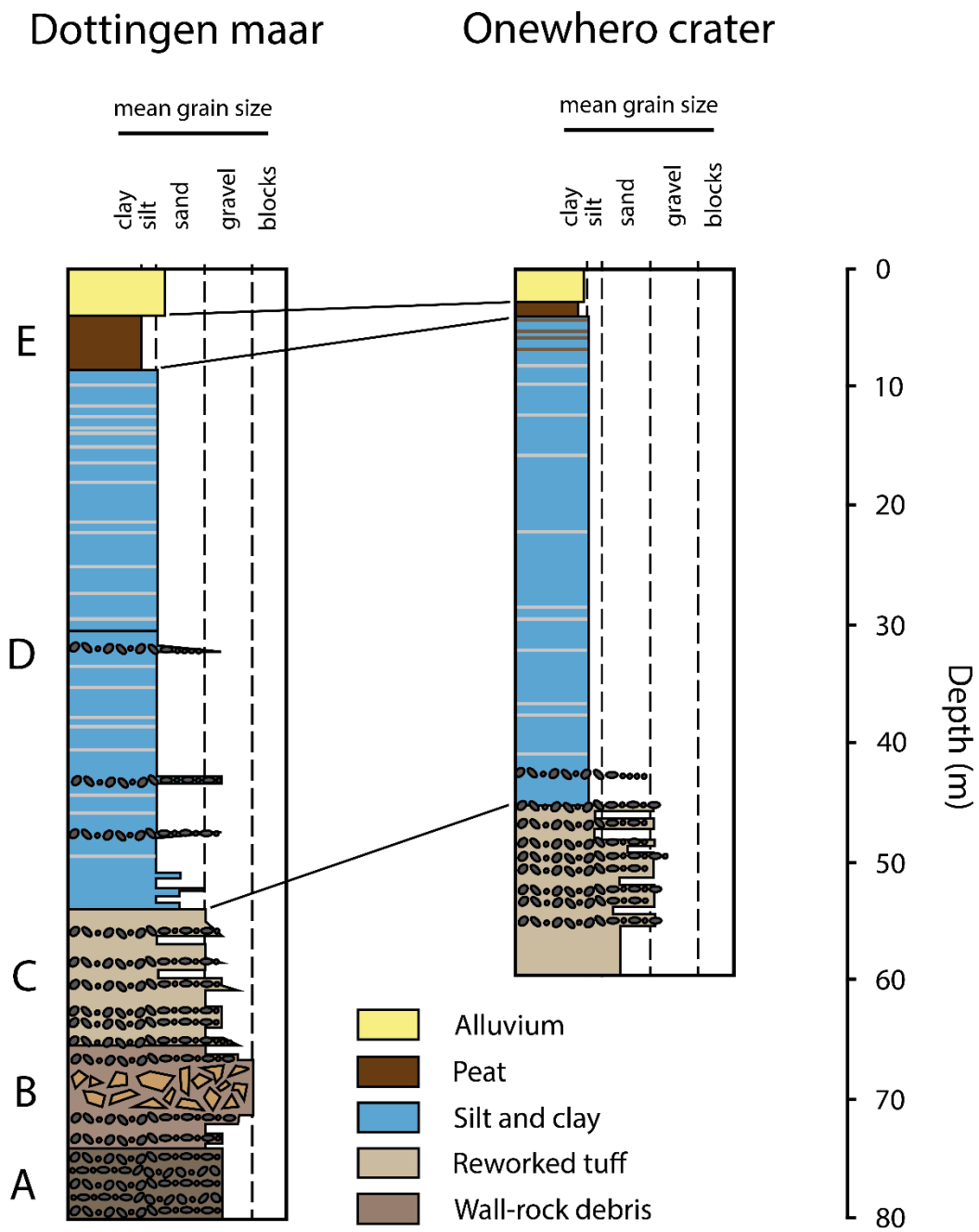

Figure 6.16: The Dottingen and Onewhero maars have comparable post-eruption sedimentary fills. The Onewhero data comes from OB3.

Zuni Salt Lake maar in the Red Hill Volcanic Field, Albuquerque, is a classic maar and has a diameter (1500 m) and surface structure comparable to the Kellyville maar (Bradbury, 1967). Zuni Salt Lake maar consists of two nested scoria cones and a shallow seasonal lake (Figure 6.17). Unlike the Kellyville maar, the scoria cones were created towards the end of eruption, and the lake that is present is saline and does not host diatoms.

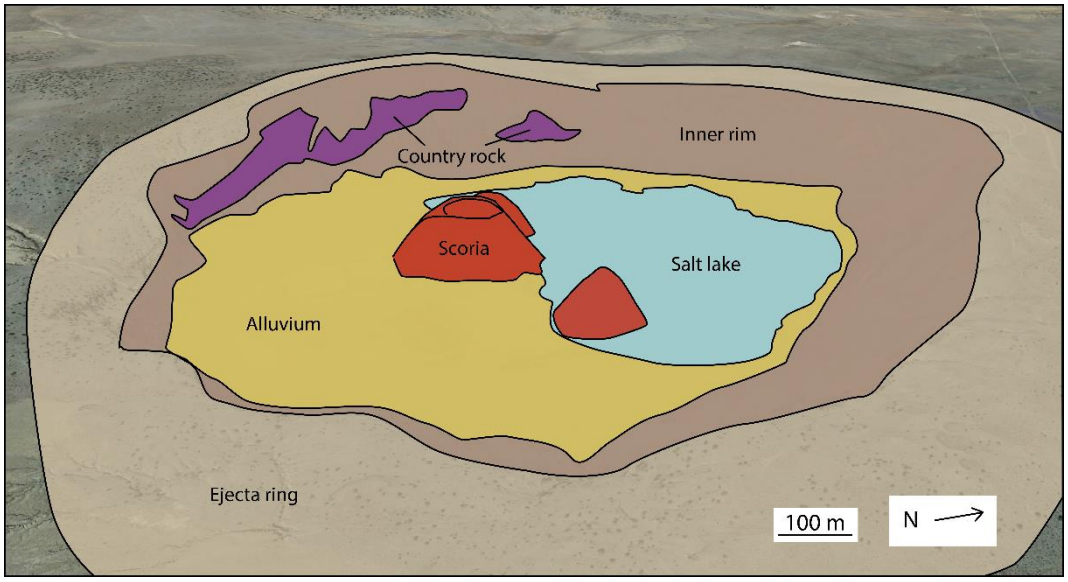

Figure 6.17: With nested scoria cones and a shallow lake, the Zuni Salt Lake maar can be likened to the Kellyville maar (base-image: Google Earth).

Lava flows in the Zuni Salt Lake maar are not visible, but probable lava flows were identified in the magnetic survey of the Kellyville crater. To the southwest of Zuni Salt Lake maar is a medium-sized scoria with >5 km long, topography-controlled lava flow (Figure 6.18). The shape and processes would have been similar to lava flows originating from Glass Hill cone in the Kellyville maar. Colchester (1968) noted that the basalt forming Glass Hill cone was fine-grained and was without visible gas vesicles. This suggests a low viscosity, which would have allowed the lava flows to travel away from the cone.

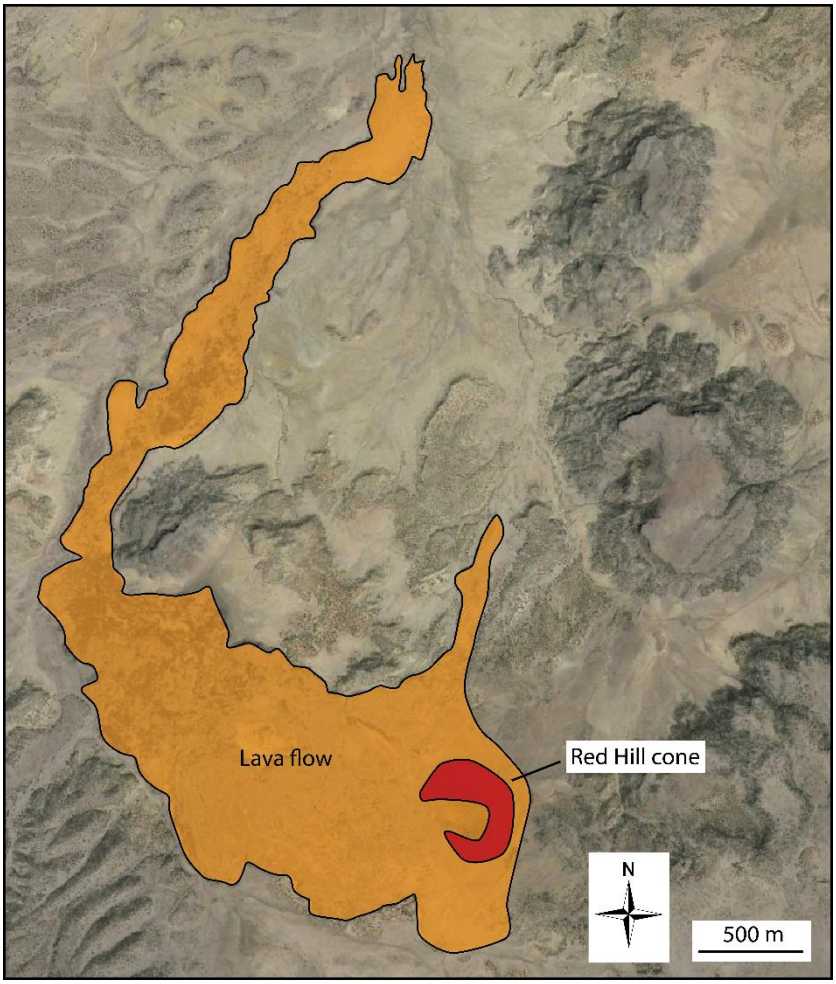

Figure 6.18: The Red Hill cone in the Red Hill Volcanic Field has a long, topography-controlled lava flow that looks similar to a lava flow identified in a magnetic survey of the Kellyville maar that originated from Glass Hill cone (base-image: Google Earth).

6.10 Future directions for further investigations of the Onewhero and Kellyville volcanic complexes

Several geological investigations could be employed to further investigate the subsurface structure of the Onewhero and Kellyville volcanic complexes. These would complement the gravity and magnetic anomalies available. Further investigations could include:

1. Drilling boreholes in strategically placed areas. In the Kellyville maar this could be through the middle of the crater (Mercer Primary School field). In the Onewhero maar this could be through the middle of the negative magnetic anomaly in the northwest of the crater and a second borehole

through the positive magnetic anomaly that stretches across the middle of the crater. Borehole drilling would provide valuable depth constraints that would improve the accuracy of the gravity models considerably.

2. A seismic survey. Even a low resolution seismic survey could allow the diatreme structures to be identified if they are present at either of the craters.

3. A resistivity survey. Resistivity investigations have been employed in several maar volcano studies to help distinguish and outline the boundaries of geological bodies in maar craters (Mrlina et al., 2009; Skacelova et al., 2010).

4. Interpretation of aeromagnetic data. There is an extensive coverage of aeromagnetic data for the South Auckland region that has not yet been publicly released. This data might highlight the position of the vents in the Onewhero and Kellyville craters as the vents are masked in the high-resolution ground-magnetic surveys that were completed in this study.

Chapter Seven: Conclusions

7.1 Geological investigation

Borehole data supplied by the Waikato Regional Council was interpreted to assist in the gravity and magnetic modelling and also in recreating an eruption history for the two maars. The boreholes revealed a 50 m accumulation of post-eruption clay-sized sediment in the northeast of the Onewhero crater (OB3). Boreholes in Mercer showed a contact between Glass Hill cone basalt flows and the Koheroa Siltstone. This meant that the vent that created Glass Hill cone probably initiated before the main, central vent. In the northeast of the Onewhero crater a sample of dry clay found on top of a recently excavated drain was scanned by the electron microscope and was found to be rich in diatom frustules. This clay was also found in the south of the crater bordering the Klondyke cone lava flow. This could confirm the presence of a paleo-lake that covered most of the crater.

7.2 Gravity investigation

Two perpendicular gravity transects across the Onewhero maar revealed a Bouguer anomaly of -5.7 mGal. Similar transects at the Kellyville maar revealed a Bouguer anomaly of +2.6 mGal. The gravity transects were used to create two-dimensional models of the crater fill using the GravCadW software package (Sheriff, 1977). The modelling required data on the densities of four geological bodies: country rock (2.3 g/cm^3 at Onewhero, 2.4 g/cm^3 at Mercer), reworked tuff (2.2 g/cm^3), post-eruption lake infill (1.3 g/cm^3), and basalt (2.9 g/cm^3). The densities were either measured independently or were taken from similar studies. The models were only constrained by data from several boreholes of questionable quality, but the two-dimensional gravity models make sense when compared to other studies (Pirrung et al., 2003; Mrlina et al., 2009; Jones, 2011). Gravity modelling of the Onewhero crater indicated a thick post-eruption infill deposit that was identified earlier in the study (Chapter 3) as being diatomaceous. This low density deposit occurs to 100 m

depth in the northwest of the crater. The positive gravity anomaly in the southeast of the crater was interpreted as a thick (10 – 20 m) lava flow that probably originated from the nearby Klondyke cone and flowed in over the top of the ejecta ring. Gravity modelling of the Kellyville crater revealed a thick accumulation of vesicular-fine basalt; this was the cause of the convex Bouguer anomalies for both of the gravity profiles. The basalt has a maximum thickness of ~60 m and it is not known whether the flows originated from Glass Hill cone or from the main vent. The basalt is overlain by varying thicknesses of post-eruption alluvium and diatomite.

7.3 Magnetic investigation

969 stations were measured in the Onewhero maar and 329 stations in the Kellyville maar using a proton magnetometer. Iron-based infrastructure was avoided over the course of the surveys to minimise outside "noise". In the Onewhero crater three major magnetic anomalies were observed. A negative anomaly in the north of the crater was interpreted as a circular basin-like feature filled with low density sediment. The shape and structure of this anomaly is consistent with an explosion crater/vent. A positive anomaly in the centre of the crater was interpreted as a feeder dyke with associated lava flows. The last major magnetic anomaly occurred in the south of the crater; it had a positive signature and was interpreted as a subsurface extension of the visible Klondyke cone lava flow nearby. In the Kellyville crater three major magnetic anomalies were observed. Two very low negative anomalies occur to the northeast of Glass Hill cone. One of these anomalies occurs in outcrop on Koheroa Road. Both of the anomalies are confirmed as being deposits of diatomite as they are neighbouring and have a similar magnetic anomaly. A high positive anomaly occurs in the west of the crater. Due to its position I can confirm this magnetic anomaly is Glass Hill cone. A lower positive anomaly forms an arc to the south of Glass Hill and this was interpreted as a subsurface lava flow.

7.4 Overall structure

By integrating the borehole data, magnetic and gravity anomalies I have suggested a simplified structure for the Onewhero and Kellyville maars. The Onewhero maar has a bowl shaped post-eruption fill that averages 40 – 60 m depth across most of the crater, it deepens rapidly in the northwest to about 100 m in the explosion crater. The low depth/diameter ratio for the Onewhero maar could be due to the weak country rock in the area that tends to create shallow diatremes compared to hard-rock diatreme emplacement (Field and Scott-Smith, 1999; Jones, 2011). The Kellyville maar has an explosion crater that is predominantly filled with basalt, either from Glass Hill cone, the main vent, or a mixture of the two. The basalt reached thicknesses greater than 60 m and is overlain with thin deposits of Taupo Volcanic Zone pumiceous sediment and diatomite.

References

Agustin-Flores, J., Nemeth, K., Cronin, S. J., Lindsay, J. M., Kereszturi, G., Brand, B. D., and Smith, I. E. M., (2014). Phreatomagmatic eruptions through unconsolidated coastal plain sequences, Maungataketake, Auckland Volcanic Field (New Zealand). *Journal of Volcanology and Geothermal Research*, 276: 46-63.

Ballance, P. F., (1974). An inter-arc flysch basin in northern New Zealand: Waitemata Group (upper Oligocene to lower Miocene). *The Journal of Geology*, 82: 439-471.

Bebbington, M. S., (2015). Spatio-volumetric hazard estimation in the Auckland Volcanic Field. *The Bulletin of Volcanology*, 77: 39-54.

Blackfield, J. J., Payne, R. J., Heggen, M. P., Riva-Caballero, A., and Plicht, J., (2014). Age and impacts of the caldera-forming Aniakchak II eruption in western Alaska. *Quaternary Research*, 82: 85-95.

Blaikie, T. N., Ailleres, L., Cas, R. A. F., and Betts, P. G., (2012). Three-dimensional potential field modelling of a multi-vent maar-diatreme – The Lake Corugulac maar, Newer Volcanics Province, south-eastern Australia. *Journal of Volcanology and Geothermal Research*, 235: 70-83.

Blaikie, T. N., Ailleres, L., Betts, P. G., and Cas, R. A. F., (2014). Interpreting subsurface volcanic structures using geologically constrained 3-D gravity inversions: Examples of maar-diatremes, Newer Volcanics Province, southeastern Australia. *Journal of Geophysical Research: Solid Earth*, 119: 3857-3878.

Bradbury, J. P., (1967). Origin, paleolimnology, and limnology of Zuni Salt Lake maar, west-central New Mexico. Ph.D. dissertation, *University of New Mexico*, Albuquerque, New Mexico.

Briggs, R. M., Okada, T., Itaya, T., Shibuya, H., and Smith, I. E. M., (1994). K-Ar ages, paleomagnetism, and geochemistry of the South Auckland Volcanic Field, North Island, New Zealand. *New Zealand Journal of Geology and Geophysics*, 37: 143-153.

Briggs, R. M., Pittari, A., and Rosenburg, M. D., (2010). Controls on volcanism in the South Auckland Volcanic Field. *GeoNZ 2010: Joint Meeting of the Geoscience Society of New Zealand: The New Zealand Geothermal Works.*

Briggs, R. M., Pittari, A., and Rosenburg, M. D., (2012). The influence of subsurface hydrogeology on the nature and localisation of volcanism in the South Auckland Volcanic Field. *Abstract Volume of the Fourth International Maar Conference*, 17-18.

Carey, R. J., Houghton, B. F., (2010). "Inheritance": an influence on the particle size of pyroclastic deposits. *Geology*, 38: 347-350.

Cas. R. A. F., (1989). Physical volcanology, in R. W. Johnson (ed.). *Intraplate Volcanism*, Cambridge University Press, Cambridge, pp. 55-87.

Cas, R. A. F., and Wright, J. V., (1987). Volcanic successions – modern and ancient. *Allen and Unwin*, London.

Cassidy, J., France, S. J., and Locke, C. A., (2007). Gravity and magnetic investigation of maar volcanoes, Auckland Volcanic Field, New Zealand. *Journal of Volcanology and Geothermal Research*, 159: 153-163.

Cook, C., Briggs, R. M., Smith, I. E. M., and Mass, R., (2005). Petrology and geochemistry of intraplate basalts in the South Auckland Volcanic Field, New Zealand: Evidence for two coeval magma suites from distinct sources. *Journal of Petrology*, 46: 473-503.

Coombs, D., Cas, R., Yosuke, K., Landis, C., McDonough, W., and Reay, A., (1986). Cenozoic volcanism in north, east and central Otago. *The Royal Society of New Zealand Bulletin*, 23: 278-312.

Discover, (2011). Following in Scott's footsteps: measuring the magnetic pole. Retrievedfrom:http://blogs.discovermagazine.com/80beats/2011/12/28/following-in-scotts-footsteps-measuring-the-magnetic-pole.

Edbrooke, S. W., Crouch, E. M., Morgans, H. E. G., and Sykes, R., (1998). Late Eocene-Oligocene Te Kuiti Group at Mount Roskill, Auckland, New Zealand. *New Zealand Journal of Geology and Geophysics*, 41: 85-93.

Edbrooke, S. W., (2001). Geology of the Auckland area. *Institute of Geological and Nuclear Sciences*, Lower Hutt, New Zealand.

Evans, M. E., and Heller, F., (2003). Environmental magnetism: principles and applications of enviromagnetics. Massachusetts, USA: *Elsevier Science.*

Everett, M. E., (2013). Near-surface applied geophysics. West Nyack, NY, USA: *Cambridge University Press*.

Field, M., and Scott-Smith., (1999) Contrasting geology and near-surface emplacement of kimberlite pipes in southern Africa and Canada. *Lithos*, 76: 214-237.

Francis, P., and Oppenheimer, C., (2004). *Volcanoes*. Oxford University Press, New York.

Gibson, A. C., (2011). Volcanology of tuff rings at Kellyville, Onewhero and Bombay, South Auckland Volcanic Field. MSc Thesis, *University of Waikato*.

Greig, D. A., (1989). A study of the Kaawa Formation aquifer system in the Manukau Lowlands. *Technical Publication 85, Auckland Regional Water Board, Auckland.*

Hayward, B.W., Kenny, J. A., and Grenfell, H. R., (2011). More volcanoes recognised in Auckland Volcanic Field. *Geoscience Society of New Zealand (Newsletter)*, 5: 11-16.

Hochstein, M.P., and Nunns, A. G., (1976). Gravity measurements across the Waikato Fault, North Island, New Zealand. *New Zealand Journal of Geology and Geophysics*, 19: 347-58.

Hornibrook, N. B., and Schofield, J. C., (1963). Stratigraphic relations in the Waitemata Group of the lower Waikato District. *New Zealand Journal of Geology and Geophysics*, 6: 38-51.

Houben, P., Kuhl, N., Dambeck, R., and Overath, J., (2013). Lateglacial to Holocene rapid crater infilling of a MIS 2 maar volcano (West-Eifel Volcanic Field, Germany): environmental history and geomorphological feedback mechanisms. *Boreas*, 42:947-958.

Isaac, M. J., Herzer, R. H., Brook, F. J., and Hayward, B. W., (1994). Cretaceous and Cenozoic sedimentary basins of New Zealand. *Institute of Geological and Nuclear Sciences Monograph B, New Zealand.*

Johnson, R. W., and Wellman, P., (1989). Framework for volcanism, in R. W. Johnson (ed.), *Intraplate Volcanism*, Cambridge University Press, Cambridge, pp. 1-53.

Jordan, S.C., Cas, R. A. F., and Hayman, P.C., (2013). The origin of a large (>3 km) maar volcano by coalescence of multiple shallow craters: Lake Purrumbete maar, southeastern Australia. *Journal of Volcanology and Geothermal Research*, 254: 5-22.

Jones, D., (2011). The geophysical characterisation of the Foulden maar. MSc Thesis, *University of Otago.*

Kear, D., (1961). Stratigraphy of the Pokeno District, Auckland. *New Zealand Journal of Geology and Geophysics*, 4: 148-164.

Kear, D., and Schofield, J. C., (1959). Te Kuiti Group. *New Zealand Journal of Geology and Geophysics*, 2: 685-717.

Kear, D., and Schofield, J. C., (1978). Geology of the Ngaruawahia subdivision, *New Zealand Department of Scientific and Industrial Research.*

Kearey, P., Brooks, M., and Hill, I., (2002). An introduction to geophysical exploration. *Blackwell Publishing*, Cornwall, United Kingdom.

Kermode, L. O., (1992). Inventory of Quaternary volcanoes and volcanic features of Northland, Auckland, South Auckland and Taranaki, *Geological Society of New Zealand.*

Lesti, C., Giordano, G., Salvini, F., and Cas, R., (2008). Volcano tectonic setting of the intraplate, Pliocene-Holocene, Newer Volcanic Province (southeast Australia): Role of crustal fracture zones. *Journal of Geophysical Research*, 113: 1-11.

Loera, H. L., Aranda-Gomez, J. J., Arzate, J. A., and Molina-Garza, R. S., (2008). Geophysical surveys of the Joya Honda maar (Mexico) and surroundings: volcanic implications. *Journal of Volcanology and Geothermal Research*, 170: 135-152.

Lorenz, V., (1973). On the formation of maars. *Bulletin Volcanologique*, 37: 183-204.

Lorenz, V., (1986). On the growth of maars and diatremes and its relevance to the formation of tuff rings. *Bulletin of Volcanology*, 170: 265-274.

Lorenz, V., (2003). Maar diatreme volcanoes, their formation, and their setting in hard-rock or soft-rock environments. *Geolines*, 15: 72-83.

Martin, U., Nemeth, K., Lorenz, V., and White, J. D. L., (2007). Introduction: Maar-diatreme volcanism. *Journal of Volcanology and Geothermal Research*, 159: 1-3.

McCraw, J., (2011). The wandering river: landforms and geological history of the Hamilton Basin. Levin, New Zealand: Graphic Press and Packaging.

Mrlina, J., Kmpf, H., Kroner, C., Mingram, J., Stebich, M., Brauer, A., Geissler, W., Kallmeyer, J., Matthes, H., and Seidl, M., (2009). Discovery of the first Quaternary maar in the Bohemian Massif, Central Europe, based on

combined geophysical and geological surveys. *Journal of Volcanology and Geothermal Research*, 182: 97-112.

Nabighian, M. N., Grauch, V. J. S., Hansen, R. O., (2005). The historical development of the magnetic method in exploration. *Geophysics*, 70: 33-61.

Nemeth, K., (2001). Phreatomagmatic volcanism of the Waipiata Volcanic Field, Otago, New Zealand. PhD Thesis, *University of Otago.*

Nemeth, K., and White, J. D.L., (2003). Reconstructing eruption processes of a Miocene monogenetic field from vent remnants: Waipiata Volcanic Field, South Island, New Zealand. *Journal of Volcanology and Geothermal Research*, 124: 1-21.

Otterloo, J., Cas, R. A. F., and Sheard, M. J., (2013). Eruption processes and deposit characteristics at the monogenetic Mt. Gambier Volcanic Complex, SE Australia: implications for alternating magmatic and phreatomagmatic activity. *The Bulletin of Volcanology*, 75: 737-758.

Pirrung, M., Fischer, C., Buchel, G., Gaupp, R., Lutz, H., and Neuffer, F. O., (2003). Lithofacies succession of maar crater deposits in the Eifel area (Germany). *Terra Nova*, 15: 125-132.

Rafferty, W. J., (1977). The volcanic geology and petrology of South Auckland. MSc Thesis, *University of Auckland.*

Rafferty, W. J., and Heming, R. F., (1979). Quaternary alkali and sub-alkalic volcanism in South Auckland, New Zealand. *Contributions to Mineralogy and Petrology*, 71: 139-150.

Rosenburg, M. D., (1991). The nature and mechanisms of phreatomagmatic volcanism in the South Auckland Volcanic Field, MSc Thesis, *University of Waikato*.

Schofield, J. C., (1958). Notes on volcanism and structure in Franklin County. *New Zealand Journal of Geology and Geophysics*, 1: 341-359.

Schultz, R., Buness, H., Gabriel, G., Pucher, R., Rolf, C., Wiederhold, H., and Wonik, T., (2005). Detailed investigation of preserved maar structures by combined geophysical surveys. *Bulletin of Volcanology*, 68: 95-106.

Sheridan, M. F., and Wohletz, K. H., (1981). Hydrovolcanic explosions: the systematics of water-pyroclast equilibrium. *Science*, 212: 1387-1389.

Sheriff, R., (1977). GravCadW, GRADIENT. *University of Montana*, MT.

Sigurdsson, H., and Houghton, B. F., (2000). Encyclopedia of Volcanoes. San Diego, USA: Academic Press.

Skacelova, Z., Rapprich, V., Valenta, J., Hartvich, F., Sramek, J., Radon, M., Gazdova, R., Novakova, L., Kolinsky, P., and Pecskay, Z., (2010). Geophysical research on the structure of partly eroded maar volcanoes: Miocene Hnojnice and Oligocene Rychnov volcanoes (northern Czech Republic). *Journal of Geosciences*, 55: 333-345.

Smith, I. E. M., (1989). Intraplate volcanism in Australasia. *Cambridge University Press*, pp. 157-162.

Sporli, K. B., and Eastwood, V. R., (1997). Elliptical boundary of an intraplate volcanic field, Auckland, New Zealand. *Journal of Volcanology and Geothermal Research*, 79: 169-179.

Statistics New Zealand. (n.d.). Auckland Region population and dwellings. Retrieved from: http://www.stats.govt.nz/Census/2013-census/profile-and-summary-reports/quickstats-about-a-place. Date retrieved: 12-10-2014.

Taylor, S. N., (2012). Volcanology of the Raventhorpe and Pokeno West Volcanic Complexes, South Auckland Volcanic Field. MSc Thesis, *University of Waikato.*

Tripathi, A. R. P., Kamp, P. J. J., and Nelson, C. S., (2014). Paleogeography of Late Eocene to earliest Miocene Te Kuiti Group, central-western North Island, New Zealand. *New Zealand Journal of Geology and Geophysics*, 57: 128-148.

Valentine, G. A. and Hirano, N., (2010). Mechanisms of low-flux intraplate volcanic fields – Basin and Range (North America) and northwest Pacific Ocean. *Geological Society of America*, 38: 55-58.

Vijevac, Z., Murphy, G., Smaill, A., Crowcroft, G. and Bowden, D., (2002). South Auckland groundwater, Kaawa Aquifer recharge study and management of the volcanic and Kaawa Aquifers. *Prepared by Auckland Council.*

Weaver, S. D. and Smith, I. E. M., (1989). New Zealand Intraplate Volcanism, in Johnson, R. W. (*ed.*), *Intraplate Volcanism,* Cambridge University Press, Cambridge, pp 157-187.

Waterhouse, B. C., (1967). Diatomite at Mercer. *Department of Industrial Research, New Zealand Geological Survey*, 35-37.

Waterhouse, B. C., (1978). Sheet N51 - Onewhero geological map of New Zealand, 1:63 360, *Department of Scientific and Industrial Research.* Wellington, New Zealand.

Waterhouse, B. C., (1980). Mercer diatomite. *New Zealand Geological Survey.*

White, P. J. and Waterhouse, B. C., (1993). Lithostratigraphy of the Te Kuiti Group: a revision. *The Royal Society of New Zealand*, 36: 255-266.

Wohletz, K. H. And Sheridan, M. F., (1983). Hydrovolcanic explosions II: evolution of basaltic tuff rings and tuff cones. *American Journal of Science*, 283: 385-413.

Woodward, D., (1971). Grv3 – Auckland gravity map of New Zealand, 1:250 000. *Department of Scientific and Industrial Research*, Wellington, New Zealand.

Appendix A – Gravity investigation

A.1 Gravity correction equations

A.1.1 Latitude correction

$$g^{l} = ge\ \frac{1 + k sin^{2}l}{sqrt\ (1 - e^{2} sin^{2}l)}$$

ge = 978032.67715 (theoretical gravity at the equator)

k = 0.001931851353 (coefficient)

e^{2} = 0.0066938002290 (coefficient)

^{l} = latitude of the gravity station in degrees (WGS84)

A.1.2 Free-air correction

$$FAC = 0.3086 * h$$

h = elevation of gravity station above sea level (m)

A.1.3 Bouguer correction

$$BC = 0.04193 ph$$

p = mean density of slab (3.67 g/cm^{3})

h = elevation of gravity station above sea level (m)

A.2 Gravity spreadsheets – raw data

A.2.1 Onewhero Y-Y' transect

Station	Time 1	Reading1	Time 2	Reading2	Time 3	Reading3	Time 4	Reading4	Average Time	Average Reading	Elapsed Time	Corrected Reading	Absolute Gravity (mGal)
B/S	**08:45:00**	**530.9**	**08:46:00**	**530.9**	**08:47:00**	**531.3**	**08:48:00**	**531.4**	**08:46:30**	**531.125**	**00:00:00**	**531.6875**	**979991.977**
1	09:05:00	440.8	09:06:00	440.9	09:07:00	441.3	09:08:00	440.6	09:06:30	440.9	00:20:00	441.74094	979984.8712
2	09:15:00	507	09:16:00	505.2	09:17:00	504.9	09:18:00	504.7	09:16:30	505.45	00:30:00	506.43016	979989.9817
3	09:26:00	540.2	09:27:00	540.9	09:28:00	540.5	09:29:00	540.1	09:27:30	540.425	00:41:00	541.55831	979992.7568
4	09:37:00	521.5	09:38:00	522.3	09:39:00	522.5	09:40:00	523.5	09:38:30	522.45	00:52:00	523.73645	979991.3489
B/S	**10:01:00**	**532.7**	**10:02:00**	**532.7**	**10:03:00**	**532.2**	**10:04:00**	**533.1**	**10:02:30**	**532.675**	**01:16:00**	**534.29558**	**979992.183**
5	10:15:00	525.2	10:16:00	525.8	10:17:00	525	10:18:00	525.1	10:16:30	525.275	01:30:00	527.09049	979991.6138
6	10:23:00	529.3	10:24:00	529.8	10:25:00	529.1	10:26:00	528.8	10:24:30	529.25	01:38:00	531.17687	979991.9367
7	10:30:00	529.3	10:31:00	530.1	10:32:00	530.1	10:33:00	531.8	10:31:30	530.325	01:45:00	532.34933	979992.0293
8	10:45:00	530.5	10:46:00	529.6	10:47:00	528.9	10:48:00	529.6	10:46:30	529.65	02:00:00	531.88316	979991.9925
9	10:51:00	526.1	10:52:00	527.3	10:53:00	526.5	10:54:00	525.7	10:52:30	526.4	02:06:00	528.71669	979991.7423
B/S	**11:13:00**	**532.8**	**11:14:00**	**533.2**	**11:15:00**	**532.3**	**11:16:00**	**532.9**	**11:14:30**	**532.8**	**02:28:00**	**535.42298**	**979992.2721**
10	11:30:00	527.5	11:31:00	528.4	11:32:00	527.1	11:33:00	527.6	11:31:30	527.65	02:45:00	530.50966	979991.884
11	11:37:00	521.9	11:38:00	522.6	11:39:00	523.5	11:40:00	522.8	11:38:30	522.7	02:52:00	525.65711	979991.5006
12	11:47:00	512.5	11:48:00	513.2	11:49:00	512.1	11:50:00	513.3	11:48:30	512.775	03:02:00	515.87133	979990.7275
13	11:53:00	502.1	11:54:00	504.8	11:55:00	503.1	11:56:00	503.4	11:54:30	503.35	03:08:00	506.52987	979989.9895
14	12:00:00	502.1	12:01:00	503.9	12:02:00	504.6	12:03:00	504.2	12:01:30	503.7	03:15:00	506.97732	979990.0249
15	12:09:00	501.4	12:10:00	499.9	12:11:00	501	12:12:00	502.5	12:10:30	501.2	03:24:00	504.60262	979989.8373

138

B/S	12:28:00	538.8	12:29:00	538.9	12:30:00	538.9	12:31:00	538.9	12:29:30	538.875	03:43:00	542.54214	979992.8345
16	13:06:00	491.5	13:07:00	491.4	13:08:00	492	13:09:00	491.9	13:07:30	491.7	04:21:00	495.89618	979989.1495
17	13:14:00	491.5	13:15:00	492.1	13:16:00	489.9	13:17:00	490.3	13:15:30	490.95	04:29:00	495.25756	979989.099
18	13:22:00	490.9	13:23:00	489.9	13:24:00	489.9	13:25:00	489.9	13:23:30	490.15	04:37:00	494.56894	979989.0446
19	13:28:00	488.8	13:29:00	488.5	13:30:00	488.7	13:31:00	487.6	13:29:30	488.4	04:43:00	492.90247	979988.913
20	13:36:00	486.9	13:37:00	486.1	13:38:00	485.5	13:39:00	486.8	13:37:30	486.325	04:51:00	490.93885	979988.7579
21	13:43:00	481.8	13:44:00	481.9	13:45:00	481.4	13:46:00	482.1	13:44:30	481.8	04:58:00	486.5113	979988.4081
22	13:51:00	479.5	13:52:00	481.8	13:53:00	480.9	13:54:00	481.5	13:52:30	480.925	05:06:00	485.74768	979988.3478
23	14:00:00	479.6	14:01:00	480.5	14:02:00	478.7	14:03:00	479.1	14:01:30	479.475	05:15:00	484.42298	979988.2431
B/S	**14:30:00**	**530.2**	**14:31:00**	**530.8**	**14:32:00**	**530.1**	**14:33:00**	**530.9**	**14:31:30**	**530.5**	**05:45:00**	**535.86564**	**979992.3071**
24	14:50:00	481.4	14:51:00	482.5	14:52:00	482.8	14:53:00	482.3	14:51:30	482.25	06:05:00	487.89409	979988.5173
25	14:56:00	482.5	14:57:00	482.1	14:58:00	482.5	14:59:00	482.8	14:57:30	482.475	06:11:00	488.20262	979988.5417
26	15:01:00	482.7	15:02:00	484	15:03:00	484.5	15:04:00	484.5	15:02:30	483.925	06:16:00	489.72223	979988.6617
27	15:06:00	480.9	15:07:00	481	15:08:00	481.7	15:09:00	481	15:07:30	481.15	06:21:00	487.01684	979988.448
28	15:13:00	482.8	15:14:00	481	15:15:00	481	15:16:00	481	15:14:30	481.45	06:28:00	487.4143	979988.4794
29	15:21:00	488.5	15:22:00	487.6	15:23:00	487.4	15:24:00	487.7	15:22:30	487.8	06:36:00	493.87567	979988.9899
30	15:27:00	498.1	15:28:00	498.1	15:29:00	497.5	15:30:00	497.8	15:28:30	497.875	06:42:00	504.03421	979989.7924
31	15:36:00	502.1	15:37:00	501.8	15:38:00	502	15:39:00	501.4	15:37:30	501.825	06:51:00	508.10951	979990.1143
32	15:52:00	517.9	15:53:00	516.7	15:54:00	517.5	15:55:00	518.1	15:53:30	517.55	07:07:00	524.05726	979991.3742
33	15:59:00	517.6	16:00:00	516.9	16:01:00	517.5	16:02:00	517.9	16:00:30	517.475	07:14:00	524.07972	979991.376
34	16:10:00	500.4	16:11:00	500.5	16:12:00	500	16:13:00	499.9	16:11:30	500.2	07:25:00	506.95786	979990.0234
35	16:16:00	481.6	16:17:00	482.9	16:18:00	481.6	16:19:00	482.1	16:17:30	482.05	07:31:00	488.89139	979988.5961
36	16:22:00	461.4	16:23:00	461.5	16:24:00	459.5	16:25:00	459.6	16:23:30	460.5	07:37:00	467.42493	979986.9003
37	16:34:00	445.8	16:35:00	443.9	16:36:00	443.8	16:37:00	444.1	16:35:30	444.4	07:49:00	451.49199	979985.6416
38	16:52:00	354.3	16:53:00	354.8	16:54:00	352.5	16:55:00	352.9	16:53:30	353.625	08:07:00	360.96759	979978.4901
B/S	**17:06:00**	**524.9**	**17:07:00**	**523.7**	**17:08:00**	**524.2**	**17:09:00**	**523.8**	**17:07:30**	**524.15**	**08:21:00**	**531.6875**	**979991.977**

139

A.2.2 Onewhero X-X' transect

Station	Time 1	Reading1	Time 2	Reading2	Time 3	Reading3	Time 4	Reading4	Average Time	Average Reading	Elapsed Time	Corrected Reading	Absolute Gravity (mGal)
B/S	**08:54:00**	**536.2**	**08:55:00**	**536.5**	**08:56:00**	**536.4**	**08:57:00**	**537.8**	**08:55:30**	**536.725**	**00:00:00**	**534.775**	**979991.977**
1	09:03:00	462.2	09:04:00	462.6	09:05:00	463.5	09:06:00	464.1	09:04:30	463.1	00:09:00	461.2693	979986.17
2	09:15:00	496.7	09:16:00	494.3	09:17:00	496	09:18:00	494.1	09:16:30	495.275	00:21:00	493.6033	979988.7244
3	09:39:00	523.2	09:40:00	523.6	09:41:00	524	09:42:00	522.9	09:40:30	523.425	00:45:00	522.0714	979990.9734
4	09:51:00	528.5	09:52:00	527.3	09:53:00	527.3	09:54:00	527.8	09:52:30	527.725	00:57:00	526.5305	979991.3257
5	09:59:00	531.3	10:00:00	532.8	10:01:00	537.1	10:02:00	537.1	10:00:30	534.575	01:05:00	533.4865	979991.8752
6	10:07:00	539.2	10:08:00	541.4	10:09:00	540.6	10:10:00	541.5	10:08:30	540.675	01:13:00	539.6925	979992.3655
B/S	**10:32:00**	**540.9**	**10:33:00**	**540.1**	**10:34:00**	**539.1**	**10:35:00**	**538.4**	**10:33:30**	**539.625**	**01:38:00**	**538.9739**	**979992.3087**
7	10:54:00	536.2	10:55:00	535.9	10:56:00	536.9	10:57:00	535.6	10:55:30	536.15	02:00:00	535.7904	979992.0572
8	11:01:00	532.1	11:02:00	532.9	11:03:00	533.4	11:04:00	533.8	11:02:30	533.05	02:07:00	532.7832	979991.8196
9	11:09:00	530.8	11:10:00	532	11:11:00	531	11:12:00	531.2	11:10:30	531.25	02:15:00	531.0892	979991.6858
10	11:18:00	526.4	11:19:00	527.2	11:20:00	526.7	11:21:00	527.5	11:19:30	526.95	02:24:00	526.9085	979991.3555
11	11:27:00	533.4	11:28:00	532.1	11:29:00	532.1	11:30:00	531.9	11:28:30	532.375	02:33:00	532.4528	979991.7935
12	11:36:00	533.2	11:37:00	532.8	11:38:00	532.9	11:39:00	532.9	11:37:30	532.95	02:42:00	533.1471	979991.8484
13	11:42:00	528.9	11:43:00	529.1	11:44:00	529.1	11:45:00	530.1	11:43:30	529.3	02:48:00	529.5766	979991.5663
B/S	**12:00:00**	**538.9**	**12:01:00**	**540.1**	**12:02:00**	**539.5**	**12:03:00**	**539.1**	**12:01:30**	**539.4**	**03:06:00**	**539.9152**	**979992.3831**
14	12:31:00	514.5	12:32:00	515.1	12:33:00	516.1	12:34:00	514.8	12:32:30	515.125	03:37:00	516.051	979990.4978
15	12:42:00	509	12:43:00	509.9	12:44:00	508.3	12:45:00	508.2	12:43:30	508.85	03:48:00	509.9218	979990.0136
16	12:50:00	512.5	12:51:00	511.9	12:52:00	512.6	12:53:00	512.2	12:51:30	512.3	03:56:00	513.4779	979990.2945

17	13:01:00	509.5	13:02:00	510.5	13:03:00	509.9	13:04:00	511.3	13:02:30	510.3	04:07:00	511.6236	979990.148
18	13:10:00	508.5	13:11:00	508.3	13:12:00	509.5	13:13:00	507.3	13:11:30	508.4	04:16:00	509.8429	979990.0074
19	13:17:00	507.8	13:18:00	509.8	13:19:00	508.5	13:20:00	506.4	13:18:30	508.125	04:23:00	509.6607	979989.993
20	13:26:00	503.1	13:27:00	503.5	13:28:00	504.2	13:29:00	503.9	13:27:30	503.675	04:32:00	505.33	979989.6508
B/S	**13:50:00**	**531.9**	**13:51:00**	**532.5**	**13:52:00**	**531.1**	**13:53:00**	**532.4**	**13:51:30**	**531.975**	**04:56:00**	**533.9481**	**979991.9117**
21	14:41:00	500.5	14:42:00	501.9	14:43:00	500.5	14:44:00	499.9	14:42:30	500.7	05:47:00	503.349	979989.4943
22	14:49:00	503.1	14:50:00	503.1	14:51:00	503.8	14:52:00	503.9	14:50:30	503.475	05:55:00	506.23	979989.7219
23	14:58:00	501.9	14:59:00	501.5	15:00:00	500.1	15:03:00	500.1	15:00:00	500.9	06:04:30	503.781	979989.5285
24	15:07:00	493.2	15:08:00	493.5	15:09:00	492.5	15:10:00	493.7	15:08:30	493.225	06:13:00	496.2186	979988.931
25	15:15:00	490.5	15:16:00	490.1	15:17:00	490.8	15:18:00	490	15:16:30	490.35	06:21:00	493.4496	979988.7123
B/S	**15:33:00**	**529.7**	**15:34:00**	**530.6**	**15:35:00**	**530.9**	**15:36:00**	**531.1**	**15:34:30**	**530.575**	**06:39:00**	**533.9132**	**979991.9089**
26	15:45:00	497.6	15:46:00	497.8	15:47:00	497.5	15:48:00	497.3	15:46:30	497.55	06:51:00	501.0472	979989.3125
27	15:54:00	495.5	15:55:00	496.4	15:56:00	496.1	15:57:00	495.1	15:55:30	495.775	07:00:00	499.3915	979989.1817
28	16:02:00	494.5	16:03:00	495.3	16:04:00	495.9	16:05:00	496.4	16:03:30	495.525	07:08:00	499.2476	979989.1703
29	16:12:00	495.5	16:13:00	497	16:14:00	497.4	16:15:00	496.9	16:13:30	496.7	07:18:00	500.5551	979989.2736
30	16:23:00	478.5	16:24:00	477	16:25:00	476.9	16:26:00	478.9	16:24:30	477.825	07:29:00	481.8259	979987.794
31	16:33:00	430	16:34:00	431.6	16:35:00	429.9	16:36:00	432.3	16:34:30	430.95	07:39:00	435.0834	979984.1014
B/S	**16:55:00**	**530.1**	**16:56:00**	**531.2**	**16:57:00**	**530.3**	**16:58:00**	**529.8**	**16:56:30**	**530.35**	**08:01:00**	**534.775**	**979991.977**

A.2.3 Kellyville Y-Y' transect

Station	Time 1	Reading1	Time 2	Reading2	Time 3	Reading3	Time 4	Reading4	Average Time	Average Reading	Elapsed Time	Corrected Reading	Absolute Gravity (mGal)
B/S	**8:41:00**	**820.2**	**8:43:00**	**819.6**	**8:44:00**	**819.6**	**8:45:00**	**821.9**	**8:43:15**	**820.325**	**00:00:00**	**824.4393**	**979991.977**
1	9:01:00	655.1	9:03:00	654.9	9:04:00	659.1	9:05:00	654.9	9:03:15	656	00:20:00	659.75686	979978.9671
2	9:12:00	740.8	9:14:00	744.2	9:15:00	745.2	9:16:00	746.1	9:14:15	744.075	00:31:00	747.63527	979985.9095
3	9:23:00	768.2	9:24:00	769.5	9:25:00	769.5	9:26:00	768.2	9:24:30	768.85	00:41:15	772.22709	979987.8522
B/S	**9:42:00**	**822.4**	**9:43:00**	**823.9**	**9:44:00**	**822.8**	**9:45:00**	**824.1**	**9:43:30**	**823.3**	**01:00:15**	**826.33752**	**979992.127**
4	9:56:00	823.5	9:57:00	824.5	9:58:00	822.9	9:59:00	823.6	9:57:30	823.625	01:14:15	826.41232	979992.1329
5	10:06:00	827.1	10:07:00	825.9	10:08:00	826.5	10:09:00	826.9	10:07:30	826.6	01:24:15	829.2086	979992.3538
6	10:17:00	840.5	10:18:00	840.5	10:19:00	841.8	10:20:00	843.4	10:18:30	841.55	01:35:15	843.96201	979993.5193
B/S	**10:35:00**	**827.5**	**10:36:00**	**827.5**	**10:37:00**	**827.5**	**10:38:00**	**828**	**10:36:30**	**827.625**	**01:53:15**	**829.71531**	**979992.3938**
7	10:50:00	879.1	10:51:00	879.1	10:52:00	883.1	10:53:00	884.9	10:51:30	881.55	02:08:15	883.37224	979996.6327
8	11:00:00	855.8	11:01:00	858.1	11:02:00	860.4	11:03:00	860.5	11:01:30	858.7	02:18:15	860.34352	979994.8134
9	11:10:00	855.1	11:11:00	854.9	11:12:00	855.8	11:13:00	855.5	11:11:30	855.325	02:28:15	856.7898	979994.5327
B/S	**11:36:00**	**825.5**	**11:37:00**	**827.3**	**11:38:00**	**826.5**	**11:39:00**	**826.7**	**11:37:30**	**826.5**	**02:54:15**	**827.50013**	**979992.2188**
10	11:43:00	833.5	11:44:00	836.8	11:45:00	836.1	11:46:00	837.1	11:44:30	835.875	03:01:15	836.75003	979992.9495
11	11:57:00	840.1	11:58:00	840.4	11:59:00	841.3	12:00:00	842.3	11:58:30	841.025	03:15:15	841.64982	979993.3366
12	12:01:00	861.2	12:02:00	861.1	12:03:00	861.4	12:04:00	861.8	12:02:30	861.375	03:19:15	861.92834	979994.9386
13	12:11:00	881.9	12:12:00	881.9	12:13:00	881.1	12:14:00	881.8	12:12:30	881.675	03:29:15	882.04962	979996.5282
14	12:19:00	889.8	12:20:00	890.5	12:21:00	891.1	12:22:00	890.8	12:20:30	890.55	03:37:15	890.78164	979997.218
B/S	**12:54:00**	**824.2**	**12:55:00**	**825.1**	**12:56:00**	**824.2**	**12:57:00**	**823.8**	**12:55:30**	**824.325**	**04:12:15**	**823.93113**	**979991.9369**
15	13:15:00	869.9	13:16:00	870	13:17:00	870	13:18:00	869.3	13:16:30	869.8	04:33:15	869.03082	979995.4997

16	13:24:00	855.9	13:25:00	855.9	13:26:00	855.5	13:27:00	855.6	13:25:30	855.725	04:42:15	854.79497	979994.3751
17	13:33:00	840.4	13:34:00	838.5	13:35:00	839.1	13:36:00	839	13:34:30	839.25	04:51:15	838.15913	979993.0609
18	13:43:00	848.1	13:44:00	848.5	13:45:00	848	13:46:00	849.1	13:44:30	848.425	05:01:15	847.15541	979993.7716
19	13:51:00	861.2	13:52:00	860.9	13:53:00	860.1	13:54:00	861.1	13:52:30	860.825	05:09:15	859.41243	979994.7399
B/S	**14:20:00**	**820.9**	**14:21:00**	**820.5**	**14:22:00**	**821.9**	**14:23:00**	**821**	**14:21:30**	**821.075**	**05:38:15**	**819.14415**	**979991.5587**
20	14:55:00	895.8	14:56:00	896.5	14:57:00	897.1	14:58:00	896.8	14:56:30	896.55	06:13:15	893.99364	979997.4718
21	15:07:00	800	15:08:00	800.7	15:09:00	800.5	15:10:00	802.8	15:08:30	801	06:25:15	798.22917	979989.9064
22	15:16:00	730.9	15:17:00	732.8	15:18:00	732.2	15:19:00	732.8	15:17:30	732.175	06:34:15	729.24333	979984.4565
23	15:27:00	698.8	15:28:00	698.7	15:29:00	700.1	15:30:00	698.5	15:28:30	699.025	06:45:15	695.89674	979981.8221
B/S	**15:47:00**	**828.1**	**15:48:00**	**827.9**	**15:49:00**	**827**	**15:50:00**	**828.7**	**15:48:30**	**827.925**	**07:05:15**	**824.4393**	**979991.977**

A.2.4 Kellyville X-X' transect

Station	Time 1	Reading1	Time 2	Reading2	Time 3	Reading3	Time 4	Reading4	Average Time	Average Reading	Elapsed Time	Corrected Reading	Absolute Gravity (mGal)
B/S	**8:38:00**	**818.7**	**8:39:00**	**818.9**	**8:40:00**	**819.4**	**8:41:00**	**818.5**	**08:39:30**	**818.875**	**00:00:00**	**812.47083**	**979991.977**
1	9:13:00	606.7	9:14:00	610.6	9:15:00	609.5	9:16:00	609.6	09:14:30	609.1	00:35:00	604.01955	979974.4043
2	9:27:00	686.9	9:28:00	687.9	9:29:00	686.5	9:30:00	688.9	09:28:30	687.55	00:49:00	682.99904	979981.1759
3	9:38:00	724.1	9:39:00	724.4	9:40:00	725.2	9:41:00	723.1	09:39:30	724.2	01:00:00	720.06506	979984.3723
B/S	**9:55:00**	**820.4**	**9:56:00**	**820.9**	**9:57:00**	**821.2**	**9:58:00**	**821.5**	**09:56:30**	**821**	**01:17:00**	**817.50801**	**979992.7257**
4	10:19:00	759.6	10:20:00	760.5	10:21:00	764.9	10:22:00	765.3	10:20:30	762.575	01:41:00	759.99071	979987.9366
5	10:30:00	755.3	10:31:00	756.5	10:32:00	755.5	10:33:00	755.2	10:31:30	755.625	01:52:00	753.45673	979987.427
6	10:42:00	784.9	10:43:00	784.2	10:44:00	785.5	10:45:00	785.5	10:43:30	785.025	02:04:00	783.31058	979990.0146
B/S	**11:05:00**	**816.1**	**11:06:00**	**813.7**	**11:07:00**	**814.1**	**11:08:00**	**813.2**	**11:06:30**	**814.275**	**02:27:00**	**813.43045**	**979992.6705**
7	11:38:00	783.3	11:39:00	783.6	11:40:00	782.8	11:41:00	784.4	11:39:30	783.525	03:00:00	783.92853	979990.3002
8	11:46:00	822.2	11:47:00	822.9	11:48:00	821.5	11:49:00	823.6	11:47:30	822.55	03:08:00	823.25609	979993.6764
9	11:54:00	807.3	11:55:00	807.8	11:56:00	807.9	11:57:00	808.7	11:55:30	807.925	03:16:00	808.93365	979992.4923
10	12:01:00	805.5	12:02:00	805.6	12:03:00	807.3	12:04:00	808.3	12:02:30	806.675	03:23:00	807.9484	979992.4376
11	12:11:00	808.2	12:12:00	809.1	12:13:00	809.5	12:14:00	810.4	12:12:30	809.3	03:33:00	810.9516	979992.7345
12	12:17:00	809.5	12:18:00	811.5	12:19:00	810.8	12:20:00	810.5	12:18:30	810.575	03:39:00	812.45353	979992.8872
B/S	**12:36:00**	**806.8**	**12:37:00**	**807.2**	**12:38:00**	**807.9**	**12:39:00**	**806.9**	**12:37:30**	**807.2**	**03:58:00**	**809.79712**	**979992.7405**
13	12:55:00	832.9	12:56:00	833.2	12:57:00	834.1	12:58:00	832.3	12:56:30	833.125	04:17:00	836.44071	979995.0843
14	13:02:00	849.9	13:03:00	851	13:04:00	850	13:05:00	849.5	13:03:30	850.1	04:24:00	853.68045	979996.5788
15	13:13:00	858.9	13:14:00	856.5	13:15:00	858.1	13:16:00	858.1	13:14:30	857.9	04:35:00	861.89647	979997.323

16	13:21:00	862.5	13:22:00	861.1	13:23:00	861.3	13:24:00	863.9	13:22:30	862.2	04:43:00	866.49904	979997.7475
17	13:30:00	866.5	13:31:00	868.5	13:32:00	869.1	13:33:00	871.9	13:31:30	869	04:52:00	873.63942	979998.3919
18	13:38:00	874.1	13:39:00	873.5	13:40:00	872.1	13:41:00	873.1	13:39:30	873.2	05:00:00	878.14199	979998.8079
19	13:47:00	879.1	13:48:00	879.4	13:49:00	877.3	13:50:00	877.5	13:48:30	878.325	05:09:00	883.60737	979999.3099
B/S	**14:16:00**	**807.3**	**14:17:00**	**810.1**	**14:18:00**	**809.8**	**14:19:00**	**810.2**	**14:17:30**	**809.35**	**05:38:00**	**815.72917**	**979993.661**
20	14:37:00	872	14:38:00	872.9	14:39:00	872.9	14:40:00	873.5	14:38:30	872.825	05:59:00	879.9984	979999.2113
21	14:46:00	871.1	14:47:00	870.7	14:48:00	872.1	14:49:00	871.4	14:47:30	871.325	06:08:00	878.83878	979999.1502
22	14:53:00	860.8	14:54:00	858.7	14:55:00	857.8	14:56:00	858.9	14:54:30	859.05	06:15:00	866.82853	979998.1585
B/S	**15:08:00**	**804.2**	**15:09:00**	**804.1**	**15:10:00**	**802.8**	**15:11:00**	**805.4**	**15:09:30**	**804.125**	**06:30:00**	**812.47083**	**979993.6005**

A.3 Gravity corrections

A.3.1 Onewhero Y-Y' transect

	Absolute G	Elevation	Latitude	Latitude correction	FAC	Bouguer correction	Simple anomaly	Regional anomaly	Residual anomaly	Bouguer anomaly
1	979984.8712	145	37.3142	978811.3038	44.747	16.2254565	1202.088979	40.2	1161.888979	-2.111021272
2	979989.9817	120	37.31478	978811.3266	37.032	13.427964	1202.259152	40.1	1162.159152	-1.840848082
3	979992.7568	108	37.31548	978811.354	33.3288	12.0851676	1202.646393	40	1162.646393	-1.353607018
4	979991.3489	114	37.31574	978811.3642	35.1804	12.7565658	1202.408462	39.9	1162.508462	-1.491538316
5	979991.6138	104	37.31658	978811.3972	32.0944	11.6375688	1200.673453	39.7	1160.973453	-3.026546998
6	979991.9367	103	37.31682	978811.4066	31.7858	11.5256691	1200.790155	39.6	1161.190155	-2.809845007
7	979992.0293	106	37.31712	978811.4184	32.7116	11.8613682	1201.461103	39.5	1161.961103	-2.038897097
8	979991.9925	103	37.31745	978811.4314	31.7858	11.5256691	1200.82122	39.4	1161.42122	-2.578779947
9	979991.7423	105	37.31776	978811.4435	32.403	11.7494685	1200.9523	39.4	1161.5523	-2.447699881
10	979991.884	110	37.31828	978811.464	33.946	12.308967	1202.057032	39.3	1162.757032	-1.242967944
11	979991.5006	103	37.3184	978811.4687	31.7858	11.5256691	1200.292068	39.2	1161.092068	-2.907931976
12	979990.7275	111	37.31857	978811.4753	34.2546	12.4208667	1201.08592	39.2	1161.88592	-2.114079842
13	979989.9895	112	37.3189	978811.4883	34.5632	12.5327664	1200.53169	39.1	1161.43169	-2.568310457
14	979990.0249	113	37.31925	978811.502	34.8718	12.6446661	1200.749999	39.1	1161.649999	-2.350001454
15	979989.8373	114	37.31951	978811.5122	35.1804	12.7565658	1200.74889	39	1161.74889	-2.251109594
16	979989.1495	114	37.31981	978811.524	35.1804	12.7565658	1200.049304	39	1161.049304	-2.950695597
17	979989.099	114	37.32008	978811.5346	35.1804	12.7565658	1199.988253	39	1160.988253	-3.011746569
18	979989.0446	116	37.32044	978811.5487	35.7976	12.9803652	1200.31312	39	1161.31312	-2.686880272

19	979988.913	116	37.32078	978811.5621	35.7976	12.9803652	1200.168121	38.9	1161.268121	-2.731879181
20	979988.7579	110	37.32103	978811.5719	33.946	12.308967	1198.822978	38.9	1159.922978	-4.077021941
21	979988.4081	110	37.3212	978811.5786	33.946	12.308967	1198.466528	38.8	1159.666528	-4.33347205
22	979988.3478	119	37.32138	978811.5857	36.7234	13.3160643	1200.169438	38.7	1161.469438	-2.530562222
23	979988.2431	113	37.32166	978811.5966	34.8718	12.6446661	1198.873592	38.6	1160.273592	-3.726408015
24	979988.5173	112	37.32204	978811.6116	34.5632	12.5327664	1198.936191	38.6	1160.336191	-3.663809474
25	979988.5417	112	37.32241	978811.6261	34.5632	12.5327664	1198.946038	38.6	1160.346038	-3.653961539
26	979988.6617	111	37.3228	978811.6414	34.2546	12.4208667	1198.854076	38.6	1160.254076	-3.745924051
27	979988.448	113	37.32318	978811.6563	34.8718	12.6446661	1199.018832	38.6	1160.418832	-3.581168156
28	979988.4794	112	37.32353	978811.6701	34.5632	12.5327664	1198.839789	38.6	1160.239789	-3.760210732
29	979988.9899	118	37.32424	978811.6979	36.4148	13.2041646	1200.502565	38.5	1162.002565	-1.997435438
30	979989.7924	116	37.32498	978811.727	35.7976	12.9803652	1200.882635	38.5	1162.382635	-1.617365425
31	979990.1143	117	37.3257	978811.7553	36.1062	13.0922649	1201.373015	38.4	1162.973015	-1.026985076
32	979991.3742	115	37.32665	978811.7926	35.489	12.8684655	1202.202188	38.4	1163.802188	-0.197812442
33	979991.376	112	37.32701	978811.8067	34.5632	12.5327664	1201.599726	38.4	1163.199726	-0.800274042
34	979990.0234	124	37.32738	978811.8212	38.2664	13.8755628	1202.592976	38.4	1164.192976	0.192975541
35	979988.5961	131	37.32783	978811.8389	40.4266	14.6588607	1202.524958	38.4	1164.124958	0.124958199
36	979986.9003	136	37.32836	978811.8597	41.9696	15.2183592	1201.791799	38.4	1163.391799	-0.608200987
37	979985.6416	148	37.32878	978811.8762	45.6728	16.5611556	1202.87701	38.4	1164.47701	0.477009911
38	979978.4901	171	37.32974	978811.9139	52.7706	19.1348487	1200.211995	38.5	1161.711995	-2.288004816

A.3.2 Onewhero X-X' transect

	Absolute G	Elevation	Latitude	Latitude correction	FAC	Bouguer correction	Simple anomaly	Regional anomaly	Residual anomaly	Bouguer anomaly
1	979986.17	145	37.3241	978811.6924	44.747	16.2254565	1202.999152	37.3	1165.699152	1.699151846
2	979988.7244	135	37.32342	978811.6657	41.661	15.1064595	1203.613236	37.4	1166.213236	2.213235718
3	979990.9734	124	37.32267	978811.6363	38.2664	13.8755628	1203.727957	37.7	1166.027957	2.027956653
4	979991.3257	133	37.32201	978811.6104	41.0438	14.8826601	1205.876435	37.8	1168.076435	4.076435393
5	979991.8752	120	37.32134	978811.5841	37.032	13.427964	1203.895162	38	1165.895162	1.895161693
6	979992.3655	123	37.32071	978811.5593	37.9578	13.7636631	1205.000272	38.1	1166.900272	2.900272142
7	979992.0572	118	37.32036	978811.5456	36.4148	13.2041646	1203.722247	38.2	1165.522247	1.522246984
8	979991.8196	116	37.32003	978811.5327	35.7976	12.9803652	1203.104231	38.3	1164.804231	0.804230978
9	979991.6858	114	37.31968	978811.5189	35.1804	12.7565658	1202.590747	38.4	1164.190747	0.190747104
10	979991.3555	110	37.31936	978811.5063	33.946	12.308967	1201.486232	38.5	1162.986232	-1.013768153
11	979991.7935	106	37.31902	978811.493	32.7116	11.8613682	1201.150777	38.6	1162.550777	-1.449223321
12	979991.8484	105	37.31869	978811.48	32.403	11.7494685	1201.02188	38.7	1162.32188	-1.678120241
13	979991.5663	106	37.31839	978811.4683	32.7116	11.8613682	1200.94829	38.8	1162.14829	-1.851710466
14	979990.4978	112	37.31764	978811.4388	34.5632	12.5327664	1201.089414	38.9	1162.189414	-1.810585964
15	979990.0136	120	37.31732	978811.4263	37.032	13.427964	1202.191371	39	1163.191371	-0.808628974
16	979990.2945	107	37.31698	978811.4129	33.0202	11.9732679	1199.928541	39.1	1160.828541	-3.171459333
17	979990.148	106	37.31668	978811.4011	32.7116	11.8613682	1199.597135	39.1	1160.497135	-3.502865307
18	979990.0074	106	37.31635	978811.3882	32.7116	11.8613682	1199.469413	39.2	1160.269413	-3.730587432
19	979989.993	105	37.31608	978811.3776	32.403	11.7494685	1199.268916	39.3	1159.968916	-4.031084356
20	979989.6508	109	37.31578	978811.3658	33.6374	12.1970673	1199.725367	39.4	1160.325367	-3.674633081
21	979989.4943	103	37.31542	978811.3517	31.7858	11.5256691	1198.4028	39.5	1158.9028	-5.097200066

22	979989.7219	99	37.3151	978811.3391	30.5514	11.0780703	1197.856162	39.6	1158.256162	-5.743838253
23	979989.5285	104	37.31482	978811.3281	32.0944	11.6375688	1198.657177	39.7	1158.957177	-5.042823453
24	979988.931	107	37.31452	978811.3163	33.0202	11.9732679	1198.661629	39.7	1158.961629	-5.038371244
25	979988.7123	105	37.31426	978811.3061	32.403	11.7494685	1198.059686	39.8	1158.259686	-5.740314301
26	979989.3125	108	37.31392	978811.2928	33.3288	12.0851676	1199.263344	39.8	1159.463344	-4.536655718
27	979989.1817	108	37.31331	978811.2689	33.3288	12.0851676	1199.156488	39.9	1159.256488	-4.743512271
28	979989.1703	109	37.31274	978811.2465	33.6374	12.1970673	1199.364189	40	1159.364189	-4.635810953
29	979989.2736	114	37.31208	978811.2206	35.1804	12.7565658	1200.476893	40	1160.476893	-3.523106776
30	979987.794	124	37.31141	978811.1943	38.2664	13.8755628	1200.990588	40.1	1160.890588	-3.109411818
31	979984.1014	135	37.31074	978811.168	41.661	15.1064595	1199.487936	40.2	1159.287936	-4.712063891

A.3.3 Kellville Y-Y' transect

	Absolute G	Elevation	Latitude	Latitude correction	FAC	Bouguer correction	Simple anomaly	Bouguer anomaly
1	979978.9671	87	37.28173	978810.0295	26.8482	8.021574	1187.76418	-0.235819763
2	979985.9095	59	37.28089	978809.9966	18.2074	5.439918	1188.680386	0.680386417
3	979987.8522	49	37.28006	978809.964	15.1214	4.517898	1188.491723	0.491722717
4	979992.1329	26	37.27925	978809.9322	8.0236	2.397252	1187.82698	-0.173020234
5	979992.3538	29	37.27831	978809.8954	8.9494	2.673858	1188.733958	0.733957571
6	979993.5193	22	37.27737	978809.8585	6.7892	2.028444	1188.421568	0.421567921
7	979996.6327	16	37.27642	978809.8212	4.9376	1.475232	1190.273857	2.273856731
8	979994.8134	19	37.27601	978809.8051	5.8634	1.751838	1189.119866	1.119866179
9	979994.5327	22	37.27554	978809.7867	6.7892	2.028444	1189.506754	1.506754278
10	979992.9495	30	37.27457	978809.7486	9.258	2.76606	1189.692849	1.692848521
11	979993.3366	23	37.27426	978809.7365	7.0978	2.120646	1188.577307	0.577307125
12	979994.9386	23	37.27389	978809.722	7.0978	2.120646	1190.193824	2.193824116
13	979996.5282	12	37.27344	978809.7043	3.7032	1.106424	1189.42068	1.420680001
14	979997.218	9	37.27298	978809.6863	2.7774	0.829818	1189.479361	1.479360781
15	979995.4997	17	37.27259	978809.671	5.2462	1.567434	1189.507528	1.507528489
16	979994.3751	19	37.2722	978809.6557	5.8634	1.751838	1188.830991	0.83099124
17	979993.0609	23	37.27177	978809.6388	7.0978	2.120646	1188.399219	0.399218964
18	979993.7716	18	37.27136	978809.6227	5.5548	1.659636	1188.044018	0.044018161
19	979994.7399	9	37.271	978809.6086	2.7774	0.829818	1187.078863	-0.921137318
20	979997.4718	10	37.27025	978809.5792	3.086	0.92202	1190.056595	2.056595227
21	979989.9064	28	37.2694	978809.5458	8.6408	2.581656	1186.419708	-1.580291547
22	979984.4565	54	37.26871	978809.5188	16.6644	4.978908	1186.62324	-1.376760134

A.3.4 Kellyville X-X' transect

	Absolute G	Elevation	Latitude	Latitude correction	FAC	Bouguer correction	Simple anomaly	Bouguer anomaly
1	979974.4043	108	37.27306	978809.6894	33.3288	12.0851676	1185.958568	-2.041432365
2	979981.1759	77	37.27332	978809.6996	23.7622	8.6162769	1186.622195	-1.377804989
3	979984.3723	67	37.27341	978809.7031	20.6762	7.4972799	1187.848065	-0.151935294
4	979987.9366	53	37.27329	978809.6984	16.3558	5.9306841	1188.663323	0.66332298
5	979987.427	48	37.2731	978809.691	14.8128	5.3711856	1187.177678	-0.822322037
6	979990.0146	43	37.27303	978809.6882	13.2698	4.8116871	1188.784453	0.784453171
7	979990.3002	36	37.2731	978809.691	11.1096	4.0283892	1187.690449	-0.309551278
8	979993.6764	22	37.27329	978809.6984	6.7892	2.4617934	1188.305337	0.305336757
9	979992.4923	25	37.27331	978809.6992	7.715	2.7974925	1187.710549	-0.289451387
10	979992.4376	30	37.27335	978809.7008	9.258	3.356991	1188.637874	0.637873947
11	979992.7345	30	37.27347	978809.7055	9.258	3.356991	1188.930067	0.930067237
12	979992.8872	26	37.27359	978809.7102	8.0236	2.9093922	1188.291199	0.291199062
13	979995.0843	21	37.27359	978809.7102	6.4806	2.3498937	1189.504795	1.504794998
14	979996.5788	18	37.27364	978809.7122	5.5548	2.0141946	1190.407251	2.407250644
15	979997.323	15	37.2737	978809.7145	4.629	1.6784955	1190.558949	2.558949264
16	979997.7475	15	37.27369	978809.7141	4.629	1.6784955	1190.983862	2.983862057
17	979998.3919	14	37.27366	978809.7129	4.3204	1.5665958	1191.432737	3.432736677
18	979998.8079	4	37.2736	978809.7106	1.2344	0.4475988	1189.884108	1.884107874
19	979999.3099	3	37.27358	978809.7098	0.9258	0.3356991	1190.190215	2.190215212
20	979999.2113	3	37.2736	978809.7106	0.9258	0.3356991	1190.090809	2.090808856
21	979999.1502	3	37.27382	978809.7192	0.9258	0.3356991	1190.021077	2.021076747
22	979998.1585	4	37.27394	978809.7239	1.2344	0.4475988	1189.221338	1.221337609

A.4 LINZ base-station tie

A.4.1 Onewhero base station tie

LINZ STATION										
#	Reading 1		Reading 2		Reading 3		Reading 4		Average time	Average reading
St 1	8:39	894.8	8:40	895.1	8:41	894.9	8:42	895.4	8:40	895.1
St 3	9:44	897.1	9:45	898.2	9:46	897.8	9:47	898.7	9:45	898.0
St 5	11:06	896.5	11:07	897.5	11:08	896.9	11:09	895.5	11:07	896.6
St 7	12:36	894.4	12:37	892.5	12:38	891.5	12:39	891.5	12:37	892.5
St 9	1:39	888.9	1:40	888.5	1:41	888.4	1:42	888.5	1:40	888.6
St 11	3:12	888.2	3:13	887.9	3:14	887.4	3:15	887.3	3:13	887.7
St 13	4:18	885.4	4:19	885.7	4:20	885.9	4:21	886.1	4:19	885.8
St 15	5:26	884.1	5:27	884.3	5:28	883.9	5:29	884.6	5:27	884.2

ONEWHERO BASE STATION										
#	Reading 1		Reading 2		Reading 3		Reading 4		Average time	Average reading
St 2	9:10	547.1	9:11	547.5	9:12	547.8	9:13	547.9	9:11	547.6
St 4	10:16	545.4	10:17	545.1	10:18	545.1	10:19	546.1	10:17	545.4
St 6	11:37	543.8	11:38	542.6	11:39	541.9	11:40	541.3	11:38	542.4
St 8	1:08	539.1	1:09	538.2	1:10	539.7	1:11	539.3	1:09	539.1
St 10	2:15	538.1	2:16	539	2:17	538.9	2:18	538.6	2:16	538.7
St 12	3:50	532.5	3:51	533.9	3:52	534.1	3:53	534.5	3:51	533.8
St 14	4:53	531.8	4:54	531.1	4:55	530.9	4:56	532.1	4:54	531.5

A.4.2 Kellyville base station tie

	LINZ STATION									
#	Reading 1		Reading 2		Reading 3		Reading 4		Average Time	Average reading
St 1	8:32	903.3	8:37	903.1	8:38	903.6	8:39	903.4	11:28	903.4
St 3	9:15	910.1	9:17	911.7	9:18	910.1	9:19	910.9	12:23	910.7
St 5	9:49	906.7	9:50	908.8	9:52	905.8	9:53	907.3	13:08	907.2
St 7	10:19	907.6	10:20	908.9	10:21	907.8	10:22	908.3	13:47	908.2
St 9	11:06	904.5	11:08	904.9	11:09	905.5	11:10	905.1	14:51	905.0
St 11	11:39	905.2	11:40	905.1	11:41	905.5	11:42	903.1	15:34	904.7
St 13	12:18	903.3	12:19	903.3	12:20	903.8	12:21	903.9	16:26	903.6
St 15	1:22	897.8	1:23	899.6	1:24	898.8	1:25	896.4	1:51	898.2
St 17	1:50	897.4	1:51	896.9	1:52	895.9	1:53	896.3	2:28	896.6
St 19	2:25	898	2:26	897.2	2:27	898.7	2:28	896.9	3:15	897.7
St 21	2:57	897.7	2:58	898	2:59	896.3	3:00	898.1	3:58	897.5
St 23	3:28	893.3	3:29	897.5	3:30	894.5	3:31	895.4	4:39	895.2
St 25	3:58	894.5	3:59	893.1	4:00	894.2	4:00	895.5	5:19	894.3
St 27	4:25	894.4	4:26	896.5	4:27	898.2	4:28	896.9	5:55	896.5

	MERCER BASE STATION

#	Reading 1		Reading 2		Reading 3		Reading 4		Average Time	Average reading
St 2	8:56	853.8	8:57	851.7	8:59	853.2	9:00	853.1	8:58	852.95
St 4	9:32	850.6	9:34	851.7	9:36	852.7	9:37	852.3	9:34	851.825
St 6	10:03	850.2	10:04	852.6	10:05	853.1	10:06	851.7	10:04	851.9
St 8	10:52	848.3	10:53	848.8	10:54	850.1	10:55	852.3	10:53	849.875
St 10	11:22	850.1	11:23	850.9	11:24	850.6	11:25	851.2	11:23	850.7
St 12	12:01	848.7	12:04	849.5	12:06	848.6	12:07	848.6	12:04	848.85
St 14	12:33	843.6	12:34	841.8	12:35	842.3	12:36	844.6	12:34	843.075
St 16	1:35	839	1:36	837.5	1:37	839.4	1:38	838.6	1:36	838.625
St 18	2:07	836	2:08	834.9	2:09	834.4	2:10	834.8	2:08	835.025
St 20	2:42	840.5	2:43	839.6	2:44	841.9	2:45	843	2:43	841.25
St 22	3:10	837.3	3:11	839.6	3:12	838.9	3:13	839.6	3:11	838.85
St 24	3:44	838.4	3:45	842.5	3:46	840.6	3:47	844.2	3:45	841.425
St 26	4:15	839.1	4:16	841.6	4:17	841.8	4:18	841.5	4:16	841

A.5 Raw two-dimensional gravity models

A.5.1 Onewhero Y – Y' transect

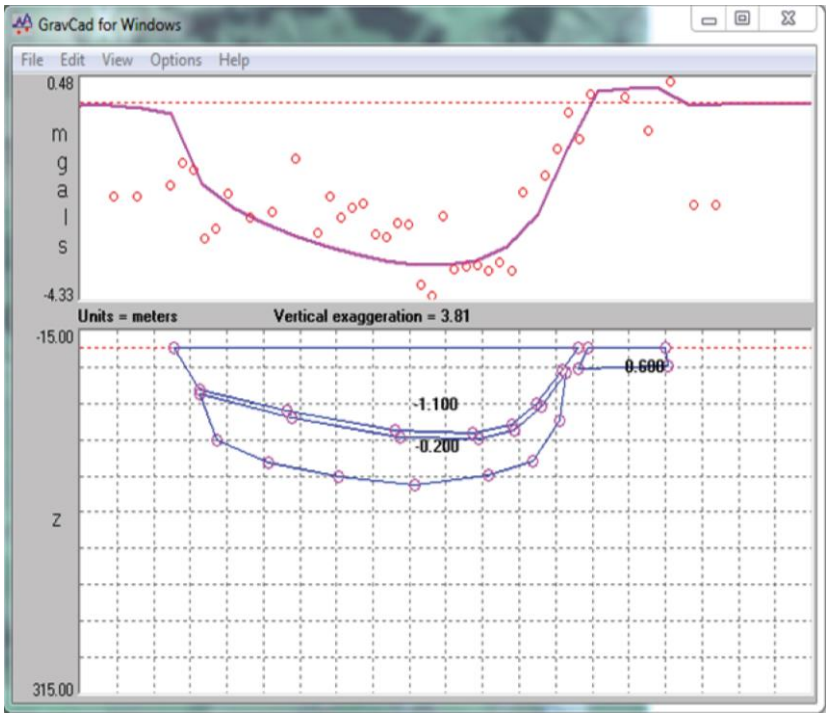

A.5.2 Onewhero X – X' transect

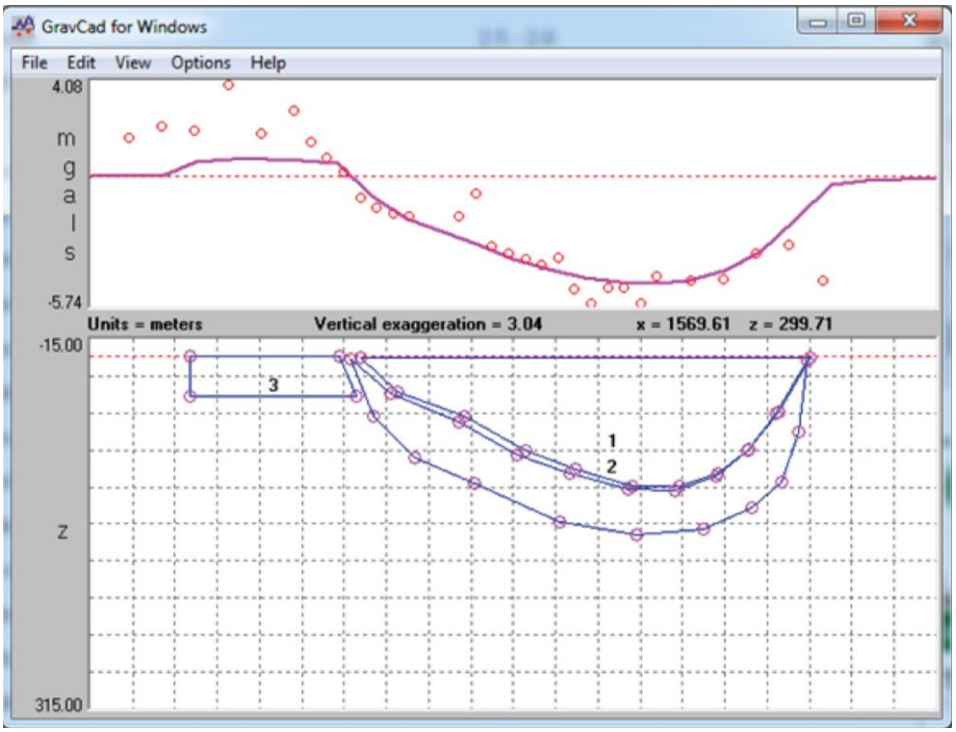

A.5.3 Kellyville Y – Y' transect

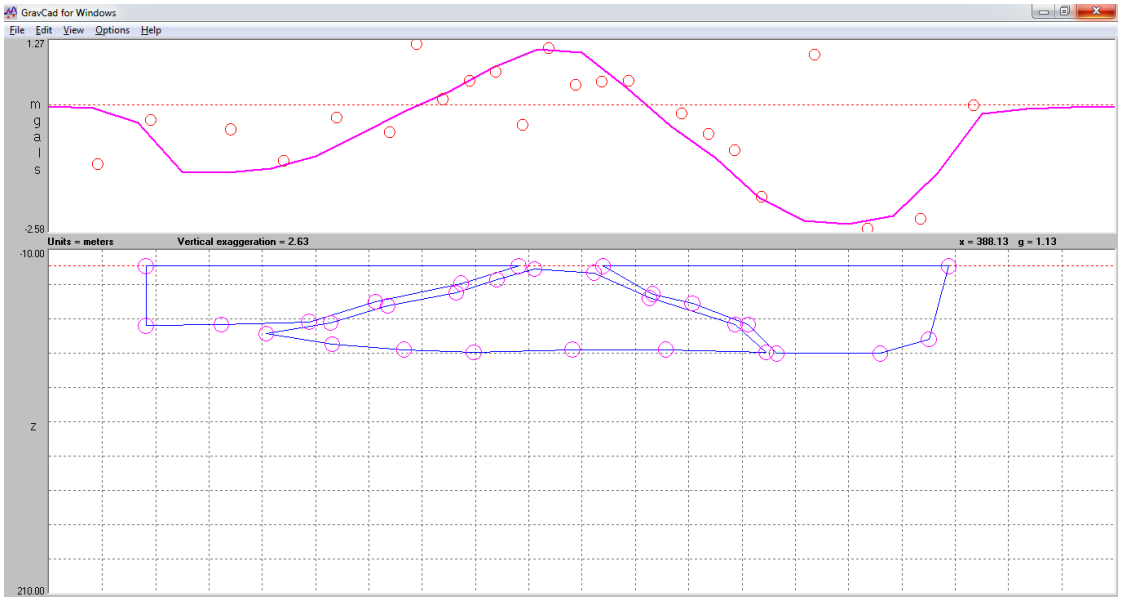

A.5.4 Kellyville X – X' transect

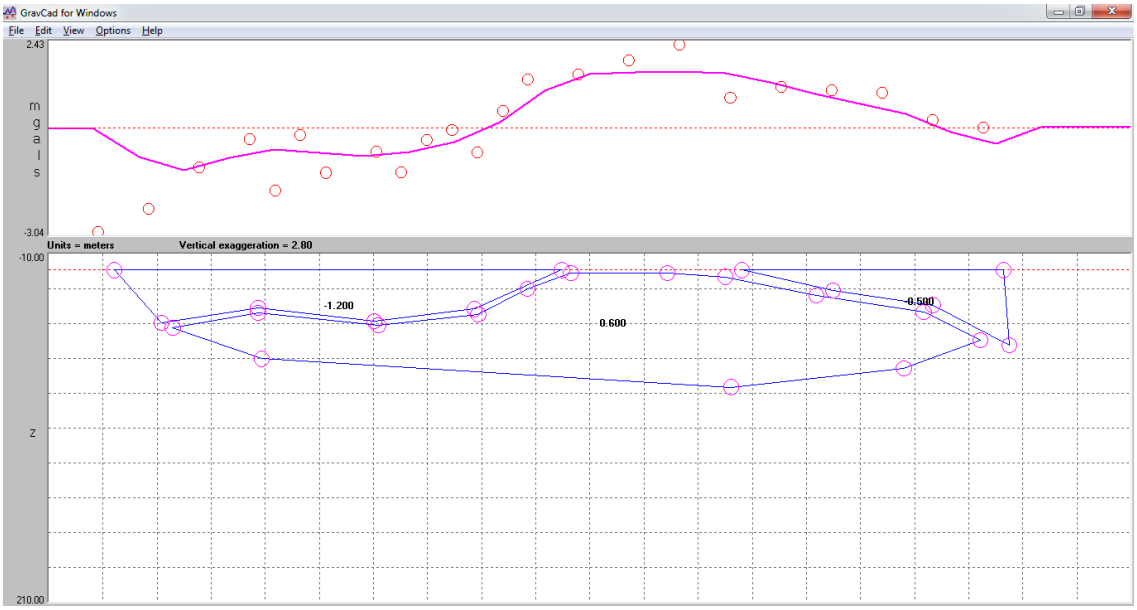

Appendix B – Magnetic investigation

B.1 Onewhero magnetic survey – raw data

Waypoint	Southing	Easting	Value	Anomaly value
1	-37.32473	174.89483	54002	-25
2	-37.32455	174.89544	53943	-84
3	-37.32428	174.89592	54019	-8
4	-37.32404	174.89548	54010	-17
5	-37.32446	174.89473	54001	-26
6	-37.32413	174.89443	54010	-17
7	-37.3238	174.89479	54019	-8
8	-37.32385	174.89414	53923	-104
9	-37.32344	174.89473	53924	-103
10	-37.32325	174.89499	54011	-16
11	-37.32309	174.89523	54013	-14
12	-37.32322	174.89552	54028	1
13	-37.32364	174.89527	54038	11
14	-37.32378	174.89555	54034	7
15	-37.32357	174.89576	54026	-1
16	-37.32336	174.89595	54027	0
17	-37.32347	174.89623	54014	-13
18	-37.32368	174.89612	54002	-25
19	-37.32391	174.89599	54029	2
20	-37.32405	174.89628	54027	0
21	-37.3238	174.89645	54021	-6
22	-37.3236	174.89656	54015	-12
23	-37.32367	174.89688	54022	-5
24	-37.32388	174.89676	54021	-6
25	-37.32412	174.89665	54013	-14
26	-37.32423	174.89691	53962	-65
27	-37.32398	174.89703	53951	-76
28	-37.32374	174.89713	53977	-50
29	-37.32509	174.89647	54001	-26
30	-37.32485	174.89662	53997	-30
31	-37.32459	174.89673	53991	-36
32	-37.32445	174.89647	54018	-9
33	-37.32438	174.89627	53977	-50

34	-37.3246	174.89618	53995	-32
35	-37.32484	174.89603	53955	-72
36	-37.32499	174.89598	53972	-55
37	-37.32521	174.89591	53811	-216
38	-37.32549	174.89576	53901	-126
39	-37.32579	174.89562	53984	-43
40	-37.32589	174.89602	54023	-4
41	-37.32559	174.89617	54008	-19
42	-37.32544	174.89671	53990	-37
43	-37.32574	174.89655	54007	-20
44	-37.32603	174.89637	53954	-73
45	-37.32514	174.89676	54029	2
46	-37.32468	174.89702	53977	-50
47	-37.3248	174.89739	53971	-56
48	-37.32528	174.89719	53856	-171
49	-37.3254	174.89755	53981	-46
50	-37.32502	174.8978	53986	-41
51	-37.32514	174.89819	53912	-115
52	-37.32565	174.89791	53912	-115
53	-37.32528	174.89857	54014	-13
54	-37.32584	174.89839	53976	-51
55	-37.32545	174.89908	53907	-120
56	-37.32575	174.89889	53920	-107
57	-37.32599	174.89878	53973	-54
58	-37.32631	174.89865	54030	3
59	-37.32662	174.89852	54075	48
60	-37.32693	174.8984	54102	75
61	-37.32703	174.89877	54119	92
62	-37.32675	174.89891	54114	87
63	-37.32644	174.89902	54106	79
64	-37.32614	174.89912	54082	55
65	-37.32585	174.89925	54051	24
66	-37.32556	174.8994	54032	5
67	-37.32569	174.89976	54039	12
68	-37.32598	174.89959	54047	20
69	-37.32627	174.89946	54067	40
70	-37.32658	174.89934	54077	50
71	-37.32688	174.89921	54094	67
72	-37.32719	174.89904	54106	79
73	-37.32728	174.89934	54082	55
74	-37.327	174.89948	54083	56
75	-37.32669	174.89963	54046	19
76	-37.3264	174.89978	54046	19
77	-37.32611	174.89993	54099	72
78	-37.32586	174.90009	54100	73
79	-37.32566	174.90014	54105	78

80	-37.32536	174.90026	54115	88
81	-37.32507	174.9004	54130	103
82	-37.32475	174.90053	54137	110
83	-37.32453	174.90065	54109	82
84	-37.32441	174.90032	54083	56
85	-37.32469	174.90014	54081	54
86	-37.32499	174.9	54130	103
87	-37.32528	174.89981	54137	110
88	-37.32548	174.8997	54073	46
89	-37.32535	174.89937	54052	25
90	-37.32506	174.89954	54025	-2
91	-37.32476	174.8997	54071	44
92	-37.32448	174.8999	54105	78
93	-37.32425	174.90004	54109	82
94	-37.32413	174.89968	54090	63
95	-37.32439	174.8995	54025	-2
96	-37.32467	174.89936	54046	19
97	-37.32496	174.8992	54032	5
98	-37.32521	174.89903	53994	-33
99	-37.32504	174.89871	53959	-68
100	-37.32477	174.89892	53849	-178
101	-37.32444	174.89909	53926	-101
102	-37.32413	174.89922	53954	-73
103	-37.32396	174.89932	53966	-61
104	-37.32373	174.89938	53985	-42
105	-37.32386	174.8997	53954	-73
106	-37.324	174.90007	54036	9
107	-37.32415	174.90041	54064	37
108	-37.32427	174.90079	54055	28
109	-37.32401	174.90093	54053	26
110	-37.32371	174.90107	54027	0
111	-37.32342	174.90121	53987	-40
112	-37.32314	174.90137	53981	-46
113	-37.32287	174.90152	53940	-87
114	-37.32303	174.90104	53912	-115
115	-37.32318	174.90069	53945	-82
116	-37.32345	174.90063	53972	-55
117	-37.32376	174.90055	54012	-15
118	-37.32407	174.90044	54042	15
119	-37.32397	174.9001	54070	43
120	-37.32368	174.9002	54018	-9
121	-37.32336	174.90028	54032	5
122	-37.32346	174.89994	54004	-23
123	-37.3234	174.89943	54010	-17
124	-37.32303	174.89964	53856	-171
125	-37.32262	174.89984	53948	-79

126	-37.32228	174.90005	53955	-72
127	-37.3224	174.90054	53986	-41
128	-37.32249	174.90102	53975	-52
129	-37.32258	174.9015	53950	-77
130	-37.32276	174.90104	53949	-78
131	-37.32294	174.90062	53949	-78
132	-37.32265	174.90077	53874	-153
133	-37.32254	174.90041	53956	-71
134	-37.32276	174.90032	53962	-65
135	-37.32312	174.90008	53953	-74
136	-37.3221	174.89987	53998	-29
137	-37.32205	174.89942	54029	2
138	-37.32239	174.89926	53995	-32
139	-37.32271	174.89911	53968	-59
140	-37.32307	174.89894	53885	-142
141	-37.32323	174.89931	53946	-81
142	-37.32288	174.8995	53906	-121
143	-37.32312	174.89769	53991	-36
144	-37.32313	174.8977	54001	-26
145	-37.32275	174.89789	53975	-52
146	-37.32241	174.89806	54035	8
147	-37.32209	174.89825	54012	-15
148	-37.32213	174.89869	54010	-17
149	-37.32247	174.89854	53993	-34
150	-37.3228	174.89836	53874	-153
151	-37.32312	174.8982	54019	-8
152	-37.32274	174.89756	54026	-1
153	-37.32241	174.89773	54085	58
154	-37.32202	174.89792	54098	71
155	-37.32181	174.89753	54087	60
156	-37.32208	174.89724	54057	30
157	-37.32239	174.89698	54071	44
158	-37.32224	174.89658	54048	21
159	-37.32244	174.89612	54049	22
160	-37.32267	174.89579	54049	22
161	-37.32288	174.89553	54029	2
162	-37.32303	174.89587	54059	32
163	-37.32278	174.89605	54063	36
164	-37.32254	174.89627	54058	31
165	-37.32264	174.89665	54045	18
166	-37.32289	174.89651	54003	-24
167	-37.32316	174.89632	54029	2
168	-37.32329	174.89666	54046	19
169	-37.323	174.89678	54029	2
170	-37.3227	174.8969	54023	-4
171	-37.32282	174.89728	54031	4

172	-37.32308	174.8971	53991	-36
173	-37.32337	174.89692	53982	-45
174	-37.32334	174.8976	53959	-68
175	-37.32341	174.89799	53913	-114
176	-37.32348	174.89837	53838	-189
177	-37.32357	174.89874	53907	-120
178	-37.32384	174.89866	53888	-139
179	-37.32417	174.89858	53876	-151
180	-37.32445	174.89845	53879	-148
181	-37.32473	174.89831	53901	-126
182	-37.32462	174.89796	53895	-132
183	-37.32431	174.89809	53898	-129
184	-37.32401	174.8982	53930	-97
185	-37.32392	174.89784	53933	-94
186	-37.3242	174.89773	53935	-92
187	-37.32452	174.89767	53924	-103
188	-37.32441	174.89728	53959	-68
189	-37.3241	174.89739	53977	-50
190	-37.32381	174.8975	53985	-42
191	-37.32444	174.89248	54011	-16
192	-37.3242	174.89262	53993	-34
193	-37.32405	174.8922	53972	-55
194	-37.32426	174.89178	53961	-66
195	-37.32373	174.89195	53992	-35
196	-37.32359	174.89157	53988	-39
197	-37.32417	174.89149	53994	-33
198	-37.32378	174.8922	53992	-35
199	-37.32412	174.893	53972	-55
200	-37.32384	174.89343	53990	-37
201	-37.32352	174.89274	54003	-24
202	-37.32386	174.89245	53974	-53
203	-37.32332	174.89234	53975	-52
204	-37.32312	174.89247	53976	-51
205	-37.32282	174.89264	53976	-51
206	-37.32254	174.89281	53995	-32
207	-37.32285	174.89342	53910	-117
208	-37.3231	174.89316	53970	-57
209	-37.32341	174.89327	53993	-34
210	-37.32363	174.89371	54003	-24
211	-37.3232	174.89428	53978	-49
212	-37.32293	174.89369	53957	-70
213	-37.323	174.8923	53945	-82
214	-37.3228	174.8916	53969	-58
215	-37.3225	174.89161	53974	-53
216	-37.32207	174.89161	53965	-62
217	-37.32243	174.89253	53963	-64

218	-37.32271	174.89246	53928	-99
219	-37.32228	174.89273	53963	-64
220	-37.32215	174.89252	53913	-114
221	-37.32206	174.89225	53971	-56
222	-37.32194	174.89197	53955	-72
223	-37.32184	174.89169	53976	-51
224	-37.32162	174.89182	53956	-71
225	-37.3217	174.89211	53916	-111
226	-37.3218	174.8924	53975	-52
227	-37.32189	174.8927	53981	-46
228	-37.32181	174.89305	53976	-51
229	-37.32171	174.89281	53955	-72
230	-37.32161	174.8926	53969	-58
231	-37.32152	174.89232	53972	-55
232	-37.32141	174.89202	53975	-52
233	-37.32131	174.89177	53982	-45
234	-37.32124	174.89255	53991	-36
235	-37.32142	174.89321	53997	-30
236	-37.32171	174.89394	53970	-57
237	-37.32196	174.89384	53995	-32
238	-37.32212	174.89412	54004	-23
239	-37.32181	174.89431	54000	-27
240	-37.32196	174.8947	53921	-106
241	-37.32229	174.89454	53955	-72
242	-37.32245	174.89493	54007	-20
243	-37.32212	174.89591	54030	3
244	-37.32206	174.89588	54045	18
245	-37.32173	174.89632	54032	5
246	-37.32151	174.89649	54006	-21
247	-37.32076	174.89704	54055	28
248	-37.32066	174.8968	54114	87
249	-37.32051	174.8964	54107	80
250	-37.32071	174.89625	54091	64
251	-37.32078	174.89655	54058	31
252	-37.32099	174.89642	54092	65
253	-37.32091	174.89616	54095	68
254	-37.32109	174.89599	53993	-34
255	-37.3212	174.89628	54074	47
256	-37.32139	174.89602	54080	53
257	-37.32126	174.89588	54081	54
258	-37.32144	174.89568	54078	51
259	-37.32179	174.89575	54023	-4
260	-37.32169	174.89549	54073	46
261	-37.32186	174.89529	54061	34
262	-37.32201	174.89556	54055	28
263	-37.32178	174.89497	54015	-12

264	-37.32157	174.89517	54053	26
265	-37.32137	174.89537	54024	-3
266	-37.32116	174.89555	54048	21
267	-37.32092	174.89573	54032	5
268	-37.32071	174.89589	54053	26
269	-37.32046	174.89598	54059	32
270	-37.32035	174.89571	54089	62
271	-37.32021	174.89543	54085	58
272	-37.3204	174.89527	54239	212
273	-37.32054	174.89553	54059	32
274	-37.32075	174.89538	54074	47
275	-37.32064	174.89512	54076	49
276	-37.32084	174.89495	53992	-35
277	-37.32096	174.89523	54063	36
278	-37.32114	174.89507	54049	22
279	-37.32102	174.8948	54060	33
280	-37.32121	174.89465	54052	25
281	-37.32136	174.8949	54038	11
282	-37.32155	174.89471	54019	-8
283	-37.32146	174.89444	54039	12
284	-37.32147	174.89404	54032	5
285	-37.32132	174.8937	54022	-5
286	-37.32119	174.89334	53988	-39
287	-37.32104	174.89297	54003	-24
288	-37.32092	174.89261	53992	-35
289	-37.3205	174.89258	53984	-43
290	-37.32023	174.89275	53976	-51
291	-37.32035	174.89308	54026	-1
292	-37.32061	174.89291	54024	-3
293	-37.32076	174.89325	54085	58
294	-37.32049	174.89342	54009	-18
295	-37.32062	174.89379	54017	-10
296	-37.32087	174.8936	54042	15
297	-37.32099	174.89399	54032	5
298	-37.3207	174.89411	54000	-27
299	-37.32079	174.89436	54032	5
300	-37.32107	174.89425	54042	15
301	-37.32057	174.89447	54046	19
302	-37.32043	174.89413	54043	16
303	-37.3203	174.89377	54053	26
304	-37.32017	174.89342	54048	21
305	-37.32004	174.89202	54041	14
306	-37.31975	174.8932	54032	5
307	-37.31946	174.89338	54006	-21
308	-37.31975	174.8941	54017	-10
309	-37.32001	174.89392	54023	-4

310	-37.31989	174.89358	54020	-7
311	-37.32016	174.89428	54043	16
312	-37.31989	174.89446	54037	10
313	-37.31996	174.89474	54051	24
314	-37.32025	174.89457	54045	18
315	-37.3196	174.89511	54067	40
316	-37.31946	174.89475	54053	26
317	-37.31934	174.8944	54072	45
318	-37.31919	174.89406	54051	24
319	-37.31905	174.89369	54039	12
320	-37.31894	174.89334	54023	-4
321	-37.31887	174.89429	54028	1
322	-37.31874	174.89394	54019	-8
323	-37.31858	174.89361	53957	-70
324	-37.31831	174.89378	54004	-23
325	-37.31803	174.89399	53948	-79
326	-37.31775	174.89417	54016	-11
327	-37.31749	174.89436	53997	-30
328	-37.31763	174.89468	54000	-27
329	-37.31791	174.89452	53950	-77
330	-37.31818	174.89433	53988	-39
331	-37.31844	174.89417	53994	-33
332	-37.31872	174.89441	54019	-8
333	-37.31844	174.89459	53935	-92
334	-37.31816	174.89478	54005	-22
335	-37.31789	174.89498	53999	-28
336	-37.31924	174.89529	53958	-69
337	-37.31909	174.89497	53962	-65
338	-37.31881	174.8951	54041	14
339	-37.31854	174.89529	54036	9
340	-37.31824	174.89545	54040	13
341	-37.31835	174.89579	54008	-19
342	-37.31861	174.89564	53983	-44
343	-37.31888	174.89545	53952	-75
344	-37.31952	174.89553	53997	-30
345	-37.31973	174.89543	54034	7
346	-37.31985	174.89571	54060	33
347	-37.31999	174.89605	54072	45
348	-37.32014	174.89635	54077	50
349	-37.31991	174.89656	54094	67
350	-37.31978	174.89624	54098	71
351	-37.31964	174.8959	54088	61
352	-37.31726	174.89659	54077	50
353	-37.3174	174.89692	54007	-20
354	-37.31752	174.89719	53740	-287
355	-37.31764	174.89751	53689	-338

356	-37.31792	174.89735	53663	-364
357	-37.31817	174.89719	53640	-387
358	-37.31804	174.89686	53696	-331
359	-37.31779	174.89698	53764	-263
360	-37.31765	174.89666	53767	-260
361	-37.31792	174.89652	53722	-305
362	-37.3182	174.89639	53748	-279
363	-37.31831	174.89675	53793	-234
364	-37.31843	174.89711	53859	-168
365	-37.31858	174.89743	53836	-191
366	-37.31884	174.89728	53814	-213
367	-37.31909	174.89711	53808	-219
368	-37.31897	174.89677	53881	-146
369	-37.31871	174.89693	53951	-76
370	-37.31859	174.89661	53950	-77
371	-37.31883	174.89648	53892	-135
372	-37.31872	174.89609	53891	-136
373	-37.31844	174.89629	53954	-73
374	-37.31898	174.89597	53958	-69
375	-37.31909	174.89643	53835	-192
376	-37.31921	174.89675	54006	-21
377	-37.31932	174.89713	53961	-66
378	-37.31945	174.89746	53993	-34
379	-37.31974	174.89735	53984	-43
380	-37.31965	174.897	53974	-53
381	-37.31953	174.89664	54033	6
382	-37.31939	174.89632	53996	-31
383	-37.31927	174.89595	54042	15
384	-37.31643	174.89639	54042	15
385	-37.31643	174.89668	54039	12
386	-37.3162	174.89681	53728	-299
387	-37.31591	174.89693	53690	-337
388	-37.31566	174.89702	53676	-351
389	-37.31579	174.89734	53586	-441
390	-37.31549	174.89754	53650	-377
391	-37.31525	174.89765	53561	-466
392	-37.31497	174.89775	53517	-510
393	-37.31468	174.89786	53483	-544
394	-37.3144	174.89797	53543	-484
395	-37.31416	174.89808	53545	-482
396	-37.31388	174.89822	53590	-437
397	-37.31398	174.89849	53612	-415
398	-37.31411	174.89884	53669	-358
399	-37.31423	174.89912	53602	-425
400	-37.31469	174.89897	53524	-503
401	-37.31462	174.8986	53463	-564

402	-37.31453	174.89823	53354	-673
403	-37.31481	174.89812	53445	-582
404	-37.31507	174.89795	53526	-501
405	-37.31533	174.89782	53496	-531
406	-37.31559	174.89765	53480	-547
407	-37.31582	174.89748	53480	-547
408	-37.31608	174.89806	53494	-533
409	-37.3162	174.8984	53478	-549
410	-37.31633	174.89739	53335	-692
411	-37.31674	174.89681	53313	-714
412	-37.317	174.89668	53538	-489
413	-37.3171	174.89699	53696	-331
414	-37.31685	174.89709	53669	-358
415	-37.3169	174.89742	53630	-397
416	-37.31665	174.89747	53655	-372
417	-37.31716	174.89733	53601	-426
418	-37.31724	174.89763	53575	-452
419	-37.31697	174.89768	53637	-390
420	-37.31673	174.89774	53598	-429
421	-37.31678	174.89813	53555	-472
422	-37.31706	174.89805	53517	-510
423	-37.31736	174.898	53463	-564
424	-37.31643	174.89635	53515	-512
425	-37.31635	174.89605	53562	-465
426	-37.31627	174.89572	53762	-265
427	-37.31601	174.89583	53815	-212
428	-37.31574	174.89593	53801	-226
429	-37.31548	174.89607	53860	-167
430	-37.31553	174.89638	53848	-179
431	-37.31562	174.89671	53834	-193
432	-37.31587	174.89661	53778	-249
433	-37.31581	174.89629	53722	-305
434	-37.31536	174.89732	53738	-289
435	-37.31507	174.89741	53744	-283
436	-37.31479	174.89754	53605	-422
437	-37.31449	174.8977	53614	-413
438	-37.31417	174.89781	53588	-439
439	-37.31389	174.89794	53627	-400
440	-37.31378	174.89758	53672	-355
441	-37.31405	174.89742	53654	-373
442	-37.31431	174.89729	53702	-325
443	-37.31457	174.89713	53723	-304
444	-37.31483	174.897	53716	-311
445	-37.31513	174.89689	53707	-320
446	-37.32267	174.90328	53685	-342
447	-37.32397	174.90279	53708	-319

448	-37.32391	174.90242	54119	92
449	-37.32383	174.90203	53887	-140
450	-37.32375	174.90167	53887	-140
451	-37.32399	174.90158	53907	-120
452	-37.32431	174.90146	53943	-84
453	-37.32458	174.90135	53956	-71
454	-37.32466	174.90172	53969	-58
455	-37.32436	174.90179	53984	-43
456	-37.32406	174.90187	53937	-90
457	-37.3241	174.90225	53926	-101
458	-37.3244	174.90219	53927	-100
459	-37.32472	174.90212	53893	-134
460	-37.32479	174.90236	53900	-127
461	-37.32454	174.90251	53912	-115
462	-37.32424	174.90267	53899	-128
463	-37.32377	174.90288	53892	-135
464	-37.3237	174.90254	53881	-146
465	-37.32361	174.90217	53897	-130
466	-37.32354	174.90182	53886	-141
467	-37.32328	174.90192	53897	-130
468	-37.32301	174.90204	53915	-112
469	-37.3227	174.90213	53897	-130
470	-37.32281	174.90248	53901	-126
471	-37.32309	174.90234	53926	-101
472	-37.32333	174.9022	53934	-93
473	-37.3234	174.90259	53908	-119
474	-37.32313	174.90272	53891	-136
475	-37.32285	174.90286	53901	-126
476	-37.32292	174.90311	53924	-103
477	-37.3232	174.90303	53948	-79
478	-37.32348	174.90292	53951	-76
479	-37.32248	174.90348	53934	-93
480	-37.32253	174.90382	53914	-113
481	-37.32263	174.90421	53971	-56
482	-37.32271	174.90459	53972	-55
483	-37.32279	174.90495	53967	-60
484	-37.32248	174.90501	53951	-76
485	-37.32218	174.90508	53955	-72
486	-37.32215	174.90473	53971	-56
487	-37.32243	174.90466	53985	-42
488	-37.32234	174.90432	53986	-41
489	-37.32203	174.9044	53973	-54
490	-37.32193	174.90403	53982	-45
491	-37.32216	174.90386	53994	-33
492	-37.32206	174.90356	54002	-25
493	-37.32181	174.90366	53992	-35

494	-37.32177	174.90337	53996	-31
495	-37.32205	174.9033	54002	-25
496	-37.32233	174.9032	54011	-16
497	-37.32236	174.90318	54000	-27
498	-37.32226	174.90281	53982	-45
499	-37.32199	174.9029	53987	-40
500	-37.32172	174.90296	53988	-39
501	-37.32163	174.90261	54008	-19
502	-37.32191	174.90247	54023	-4
503	-37.3222	174.90235	54031	4
504	-37.32214	174.90197	54018	-9
505	-37.32184	174.90201	53992	-35
506	-37.32153	174.90208	53995	-32
507	-37.32148	174.90174	54027	0
508	-37.32172	174.9016	54047	20
509	-37.32201	174.90153	54058	31
510	-37.32195	174.90116	54037	10
511	-37.32168	174.90129	54005	-22
512	-37.32137	174.90133	54011	-16
513	-37.32142	174.90077	54045	18
514	-37.32115	174.90087	54067	40
515	-37.32086	174.901	54067	40
516	-37.32056	174.90106	54081	54
517	-37.32027	174.90113	54075	48
518	-37.31997	174.90123	54056	29
519	-37.31965	174.90133	54025	-2
520	-37.31957	174.90096	53978	-49
521	-37.31985	174.90087	53923	-104
522	-37.32012	174.90076	53897	-130
523	-37.32043	174.90068	53954	-73
524	-37.32074	174.90055	53956	-71
525	-37.32101	174.90047	54055	28
526	-37.32134	174.90039	54075	48
527	-37.32135	174.90021	54094	67
528	-37.32103	174.90028	54085	58
529	-37.32075	174.90037	54065	38
530	-37.32045	174.90044	54098	71
531	-37.32015	174.90052	54084	57
532	-37.31986	174.9006	54051	24
533	-37.31956	174.90067	54004	-23
534	-37.31949	174.90032	53945	-82
535	-37.31976	174.90021	53885	-142
536	-37.32003	174.90015	53856	-171
537	-37.32033	174.90005	53921	-106
538	-37.3206	174.89994	53978	-49
539	-37.32088	174.89983	54038	11

540	-37.32118	174.89976	54048	21
541	-37.32145	174.89964	54101	74
542	-37.32174	174.89942	54104	77
543	-37.32149	174.89948	54076	49
544	-37.32122	174.89956	54058	31
545	-37.32094	174.89961	54097	70
546	-37.32066	174.8997	54115	88
547	-37.32037	174.89977	54109	82
548	-37.32009	174.89985	54086	59
549	-37.31981	174.89996	54026	-1
550	-37.31953	174.90006	53992	-35
551	-37.31944	174.89974	53935	-92
552	-37.31967	174.89965	53875	-152
553	-37.31995	174.89956	53847	-180
554	-37.32024	174.8995	53911	-116
555	-37.32048	174.89943	53972	-55
556	-37.3208	174.89932	54027	0
557	-37.32108	174.89923	54071	44
558	-37.3214	174.89915	54111	84
559	-37.32165	174.89908	54124	97
560	-37.32162	174.89891	54118	91
561	-37.32132	174.899	54096	69
562	-37.32102	174.89909	54104	77
563	-37.32076	174.89921	54123	96
564	-37.32042	174.89928	54124	97
565	-37.3201	174.8993	54040	13
566	-37.31979	174.89944	54060	33
567	-37.31948	174.89955	54002	-25
568	-37.31939	174.89925	53935	-92
569	-37.31969	174.89914	53859	-168
570	-37.31997	174.89906	53810	-217
571	-37.32028	174.89897	53921	-106
572	-37.32057	174.89887	53985	-42
573	-37.3209	174.89878	54041	14
574	-37.32119	174.89866	54083	56
575	-37.32149	174.89854	54113	86
576	-37.32151	174.89839	54123	96
577	-37.3212	174.89847	54112	85
578	-37.32087	174.89852	54110	83
579	-37.32056	174.89862	54123	96
580	-37.32024	174.8987	54110	83
581	-37.31994	174.89877	54080	53
582	-37.31963	174.89889	54038	11
583	-37.31928	174.89894	53987	-40
584	-37.31921	174.89861	53925	-102
585	-37.31958	174.8986	53928	-99

586	-37.31988	174.89857	53984	-43
587	-37.32018	174.8984	54035	8
588	-37.32049	174.89832	54076	49
589	-37.3208	174.89823	54108	81
590	-37.3211	174.89814	54121	94
591	-37.32139	174.89805	54118	91
592	-37.32142	174.89783	54116	89
593	-37.3211	174.89791	54119	92
594	-37.32079	174.89799	54108	81
595	-37.32049	174.89806	54082	55
596	-37.32018	174.89817	54043	16
597	-37.31985	174.89824	53995	-32
598	-37.31953	174.89836	53928	-99
599	-37.31924	174.89844	53867	-160
600	-37.31914	174.8981	53784	-243
601	-37.31946	174.89799	53856	-171
602	-37.31978	174.89791	53949	-78
603	-37.32006	174.89782	53979	-48
604	-37.32038	174.89774	54048	21
605	-37.3207	174.89766	54037	10
606	-37.32099	174.89757	54086	59
607	-37.32132	174.89745	54106	79
608	-37.32102	174.90395	54045	18
609	-37.32109	174.90432	54050	23
610	-37.32116	174.90469	54004	-23
611	-37.3212	174.90502	54002	-25
612	-37.32129	174.90538	53979	-48
613	-37.32157	174.90531	54018	-9
614	-37.32187	174.90521	54012	-15
615	-37.3218	174.90486	54017	-10
616	-37.32152	174.90494	54026	-1
617	-37.32146	174.90457	54007	-20
618	-37.32172	174.90449	54007	-20
619	-37.32167	174.90411	54037	10
620	-37.32136	174.90414	54049	22
621	-37.32131	174.90381	53986	-41
622	-37.32159	174.90373	54042	15
623	-37.32159	174.90344	53958	-69
624	-37.32152	174.90308	54058	31
625	-37.32142	174.90272	54062	35
626	-37.32136	174.90237	54077	50
627	-37.3213	174.90199	54088	61
628	-37.32122	174.90162	54097	70
629	-37.32113	174.90125	54105	78
630	-37.32084	174.90133	54103	76
631	-37.32093	174.9017	54099	72

632	-37.32101	174.90208	54093	66
633	-37.32109	174.90245	54085	58
634	-37.32118	174.90281	54075	48
635	-37.32127	174.90317	54065	38
636	-37.32135	174.90353	54040	13
637	-37.32107	174.90364	54058	31
638	-37.32099	174.90329	54073	46
639	-37.32092	174.90293	54079	52
640	-37.32084	174.90256	54087	60
641	-37.32076	174.9022	54092	65
642	-37.32069	174.90184	54093	66
643	-37.32061	174.90148	54091	64
644	-37.32139	174.90626	53993	-34
645	-37.32165	174.90637	53996	-31
646	-37.32192	174.90646	53989	-38
647	-37.3222	174.90654	53992	-35
648	-37.32252	174.90656	53959	-68
649	-37.3228	174.90653	53994	-33
650	-37.32307	174.90643	53995	-32
651	-37.32298	174.9061	54006	-21
652	-37.32267	174.90614	54004	-23
653	-37.3226	174.90574	54002	-25
654	-37.32289	174.90569	53986	-41
655	-37.32282	174.90535	53984	-43
656	-37.32252	174.9054	53980	-47
657	-37.32222	174.90546	53993	-34
658	-37.32195	174.90554	53934	-93
659	-37.32165	174.90562	53997	-30
660	-37.32136	174.90567	53999	-28
661	-37.32141	174.90601	53915	-112
662	-37.32169	174.90598	53950	-77
663	-37.32199	174.90693	54002	-25
664	-37.32196	174.90596	54002	-25
665	-37.32229	174.9059	53920	-107
666	-37.32249	174.90691	53934	-93
667	-37.32277	174.90683	53980	-47
668	-37.32305	174.90674	53966	-61
669	-37.3231	174.90707	53945	-82
670	-37.32318	174.90746	53956	-71
671	-37.3229	174.90751	53967	-60
672	-37.32281	174.90716	53976	-51
673	-37.32253	174.90721	53965	-62
674	-37.32263	174.90757	53986	-41
675	-37.32222	174.90683	53978	-49
676	-37.32225	174.90717	53972	-55
677	-37.32232	174.90753	53953	-74

678	-37.32236	174.90786	53955	-72
679	-37.32209	174.90792	53949	-78
680	-37.32178	174.90798	53976	-51
681	-37.32173	174.90764	53978	-49
682	-37.32203	174.90758	53987	-40
683	-37.32197	174.90721	53988	-39
684	-37.32167	174.90725	53991	-36
685	-37.32162	174.90689	53992	-35
686	-37.32193	174.90687	53996	-31
687	-37.32132	174.90654	53996	-31
688	-37.32136	174.90688	53988	-39
689	-37.32141	174.90721	53979	-48
690	-37.32145	174.90757	53954	-73
691	-37.32151	174.90794	53945	-82
692	-37.32124	174.90805	53973	-54
693	-37.32117	174.90768	53988	-39
694	-37.32111	174.90732	53995	-32
695	-37.32104	174.90695	53975	-52
696	-37.32083	174.9072	53958	-69
697	-37.32091	174.90755	53959	-68
698	-37.32098	174.90792	53937	-90
699	-37.32101	174.90827	53974	-53
700	-37.32072	174.90836	53970	-57
701	-37.32067	174.90797	53922	-105
702	-37.3206	174.90759	53988	-39
703	-37.32036	174.90732	53960	-67
704	-37.32035	174.90698	53941	-86
705	-37.32026	174.90658	53943	-84
706	-37.32021	174.90621	54012	-15
707	-37.32049	174.90614	53843	-184
708	-37.32054	174.90648	53983	-44
709	-37.32065	174.90681	53924	-103
710	-37.32096	174.90669	53989	-38
711	-37.32089	174.90629	54013	-14
712	-37.32082	174.90593	54010	-17
713	-37.32122	174.90627	54011	-16
714	-37.32115	174.9059	54034	7
715	-37.32108	174.90544	54050	23
716	-37.32102	174.90509	54029	2
717	-37.32073	174.9052	53924	-103
718	-37.32046	174.9053	53963	-64
719	-37.3205	174.90552	54023	-4
720	-37.32077	174.90549	54077	50
721	-37.32073	174.90368	54080	53
722	-37.32068	174.90328	54086	59
723	-37.32062	174.90289	54091	64

724	-37.32055	174.90253	54086	59
725	-37.32048	174.90217	54084	57
726	-37.32042	174.9018	54074	47
727	-37.32035	174.90142	54040	13
728	-37.32006	174.90153	54056	29
729	-37.32012	174.90193	54070	43
730	-37.32016	174.90233	54076	49
731	-37.32022	174.90269	54080	53
732	-37.32028	174.90307	54080	53
733	-37.32037	174.90343	54072	45
734	-37.3204	174.90381	54045	18
735	-37.32015	174.90388	54063	36
736	-37.32008	174.90357	54064	37
737	-37.32001	174.90324	54058	31
738	-37.31994	174.90291	54042	15
739	-37.31989	174.90258	54031	4
740	-37.31983	174.90227	54014	-13
741	-37.31978	174.90194	53989	-38
742	-37.31973	174.90161	53801	-226
743	-37.31874	174.89823	53733	-294
744	-37.31846	174.89831	53670	-357
745	-37.31817	174.89841	53602	-425
746	-37.31789	174.89851	53527	-500
747	-37.31759	174.89861	53463	-564
748	-37.31733	174.89871	53423	-604
749	-37.31735	174.89912	53375	-652
750	-37.31742	174.89953	53507	-520
751	-37.31782	174.89937	53538	-489
752	-37.31822	174.89922	53621	-406
753	-37.31852	174.89913	53705	-322
754	-37.3188	174.89902	53758	-269
755	-37.31873	174.89868	53766	-261
756	-37.31844	174.89873	53706	-321
757	-37.31815	174.89882	53635	-392
758	-37.31784	174.89892	53558	-469
759	-37.31754	174.89903	53482	-545
760	-37.31727	174.89989	53283	-744
761	-37.31758	174.89982	53392	-635
762	-37.31788	174.89972	53491	-536
763	-37.31817	174.89963	53585	-442
764	-37.31846	174.89953	53662	-365
765	-37.31877	174.89947	53734	-293
766	-37.31854	174.89993	53747	-280
767	-37.31826	174.90003	53671	-356
768	-37.31797	174.90014	53582	-445
769	-37.31768	174.90023	53482	-545

770	-37.3174	174.90035	53378	-649
771	-37.31742	174.90065	53265	-762
772	-37.31774	174.90054	53242	-785
773	-37.31801	174.90044	53365	-662
774	-37.31828	174.90036	53472	-555
775	-37.31854	174.90029	53568	-459
776	-37.31884	174.90021	53655	-372
777	-37.31911	174.90013	53737	-290
778	-37.31918	174.9005	53813	-214
779	-37.3189	174.90057	53831	-196
780	-37.31861	174.90067	53757	-270
781	-37.31832	174.90077	53669	-358
782	-37.31804	174.90086	53574	-453
783	-37.31777	174.90094	53463	-564
784	-37.31752	174.90102	53347	-680
785	-37.31886	174.90065	53240	-787
786	-37.31895	174.901	53778	-249
787	-37.31902	174.90137	53807	-220
788	-37.31932	174.9013	53888	-139
789	-37.31927	174.90094	53860	-167
790	-37.3194	174.90163	53924	-103
791	-37.31948	174.90197	53956	-71
792	-37.31953	174.90234	53956	-71
793	-37.3196	174.90273	53987	-40
794	-37.31967	174.90311	54016	-11
795	-37.31972	174.90349	54049	22
796	-37.31979	174.90386	54066	39
797	-37.3195	174.90391	54015	-12
798	-37.31944	174.90353	54023	-4
799	-37.31936	174.90315	54009	-18
800	-37.31929	174.90279	53984	-43
801	-37.31922	174.90239	53953	-74
802	-37.31915	174.902	53911	-116
803	-37.3191	174.90168	53867	-160
804	-37.3194	174.90419	53833	-194
805	-37.31933	174.90384	54018	-9
806	-37.31928	174.90352	54006	-21
807	-37.319	174.90357	53973	-54
808	-37.31906	174.90392	53938	-89
809	-37.31914	174.90427	53970	-57
810	-37.31886	174.90437	53981	-46
811	-37.3188	174.90395	53927	-100
812	-37.31876	174.90362	53923	-104
813	-37.31849	174.90375	53885	-142
814	-37.31861	174.90406	53835	-192
815	-37.31869	174.9044	53893	-134

816	-37.31841	174.90445	53911	-116
817	-37.3185	174.9038	53893	-134
818	-37.31824	174.90387	53847	-180
819	-37.31831	174.9042	53801	-226
820	-37.31805	174.90434	53853	-174
821	-37.31813	174.90461	53833	-194
822	-37.31791	174.90476	53841	-186
823	-37.3178	174.90439	53854	-173
824	-37.31775	174.90401	53813	-214
825	-37.31807	174.9039	53735	-292
826	-37.31633	174.90022	53767	-260
827	-37.31639	174.90054	53032	-995
828	-37.31646	174.90092	52996	-1031
829	-37.31653	174.90132	52976	-1051
830	-37.31684	174.90123	52989	-1038
831	-37.31716	174.90115	53016	-1011
832	-37.31711	174.90077	53093	-934
833	-37.31681	174.90084	53105	-922
834	-37.31672	174.90044	53017	-1010
835	-37.31702	174.90034	53043	-984
836	-37.31697	174.90001	53133	-894
837	-37.31669	174.90012	53166	-861
838	-37.31617	174.90028	53085	-942
839	-37.31589	174.90039	53017	-1010
840	-37.31558	174.90049	53017	-1010
841	-37.31569	174.90087	53061	-966
842	-37.31597	174.90075	53044	-983
843	-37.31624	174.90064	53000	-1027
844	-37.31632	174.90102	52984	-1043
845	-37.31602	174.90113	52977	-1050
846	-37.31574	174.90123	52970	-1057
847	-37.31584	174.90161	52997	-1030
848	-37.31612	174.90151	53046	-981
849	-37.31641	174.90144	53022	-1005
850	-37.31567	174.90187	52993	-1034
851	-37.31574	174.90228	52989	-1038
852	-37.31603	174.90225	53089	-938
853	-37.31611	174.90257	53196	-831
854	-37.31599	174.9019	53148	-879
855	-37.31545	174.90173	53224	-803
856	-37.31515	174.90181	53089	-938
857	-37.31485	174.90191	53162	-865
858	-37.31454	174.90199	53194	-833
859	-37.31421	174.90209	53357	-670
860	-37.31359	174.90223	53354	-673
861	-37.31474	174.90155	53258	-769

862	-37.31503	174.90143	53165	-862
863	-37.31528	174.90132	53157	-870
864	-37.31523	174.90096	53253	-774
865	-37.31491	174.90102	53345	-682
866	-37.31458	174.9011	53346	-681
867	-37.31454	174.9008	53254	-773
868	-37.31485	174.90071	53805	-222
869	-37.31516	174.90059	53236	-791
870	-37.31704	174.89969	53135	-892
871	-37.31673	174.89982	53058	-969
872	-37.31643	174.89994	53026	-1001
873	-37.31616	174.90003	53013	-1014
874	-37.31587	174.90012	53077	-950
875	-37.3158	174.89974	53086	-941
876	-37.31609	174.89966	53136	-891
877	-37.31636	174.89953	53197	-830
878	-37.31667	174.89944	53280	-747
879	-37.31699	174.89932	53327	-700
880	-37.31691	174.89891	53261	-766
881	-37.31661	174.89899	53204	-823
882	-37.31634	174.89906	53168	-859
883	-37.31604	174.89913	53161	-866
884	-37.31573	174.8992	53173	-854
885	-37.31539	174.89933	53223	-804
886	-37.31511	174.8994	53298	-729
887	-37.3148	174.89946	53245	-782
888	-37.3149	174.89982	53170	-857
889	-37.3152	174.89976	53129	-898
890	-37.3155	174.89972	53090	-937
891	-37.31549	174.90006	53149	-878
892	-37.3152	174.90018	53474	-553
893	-37.31415	174.90095	53464	-563
894	-37.3143	174.90143	53466	-561
895	-37.31447	174.90212	53544	-483
896	-37.31409	174.90227	53602	-425
897	-37.31398	174.90168	53618	-409
898	-37.31369	174.90169	53549	-478
899	-37.31388	174.90122	53557	-470
900	-37.31356	174.90128	53624	-403
901	-37.31339	174.90096	53533	-494
902	-37.31336	174.90058	53548	-479
903	-37.31329	174.9002	53666	-361
904	-37.3136	174.90008	53511	-516
905	-37.31391	174.89998	53421	-606
906	-37.31423	174.89985	53377	-650
907	-37.31452	174.89969	53356	-671

908	-37.31467	174.90001	53304	-723
909	-37.31436	174.90015	53400	-627
910	-37.31403	174.90023	53490	-537
911	-37.3137	174.90029	53476	-551
912	-37.31376	174.9007	53569	-458
913	-37.31406	174.90059	53489	-538
914	-37.31437	174.9005	53399	-628
915	-37.31479	174.90037	53277	-750
916	-37.32001	174.90637	53966	-61
917	-37.32009	174.90678	53979	-48
918	-37.32017	174.90718	53968	-59
919	-37.32023	174.90759	53981	-46
920	-37.3203	174.90799	53982	-45
921	-37.32036	174.9084	53982	-45
922	-37.32005	174.90853	53953	-74
923	-37.31995	174.9081	53957	-70
924	-37.31985	174.90769	53960	-67
925	-37.31975	174.90732	53943	-84
926	-37.31966	174.9069	54005	-22
927	-37.3196	174.90653	53936	-91
928	-37.31934	174.90651	53916	-111
929	-37.31941	174.90692	53899	-128
930	-37.31949	174.90732	53958	-69
931	-37.31957	174.9077	53956	-71
932	-37.31963	174.90809	53949	-78
933	-37.31969	174.90848	53944	-83
934	-37.31949	174.90877	53837	-190
935	-37.31918	174.90885	53836	-191
936	-37.3189	174.90895	53835	-192
937	-37.31881	174.90845	53935	-92
938	-37.31871	174.90797	53932	-95
939	-37.31863	174.90758	53836	-191
940	-37.31894	174.90748	53934	-93
941	-37.31904	174.90788	53941	-86
942	-37.3191	174.90828	53947	-80
943	-37.31919	174.90859	53934	-93
944	-37.31944	174.90846	53948	-79
945	-37.31939	174.90806	53904	-123
946	-37.31933	174.9077	53914	-113
947	-37.31925	174.90735	53921	-106
948	-37.31921	174.90716	53927	-100
949	-37.31913	174.90678	53940	-87
950	-37.31904	174.9064	53919	-108
951	-37.31896	174.90604	53877	-150
952	-37.3187	174.9061	53913	-114
953	-37.3184	174.90625	53913	-114

954	-37.31843	174.90664	53893	-134
955	-37.31849	174.90701	53923	-104
956	-37.31855	174.9074	53915	-112
957	-37.31887	174.90728	53922	-105
958	-37.31882	174.9069	53928	-99
959	-37.31882	174.90647	53920	-107
960	-37.31895	174.90552	53872	-155
961	-37.31867	174.90564	53903	-124
962	-37.31838	174.90576	53902	-125
963	-37.31831	174.90534	53895	-132
964	-37.31863	174.90528	53891	-136
965	-37.31895	174.90522	53894	-133
966	-37.31919	174.90565	53832	-195
967	-37.31934	174.90606	53933	-94
968	-37.31965	174.90601	53959	-68
969	-37.31961	174.90558	53958	-69

B.2 Kellyville magnetic survey – raw data

Waypoint	Southing	Easting	Value	Anomaly value
1	-37.27564	175.06168	53957	-3
2	-37.27526	175.06165	53642	-318
3	-37.27497	175.06183	53309	-651
4	-37.27467	175.06194	53741	-219
5	-37.27439	175.06199	53886	-74
6	-37.27404	175.06206	53892	-68
7	-37.2736	175.06207	53825	-135
8	-37.2732	175.06204	53778	-182
9	-37.2729	175.06205	53805	-155
10	-37.27249	175.06155	53775	-185
11	-37.27272	175.06129	53834	-126
12	-37.27306	175.06139	53795	-165
13	-37.27324	175.06103	53771	-189
14	-37.27346	175.06150	53946	-14
15	-37.27374	175.06165	53845	-115
16	-37.27389	175.06124	53857	-103
17	-37.27421	175.06136	53491	-469
18	-37.27457	175.06135	53633	-327
19	-37.27472	175.06086	53799	-161
20	-37.27425	175.06066	53699	-261
21	-37.27418	175.06049	52563	-1397
22	-37.27445	175.06020	52848	-1112
23	-37.27462	175.06019	52871	-1089
24	-37.27464	175.06055	53324	-636
25	-37.27482	175.06040	53681	-279
26	-37.27494	175.06025	54112	152
27	-37.27507	175.06002	53729	-231
28	-37.2748	175.06000	53875	-85
29	-37.2746	175.06013	53839	-121
30	-37.27449	175.06005	53118	-842
31	-37.27433	175.05996	53561	-399
32	-37.27427	175.05963	53749	-211
33	-37.27403	175.05972	53222	-738
34	-37.27396	175.05933	53260	-700
35	-37.27414	175.05939	53359	-601
36	-37.2741	175.05912	53347	-613
37	-37.27406	175.05881	53512	-448
38	-37.27389	175.05846	54112	152
39	-37.27407	175.05839	54793	833
40	-37.27457	175.05869	54708	748

41	-37.27445	175.05837	54271	311
42	-37.27434	175.05818	53570	-390
43	-37.27419	175.05785	53925	-35
44	-37.2741	175.05734	54450	490
45	-37.2743	175.05722	53939	-21
46	-37.27441	175.05694	54247	287
47	-37.27461	175.05664	54708	748
48	-37.27493	175.05654	54775	815
49	-37.27532	175.05649	54012	52
50	-37.27565	175.05644	54220	260
51	-37.27598	175.05649	53890	-70
52	-37.27619	175.05657	54719	759
53	-37.27615	175.05680	54254	294
54	-37.27585	175.05700	53513	-447
55	-37.2757	175.05671	53389	-571
56	-37.27556	175.05719	54105	145
57	-37.27534	175.05686	54623	663
58	-37.27531	175.05740	54593	633
59	-37.27501	175.05700	54394	434
60	-37.27494	175.05757	54367	407
61	-37.2747	175.05723	54351	391
62	-37.27473	175.05777	54014	54
63	-37.2745	175.05760	54081	121
64	-37.27452	175.05797	54211	251
65	-37.27462	175.05819	53776	-184
66	-37.275	175.05805	54388	428
67	-37.27527	175.05788	53975	15
68	-37.27568	175.05763	53818	-142
69	-37.27587	175.05799	53755	-205
70	-37.27538	175.05804	54024	64
71	-37.27506	175.05819	54359	399
72	-37.27471	175.05838	54027	67
73	-37.27483	175.05867	53788	-172
74	-37.27515	175.05854	54053	93
75	-37.27533	175.05878	54021	61
76	-37.27519	175.05921	54298	338
77	-37.27624	175.05785	53817	-143
78	-37.27607	175.05887	53178	-782
79	-37.2758	175.05955	53537	-423
80	-37.27597	175.05992	53446	-514
81	-37.27567	175.06045	53910	-50
82	-37.27545	175.06097	53692	-268
83	-37.27523	175.06127	53144	-816
84	-37.2759	175.06183	54079	119
85	-37.27604	175.06233	54021	61
86	-37.27633	175.06214	54044	84

87	-37.2766	175.06186	54048	88
88	-37.2765	175.06155	54126	166
89	-37.27636	175.06122	54268	308
90	-37.27624	175.06083	54320	360
91	-37.27638	175.06057	54098	138
92	-37.27658	175.06028	54218	258
93	-37.2768	175.06009	54014	54
94	-37.27703	175.06046	54131	171
95	-37.27723	175.06080	54221	261
96	-37.2774	175.06116	54089	129
97	-37.27762	175.06161	54082	122
98	-37.2778	175.06206	54026	66
99	-37.27791	175.06240	54007	47
100	-37.27824	175.06210	53893	-67
101	-37.27868	175.06177	53978	18
102	-37.27873	175.06130	53898	-62
103	-37.27856	175.06083	53969	9
104	-37.27841	175.06053	54022	62
105	-37.27825	175.06015	54071	111
106	-37.27811	175.05972	54106	146
107	-37.27783	175.05984	54146	186
108	-37.27777	175.06024	54228	268
109	-37.27756	175.06053	54246	286
110	-37.27729	175.06010	54091	131
111	-37.27661	175.06021	54296	336
112	-37.27659	175.06070	54110	150
113	-37.27671	175.06107	54135	175
114	-37.27692	175.06152	54115	155
115	-37.27712	175.06177	54118	158
116	-37.27733	175.06206	54084	124
117	-37.27731	175.06243	54051	91
118	-37.27709	175.06270	54078	118
119	-37.27684	175.06297	53819	-141
120	-37.27666	175.06307	54136	176
121	-37.27654	175.06298	54039	79
122	-37.27675	175.06270	54075	115
123	-37.27688	175.06242	54041	81
124	-37.27673	175.06213	54057	97
125	-37.27635	175.06204	54066	106
126	-37.27614	175.06187	54125	165
127	-37.27675	175.05893	54382	422
128	-37.27699	175.05953	54321	361
129	-37.27759	175.05935	54158	198
130	-37.278	175.05927	54240	280
131	-37.27788	175.05903	54356	396
132	-37.27749	175.05900	53723	-237

133	-37.27701	175.05909	54434	474
134	-37.27721	175.05868	53681	-279
135	-37.27761	175.05850	54217	257
136	-37.27788	175.05835	54301	341
137	-37.27813	175.05805	54166	206
138	-37.27811	175.05789	54231	271
139	-37.2786	175.05770	54114	154
140	-37.27914	175.05760	53908	-52
141	-37.27935	175.05704	53941	-19
142	-37.27939	175.05623	53855	-105
143	-37.27907	175.05601	53999	39
144	-37.27874	175.05651	54032	72
145	-37.27811	175.05699	54005	45
146	-37.27776	175.05744	54158	198
147	-37.27742	175.05798	54450	490
148	-37.27688	175.05831	53515	-445
149	-37.27687	175.05765	52731	-1229
150	-37.27718	175.05714	54689	729
151	-37.27708	175.05728	54597	637
152	-37.27703	175.05738	54051	91
153	-37.27697	175.05747	53016	-944
154	-37.27691	175.05756	52478	-1482
155	-37.27687	175.05763	52713	-1247
156	-37.27682	175.05773	52519	-1441
157	-37.27694	175.05779	52062	-1898
158	-37.27703	175.05769	53228	-732
159	-37.277	175.05772	52905	-1055
160	-37.27714	175.05767	53700	-260
161	-37.27723	175.05760	54539	579
162	-37.27728	175.05749	54881	921
163	-37.2774	175.05734	54678	718
164	-37.27738	175.05720	54591	631
165	-37.27733	175.05707	54563	603
166	-37.27724	175.05690	54592	632
167	-37.27696	175.05663	54404	444
168	-37.27703	175.05634	54177	217
169	-37.27725	175.05628	54122	162
170	-37.27768	175.05610	54158	198
171	-37.27808	175.05587	53467	-493
172	-37.27811	175.05550	53767	-193
173	-37.27783	175.05551	53860	-100
174	-37.27817	175.05509	53786	-174
175	-37.27809	175.05481	53850	-110
176	-37.27781	175.05454	53831	-129
177	-37.27753	175.05433	53780	-180
178	-37.27716	175.05400	53691	-269

179	-37.27696	175.05461	53885	-75
180	-37.27705	175.05512	53982	22
181	-37.27713	175.05560	53940	-20
182	-37.27706	175.05616	54138	178
183	-37.27692	175.05680	54506	546
184	-37.27685	175.05709	54397	437
185	-37.2768	175.05735	53273	-687
186	-37.27674	175.05754	53076	-884
187	-37.27671	175.05769	52374	-1586
188	-37.27668	175.05787	52724	-1236
189	-37.27661	175.05814	53499	-461
190	-37.2766	175.05842	54034	74
191	-37.27486	175.05608	54025	65
192	-37.2751	175.05597	54597	637
193	-37.27535	175.05592	54514	554
194	-37.27561	175.05581	53912	-48
195	-37.27566	175.05556	54165	205
196	-37.27547	175.05526	54113	153
197	-37.27596	175.05570	53791	-169
198	-37.27622	175.05588	54373	413
199	-37.27639	175.05589	54947	987
200	-37.27639	175.05582	54620	660
201	-37.27624	175.05558	54738	778
202	-37.27612	175.05524	55092	1132
203	-37.27641	175.05543	54105	145
204	-37.27649	175.05559	54101	141
205	-37.27659	175.05560	53973	13
206	-37.27656	175.05529	54015	55
207	-37.27638	175.05507	53985	25
208	-37.27611	175.05490	53967	7
209	-37.2761	175.05457	53473	-487
210	-37.27583	175.05427	53907	-53
211	-37.27544	175.05411	54015	55
212	-37.27522	175.05402	53978	18
213	-37.27528	175.05425	54155	195
214	-37.27503	175.05424	54197	237
215	-37.27486	175.05428	54374	414
216	-37.27513	175.05442	54226	266
217	-37.27501	175.05462	54438	478
218	-37.2752	175.05472	54324	364
219	-37.27543	175.05491	54284	324
220	-37.27464	175.05449	54509	549
221	-37.27433	175.05425	54519	559
222	-37.27429	175.05474	55111	1151
223	-37.27433	175.05512	55235	1275
224	-37.27474	175.05504	55076	1116

225	-37.27477	175.05556	54433	473
226	-37.27462	175.05585	53694	-266
227	-37.27499	175.05611	53950	-10
228	-37.27429	175.05566	53509	-451
229	-37.27415	175.05525	54296	336
230	-37.27375	175.05534	53722	-238
231	-37.27367	175.05511	53838	-122
232	-37.27391	175.05449	55036	1076
233	-37.27348	175.05467	54131	171
234	-37.27338	175.05443	54117	157
235	-37.27366	175.05417	54316	356
236	-37.27415	175.05386	54557	597
237	-37.27433	175.05370	54200	240
238	-37.27393	175.05347	54427	467
239	-37.27345	175.05328	54099	139
240	-37.2736	175.05374	54335	375
241	-37.27323	175.05390	54159	199
242	-37.2735	175.05503	53826	-134
243	-37.27385	175.05585	53009	-951
244	-37.27409	175.05638	53202	-758
245	-37.27395	175.05671	50645	-3315
246	-37.27381	175.05683	50680	-3280
247	-37.27373	175.05705	51693	-2267
248	-37.27363	175.05742	51802	-2158
249	-37.27351	175.05822	53002	-958
250	-37.27341	175.05872	54166	206
251	-37.27305	175.05798	53365	-595
252	-37.27305	175.05839	53455	-505
253	-37.27311	175.05874	52564	-1396
254	-37.27265	175.05873	53432	-528
255	-37.27266	175.05893	52840	-1120
256	-37.27313	175.05904	53346	-614
257	-37.27342	175.05899	53929	-31
258	-37.27328	175.05955	53489	-471
259	-37.27306	175.06000	53575	-385
260	-37.27287	175.06018	53559	-401
261	-37.27249	175.06034	53242	-718
262	-37.27232	175.06008	53347	-613
263	-37.27257	175.05977	53536	-424
264	-37.2727	175.05943	53720	-240
265	-37.27283	175.05925	54048	88
266	-37.2725	175.05914	54147	187
267	-37.27232	175.05943	54044	84
268	-37.27228	175.05919	53978	18
269	-37.27213	175.05912	53798	-162
270	-37.27188	175.05889	52668	-1292

271	-37.27162	175.05860	52872	-1088
272	-37.27146	175.05836	53316	-644
273	-37.27183	175.05844	53501	-459
274	-37.27213	175.05867	53441	-519
275	-37.27213	175.05821	53078	-882
276	-37.27249	175.05807	53019	-941
277	-37.27313	175.05766	52239	-1721
278	-37.27322	175.05718	52589	-1371
279	-37.27339	175.05664	53546	-414
280	-37.2737	175.05622	54058	98
281	-37.27345	175.05574	52326	-1634
282	-37.27315	175.05630	53807	-153
283	-37.27298	175.05684	53529	-431
284	-37.27286	175.05735	53586	-374
285	-37.27327	175.05533	50999	-2961
286	-37.27293	175.05515	54135	175
287	-37.27283	175.05561	54460	500
288	-37.27259	175.05617	54273	313
289	-37.27245	175.05666	53884	-76
290	-37.27232	175.05722	54048	88
291	-37.27209	175.05760	53571	-389
292	-37.27182	175.05767	53300	-660
293	-37.27191	175.05723	53457	-503
294	-37.27203	175.05664	53724	-236
295	-37.2722	175.05597	53913	-47
296	-37.27245	175.05536	54078	118
297	-37.2721	175.05554	54216	256
298	-37.27152	175.05593	54063	103
299	-37.27121	175.05624	53974	14
300	-37.27079	175.05658	53644	-316
301	-37.27024	175.05605	53763	-197
302	-37.27026	175.05542	53803	-157
303	-37.27038	175.05464	53741	-219
304	-37.27045	175.05390	53874	-86
305	-37.27053	175.05359	53869	-91
306	-37.27057	175.05342	53863	-97
307	-37.27057	175.05324	53993	33
308	-37.27049	175.05322	53981	21
309	-37.27047	175.05307	53961	1
310	-37.27039	175.05314	54054	94
311	-37.27054	175.05291	53985	25
312	-37.27051	175.05291	54046	86
313	-37.2707	175.05304	54039	79
314	-37.27095	175.05313	53965	5
315	-37.271	175.05367	53787	-173
316	-37.27097	175.05413	53617	-343

317	-37.27106	175.05469	53575	-385
318	-37.2712	175.05524	54560	600
319	-37.27193	175.05515	53749	-211
320	-37.27176	175.05460	54127	167
321	-37.2716	175.05407	54150	190
322	-37.27151	175.05344	54176	216
323	-37.27192	175.05344	53748	-212
324	-37.27191	175.05400	54183	223
325	-37.27183	175.05451	54336	376
326	-37.272	175.05504	54166	206
327	-37.27241	175.05497	54149	189
328	-37.27235	175.05452	54393	433
329	-37.27337	175.05470	54446	486